Flame Spread on Composite Materials for use in High Speed Craft

by

Mark T. Wright

A Thesis

Submitted to the Faculty

of the

WORCESTER POLYTECHNIC INSTITUTE

in partial fulfillment of the requirements for the

Degree of Master of Science

in

Fire Protection Engineering

August 1999

APPROVED:

Professor Jonathan Barnett, Ph.D., Major Advisor

Professor Nicholas Dembsey, Ph.D, Co-Advisor

Jason Averill, M.S. FPE, NIST, Reader

Professor David Lucht, P.E., Head of Department

Abstract

The use of advanced materials in the construction of high-speed craft is becoming more commonplace. However, there are certain requirements set in the High Speed Craft Code (published by IMO) that restrict the use of materials based on results from full scale room fire testing (ISO 9705). An obvious benefit would be gained by simulating the results of these full-scale tests using bench scale data from the Cone Calorimeter and LIFT apparatus.

A flame-spread algorithm developed by Henri Mitler at the National Institute of Standards and Technology was selected for implementation into the zone fire model CFAST. This algorithm was modified from its original form, so that it could simulate flame spread on wall/ceiling lining materials for both sidewall and corner scenarios, including ISO 9705 as prescribed in the High Speed Craft Code. Changes to the algorithm included geometry of flame spread across the ceiling, flame height, radiation exchange, ignition burner heat flux maps, and multiple pyrolysis zones. The new flame spread algorithm was evaluated against room corner test data from four different marine composite materials tested per ISO 9705.

Acknowledgements

Thanks to Professor Barnett and Professor Dembsey for their interest and support of this research and for their patience with my seemingly endless stream of questions. Their high standards have pushed me to great academic highs and reminded me of the value of hard work at the end of the day.

Thanks to my reader Jason Averill, who was kind enough to take time out of his busy schedule and make this a better document.

Thanks to the staff at NIST who has given their support in the use of CFAST, especially Glenn Forney, Rick Peacock, and Paul Reneke.

Thanks to Henri Mitler for his support of my work and for providing me with the source code to his original algorithm. This project certainly wouldn't have been possible without it!

Thanks to Terry Fay and Chris Lautenberger for their large amount of help in debugging the code of this algorithm and running simulations.

Thanks to Jay Ierardi and the rest of the crew in the computational fire modeling lab, who put up with endless hours of complaining and provided the necessary camaraderie to relieve some of the pain.

Thanks to my parents and sister, whose encouragement and understanding throughout this process was enormously helpful. I wouldn't have finished without it.

Finally, the support of the Department of Transportation, Maritime Administration, Agreement # DTMA 91-97-H-0002 – "Internationally Competitive Fast Ferries and Composite Ship Technologies" is greatly appreciated.

"*If I have seen farther than others, it is because I was standing on the shoulders of giants*." – Sir Issac Newton

Executive Summary

An algorithm that simulates the spread of flame in a compartment corner configuration has been developed. This objective was accomplished by selecting an appropriate flame spread algorithm from the literature, enhancing it to simulate the room corner configuration, implementing it within a zone fire model, and testing the algorithm by comparing its predictions with experimental data.

The first step in this process was to select a pre-existing flame spread algorithm from the literature for implementation into the zone fire model CFAST[26,27]. Numerous algorithms were identified and inspected on a general level. Many of these algorithms were not representative of compartment fire conditions, so they were eliminated from the list of potential candidates. Algorithms developed by Quintiere[31], Karlsson[19], and Mitler[23,24] were the best candidates, and were analyzed in greater detail. Mitler's algorithm was selected for this project, based primarily on the detail represented in calculations of upward flame spread, pyrolysis rate, and heat flux from burner and wall flames to wall/ceiling surfaces. This algorithm uses small, discrete elements, allowing a detailed distribution of these parameters to be calculated.

The next step was to develop this algorithm so that it could simulate the ignition and burning of wall/ceiling lining materials in the room corner configuration. Many changes were necessary, because the original algorithm was developed for a room side-wall configuration. The changes were as follows:

- The geometry of flame spread on the ceiling was set to quarter-circular,
- the flame height correlation was revised to be representative of the room corner,
- the radiation exchange in the corner was detailed via a radiation network calculation,
- the description of total heat flux from the ignition burner in the corner was improved through the use of heat flux maps, and
- the burnout simulation was improved by allowing multiple pyrolysis zones to exist.

Once these modifications were made, the new algorithm was implemented into CFAST[26,27].

The last task was to test the predictive capabilities of the new flame spread algorithm. A set of experimental data was available for several marine composite materials, which included results from the Cone Calorimeter, LIFT apparatus, and full-scale ISO 9705 room corner test (standard test method for fire performance of wall/ceiling linings in a compartment corner). Four of the marine composite materials were selected for testing the algorithm because they had the most complete material property data, and represented a varied range of full-scale experimental behavior. Three of these materials were fire retarded and one was non-fire retarded. The next step was to formulate the material property data into a self-consistent set of inputs for the algorithm, and alter important input parameters to establish the sensitivity of the algorithm to these variables. These variables were thermal inertia, Cone Calorimeter heat release rate curve, material emissivity, flame transmissivity, ignition temperature, minimum temperature for lateral flame spread, and the lateral flame spread parameter. A sensitivity matrix was

developed to organize the changes to the key input variables and numerous simulations were then conducted as outlined in this matrix.

The new algorithm predicted the experimental behavior of the non-fire retarded material with only 20-30% error, but was not as successful for two of the three fire retarded materials. A hypothesis was made that the full-scale effects of the fire retardants may not be well represented in the small-scale tests, leading to errant simulation results. The results from the simulations based on the sensitivity matrix showed that the algorithm was most sensitive to variations in the Cone Calorimeter curve, thermal inertia ($k\rho c_p$), and ignition temperature. Additionally, the algorithm was shown to be numerically stable.

Recommendations for further work include a study of the behavior of fire retardants, additional simulation of non-fire retarded materials, and verification of calculations involving ceiling mass loss rates, multiple pyrolysis zones, heat flux maps, and the flame transmissivity factor (used in the radiation network to account for the attenuation of radiation as it passes through a flame).

Table of Contents

List of Figures

List of Tables

Nomenclature

SYBMOLS

A_k	m^2	Surface area of element *k*
A_f	m^2	Flame area (Karlsson[19])
A_p	m^2	Pyrolysis area (Karlsson[19])
a	m	Configuration factor dimension
b	m	Configuration factor dimension
c	m	Configuration factor dimension
c_p	J/kg-K or kJ/kg-K	Specific heat at constant pressure
C_s	g/g	Soot mass concentration in the upper layer
D	m	Characteristic dimension of ignition burner
F_{k-j}	(ND)†	Configuration factor between elements *k* and *j*
g	m/sec2	Acceleration of gravity
ΔH_{eff}	kJ/g	Effective heat of combustion
$\Delta H_{net,c}$	kJ/g	Net heat of complete combustion
ΔH_{rad}	kJ/g	Radiative heat of combustion
H	m	Configuration factor dimension
k	W/m-K or kW/m-K	Material thermal conductivity
K	L/mg-m	A constant used in the gas emissivity calculation (0.47)
L	m	Configuration factor dimension
L	kJ/g	Effective heat of gasification (Quintiere[31])
$\dot{Q}$	W or kW	Heat release rate
$\dot{Q}''$	kW/m^2	Energy release rate per unit area of a material (Quintiere[31])
$\dot{Q}_l$	W/m^2 or kW/m^2	Heat release rate per unit width
$\dot{Q}_D^*$	(ND)†	Non-dimensional heat release rate (uses $\dot{Q}$)
$\dot{Q}_l^*$	(ND)†	Non-dimensional heat release rate (uses $\dot{Q}_l$)
Q_k	W or kW	Energy supplied to the surface of element *k* by some other means than the radiation in the enclosure
q_k	W/m^2 or kW/m^2	Energy flux supplied to the surface of element *k* by some other means than the radiation in the enclosure
$q_{o,k}$	W/m^2 or kW/m^2	Outgoing radiant flux from the surface of element *k*
$q_{i,k}$	W/m^2 or kW/m^2	Incident radiant flux to the surface of element *k*
$\dot{q}_f''$	W/m^2 or kW/m^2	Flame heat flux (Quintiere[31],Karlsson[19])
R_k	W/m^2 or kW/m^2	External flux (from burner and wall flames) added to radiation network at element *k*
r	m	Configuration factor dimension
S	m	Physical pathlength through the upper gas layer (mean beam length)
S	m	Dimension used in configuration factor derivation

t	sec	time
t_{ig}	sec	Characteristic ignition time (Quintiere[31],Karlsson[19])
T_{gas}	K	Upper layer gas temperature
T_k	K	Surface temperature of element k
T_o	K	Ambient temperature
T_s	K	Surface temperature (Quintiere[31],Karlsson[19])
$T_{s,min}$	K	Minimum surface temperature for lateral flame spread
x_p	m	Lateral pyrolysis front (Quintiere[31])
y_p	m	Height of pyrolysis zone (Quintiere[31])
y_f	m	Flame height (Quintiere[31])
Z_f	m	Flame height
Z_p	m	Height of pyrolysis zone

GREEK SYMBOLS

$\bar{\alpha}_{k-j}$	(ND) †	Absorptivity of gas layer between elements k and j
α_{flame}	(ND)†	Absorptivity of flames from the burning material
χ_A	(ND)†	Combustion efficiency
χ_R	(ND)†	Radiative fraction of heat release rate
δ	M	Material thickness
δ_{kj}	(ND)†	Kronecker delta (equals 1 when $k = j$, otherwise equals 0)
ε_{flame}	(ND)†	Emissivity of flames from the burning material
ε_g	(ND)†	Emissivity of the upper gas layer
ε_k	(ND)†	Material surface emissivity of element k
Φ	kW^2/m^3	Lateral flame spread parameter
φ	Radians	Angle used in configuration factor derivation
κ_s	1/m	Soot emission coefficient
θ_1	Radians	Angle used in configuration factor derivation
θ_2	Radians	Angle used in configuration factor derivation
ρ	M	Dimension used in configuration factor derivation
ρ	kg/m^3	Material density
ρ_o	kg/m^3	Ambient air density
ρ_k	(ND)†	Material surface reflectivity of element k
σ	kW/m^2K^4	Stefan-Boltzmann constant ($5.67e^{-11}$)
$\tau_{fl,k}$	(ND)†	Transmissivity of the flame in front of element k
$\bar{\tau}_{k-j}$	(ND)†	Transmissivity of gas layer between elements k and j

Notes:
† Dimensionless variable

1.0 Introduction

Composite materials have been used for numerous years in the recreational boating industry. A typical example would be a fiberglass hull on a small fishing boat. Several characteristics of these materials make them desirable in marine applications, including[9]:

- High strength to weight ratio,
- high stiffness,
- high fatigue resistance, and
- high corrosion resistance.

These characteristics can also benefit the commercial marine industry, particularly in the domain of high-speed craft where lightweight materials are an essential part of shipbuilding. However, the International Maritime Organization closely regulates the use of these materials on high-speed craft.

The International Code of Safety for High-Speed Craft[14] is the code dealing with the construction and operation of these type of vessels. It allows the use of alternate building materials, instead of the industry standard steel or aluminum. If such materials are to be used according to the code, they must first be qualified as a "Fire Restricting Material" by provisions in the Fire Test Procedures (FTP) code[13] that outline requirements to limit heat release rate, smoke production, and flame spread. More specifically, these requirements are:

(1) The time average of HRR excluding the HRR from the ignition source does not exceed 100kW,
(2) The maximum HRR excluding the HRR from the ignition source does not exceed 500 kW averaged over any 30 second period of time during the test,
(3) The time average of the smoke production rate does not exceed 1.4 m^2/sec,
(4) The maximum value of the smoke production rate does not exceed 8.3m^2/sec averaged over any period of 60 seconds during the test,
(5) Flame spread must not reach any further down the walls of the test room than 0.5m from the floor excluding the area which is within 1.2m from the corner where the ignition source is located, and
(6) No flaming drops or debris of the test sample may reach the floor of the test room outside the area, which is within 1.2m from the corner where the ignition source is located.

The basic experimental setup used to test these requirements is the ISO9705 room corner test[16]. This is a standard test method for determining the performance of wall and ceiling lining materials, when exposed to a fire from an ignition burner placed in the corner of a full-size compartment. Since full scale testing of these materials is particularly expensive, a desirable alternative is to simulate full-scale tests based on results from small-scale tests such as the Cone Calorimeter[15]. Thus, the main goal of this project was to attempt simulation of the behavior of composite materials in a full-scale room corner test using model input data from small-scale experiments. The basic

method chosen to achieve this goal was to use a zone fire model for the simulation of general room conditions, with the addition of a pre-existing algorithm to track flame spread in the compartment corner. The flame-spread algorithm calculates the total heat release rate and physical limits of burning. Therefore, it can provide guidance on the Fire Restricting Material requirements (1), (2), and (5). The zone fire model calculates species production (including smoke), thus providing guidance on requirements (3) and (4). Requirement (6) was considered to be beyond the scope of this project, as this type of material behavior is not readily predicted.

The zone fire model chosen for this project was CFAST[26,27], developed by the National Institute of Standards and Technology. It calculates properties of the upper and lower layers, including gas temperatures, wall surface temperatures, species concentrations, layer thickness, and vent flows. CFAST also provides simulation of other phenomena, such as mechanical ventilation and ignition of objects within the compartment. This model has general acceptance in the fire protection community, which was a major factor in its selection for this project [17,4].

The selection of an appropriate flame spread algorithm is described in Chapter 2. Numerous flame-spread algorithms were identified, however most were eliminated as potential candidates because they did not represent compartment fire conditions. Algorithms developed by Quintiere[31], Karlsson[19], and Mitler[23,24] were studied and compared in more detail. The algorithm developed by Mitler was selected for use in this project because it simulates compartment fire conditions and includes the most detailed representation of upward flame spread, pyrolysis, and distribution of heat flux from burner and wall flames to the wall/ceiling surfaces.

Mitler's original algorithm was intended to simulate the spread of flames on a compartment wall away from a corner. Since the goal of this project is to simulate flame spread in the compartment corner, several changes to the algorithm were necessary. Chapter 3 discusses the changes made to the original algorithm, including geometry of the flame spread over the ceiling, flame height, enhanced radiative exchange, heat flux maps, and multiple pyrolysis zones.

Chapters 4 and 5 describe issues surrounding the integration of the new flame spread algorithm into CFAST[26,27], and other details regarding the source code modifications needed to implement the changes specified in Chapter 3. Also provided is a basic description of how the new flame spread algorithm works within CFAST. All changes were formed in a way that allows the user to select various options (simulate the corner configuration, use the heat flux maps, etc.) via the input to the algorithm. Thus, the original sidewall algorithm is preserved and may still be used for simulations.

The new flame spread algorithm was evaluated against experimental data for four marine composite materials. Data from small-scale experiments (Cone Calorimeter and LIFT apparatus) were used to create a self-consistent set of model inputs, and the algorithm output was compared to experimental results from full-scale ISO 9705 tests on these materials. Additionally, a sensitivity analysis of important input parameters was conducted, along with simulation of the potential effects of fire retardants present in three of the four evaluated materials. The results of these evaluations are provided in Chapter 6, followed by conclusions and recommendations for future work in Chapter 7.

2.0 Algorithm Selection

The first step in the development of a corner flame spread algorithm was to select an existing algorithm as a basis from which to work. This algorithm would then be implemented into the zone fire model CFAST [26,27], and changes made as necessary to suit the room corner geometry. Several different flame spread algorithms were identified in the literature and are described briefly in the following section.

2.1 Description of Various Flame Spread Algorithms

The following algorithms describe simulation of various flame-spread conditions with differing degrees of detail.

- Quintiere[31]
  The algorithm developed by Quintiere is intended to simulate "the ignition, flame spread, burnout, and burning rate of wall and ceiling materials subject to a corner fire ignition source in a room." Based on an experimental setup similar to ISO 9705[16], this algorithm calculates ignition from a square burner in a room corner, upward and lateral flame spread on the wall surfaces, and subsequent flame spread across the ceiling and down the wall from the ceiling. The primary outputs from this algorithm are total heat release rate, flame height, and a detailed time history of pyrolysis and burnout front positions. As this algorithm is based on room corner experiments, it is representative of compartment fire conditions.

- Karlsson[19]

  This algorithm is based on two separate room corner scenarios with different scale sizes (full and 1/3 room). The full-scale room is the same as the ISO 9705[16] room. Two separate algorithms were also developed to simulate different wall/ceiling lining conditions. Model A is based on the room with the lining material mounted on both the walls and ceiling. Model B is based on the room with the lining material on only the walls. The ceiling is considered inert in Model B. Model A simulates ignition of the walls behind the burner, and flame spread across the ceiling and along the wall-ceiling interface. Model B simulates ignition of the walls behind the burner, and the spread along "arms" at the ceiling wall interface. Subsequent downward spread from the "arms" is also simulated. The main outputs from these algorithms are total heat release rate, pyrolysis area, flame area, and fluxes to the lower walls. This algorithm is representative of compartment fire conditions.

- Mitler [23,24]

  Mitler's algorithm is designed to "predict the ignition of, and the subsequent rate and extent of fire spread of flat walls in a room using the fire properties of the materials involved." Simulation of the spread of fire to the ceiling in this configuration is also considered, as well as lateral spread. A line burner was the simulated ignition source. The wall and ceiling are divided into many horizontal elements, where temperature,

incident flux, mass loss rate (after ignition), and burnout are individually tracked. The main outputs of this algorithm are total heat release rate, pyrolysis and burnout locations, flame heights, heat flux distributions, mass loss rate, and width of the upper layer and lower layer pyrolysis zones on the wall. This configuration is representative of compartment fire conditions.

- Beyler, Hunt, Iqbal, and Williams[6]
  This algorithm is based on experiments of vertical flame spread on a vertical panel, using a line burner as the ignition source. Vertical flame spread is simulated on a flat panel subject to ignition via a line burner. The vertical panel is subdivided into many elements, each of which is tracked independently. The main outputs of the algorithm are total heat release rate, flame height, surface temperature of the elements, mass loss rate, and pyrolysis and burnout locations. Lateral flame spread or flame spread along the ceiling/wall interface is not considered in this algorithm. This configuration is not representative of room fire conditions as it simulates upward spread in an open experimental condition (i.e. under a hood).

- Kulkarni, Brehob, Manohar, and Nair[20]
  This algorithm is a mix of experimental and theoretical constructions. It is an open configuration (no ceiling) algorithm that attempts to describe an experimental setup for vertical flame spread. The experimental setup consists of a vertical sample that is ignited by a line burner, and could optionally be heated by two radiant panels to simulate external flux. The main outputs of this algorithm are surface temperature, forward heating flux, flame height, local mass loss rate, and pyrolysis and burnout fronts. This algorithm does not account for lateral spread and is not generally representative of room fire conditions, although the two external fluxes could be used to approximate crude room fire conditions (upper and lower layer simulation).

- Ahmed, Dietenberger, and Jones[1]
  This algorithm provides flame spread modeling of pool and wall fires (which can be incline planes), where the basic shape of an octagon was used to describe the advancement of the flame front. The surface in consideration was discretized into a grid that controlled the movement of the octagon vertices. The main outputs are total heat release rate and pyrolysis front locations. This algorithm is representative of compartment fire conditions.

- Ohlemiller and Dolan[25]
  This algorithm is based on experiments using the LIFT apparatus for honeycomb sandwich panels, and high-density composite armor. The algorithm simulates ignition and delay times and lateral flame spread velocity for these materials. Problems with material behavior during the testing made results from the algorithm somewhat unreliable. This algorithm is not representative of room fire conditions because it only simulates the behavior of the material in the LIFT apparatus.

- Qian, Cheng, and Saito[30]
  This algorithm was developed from experimental results and observations based on a small-scale room (1m x 1m x 1.6m) with PMMA lining the walls and ceiling. Line burners were used to ignite the samples in the corner at the bottom of the test room. The algorithm combines several empirical correlations to form a single equation for the pyrolysis height as a function of time. The main outputs are flame height, heat flux to the wall, wall surface temperature, and pyrolysis front position. Vertical flat wall and corner configurations are valid for this algorithm, although room feedback effects are not included and the results may not scale up to a full room accurately.

- Baroudi, Kokkala, and Parker[5]
  This algorithm is based on experimental data relating to flame spread on a vertical surface (primarily wood) that resides in a room with a high ceiling. This algorithm is similar to the other algorithms, as it calculates flame height, wall surface temperature, pyrolysis height, etc. as a function of time, however because the primary focus for this study was for vertical walls in high, open spaces, room effects are not considered.

Most of these algorithms provided reasonable results for the situation that they were attempting to simulate, however most were removed as potential candidates for implementation into CFAST[26,27]. The primary reason for this was that most of these algorithms were not developed to simulate a compartment configuration. This characteristic is important to the project because the behavior of marine composite materials in the ISO 9705[16] compartment corner test is the desired simulation goal. The algorithm developed by Ahmed, et al.[1] was eliminated from the scope of study based on reported numerical issues [personal communication with Dr. Jonathan Barnett at Worcester Polytechnic Institute].

The algorithms developed by Quintiere[31], Karlsson[19] and Mitler[23,24] warranted further investigation as they simulated compartment conditions and were sufficiently detailed. The following sections describe the comparison of these algorithms, and the final selection.

2.2 Study of Selected Algorithms

Quintiere[31], Karlsson[19], and Mitler's[23,24] algorithms were examined in more depth to determine which one would be the best choice for implementation into CFAST. In examining these algorithms, several similar modules were identified in each that could be used for comparing the algorithms. These modules are as follows:

1) Upward (concurrent) spread mechanism
2) Pyrolysis algorithm
3) Heat flux from burner and wall flames to the wall/ceiling surfaces
4) Lateral (opposed) spread mechanism
5) Regression (burn-through)
6) Surface temperature
7) Upper layer gas temperature

Each model uses a simple one-dimensional heat transfer algorithm to calculate the surface temperature; therefore its inclusion in the following analysis is not necessary. The last item in the list is also not included because it is handled by the zone fire model. Thus, the upper gas layer temperature will be calculated in the same manner for each algorithm.. The following tables review the remainder of the modules for each algorithm.

Table 2-1 – Overview of modules in Quintiere's algorithm

MODULE	DESCRIPTION
Upward (concurrent) spread mechanism	The basic upward spread module in this algorithm is based upon the work done by Saito, Quintiere, and Williams (SQW)[28]. The differential equation governing upward spread is: $\frac{dy_p}{dt} = \frac{y_f - y_p}{t_{ig}}$ (2-1) where y_f is the flame height, y_p is the pyrolysis height, and t_{ig} is an ignition time defined as: $t_{ig} = \frac{\pi}{4} k\rho c_p \left[\frac{T_{ig} - T_s}{\dot{q}''_f} \right]^2$ (2-2) $k\rho c_p$ is the thermal inertia of the wall/ceiling material, T_{ig} is the ignition temperature, T_s is the global average surface temperature, and q''_f is the flame heat flux beyond the burning region (specified as constant at 30 kW/m^2).
Pyrolysis algorithm	A material parameter $\Delta H_{eff}/L$ (heat of combustion divided by an effective heat of gasification) is defined by Quintiere that characterizes the burning behavior of a material. Specifically it allows the peak heat release rate to be found under differing flux conditions via the following equation: $\dot{Q}'' = \frac{\Delta H_{eff}}{L} \left(\dot{q}''_f - \sigma T_{ig}^4 + \sigma T_{gas}^4 \right)$ (2-3) where $\dot{q}''_f$ is the incident flame heat flux over the pyrolysis region, σT_{ig}^4 is the re-radiation flux loss, and σT_{gas}^4 is the incident heat flux from the room, maximized as a blackbody with a view factor of one. As q''_f and σT_{ig}^4 are constants, the change in peak heat release rate varies only with T_{gas}. The above equation represents the pyrolysis algorithm because the material dependent parameter $\Delta H_{eff}/L$ controls the way the heat release rate changes for a given incident flux.
Heat flux from burner and wall flames to the wall/ceiling surfaces	Heat flux to the walls from the burner/wall flames within the pyrolysis region is assumed constant at 60kW/m^2 Heat flux to the walls from the extended flame length (beyond the pyrolysis region) is also considered constant at 30kW/m^2.
Lateral (opposed) spread	The following form is in use for all three algorithms: $\frac{dx_p}{dt} = \frac{\Phi}{k\rho c_p \left(T_{ig} - T_s \right)^2}$ (2-4) where x_p is the lateral pyrolysis front, and Φ and $T_{s,min}$ are material derived

	parameters from the test procedure of ASTM E-1321 (LIFT apparatus)[3]. T_s must be greater than $T_{s,min}$ for lateral flame spread to occur.
Regression and burn-through	A burnout time parameter is used, which is the total available energy per unit area for a given material, divided by the instantaneous energy release rate. The total available energy is obtained from the cone data.

Table 2-2 – Overview of modules in Karlsson's algorithm

MODULE	DESCRIPTION
Upward (concurrent) spread mechanism	As with Quintiere's[31] algorithm, this is based on the SQW[28] equation. However, it is derived in areas instead of lengths: $\frac{dA_p}{dt} = \frac{A_f - A_p}{t_{ig}}$ (2-5) where A_p is the pyrolysis area and A_f is the flame area. t_{ig} is the same as in Quintiere's algorithm, except for q''_f which is specified as 45kW/m^2. However, since the entire wall behind the burner is assumed to ignite instantaneously, this actually only governs spread across the ceiling and along the wall/ceiling interface.
Pyrolysis algorithm	This is based on the Cone Calorimeter heat release rate curve for the material, tested at 50kW/m^2. No account is taken for changing mass loss rates versus changing incident fluxes.
Heat flux from burner and wall flames to the wall/ceiling surfaces	Constants are defined that are used within this algorithm for the burner heat flux to the wall (pre-ignition) and the flux to the virgin material ahead of the pyrolysis front. These are set at 45kW/m^2 and 35kW/m^2 respectively. In order to calculate the surface temperature of the wall beneath the hot gas layer (beyond the area of wall directly behind the burner), a heat flux term that varies with height is used: $\dot{q}'' = \varepsilon_g F_g \sigma\left(T_g^4 - T_o^4\right) + \varepsilon_f F_f \sigma\left(T_f^4 - T_o^4\right) + \varepsilon_p F_p \sigma\left(T_p^4 - T_o^4\right)$ (2-6) where the subscripts g, f, and p denote gas layer, flame, and pyrolyzing wall material, respectively. The configuration factor for the flame and pyrolyzing wall material was assumed to be equal. Additionally, the flame temperature was taken to be ~1100K, the pyrolyzing material temperature was taken to be ~750K, and the flame and pyrolyzing material emission coefficients were each taken to be 0.5.
Lateral (opposed) spread	The same form as Quintiere[31] is used in this algorithm.
Regression and burn-through	This is not explicitly discussed in the report. It could be tied to the use of the actual HRR curve from the Cone Calorimeter. Burnout/regression would generally then be seen as the decrease of HRR near the end of the curve.

Table 2-3 – Overview of modules in Mitler's algorithm

MODULE	DESCRIPTION
Upward (concurrent) spread mechanism	An elemental approach is taken in this algorithm as upward spread is calculated as a moving ignition front. The height of the pyrolysis front is assumed to be the highest element that has reached the ignition temperature. At each time step the surface temperatures are updated, and the location of the pyrolysis front is moved to the newest elements that have reached the ignition temperature. Several routines are coupled and converged to a solution at each time step (after ignition at one or more consecutive nodes) These routines are: • Mass loss rate • Total power output • Flame height • Total flux from the upper layer gases • Fluxes from the flames (material and burner) • Surface temperature Each of these parameters (except flame height) is tracked independently for each element. At each time step, a new height for the pyrolysis front is calculated based on these variables.
Pyrolysis algorithm	This is based on the mass loss rate from the Cone Calorimeter data at an arbitrary irradiance level. This data is scaled in time based on the irradiance level to the surface versus irradiance levels used in the cone. A mass loss rate at every burning node can then be calculated based on the incident flux to the material, and the time after ignition of that node.
Heat flux from burner and wall flames to the wall/ceiling surfaces	Convective flux is calculated depending on which region is under consideration: • In the pyrolyzing zone • Beyond the pyrolyzing zone Radiative flux is calculated from the following sources in the indicated regions: • From the burner-below peak flux level (approximately 1/3 of the flame height) • From the burner-above peak flux level • From the burning walls-low within the pyrolysis zone • From the burning walls-high within the pyrolysis zone • From the burning walls-above the pyrolysis zone • Above flame height (a total radiative flux that decays exponentially with height) An additional flux is added to upper and lower walls from ceiling burning, using appropriate configuration factors. A room feedback flux to the upper and lower walls is also applied.
Lateral (opposed) spread	This is in the same form used by Quintiere[31] and Karlsson[19]. However, different spread rates are accounted for on the upper and lower layer walls by using different surface temperatures for these walls.

Table 2-3 – Overview of modules in Mitler's algorithm (cont'd)

Regression, burn-through	Cumulative mass loss calculated at each node. Burn-through is achieved at an element when the mass available at that element has been completely pyrolyzed.

2.3 Selection of the Algorithm

The next step in the algorithm selection process was to rank them in multiple categories from most desirable to least desirable. For this purpose, three of the previously described modules and three other general algorithm characteristics were selected as the categories for comparison. The modules chosen for this part of the analysis are the most important of the five used in the above study because they are most likely to strongly affect simulation performance. The modules selected were:

1) Upward spread mechanism
2) Pyrolysis algorithm
3) Heat flux from burner and wall flames to the wall/ceiling surfaces

In the following discussion Mitler, Quintiere, and Karlsson refer to [23,24], [31], and [19], respectively.

Upward Spread

Mitler's algorithm was clearly the best in this category. Flame height, radiative flux, convective flux, total mass loss rate, and wall temperatures are coupled and converged to a solution for the pyrolysis front position at each time step. The entire wall is also discretized into elemental strips, so that ignition can occur at only one strip, or over a range of strips. Quintiere's algorithm follows, in that ignition occurs over the portion of the wall behind the ignition burner flame, and then spreads upward and across then ceiling from there using the SQW[28] equation. Karlsson's algorithm is last in this category because the entire wall (floor to ceiling) behind the ignition burner is assumed to ignite at once, and concurrent spread occurs only along the wall/ceiling interface and over the ceiling.

Pyrolysis Algorithm

Mitler is the best choice in this category because the pyrolysis rate is tracked independently at each ignited element based on a total incident flux at that element. Quintiere follows closely because it also adjusts the mass loss rate based on net flux. However, this is done over a broad area instead of being a function of height. Karlsson does not adjust the mass loss rate according to net flux, therefore it is the least favorable in this category.

Heat Flux from Burner and Wall Flames to the Wall/ceiling Surfaces

Mitler is the best in this category because it considers a heat flux that varies with height, and calculates the convective and radiative components of this flux separately. Karlsson and Quintiere are less desirable, since they assume a constant flux over the entire pyrolysis region and a separate constant flux over the pre-heating area. Karlsson is

slightly better than Quintiere in this category because the lower wall is discretized into strips. Using these strips, the flux can be calculated as a function of height in order to supplement the downward spread module.

Three general algorithm characteristics were also chosen for comparison, although they were not considered as important as the above modules because they are qualitative in nature. These characteristics were:

1) How well is the ceiling spread simulated?
2) How well is the corner configuration simulated?
3) What is the level of difficulty in implementing the algorithm into CFAST[26,27]?

Ceiling Spread Simulation

In this category, Quintiere is the best, as the geometry of spread on the corner ceiling is intuitively reasonable (radial progression from the corner) and wall/ceiling interface spread is also well defined. Karlsson follows in that it considers wall/ceiling interface spread in a manner similar to Quintiere. However, spread on the ceiling does not have a defined shape, only an area. It is more difficult to compare Mitler for this category because it was developed for the sidewall configuration, however it was considered to be the least desirable of the algorithms in this category. The ceiling is made from a "high" wall that is "folded down" at the ceiling height to make a ceiling. Flame spread over the ceiling continues in the same manner as the wall, except that an area is subtracted for the spread of "arm extensions" along the wall/ceiling interface. These "arms" are not well defined by the algorithm, and the width of the area of flame spread on the ceiling was not clearly defined in the algorithm's original development.

Corner Configuration Simulation

Based on the above considerations, Quintiere seemed to be the best simulation of the corner configuration based on a defined geometry and flux calculation, followed by Karlsson. Mitler does not simulate the corner configuration, so it ranks last. However, the structure of the model allows it to be modified for this configuration.

Implementation Difficulty

This category is more qualitative than the others, however Quintiere would be the easiest to implement based on the fact that a version of this algorithm already exists within the CFAST[26,27] structure. Karlsson and Mitler follow, where Karlsson would be slightly easier because the algorithm itself is not as complex as Mitler's.

Table 2-4 – Summary of algorithm comparison

	Mitler[23,24]	Quintiere[31]	Karlsson[19]
Upward wall spread	1	2	3
Pyrolysis Algorithm	1	2	3
Heat Flux to	1	2	3

Surface			
Ceiling Spread Simulation	3	1	2
Corner Configuration Simulation	3	1	2
Implementation Difficulty	3	1	2

Note: 1 is most desirable, 3 is least desirable

As can be seen from Table 2-4, Mitler's algorithm has a clear advantage in terms of how well it deals with the relevant physics of the problem. It would also be the most difficult to implement. It suffered in the other two categories, mainly because it is currently designed for the sidewall configuration. Adapting this algorithm to the corner configuration would resolve the ceiling spread issue by constraining the geometry of the flame spread on the ceiling.

Quintiere's algorithm has the clear advantage as a compartment corner algorithm in its present form. The physics of the algorithm are respectable, but do not approach the detail contained in Mitler's algorithm. Implementation of Quintiere's algorithm would be the easiest, as a simple form of it is already present in the CFAST[26,27] source code.

As this comparison shows, Karlsson's algorithm is the least desirable out of the three. It has the least detailed physics and does not simulate the corner as well as Quintiere's algorithm. Because of these factors, Karlsson's algorithm was taken out of consideration at this point.

Mitler's algorithm was chosen over Quintiere's algorithm for this project. This was done for three reasons. The first reason is that the physics in Mitler's algorithm are very detailed and were thought to simulate the fire spread more accurately once the algorithm had been developed for the corner configuration. Next, this algorithm is based on compartment fire conditions. This characteristic allows simulation of the ISO 9705[16] room corner configuration, after modification for the corner scenario. Finally, an undergraduate project team was already in the process of implementing Quintiere's algorithm into CFAST[26,27] as a part of their senior project[2]. Working on the development of two flame spread models was thought to be more beneficial, as they could both be compared to experimental results to determine their accuracy.

3.0 Algorithm Development

Although the flame spread algorithm developed by Mitler[23,24] is clearly the best choice in terms of the detail of physical phenomena included, the original algorithm was designed to simulate a flame spread in a compartment side-wall configuration. The algorithm had to be enhanced for a corner scenario, in order to satisfy the objectives of this project. In particular, simulation of ISO 9705[16] was desirable because it is the test procedure used to qualify materials as "Fire Restricting Materials"[12].

Several aspects of the algorithm required modification in order to suit the corner configuration. These were as follows:

- The geometry of the flame spread over the ceiling,
- The burner flame height correlation used for the corner configuration,
- Radiation due to the corner geometry,
- The incident flux from the corner burner, and
- The altered mass loss rate expressions to compliment the geometry.

3.1 Geometric Considerations

The original form of Mitler's[23,24] algorithm was intended to simulate the spread of flame on a vertical wall surface and ceiling in a compartment. In the original model, it was assumed that the ignition burner was somewhere near the center of a wall (away from compartment corners), although the height at which the ignition source could be placed was arbitrary. The modeled ignition source was a line burner placed flush against the wall. Once started, the algorithm would simulate the heating and ignition of the wall lining material, and subsequent movement of the pyrolysis front up the wall. Once the pyrolysis front reached the ceiling, it split into two "arm extensions" along the wall/ceiling interface and a ceiling pyrolysis zone. Lateral flame spread was also calculated once the temperature of the extended walls in the upper and lower layers of the room reached a critical temperature. The entire burnable area was divided into thin, horizontal elements, where parameters (surface temperature, total incident flux, mass loss rate, etc.) were independently tracked. Figure 3-1 shows the geometry of the original algorithm. Note that the value for H shown in the figure would represent the distance between the top of the burner and the ceiling (a "virtual ceiling height"), for the case where the top of the burner is located above floor level.

The change in geometry of flame spread on the walls themselves is easily dealt with when developing the algorithm for the corner situation. This area of spread is simply "folded" into the corner along the centerline shown in Figure 3-1. The change in geometry of flame spread across the ceiling is more difficult to define. In its original form, Mitler's[23,24] algorithm has only one geometric constraint on the spread of flame across the ceiling, the single ceiling/wall interface. With only one constraint, the geometry of flame spread across the ceiling is hard to determine particularly when considering its width (*2** [(W_u*/2) –delta*] as illustrated in Figure 3-1). There is much discussion by Mitler[24] about determining this width, although no firm conclusions were drawn. Altering Mitler's algorithm for the corner configuration creates a more bounded

geometry, as the two corner walls constrain the flame spread across the ceiling. Defining the shape of flame spread across the ceiling is necessary for the proper calculation of the pyrolysis and burnout fronts and the enhanced radiation effect. Three potential geometric spread patterns were identified for the movement of the flame and pyrolysis fronts over the ceiling; these being square, triangular, and quarter-circular.

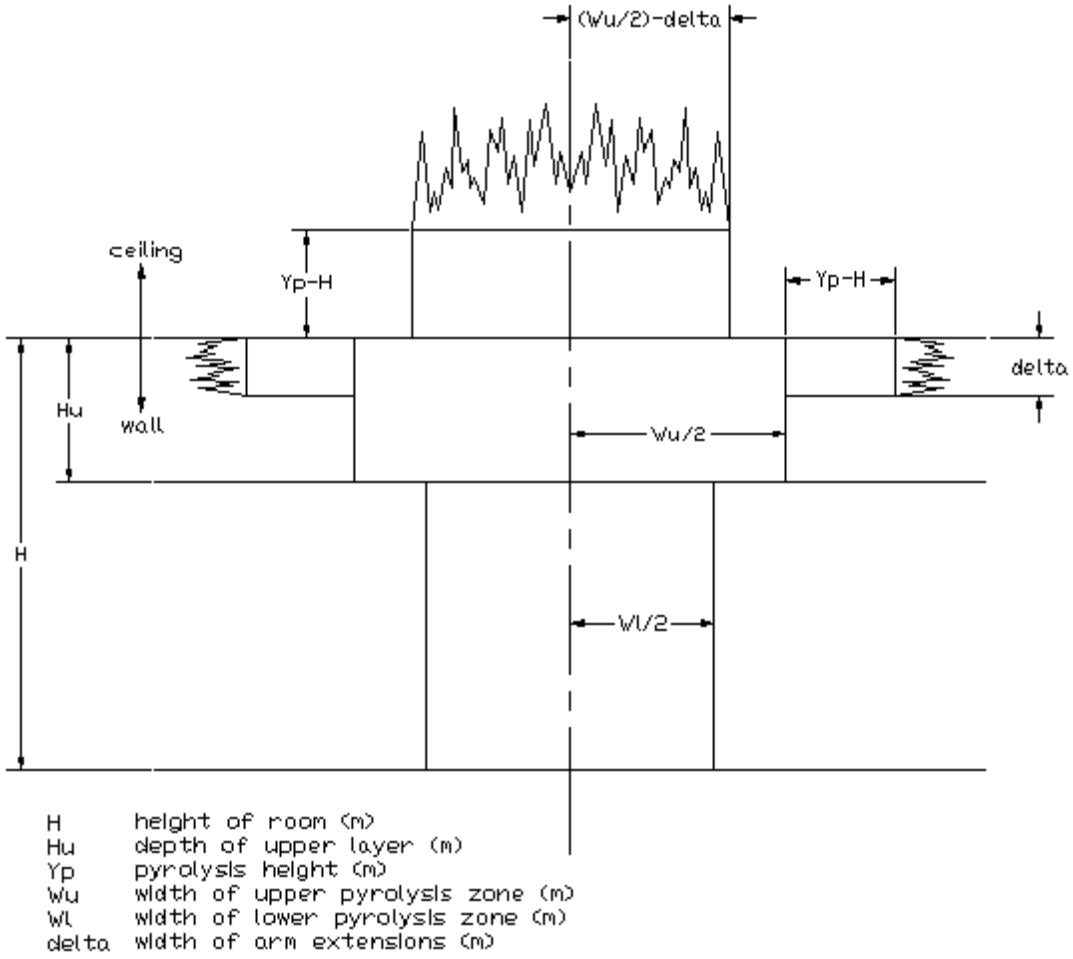

Figure 3-1 – The geometry of flame spread in the original algorithm[23,24]

3.1.1 Square Geometry

The square geometry of flame spread across the ceiling is shown in Figure 3-2. As can be seen from the figure this pattern is derived simply by "folding" the existing ceiling spread into the corner, much like folding the lid of a cardboard box. The movement of the pyrolysis front across the ceiling would then proceed in the same manner as the original algorithm. The "folding" results in an overlap region in the flame and pyrolysis fronts that must be removed in order to make the geometry physically correct. The overlapped pyrolysis area could be simply subtracted, however, the overlapping of the extended flames is particularly difficult to handle because the flames

are representative of both an area *and* a flow of gas. Figure 3-3 shows a more detailed plan view of the flame spread on the ceiling for this geometry. Because of the gas flow, there may also be an extended flame area to the sides of the pyrolysis zones as indicated in the figure. Because there is uncertainty in dealing with these overlapping regions, this geometry of spread was not selected for use in the room-corner version of Mitler's[23,24] algorithm.

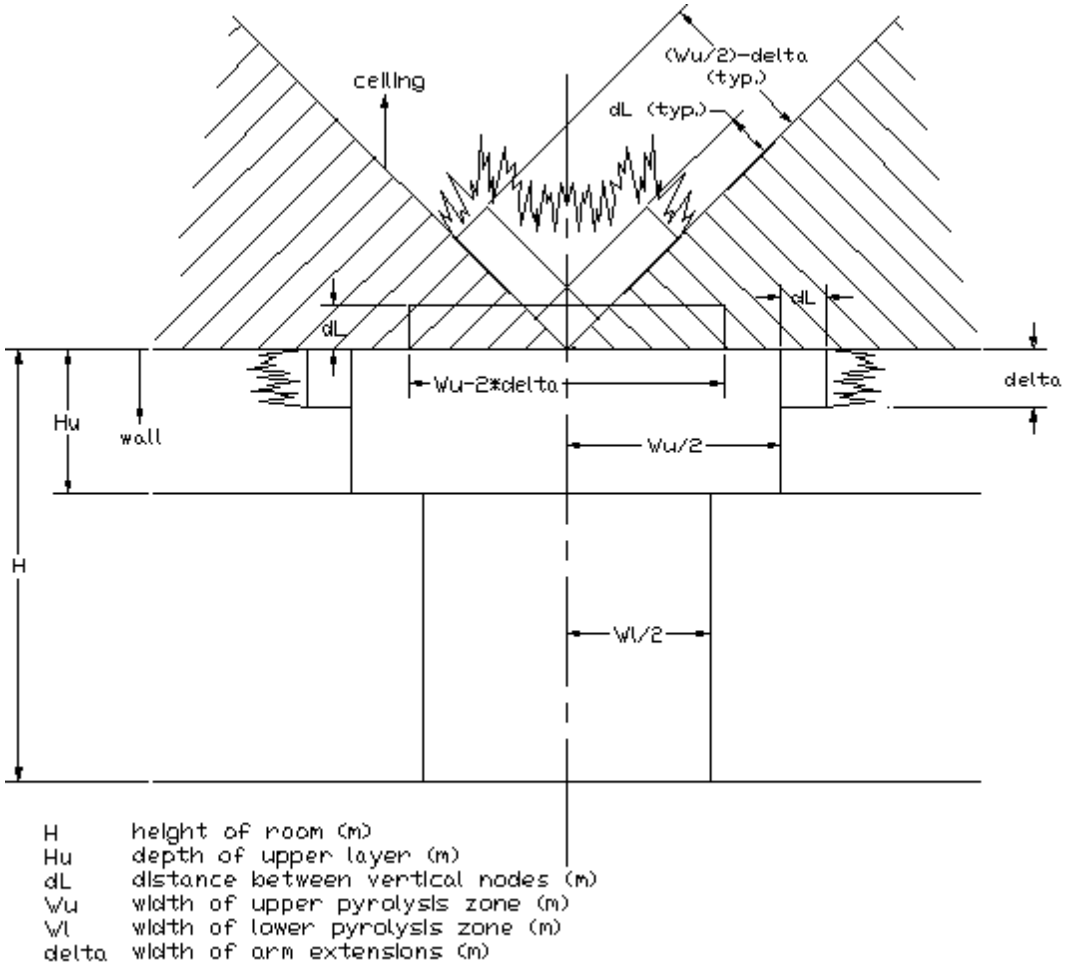

Figure 3-2 – Square geometry for ceiling flame spread (the "folding")

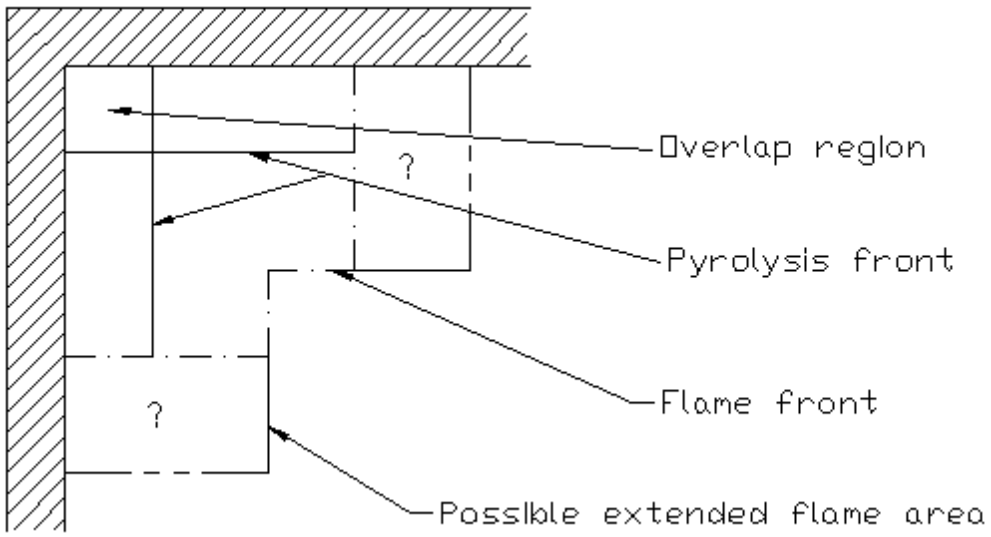

Figure 3-3 – Plan view of the square geometry of flame spread on the ceiling

3.1.2 Triangular Geometry

The triangular ceiling spread pattern is shown in Figure 3-4. The basic idea of this geometry is that the spread across the ceiling in the corner proceeds in the shape of an isosceles triangle, with the equal (shorter) sides being flush with the corner walls. Figure 3-5 shows a detailed plan view of this ceiling spread geometry. An initial pyrolysis zone must be defined once the pyrolysis front reaches the ceiling. This is accomplished by one of two methods. The first is to use a triangular area equivalent to the area of the first ceiling element that would be ignited using the original sidewall geometry. The second would be to use an equivalent length based on the width of the first ignited ceiling element in the original algorithm. The hypotenuse of the triangle ("D" in Figure 3-5) could be set equal to the entire original width, one of the shorter sides of the triangle ("B" in Figure 3-5) could be set equal to one-half of the original element width, or another similar construction could be implemented. The manner in which further spread occurs is also important. The growth could be based on increasing the length of the side of the ceiling pyrolysis triangle along the wall/ceiling interface ("B" in Figure 3-5). Alternatively, the growth could occur by increasing the "height" of the triangle along the centerline shown in Figure 3-4. Each of these methods would produce a different rate of pyrolysis area spread because the widths of the elements would be different. The growth along the "height" would produce the largest triangles and therefore the greatest heat release rate and fire growth.

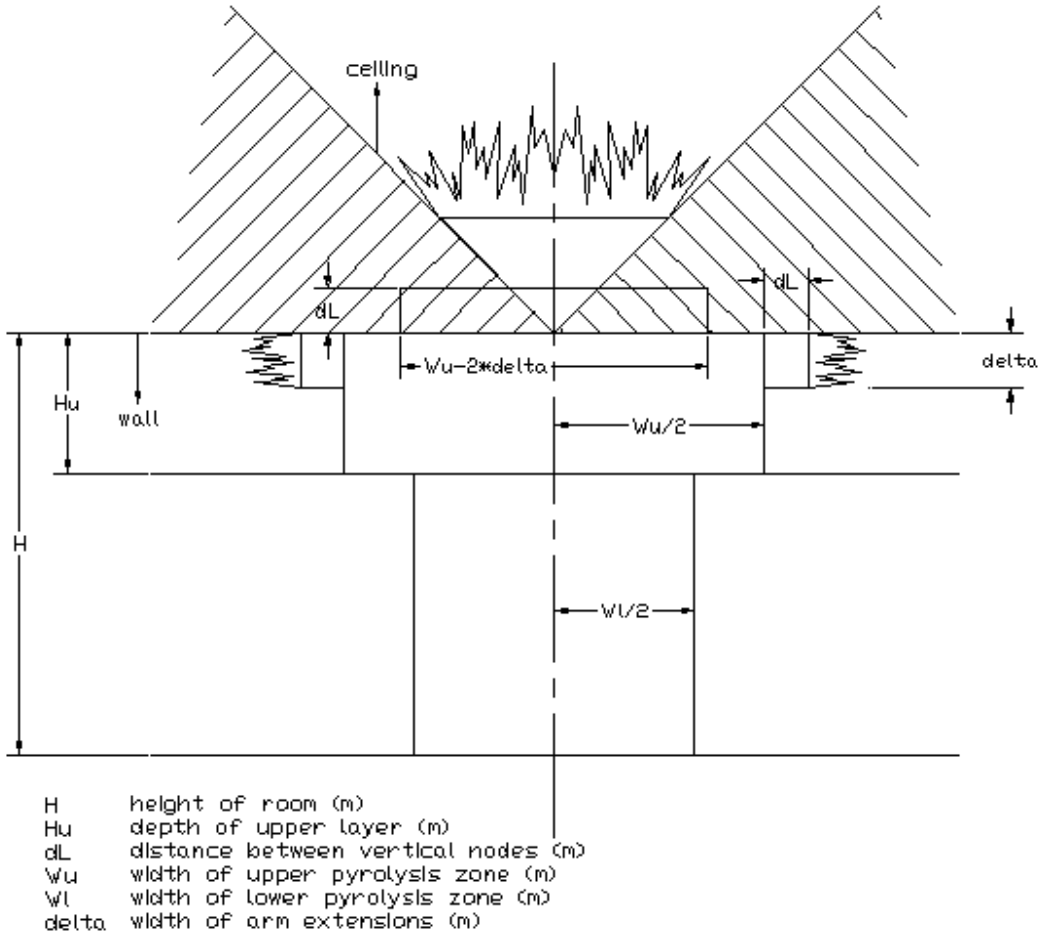

Figure 3-4 – Triangular geometry for ceiling flame spread

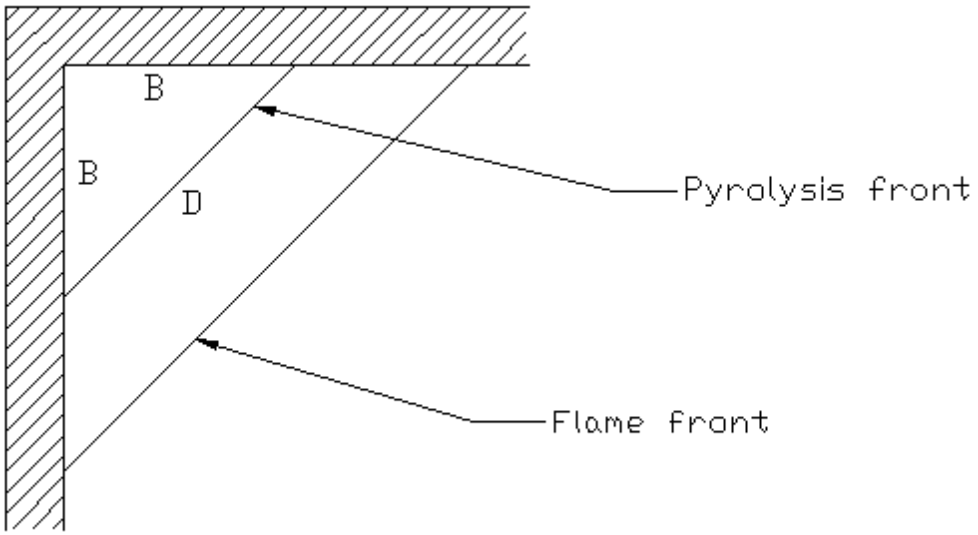

Figure 3-5 – Plan view of the triangular flame spread geometry on the ceiling

3.1.3 Quarter-circular Geometry

The quarter-circular flame spread geometry is shown in Figure 3-6. In this geometry, the pyrolysis front spreads out radially from the corner. As with the triangular geometry, the initial pyrolysis area must be defined. One choice would be to use an equivalent area in a manner similar to that described for the triangular geometry. The other options would be to use an equivalent length from the original algorithm and apply it to either an arc length (full width of the original element), the radius (half-width of the original element), or a similar construction. Growth of the pyrolysis area is simplified as radial progression is constant for all angles, unlike the triangle as described above. Figure 3-7 shows a plan view of the quarter-circular flame spread geometry on the ceiling.

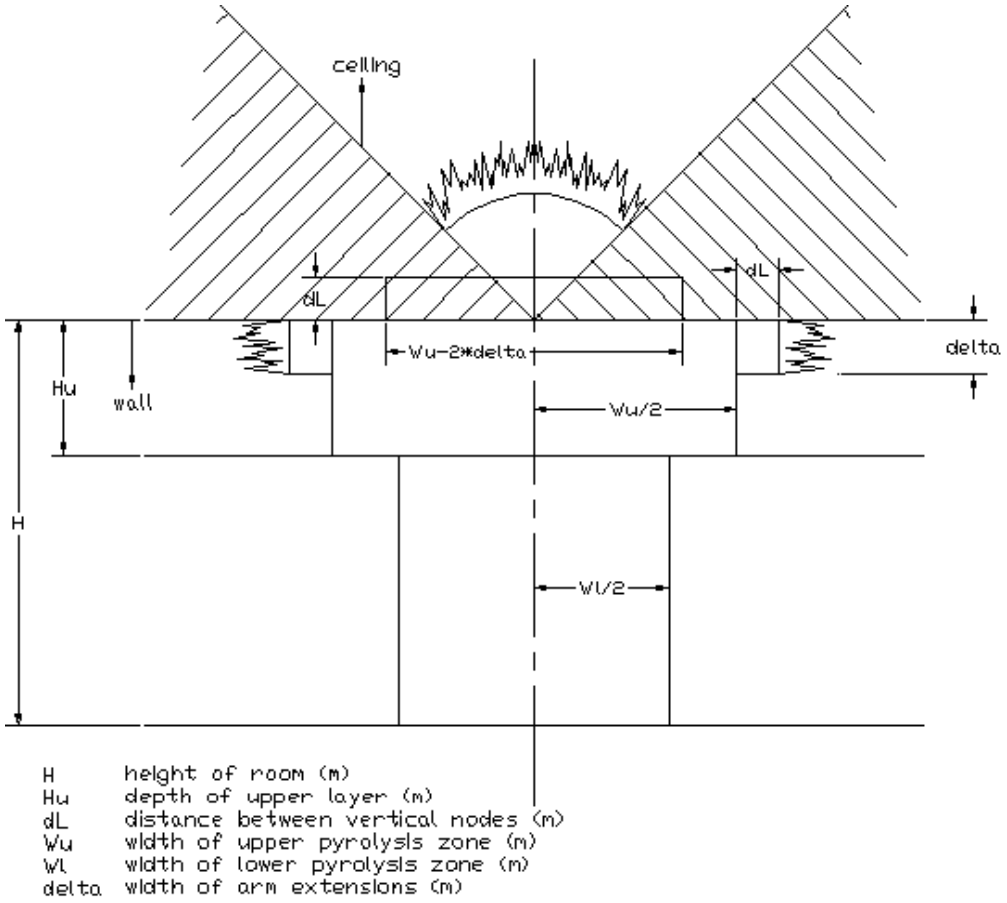

Figure 3-6 – Quarter-circular geometry for ceiling flame spread

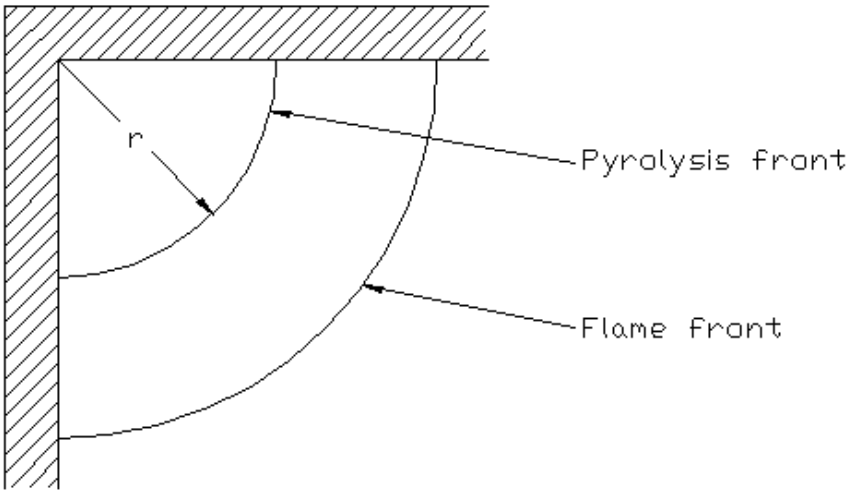

Figure 3-7 – Plan view of the quarter-circular geometry of flame spread on the ceiling

The quarter-circular geometry was chosen for the new algorithm. This was done for several reasons:

- The geometry of spread is intuitively realistic,
- The radiation calculations are slightly easier with the circular geometry versus the triangular geometry (i.e. simpler derivation of view factors),
- The pyrolysis area spread rate is not dependent on where the "line of growth" is placed, as in the triangular geometry, and
- The use of this geometry allows direct comparison between the new algorithm, and that of Quintiere[31].

3.2 Corner Flame Height Correlation

In addition to geometric changes, the height of flames in the compartment corner are different from those against the center of a compartment wall[8]. Thus, a change in the calculation of flame height was necessary. Originally, separate correlations for line and square burners for both sidewall *and* corner positions were proposed for the algorithm. However, little information was available in the literature describing the behavior of line burners in a compartment corner or square burners against the center of a compartment wall. Therefore, the algorithm was restricted to a line burner for the compartment sidewall case, and a square burner for the compartment corner case.
In order to derive a suitable corner flame height from a square burner, several correlations were compared using the non-dimensional terms $\dot{Q}_D^*$ (for square burners) [8] or $\dot{Q}_l^*$ (for line burners)[8] and Z_f / D:

$$\dot{Q}_D^* = \frac{\dot{Q}}{\rho_o c_p T_o g^{1/2} D^{5/2}} \tag{3-1}$$

or

$$\dot{Q}_l^* = \frac{\dot{Q}_l}{\rho_o c_p T_o g^{1/2} D^{3/2}} \tag{3-2}$$

Note that the variable D represents length of the side for the square burners or the width of the slot for the line burners in these correlations.

The main difference between these two equations is that the heat release rate $\dot{Q}_l$ is specified per unit width (kW/m) for the line burner correlation. At ambient conditions, the term $\rho_o c_p T_o g^{1/2}$ can be approximated as 1110 (kW/m$^{5/2}$) [21]. The line burner correlations were included for reference purposes in the process of developing a suitable correlation.

Three correlations for square burners in the corner were identified during this exercise. The first was developed by Hasemi and Tokunaga[11] for square burners in an

open corner configuration. The correlation is intended to describe heat output levels circa 100kW. The expression is:

$$\frac{Z_f}{D} = 3.65\dot{Q}_D^{*\,2/3} \tag{3-3}$$

The next correlation (identified by Dillon[7]) was developed by Kokkala based on a visible flame boundary temperature of between 400 and 500°C. His experiments were carried out over a wide range of burner sizes (0.17m to 0.5m) and heat outputs (40kW to 300kW) in an open corner configuration. The developed expressions are:

$$\begin{aligned} \frac{Z_f}{D} &= -1.73 + 4.96\dot{Q}_D^{*\,2/3} \quad for \quad \dot{Q}_D^* < 8.6 \\ \frac{Z_f}{D} &= 15.6 + 0.4\dot{Q}_D^* \quad for \quad \dot{Q}_D^* > 8.6 \end{aligned} \tag{3-4}$$

The last correlation for a square burner flame height in a compartment corner (also identified by Dillon[7]) was originally developed by Heskestad and revised by Kokkala. The original equation was for a pool fire. The modified expression is as follows:

$$\frac{Z_f}{D} = -2.04 + 6.62\dot{Q}_D^{*\,2/5} \tag{3-5}$$

The following three expressions for line burners against a wall are used for reference. The original equation from each reference has been converted to non-dimensional form in the following sets of equations.

Mitler's[23] correlation:

Original equation: $$Z_f = 0.14\left(\dot{Q}_l\right)^{1/2} \tag{3-6}$$

Non-dimensional form: $$\frac{Z_f}{D} = 4.64\left(\dot{Q}_l^*\right)^{1/2} D^{-1/4} \tag{3-7}$$

Kulkarni's[20] correlation:

Original equation: $$Z_f = 0.0433\left(\dot{Q}_l\right)^{2/3} \tag{3-8}$$

Non-dimensional form: $$\frac{Z_f}{D} = 4.614\left(\dot{Q}_l^*\right)^{2/3} \tag{3-9}$$

Beyler's[**6**] correlation:

Original equation: $$Z_f = 0.052\left(\dot{Q}_l\right)^{2/3} \tag{3-10}$$

Non-dimensional form: $$\frac{Z_f}{D} = 5.54\left(\dot{Q}_l^*\right)^{2/3} \tag{3-11}$$

A summary of the various correlations used in the comparison is shown in Table 3-1.

Table 3-1 – Summary of flame height correlations used for comparison

Author	Correlation	Type
Mitler[23]	$\frac{Z_f}{D} = 4.64\left(\dot{Q}_l^*\right)^{1/2} D^{-1/4}$	Side-wall (line)
Kulkarni[20]	$\frac{Z_f}{D} = 4.614\left(\dot{Q}_l^*\right)^{2/3}$	Side-all (line)
Beyler[6]	$\frac{Z_f}{D} = 5.54\left(\dot{Q}_l^*\right)^{2/3}$	Side-wall (line)
Hasemi and Tokunaga[21]	$\frac{Z_f}{D} = 3.65\dot{Q}_D^{*2/3}$	Corner (square)
Kokkala (from Dillon[7])	$\frac{Z_f}{D} = -1.73 + 4.96\dot{Q}_D^{*2/3} \quad for \quad \dot{Q}_D^{*2/3} < 8.6$ $\frac{Z_f}{D} = 15.6 + 0.4\dot{Q}_D^* \quad for \quad \dot{Q}_D^{*2/3} > 8.6$	Corner (square)
Heskestad (from Dillon[7])	$\frac{Z_f}{D} = -2.04 + 6.62\dot{Q}_D^{*2/5}$	Corner (square)

Values were obtained from each correlation for Z_f/D versus $\dot{Q}^*$. Figure 3-8 shows each correlation separately. The graph illustrates that both the wall correlations and the corner correlations group together. Because of the grouping behavior, the sets of values from each type were averaged to get an average curve for the corner (square) and wall (line) correlations as shown in Figure 3-9. A good first order approximation of flame height from a square burner in a compartment corner would be to use a curve fit to the average corner correlation curve. Figure 3-9 shows the curve fit to the square correlation average, which has the following equation:

$$\frac{Z_f}{D} = -1.7 + 5.8\left(\dot{Q}_D^*\right)^{1/2} \tag{3-12}$$

This is the expression that replaced Mitler's original flame height correlation when simulating the corner configuration. The height of the pyrolysis zone (Z_p) is also taken into account when the algorithm calculates flame height. Thus, equation (3-12) was used to solve for Z_{fo} in the following flame height equation used in the flame-spread algorithm:

$$Z_f = \left(Z_{fo}^4 + Z_p^4\right)^{1/4} \tag{3-13}$$

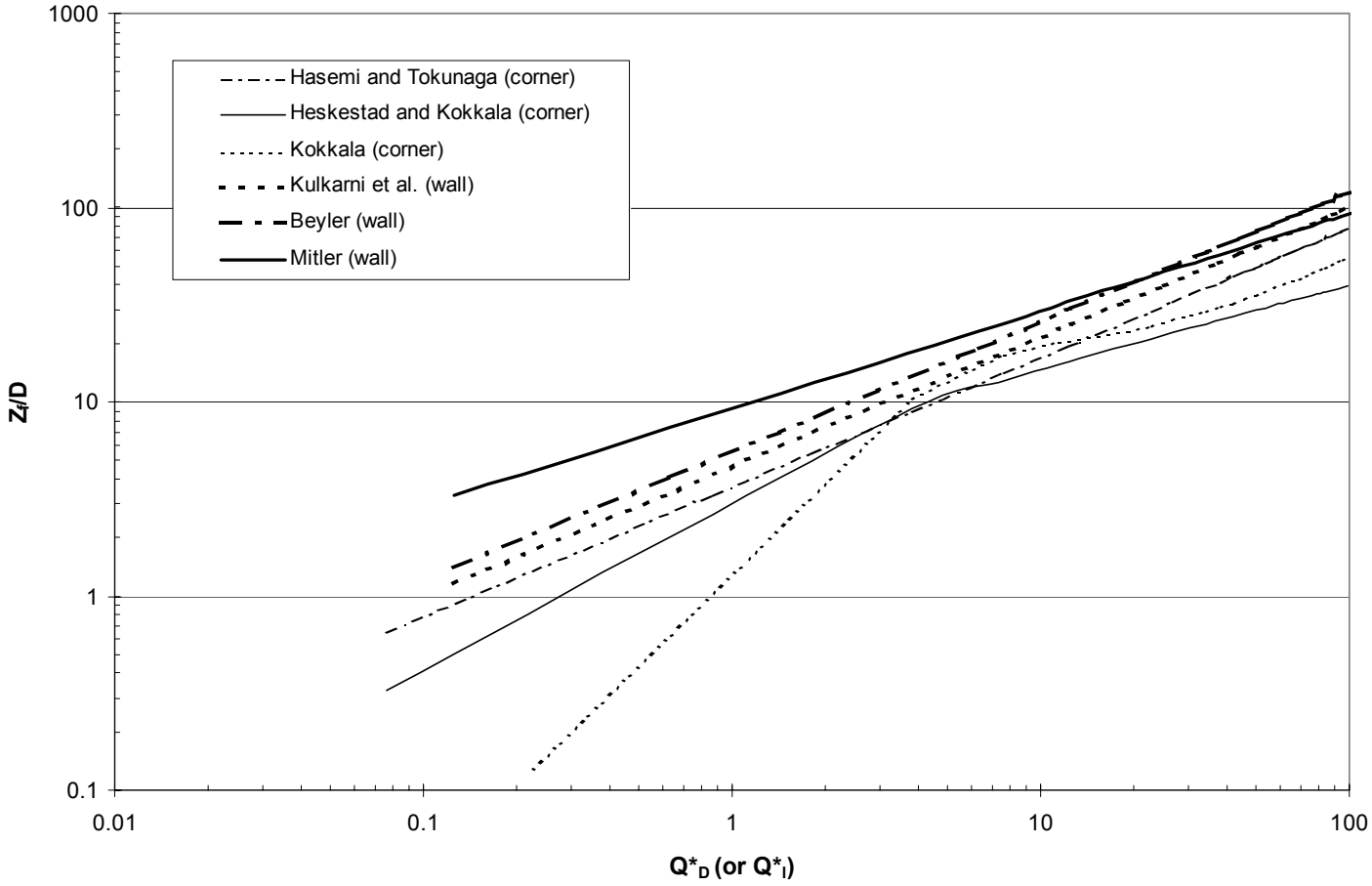

NOTE: The values for the wall correlations use Q^*_I and and the corner correlations use Q^*_D

Figure 3-8 – Comparison of various flame height correlations

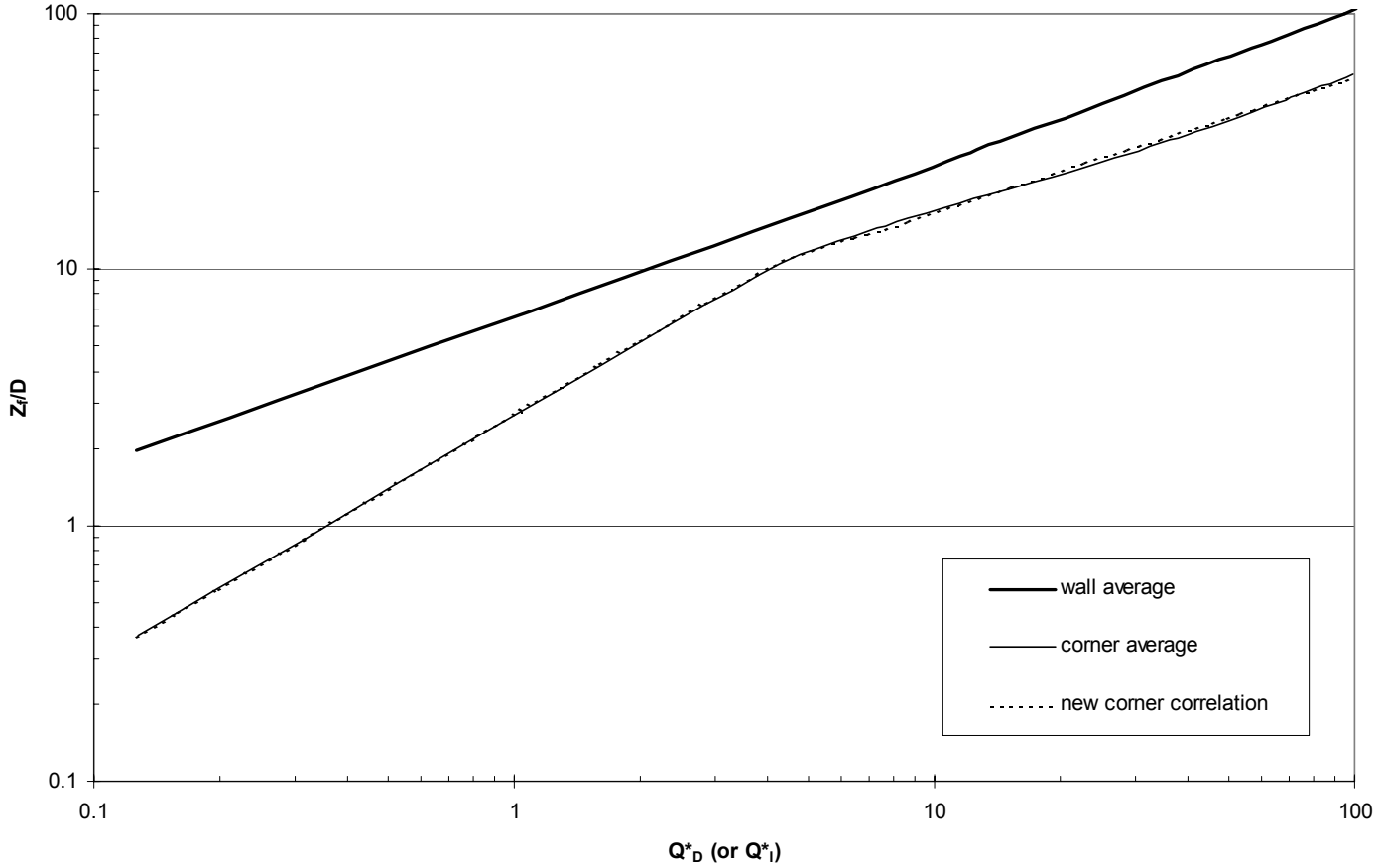

NOTE: The values for the wall correlations use Q*l and the corner correlations use Q*D

Figure 3-9 – Comparison of correlation averages with a curve fit to the corner average

3.3 Enhanced Corner Radiation

The radiation incident on the wall and ceiling elements of the algorithm is enhanced in the corner configuration. In the sidewall configuration, the wall elements do not view each other because they are in the same plane. In the corner configuration the walls are perpendicular, allowing them to "see" each other, thus enhancing the total incident flux at each element in addition to radiative feedback from ceiling elements and a hot gas layer. The total incident flux at each element is important because it influences the mass loss rate for that element if it is pyrolyzing, and determines the degree of preheating in the case of a non-pyrolyzing element. In the original sidewall algorithm the radiative fluxes included were as follows:

1) Radiation from the line burner flame to the wall
2) Radiation from the burning wall material flame to the wall
3) Uniform flux to the upper part of the wall, based on radiation from the flames on the ceiling and/or other sources such as a hot gas layer
4) Uniform flux to the lower part of the wall, based on radiation from the flames on the ceiling and/or other sources such as a hot gas layer
5) Flux to the flame arm extensions along the ceiling/wall interface from the flames on the ceiling

In addition to these fluxes, the corner configuration requires the calculation of the radiation exchange between the hot corner walls and ceiling, because the corner geometry allows radiation from one wall to reach the other wall and the ceiling. A more detailed flux distribution is also desirable, as opposed to the uniform fluxes used in the sidewall algorithm. In order to accomplish these tasks, a subroutine was written that generates a general radiation network for the corner configuration. The network accounts for radiative exchange between the walls, ceiling, and a hot gas layer. The calculated radiative flux from the burner and wall flames is added as an external flux. Also included is a factor to attenuate radiation as it passes through a flame when going between elements. This routine is based on assumptions that both the walls and the upper layer gas are gray bodies with uniform properties. The approach taken to solve this problem was to break up the geometry of the corner into five separate zones and the upper gas layer. As shown in Figure 3-10, the five zones are:

1) The upper zone, wall 1 (horizontal, rectangular elements in the upper gas layer),
2) the lower zone, wall 1 (horizontal, rectangular elements below the upper gas layer),
3) the lower zone, wall 2 (horizontal, rectangular elements below the upper gas layer),
4) the upper zone, wall 2 (horizontal, rectangular elements in the upper gas layer), and
5) the ceiling (broken into quarter-circular elements).

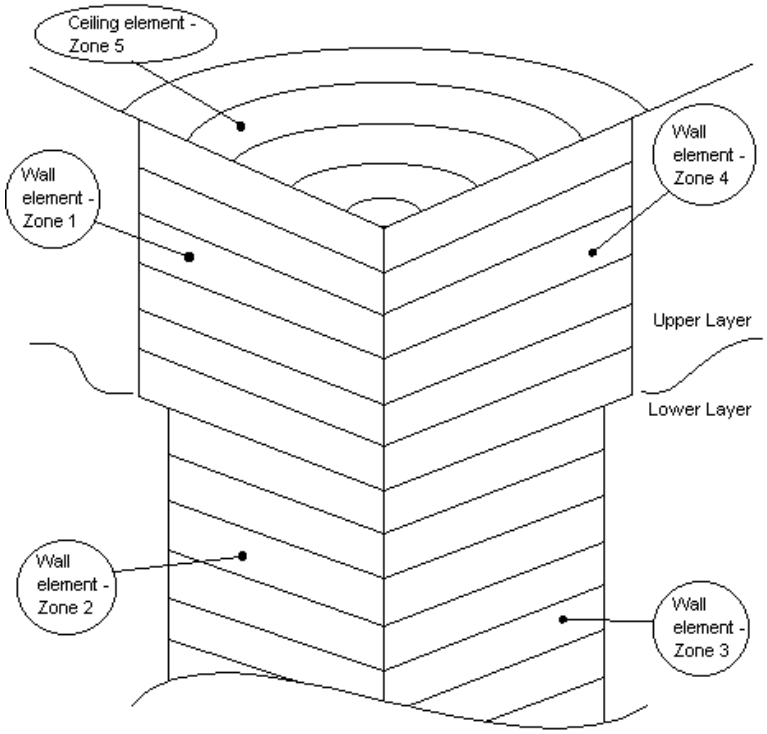

Figure 3-10 – Geometry of the elements used in the radiation network

Each time the radiation network is used by the flame spread algorithm, the input variables to the network are taken from the algorithm and CFAST at the current time-step. The input variables taken from the flame spread algorithm are temperature and external flux distribution over the walls and ceiling, material emissivity, room dimensions, gas layer interface height, width of the lower pyrolysis zones, width of the upper pyrolysis zones, and the radius of the ceiling zone. The upper gas layer is defined by properties provided by CFAST. Currently, the gas layer properties are soot mass concentration, soot emission coefficient, temperature, partial pressure of carbon dioxide, and partial pressure of water vapor. The width of each element is set to approximately 0.12m (10 elements per zone for a 2.4m wall height). During initial development and testing of this routine, this element size was found to provide adequate resolution while allowing acceptable execution times (see Figures 3-11 and 3-12). Note that this radiation network was written specifically for the new flame spread algorithm. This means that the same geometric limitations apply (i.e. roughly a standard sized compartment is valid).

Two general options also exist within the routine. First, the inclusion of the gas layer can be toggled on or off. Secondly, an option to calculate accurate beam lengths for the gas layer calculations is included. The intention of this option was to calculate the exact length of gas that radiation must pass through between any two arbitrary elements, instead of using a global mean beam length. This method produced some difficulties and uncertain results during initial testing, so it was not pursued further. It is recommended that the user not select this option at this time. The main output of this subroutine is the incident radiant flux distribution to the elements in the corner configuration.

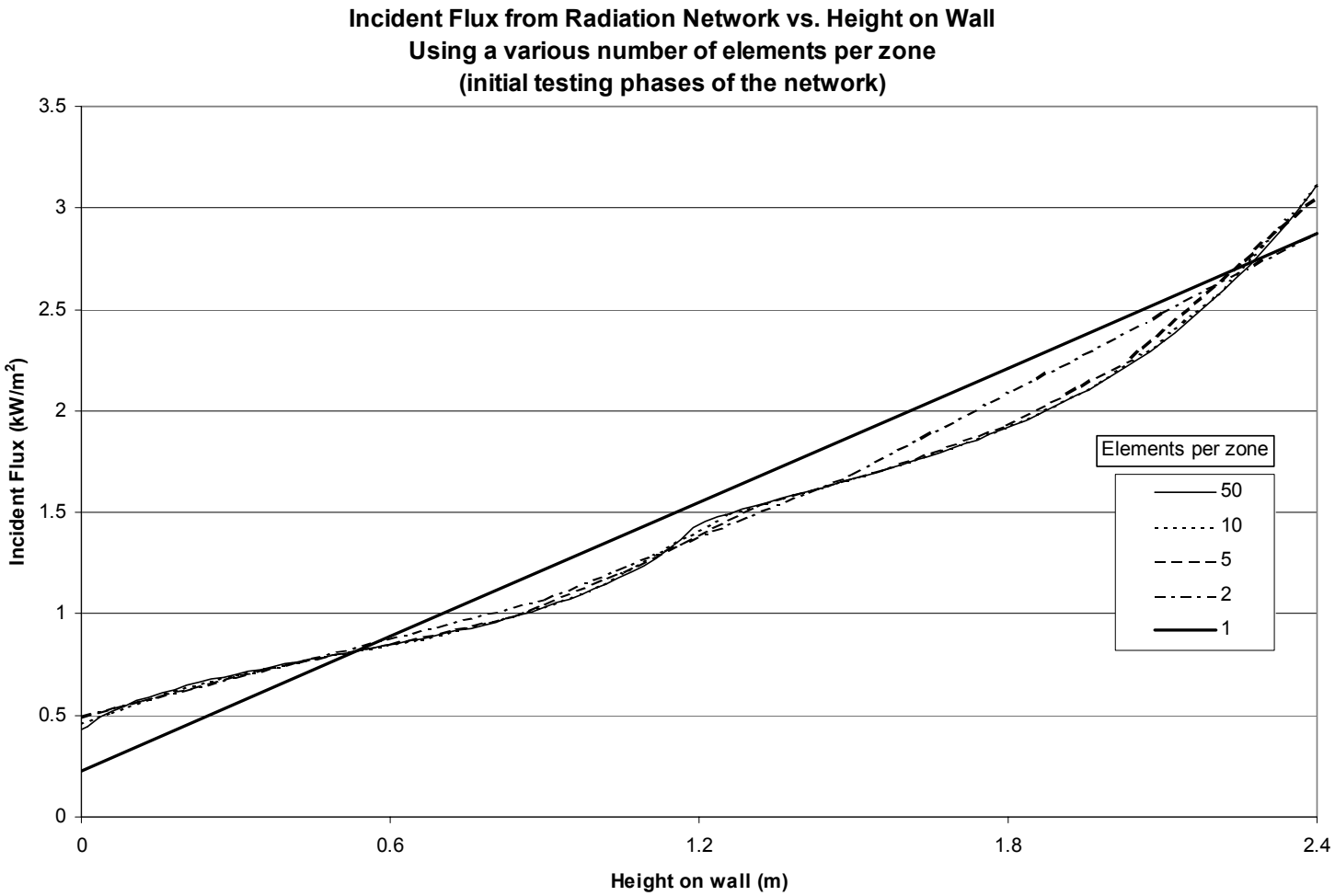

Figure 3-11 – Radiation network output resolution versus number of elements used per zone

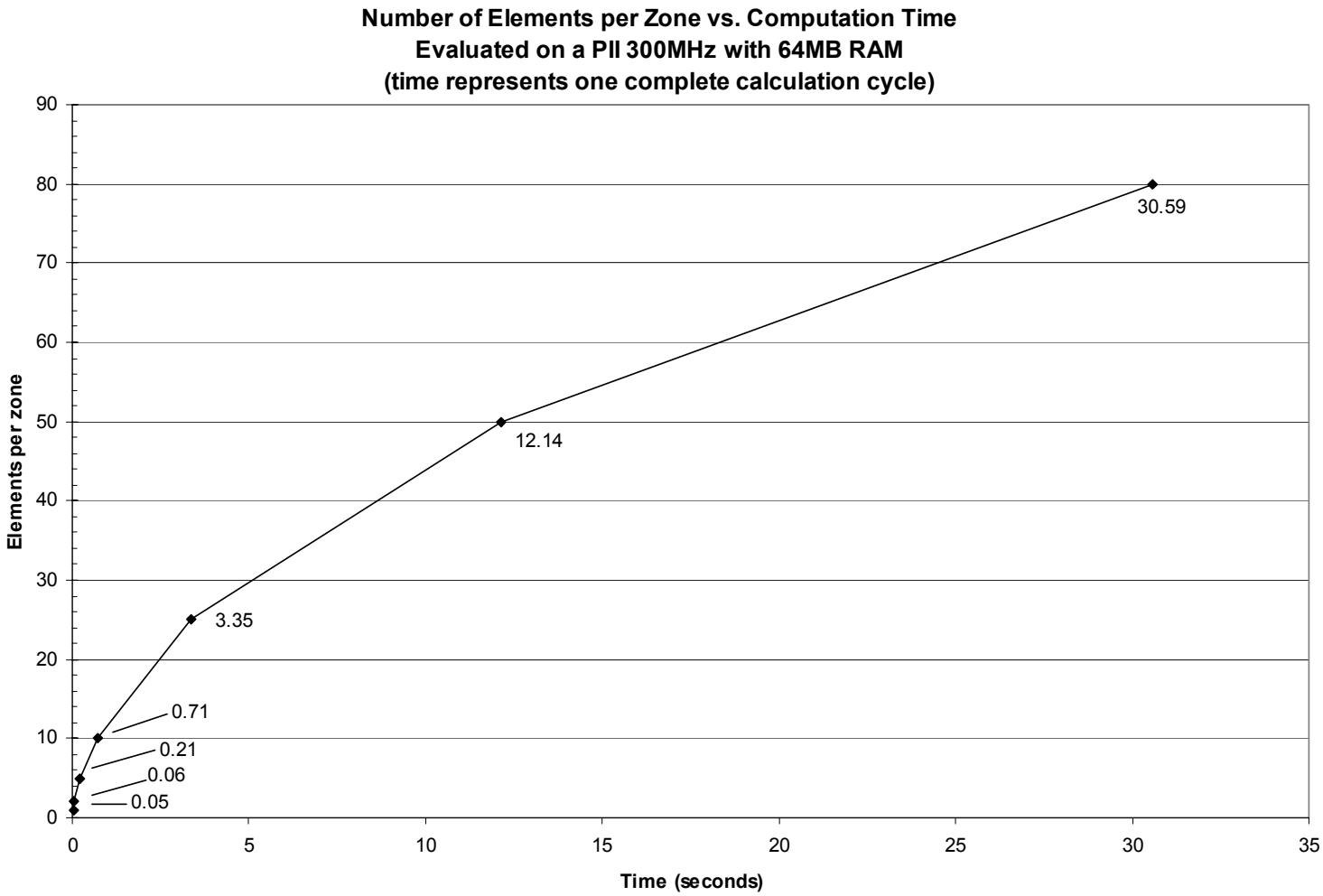

Figure 3-12 – Required solution time for various numbers of elements per zone

The following sections will describe the derivation of the radiation network equations, configuration factors, and the upper gas layer emissivity calculation. Details about the actual structure and subroutines for the network radiation exchange program are in Appendices D and E.

3.3.1 Derivation of Radiation Network Equations

The basics of this derivation are similar to those found in Siegel and Howell[29] (Chapters 7 and 13), however two new variables have been added to the formula. One is an external flux representing radiative flux from the burner and wall flames to the wall, and the other is radiation attenuation by the flame as it passes from one wall element to another. The attenuation is only considered for elements actually behind a flame. Currently, the radiation network does not distinguish between the ignition burner flame and flames from the burning walls/ceiling. This factor is simply applied when an element is within the calculated flame height. A general equation for a radiation network that is solvable via matrix inversion is the desired result in this derivation. The base equation for this derivation is:

$$Q_k = q_k A_k = \left(q_{o,k} - q_{i,k}\right) A_k \tag{3-14}$$

Q_k represents the energy flux supplied to the surface element k by some means other than radiation, which is necessary to hold the temperature of the element steady. The subscripts i and o represent incoming and outgoing radiative flux, respectively. The variable $q_{o,k}$ is defined by the following:

$$q_{o,k} = \varepsilon_k \sigma T_k^4 + \rho_k q_{i,k} \tag{3-15}$$

Assuming that the reflectivity (ρ_k) is equal to $(1-\varepsilon_k)$, and solving for $q_{i,k}$ gives:

$$q_{i,k} = \frac{q_{o,k} - \varepsilon_k \sigma T_k^4}{1-\varepsilon_k} \tag{3.16}$$

The flame transmissivity factor to account for attenuation of the incoming radiation as it passes through a flame is applied by simple multiplication as follows:

$$q_{i,k} = \tau_{fl,k} \frac{q_{o,k} - \varepsilon_k \sigma T_k^4}{1-\varepsilon_k} \tag{3.17}$$

Adding the new term for external flux (R_k) results in the following equation:

$$q_{i,k} = \tau_{fl,k} \frac{q_{o,k} - \varepsilon_k \sigma T_k^4}{\left(1-\varepsilon_k\right)} + R_k \tag{3-18}$$

Substituting (3-18) into (3-14) and solving for q_k creates the following expression:

$$\frac{Q_k}{A_k} = q_k = \frac{\varepsilon_k}{\left(1-\varepsilon_k\right)} \left[\tau_{fl,k} \sigma T_k^4 - \tau_{fl,k} q_{o,k} - R_k \frac{\left(1-\varepsilon_k\right)}{\varepsilon_k} \right. \tag{3-19}$$

Another way to solve for the incoming flux is:

$$q_{i,k} = \sum_{j=1}^{N} F_{k-j} q_{o,j} \tag{3.20}$$

where F_{k-j} is the configuration factor between elements k and j. Applying the flame transmissivity factor and external flux as before yields:

$$q_{i,k} = \tau_{fl,k} \sum_{j=1}^{N} F_{k-j} q_{o,j} + R_k \tag{3-21}$$

Substituting (3-21) into (3-14) and solving for q_k creates a second equation similar to (3-19):

$$\frac{Q_k}{A_k} = q_k = q_{o,k} - \tau_{fl,k} \sum_{j=1}^{N} F_{k-j} q_{o,j} + R_k \tag{3-22}$$

Equations (3-19) and (3-22) are used to obtain the general solution for the radiation network. In order to clarify this procedure for obtaining the general expression, an example for three gray surfaces in an enclosure is shown here. The addition of a gray absorbing medium (the upper gas layer), an external flux (radiation from flames), and attenuation of radiation (between wall elements by flame) are all included. First, equations (3-19) and (3-22) are written for each surface:

$$q_1 = \frac{\varepsilon_1}{(1-\varepsilon_1)} \left[\tau_{fl,1} \sigma T_1^4 - \tau_{fl,1} q_{o,1} - R_1 \frac{(1-\varepsilon_1)}{\varepsilon_1} \right. \tag{3-23}$$

$$q_2 = \frac{\varepsilon_2}{(1-\varepsilon_2)} \left[\tau_{fl,2} \sigma T_2^4 - \tau_{fl,2} q_{o,2} - R_2 \frac{(1-\varepsilon_2)}{\varepsilon_2} \right. \tag{3-24}$$

$$q_3 = \frac{\varepsilon_3}{(1-\varepsilon_3)} \left[\tau_{fl,3} \sigma T_3^4 - \tau_{fl,3} q_{o,3} - R_3 \frac{(1-\varepsilon_3)}{\varepsilon_3} \right. \tag{3-25}$$

$$q_1 = q_{o,1} - \tau_{fl,1} F_{1-1} q_{o,1} - \tau_{fl,1} F_{1-2} q_{o,2} - \tau_{fl,1} F_{1-3} q_{o,3} + R_1 \tag{3-26}$$

$$q_2 = q_{o,2} - \tau_{fl,2} F_{2-1} q_{o,1} - \tau_{fl,2} F_{2-2} q_{o,2} - \tau_{fl,2} F_{2-3} q_{o,3} + R_2 \tag{3-27}$$

$$q_3 = q_{o,3} - \tau_{fl,3} F_{3-1} q_{o,1} - \tau_{fl,3} F_{3-2} q_{o,2} - \tau_{fl,3} F_{3-3} q_{o,3} + R_3 \tag{3-28}$$

Solving (3-23), (3-24), and (3-25) for $q_{o,1}$, $q_{o,2}$, and $q_{o,3}$ respectively, and combining these results with (3-26), (3-27), and (3-28) yields:

$$\begin{aligned} q_1 = \frac{1}{\tau_{fl,1}} \Bigg[& \tau_{fl,1} \sigma T_1^4 - q_1 \frac{(1-\varepsilon_1)}{\varepsilon_1} - R_1 \frac{(1-\varepsilon_1)}{\varepsilon_1} \\ & - \frac{\tau_{fl,1}}{\tau_{fl,1}} F_{1-1} \left[\tau_{fl,1} \sigma T_1^4 - q_1 \frac{(1-\varepsilon_1)}{\varepsilon_1} - R_1 \frac{(1-\varepsilon_1)}{\varepsilon_1} \right] \\ & - \frac{\tau_{fl,1}}{\tau_{fl,2}} F_{1-2} \left[\tau_{fl,2} \sigma T_2^4 - q_2 \frac{(1-\varepsilon_2)}{\varepsilon_2} - R_2 \frac{(1-\varepsilon_2)}{\varepsilon_2} \right] \\ & - \frac{\tau_{fl,1}}{\tau_{fl,3}} F_{1-3} \left[\tau_{fl,3} \sigma T_3^4 - q_3 \frac{(1-\varepsilon_3)}{\varepsilon_3} - R_3 \frac{(1-\varepsilon_3)}{\varepsilon_3} \right] + R_1 \end{aligned} \tag{3-29}$$

$$
\begin{aligned}
q_2 = \frac{1}{\tau_{fl,2}}\Bigg[& \tau_{fl,2}\sigma T_2^4 - q_2\frac{(1-\varepsilon_2)}{\varepsilon_2} - R_2\frac{(1-\varepsilon_2)}{\varepsilon_2}\Bigg] \\
& - \frac{\tau_{fl,2}}{\tau_{fl,1}}F_{2-1}\Bigg[\tau_{fl,1}\sigma T_1^4 - q_1\frac{(1-\varepsilon_1)}{\varepsilon_1} - R_1\frac{(1-\varepsilon_1)}{\varepsilon_1}\Bigg] \\
& - \frac{\tau_{fl,2}}{\tau_{fl,2}}F_{2-2}\Bigg[\tau_{fl,2}\sigma T_2^4 - q_2\frac{(1-\varepsilon_2)}{\varepsilon_2} - R_2\frac{(1-\varepsilon_2)}{\varepsilon_2}\Bigg] \\
& - \frac{\tau_{fl,2}}{\tau_{fl,3}}F_{2-3}\Bigg[\tau_{fl,3}\sigma T_3^4 - q_3\frac{(1-\varepsilon_3)}{\varepsilon_3} - R_3\frac{(1-\varepsilon_3)}{\varepsilon_3}\Bigg] + R_2
\end{aligned}
\tag{3-30}
$$

$$
\begin{aligned}
q_3 = \frac{1}{\tau_{fl,3}}\Bigg[& \tau_{fl,3}\sigma T_3^4 - q_3\frac{(1-\varepsilon_3)}{\varepsilon_3} - R_3\frac{(1-\varepsilon_3)}{\varepsilon_3} \\
& - \frac{\tau_{fl,3}}{\tau_{fl,1}}F_{3-1}\Bigg[\tau_{fl,1}\sigma T_1^4 - q_1\frac{(1-\varepsilon_1)}{\varepsilon_1} - R_1\frac{(1-\varepsilon_1)}{\varepsilon_1}\Bigg] \\
& - \frac{\tau_{fl,3}}{\tau_{fl,2}}F_{3-2}\Bigg[\tau_{fl,2}\sigma T_2^4 - q_2\frac{(1-\varepsilon_2)}{\varepsilon_2} - R_2\frac{(1-\varepsilon_2)}{\varepsilon_2}\Bigg] \\
& - \frac{\tau_{fl,3}}{\tau_{fl,3}}F_{3-3}\Bigg[\tau_{fl,3}\sigma T_3^4 - q_3\frac{(1-\varepsilon_3)}{\varepsilon_3} - R_3\frac{(1-\varepsilon_3)}{\varepsilon_3}\Bigg] + R_3
\end{aligned}
\tag{3-31}
$$

Rearranging these equations so that *q's* are on the left hand side gives:

$$
\begin{aligned}
& q_1\Bigg(1 + \frac{(1-\varepsilon_1)}{\varepsilon_1\tau_{fl,1}} - F_{1-1}\frac{\tau_{fl,1}}{\tau_{fl,1}}\frac{(1-\varepsilon_1)}{\varepsilon_1}\Bigg) - q_2\Bigg(F_{1-2}\frac{\tau_{fl,1}}{\tau_{fl,2}}\frac{(1-\varepsilon_2)}{\varepsilon_2}\Bigg) - q_3\Bigg(F_{1-3}\frac{\tau_{fl,1}}{\tau_{fl,3}}\frac{(1-\varepsilon_3)}{\varepsilon_3}\Bigg) \\
& = (1-F_{1-1})\tau_{fl,1}\sigma T_1^4 - F_{1-2}\tau_{fl,1}\sigma T_2^4 - F_{1-3}\tau_{fl,1}\sigma T_3^4 + \frac{\tau_{fl,1}}{\tau_{fl,1}}F_{1-1}R_1\frac{(1-\varepsilon_1)}{\varepsilon_1} \\
& \quad + \frac{\tau_{fl,1}}{\tau_{fl,2}}F_{1-2}R_2\frac{(1-\varepsilon_2)}{\varepsilon_2} + \frac{\tau_{fl,1}}{\tau_{fl,3}}F_{1-3}R_3\frac{(1-\varepsilon_3)}{\varepsilon_3} - R_1\frac{(1-\varepsilon_1)}{\varepsilon_1\tau_{fl,1}} + R_1
\end{aligned}
\tag{3-32}
$$

$$
\begin{aligned}
& -q_1\Bigg(F_{2-1}\frac{\tau_{fl,2}}{\tau_{fl,1}}\frac{(1-\varepsilon_1)}{\varepsilon_1}\Bigg) + q_2\Bigg(1 + \frac{(1-\varepsilon_2)}{\varepsilon_2\tau_{fl,2}} - F_{2-2}\frac{\tau_{fl,2}}{\tau_{fl,2}}\frac{(1-\varepsilon_2)}{\varepsilon_2}\Bigg) - q_3\Bigg(F_{2-3}\frac{\tau_{fl,2}}{\tau_{fl,3}}\frac{(1-\varepsilon_3)}{\varepsilon_3}\Bigg) \\
& = -F_{2-1}\tau_{fl,2}\sigma T_1^4 + (1-F_{2-2})\tau_{fl,2}\sigma T_2^4 - F_{2-3}\tau_{fl,2}\sigma T_3^4 + \frac{\tau_{fl,2}}{\tau_{fl,1}}F_{2-1}R_1\frac{(1-\varepsilon_1)}{\varepsilon_1} \\
& \quad + \frac{\tau_{fl,2}}{\tau_{fl,2}}F_{2-2}R_2\frac{(1-\varepsilon_2)}{\varepsilon_2} + \frac{\tau_{fl,2}}{\tau_{fl,3}}F_{2-3}R_3\frac{(1-\varepsilon_3)}{\varepsilon_3} - R_2\frac{(1-\varepsilon_2)}{\varepsilon_2\tau_{fl,2}} + R_2
\end{aligned}
\tag{3-33}
$$

$$-q_1\left(F_{3-1}\frac{\tau_{fl,3}}{\tau_{fl,1}}\frac{(1-\varepsilon_1)}{\varepsilon_1}\right.-q_2\left(F_{3-2}\frac{\tau_{fl,3}}{\tau_{fl,2}}\frac{(1-\varepsilon_2)}{\varepsilon_2}\right.+q_3\left(1+\frac{(1-\varepsilon_3)}{\varepsilon_3\tau_{fl,3}}-F_{3-3}\frac{\tau_{fl,3}}{\tau_{fl,3}}\frac{(1-\varepsilon_3)}{\varepsilon_3}\right.$$

$$=-F_{3-1}\tau_{fl,3}\sigma T_1^4-F_{3-2}\tau_{fl,3}\sigma T_2^4+(1-F_{3-3})\tau_{fl,3}\sigma T_3^4+\frac{\tau_{fl,3}}{\tau_{fl,1}}F_{3-1}R_1\frac{(1-\varepsilon_1)}{\varepsilon_1} \tag{3-34}$$

$$+\frac{\tau_{fl,3}}{\tau_{fl,2}}F_{3-2}R_2\frac{(1-\varepsilon_2)}{\varepsilon_2}+\frac{\tau_{fl,3}}{\tau_{fl,3}}F_{3-3}R_3\frac{(1-\varepsilon_3)}{\varepsilon_3}-R_3\frac{(1-\varepsilon_3)}{\varepsilon_3\tau_{fl,3}}+R_3$$

Equations (3-32), (3-33), and (3-34) can be written in the following compact form:

$$\sum_{j=1}^{N}\left[\delta_{kj}\left(1+\frac{(1-\varepsilon_j)}{\varepsilon_j\tau_{fl,j}}\right)-F_{k-j}\frac{\tau_{fl,k}}{\tau_{fl,j}}\frac{(1-\varepsilon_j)}{\varepsilon_j}\right]q_j$$

$$=\sum_{j=1}^{N}(\delta_{kj}-F_{k-j})\tau_{fl,k}\sigma T_j^4+\frac{\tau_{fl,k}}{\tau_{fl,j}}F_{k-j}R_j\frac{(1-\varepsilon_j)}{\varepsilon_j}-\delta_{kj}R_k\left(\frac{(1-\varepsilon_k)}{\varepsilon_k\tau_{fl,k}}+1\right) \tag{3-35}$$

Since this equation is in the same form as equation 7-31 from Siegel and Howell[29], the same derivation applied in Chapter 13 of Siegel and Howell for the addition of an absorbing gray medium applies. The final form of the radiation network equation is then:

$$\sum_{j=1}^{N}\left[\delta_{kj}\left(1+\frac{(1-\varepsilon_j)}{\varepsilon_j\tau_{fl,j}}\right)-F_{k-j}\frac{\tau_{fl,k}}{\tau_{fl,j}}\frac{(1-\varepsilon_j)}{\varepsilon_j}\overline{\tau}_{k-j}\right]q_j$$

$$=\sum_{j=1}^{N}(\delta_{kj}-F_{k-j}\overline{\tau}_{k-j})\tau_{fl,k}\sigma T_j^4+\frac{\tau_{fl,k}}{\tau_{fl,j}}F_{k-j}R_j\frac{(1-\varepsilon_j)}{\varepsilon_j}-\delta_{kj}R_k\left(\frac{(1-\varepsilon_k)}{\varepsilon_k\tau_{fl,k}}+1\right) \tag{3-36}$$

$$-F_{k-j}\overline{\alpha}_{k-j}\sigma T_{gas}^4$$

The terms $\overline{\alpha}_{k-j}$, $\overline{\tau}_{k-j}$, and T_{gas} represent the absorptivity, transmissivity, and temperature of the upper gas layer, respectively. This equation is then written for each element *k* for *k* equal 1 to N, to arrive at N equations that must be solved simultaneously. The method chosen to solve these equations was matrix inversion. Each equation can be written in a simpler form as:

$$\sum_{j=1}^{N}a_{kj}q_j=C_k \tag{3-37}$$

In this equation,

$$a_{kj}=\delta_{kj}\left(1+\frac{(1-\varepsilon_j)}{\varepsilon_j\tau_{fl,j}}\right.-F_{k-j}\frac{\tau_{fl,k}}{\tau_{fl,j}}\frac{(1-\varepsilon_j)}{\varepsilon_j}\overline{\tau}_{k-j} \tag{3-38}$$

and

$$C_k = \sum_{j=1}^{N} \left(\delta_{kj} - F_{k-j}\overline{\tau}_{k-j} \right) \tau_{fl,k} \sigma T_j^4 + \frac{\tau_{fl,k}}{\tau_{fl,j}} F_{k-j} R_j \frac{\left(1-\varepsilon_j\right)}{\varepsilon_j} - \delta_{kj} R_k \left(\frac{\left(1-\varepsilon_k\right)}{\varepsilon_k \tau_{fl,k}} + 1 \right. \\ \left. - F_{k-j}\overline{\alpha}_{k-j} \sigma T_{gas}^4 \right) \tag{3-39}$$

For N elements, the set of equations takes on the form:

$$\begin{array}{ccccccccccc} a_{11}q_1 & + & a_{12}q_2 & + & \cdots & + & a_{13}q_3 & + & \cdots & + & a_{1N}q_N = C_1 \\ a_{21}q_1 & + & a_{22}q_2 & + & \cdots & + & a_{23}q_3 & + & \cdots & + & a_{2N}q_N = C_2 \\ \vdots & & \vdots & & & & \vdots & & & & \vdots \quad \vdots \\ a_{k1}q_1 & + & a_{k2}q_2 & + & \cdots & + & a_{k3}q_3 & + & \cdots & + & a_{kN}q_N = C_k \\ \vdots & & \vdots & & & & \vdots & & & & \vdots \quad \vdots \\ a_{N}q_1 & + & a_{N2}q_2 & + & \cdots & + & a_{N3}q_3 & + & \cdots & + & a_{NN}q_N = C_N \end{array} \tag{3-40}$$

Matrices $[a]$, $[q]$, and $[C]$ can then be defined as:

$$[a] = \begin{bmatrix} a_{11} & a_{12} & \cdots & a_{1j} & \cdots & a_{1N} \\ a_{21} & a_{22} & \cdots & a_{2j} & \cdots & a_{2N} \\ \vdots & \vdots & & \vdots & & \vdots \\ a_{k1} & a_{k2} & \cdots & a_{kj} & \cdots & a_{kN} \\ \vdots & \vdots & & \vdots & & \vdots \\ a_{N1} & a_{N2} & \cdots & a_{Nj} & \cdots & a_{NN} \end{bmatrix} \quad [q] = \begin{bmatrix} q_1 \\ q_2 \\ \vdots \\ q_k \\ \vdots \\ q_N \end{bmatrix} \quad [C] = \begin{bmatrix} C_1 \\ C_2 \\ \vdots \\ C_k \\ \vdots \\ C_N \end{bmatrix} \tag{3-41}$$

By the above definitions,

$$[a][q]=[C], \quad [q]=[a]^{-1}[C] \tag{3-42}$$

Using matrix inversion (LU decomposition and back-substitution were selected in this case) the values of q_k can be obtained from equation (3-42). The incident radiative flux $(q_{i,k})$ on each element k must be found using the values of q_k. First, equation (3-18) is solved for $q_{o,k}$:

$$q_{o,k} = \left(q_{i,k} - R_k \right) \left[\frac{\left(1-\varepsilon_k\right)}{\tau_{fl,k}} + \varepsilon_k \sigma T_k^4 \right. \tag{3-43}$$

Equation (3-43) is then substituted into equation (3-14), and solved for $q_{i,k}$:

$$q_{i,k} = \left[q_k + R_k \frac{\left(1-\varepsilon_k\right)}{\tau_{fl,k}} - \varepsilon_k \sigma T_k^4 \right] \left(\frac{\tau_{fl,k}}{1-\varepsilon_k-\tau_{fl,k}} \right) \tag{3-44}$$

The flux distribution resulting from this equation is used in the flame-spread algorithm.

3.3.2 Configuration Factors used in the Radiation Network

The next step was to determine the various configuration factors between the elements. Configuration factor algebra and reciprocity relations were used to derive the various configuration factors between each of the elements. Two basic configuration factors were used. The first configuration factor is found in most standard radiation texts[29, 22], and describes two finite area rectangles that are contiguous along one edge, and are perpendicular to each other (see Figure 3-13).

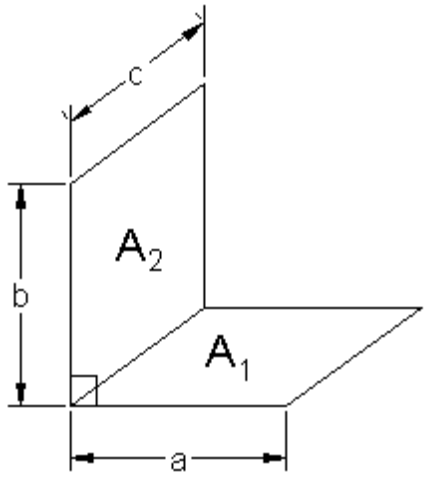

$$V = \frac{b}{c}$$

$$U = \frac{a}{c}$$

Figure 3-13 – Configuration factor for perpendicular rectangular areas

The equation for the this view factor is:

$$F_{1-2} = \frac{1}{\pi U}\left(\begin{array}{l} U\tan^{-1}\frac{1}{U} + V\tan^{-1}\frac{1}{V} - \sqrt{V^2+U^2}\,\tan^{-1}\frac{1}{\sqrt{V^2+U^2}} \\ +\frac{1}{4}\ln\left\{ \frac{\left(1+U^2\right)\left(1+V^2\right)}{1+U^2+V^2}\left[\frac{U^2\left(1+U^2+V^2\right)}{\left(1+U^2\right)\left(U^2+V^2\right)}\right]^{U^2}\left[\frac{V^2\left(1+V^2+U^2\right)}{\left(1+V^2\right)\left(V^2+U^2\right)}\right]^{V^2} \right| \end{array} \right) \tag{3-45}$$

Configuration factor algebra was used in two cases for wall element to wall element exchange between zones 1 and 3, or 2 and 4 (Figure 3-10):

1) Wall elements touch only on one corner (lowest element in zone 1 to highest element in zone 3 (analogously from zone 4 to zone 2))
2) Wall elements are separated (all other elements in zone 1 to all other elements in zone 3 (analogously from zone 4 to zone 2))

The second basic factor is for a differential element to a finite area quarter circle. The differential element is in a plane that is perpendicular and contiguous to one of the straight edges of the quarter-circular area (see Figure 3-14). This configuration factor was

derived because it was not found in the literature. The details of this derivation will not be presented here, but are available in Appendix A. The equation for this configuration factor is:

$$F_{d1-2} = \frac{1}{4\pi L}\left[\begin{array}{l} \ln\left(H^2 + r^2 + L^2 + 2rL\right)H - 2\tan^{-1}\left(\frac{-r+L}{H}\right)L \\ \quad - \ln\left(H^2 + r^2 + L^2\right)H + 2\tan^{-1}\left(\frac{L}{H}\right)L \end{array}\right] \tag{3-46}$$

In order to obtain the configuration factor for a quarter-circular *strip* to a wall element, configuration factor algebra must again be used, although in this case simple subtraction is sufficient. The exchange between an entire wall element and a ceiling element must be done using an average, since the basic configuration factor is for a differential area (wall) to a finite area (ceiling).

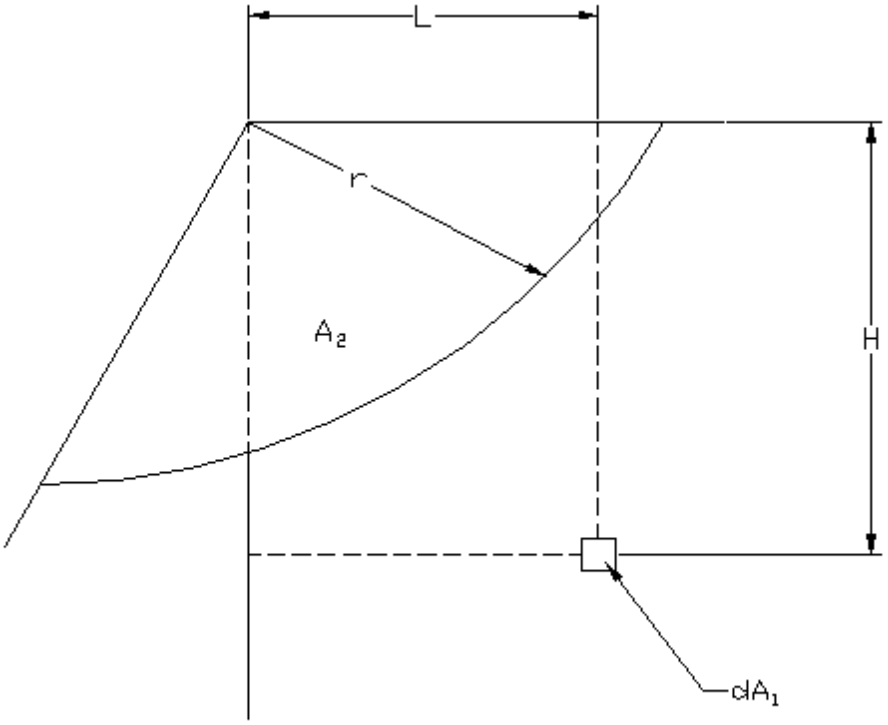

Figure 3-14 – Configuration factor for a differential element to a quarter circle

A grid of points is generated for the wall element under consideration and the configuration factor at each of these points to the ceiling element is calculated. The average of all of these values is used as the configuration factor from the entire wall element to the ceiling element. Currently, the grid on the wall element is set at 60 (length) by 4 (width). During initial testing, these values provided numerical stability, while allowing for relatively quick calculations.

3.3.3 Upper Gas Layer Emissivity Calculations

The final step in determining the exchange between the walls/ceiling and the hot gas layer is to calculate the absorptivity of the hot gas layer for use in equation (3-36). For this part of the calculations, the assumption is made that the absorptivity is equal to the emissivity and the transmissivity is equal to one minus the absorptivity. The equation used to calculate the emissivity of the hot gas layer is from the Tien, et al.[35]:

$$\varepsilon_t = \left(1 - e^{-\kappa_s S}\right) + \varepsilon_g e^{-\kappa_s S} \tag{3-47}$$

By default, the value for S is set to the mean beam length of the gas layer. The emissivity of the gas layer without the soot is calculated in the usual way, using the partial pressures of H_2O and CO_2, mean beam length, and the Hottel[35] charts. A subroutine was borrowed directly from the source code of the WPI/Fire model[33] for this purpose. The value for κ_s (soot emission coefficient) is calculated as:

$$\kappa_s = 1000 \rho_o K C_s \tag{3-48}$$

The terms ρ_o, K, and C_s are the ambient air density, a derived constant equal to 0.47 L/mg-m[32], and the soot mass concentration in the upper layer, respectively. The factor of 1000 is needed to convert the density from kg/m^3 to mg/L.

3.4 Experimental Corner Heat Flux Map

The next step in the development process was to alter the heat flux from the ignition source. The original flame spread algorithm simulated heat flux from a line burner placed against the center of a compartment wall using specific expressions. Clearly, a different approach is necessary for a square burner in the compartment corner configuration. Little information was found in the literature identifying specific expressions for heat flux from a square burner to a wall in the corner, however some experimental information on the flux distribution in this configuration was recorded by Dillon[7]. Based on the ISO 9705[16] room corner configuration, the experiments were conducted that used thin steel plates mounted on the walls and ceiling. A grid of thermocouples was attached to the unexposed side of the steel, and a square burner was placed in the corner. Experiments were conducted at steady state burner heat release rates of 100kW and 300kW. The heat flux distributions were then calculated from the thermocouple readings and heat transfer theory. Figures 3-15 and 3-16 show the heat flux distributions from the 100kW burner on the wall and ceiling, respectively without room feedback effects. Figures 3-17 and 3-18 show the heat flux distributions from the 300kW burner on the wall and ceiling, respectively without room feedback effects. For clarity, sections of extrapolation were drawn on the graphs because no thermocouples were placed directly on the intersection between the wall and ceiling. The charts provide two-dimensional distributions for the flux, however the model only requires a one-dimensional distribution of the flux (i.e. flux vs. height or radius). Therefore, values for the fluxes were taken along the lines indicated in the figures.

The original flux distributions taken from figures 3-15 through 3-18 caused the model to behave somewhat unrealistically. Ignition would always be simulated on the wall just below the ceiling. This indicates that the model is operating correctly as initial ignition is simulated at the location of highest flux, but general observation on room

corner fire experiments indicates that sustained ignition occurs further down the wall, closer to the burner. Because of this discrepancy, the fluxes were altered to ensure ignition at the area of elevated flux on the wall above the burner (e.g. 67.5cm to 112.5cm in Figure 3-15). In order to remove the area of high flux near the ceiling, the flux was set constant above the area of elevated flux on the wall just above the burner. For the 100kW burner distribution, the flux was decreased to 30kW/m^2 at a height of approximately 130cm (Figure 3-15) and set constant until the 30kW/m^2 boundary was reached on the ceiling. The flux decreased as shown in Figure 3-16 beyond that boundary. A similar procedure was followed for the 300kW burner distribution, except the cutoff was 60kW/m^2 at a height of approximately 170cm (Figure 3-17).

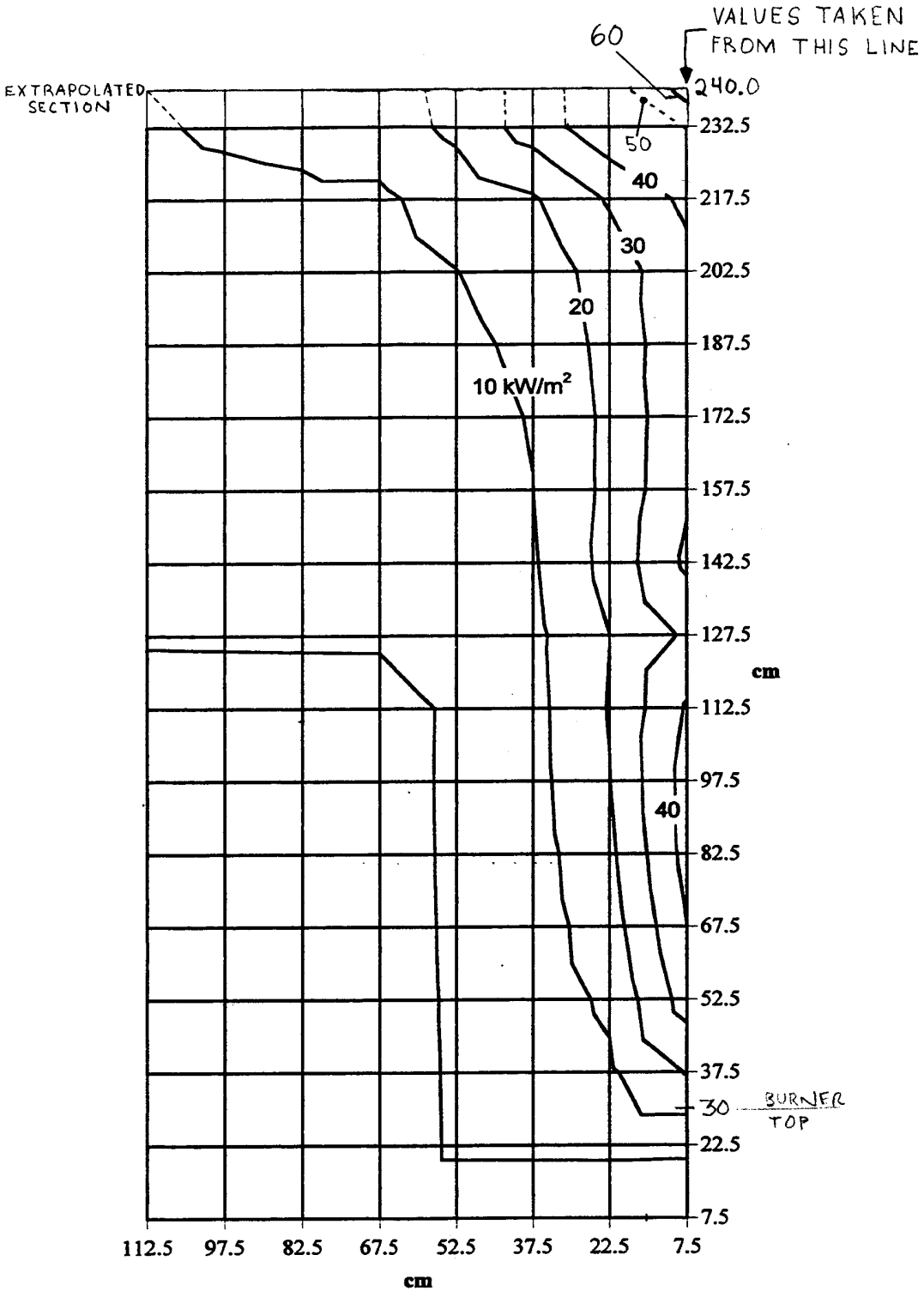

Figure 3-15 – Incident Fire Plume Heat Flux Distribution to Wall – 100kW Square Burner[7]

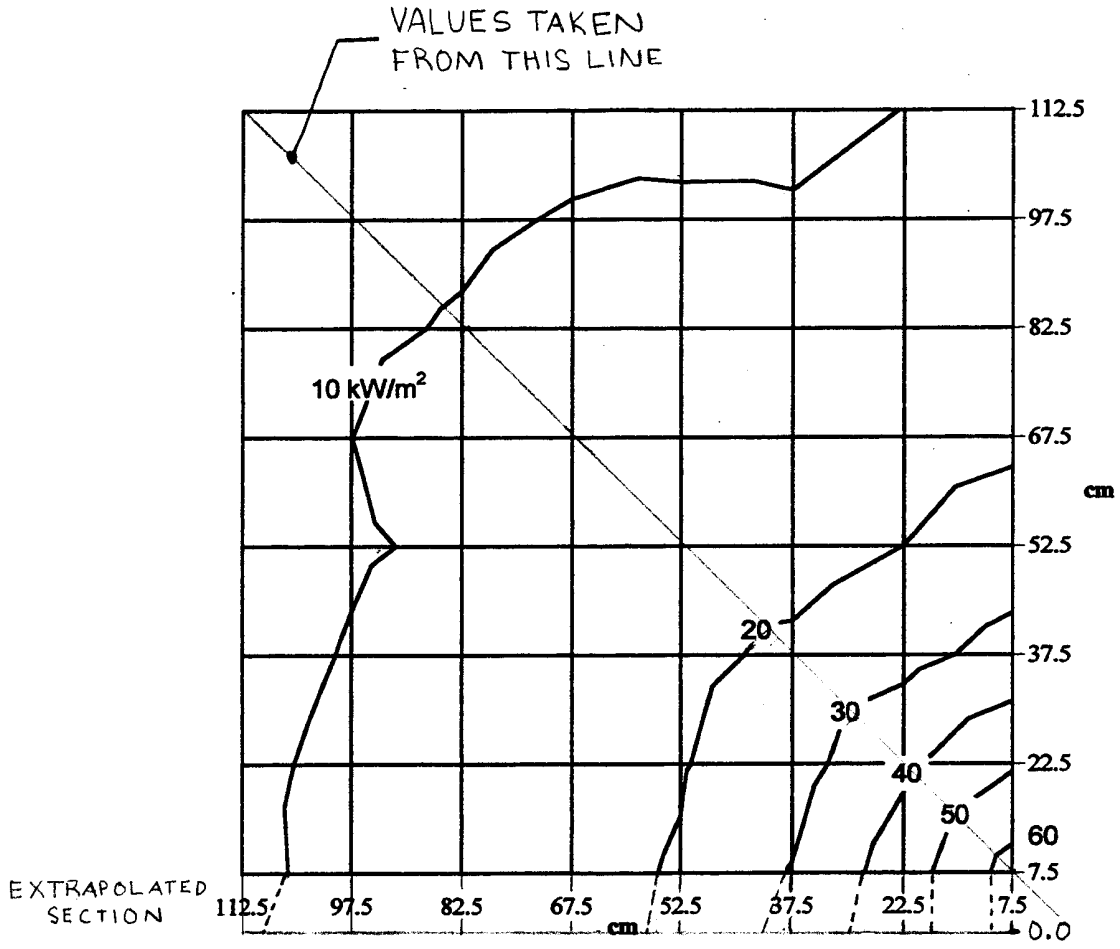

Figure 3-16 – Incident Fire Plume Heat Flux Distribution to Ceiling – 100kW Square Burner[7]

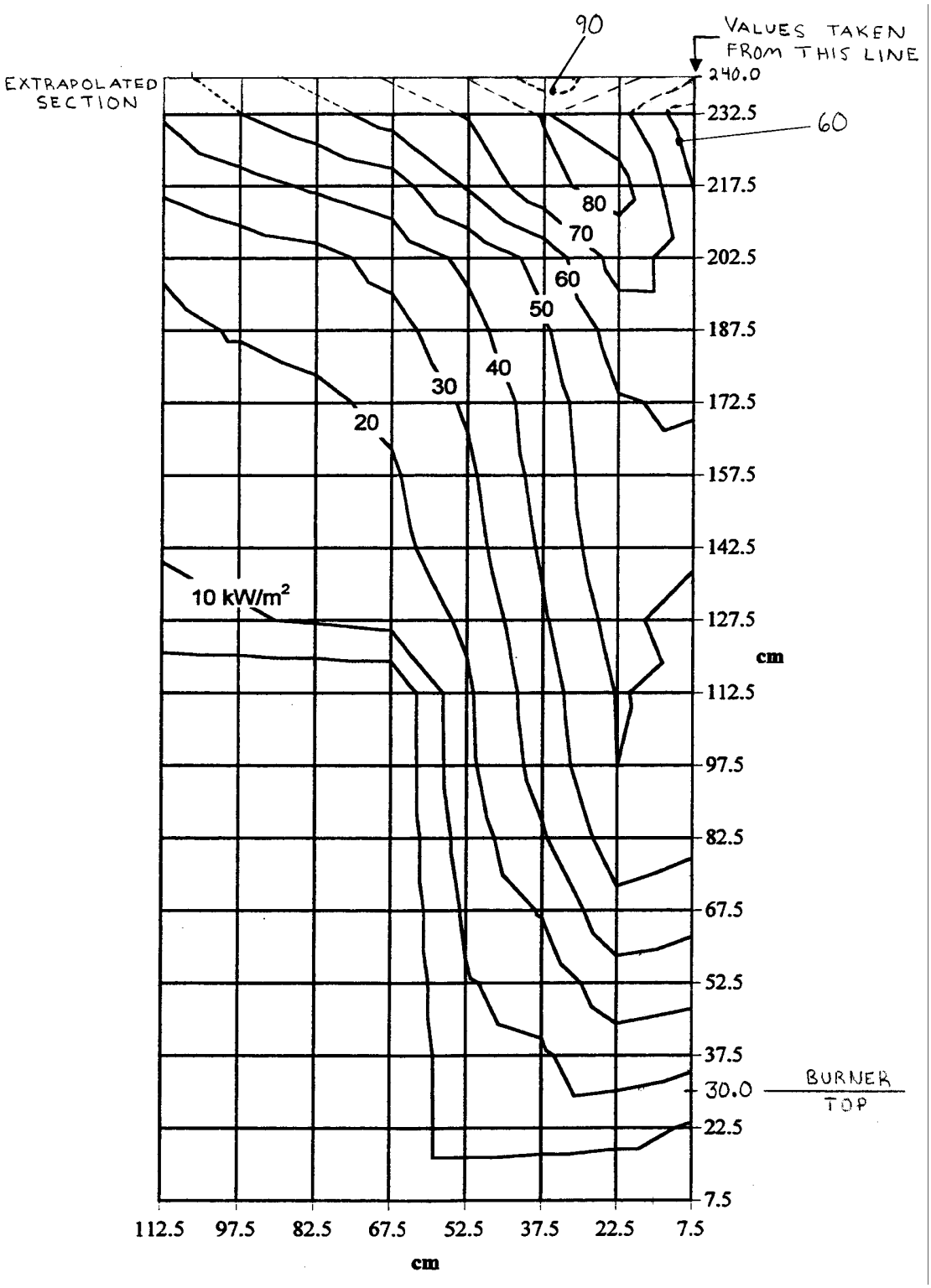

Figure 3-17 – Incident Fire Plume Heat Flux Distribution to Wall – 300kW Square Burner[7]

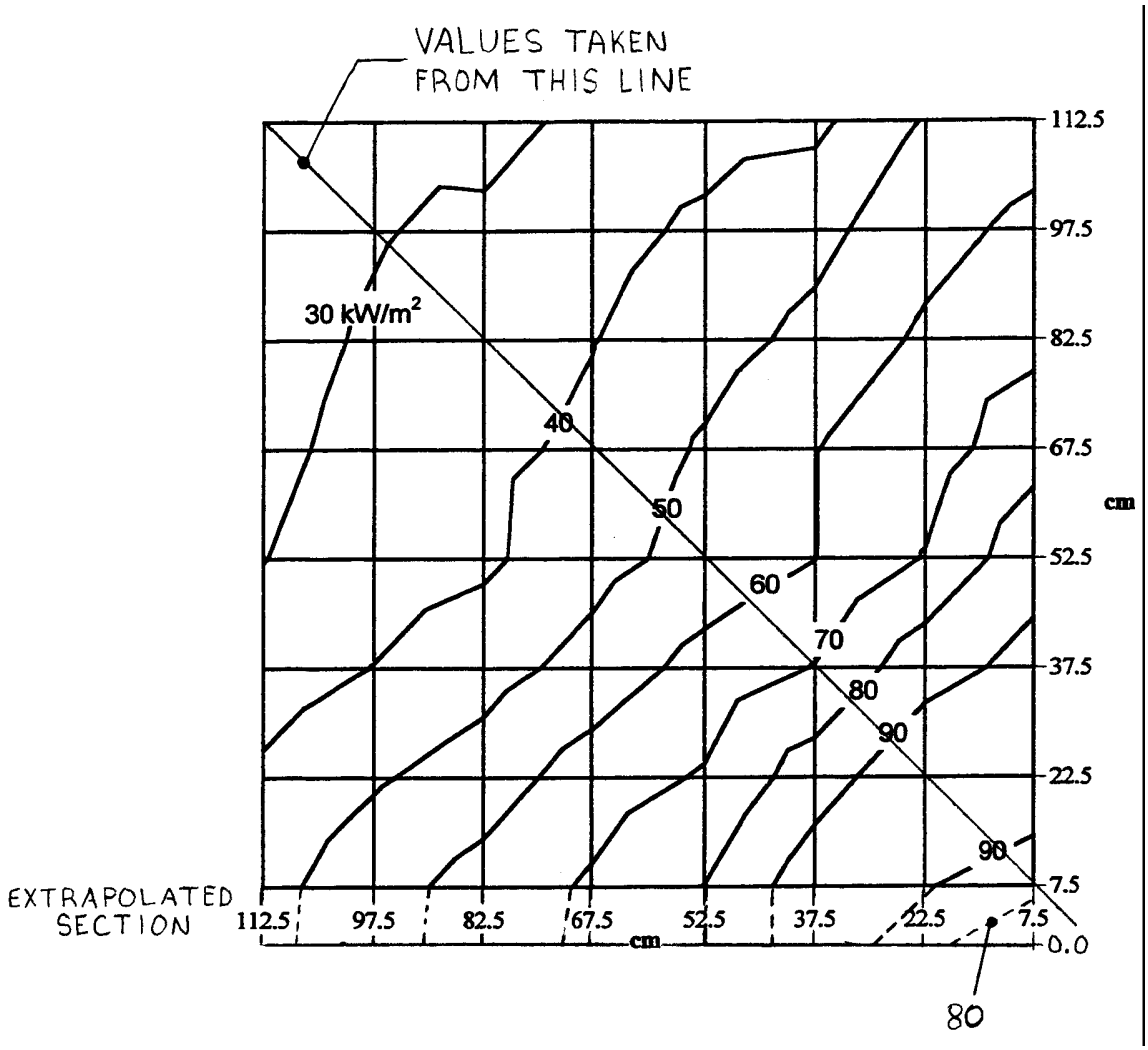

Figure 3-18 – Incident Fire Plume Heat Flux Distribution to Wall – 300kW Square Burner[7]

3.5 Multiple Pyrolysis Zones

This section describes the change in the method of tracking pyrolysis zones in the flame-spread algorithm. Although this change does not specifically deal with the conversion to the room corner configuration, it is included here because it is a fundamental modification to the original algorithm. The original algorithm allowed only one pyrolysis zone at any given time in the simulation. After ignition, simulation of both upward and downward spread from the initial ignition zone would occur until an element had burned out. At this point in the simulation, the lower bound of pyrolysis would be moved up to the burnout location and all elements below this point would be assumed burnt out. This often led to the situation where a significant number of elements would be burnt out when there was still burnable material remaining at these elements. In order to correct this problem, the shift in the lower pyrolysis bound at burnout was removed. Burnout is now controlled by the remaining fuel at each node. The algorithm tracks the

locations of multiple pyrolysis and burnout fronts, although these values are not used further in the algorithm in calculation of flame height, total flux, etc. It is important to note that once multiple pyrolysis zones exist (and they are sufficiently far apart), the validity of the flame height and heat flux calculations is questionable because the algorithm was derived for only one pyrolysis zone.

4.0 Implementation of the Flame Spread Algorithm into CFAST

Although some programming issues have been mentioned in previous chapters, details about the implementation of the flame spread algorithm into the zone model CFAST[26,27] have not been discussed. This chapter will provide those details. Note that all programming has been done in FORTRAN, as both CFAST and the original algorithm were written in this programming language. A description of pertinent CFAST structures and procedures will be given, followed by a description of the main subroutines of the flame spread algorithm and a description of general use of the resulting program.

4.1 CFAST Structure

CFAST is a zone model that was originally developed as the fire model for HAZARD I, and has been continually updated and improved over the past 16 years [26]. The model is now quite complex, as it is able to simulate multiple fires, multiple rooms, mechanical ventilation, species production and deposition, and a myriad of other effects related to compartment fires. In order to allow future effects to be added to the general simulation, the actual programming of CFAST was performed in a modular fashion. Figure 4-1 depicts the overall structure of the CFAST model. As seen in the figure, all of the main physics calculated by the program are broken into subroutines that calculate one particular phenomenon. Since the focus of the work is to model a compartment corner fire, the primary subroutine of interest is *FIRES*. This subroutine calculates phenomena related to combustion such as mass loss rate, heat release rate, species production, etc. for two classifications of fires.

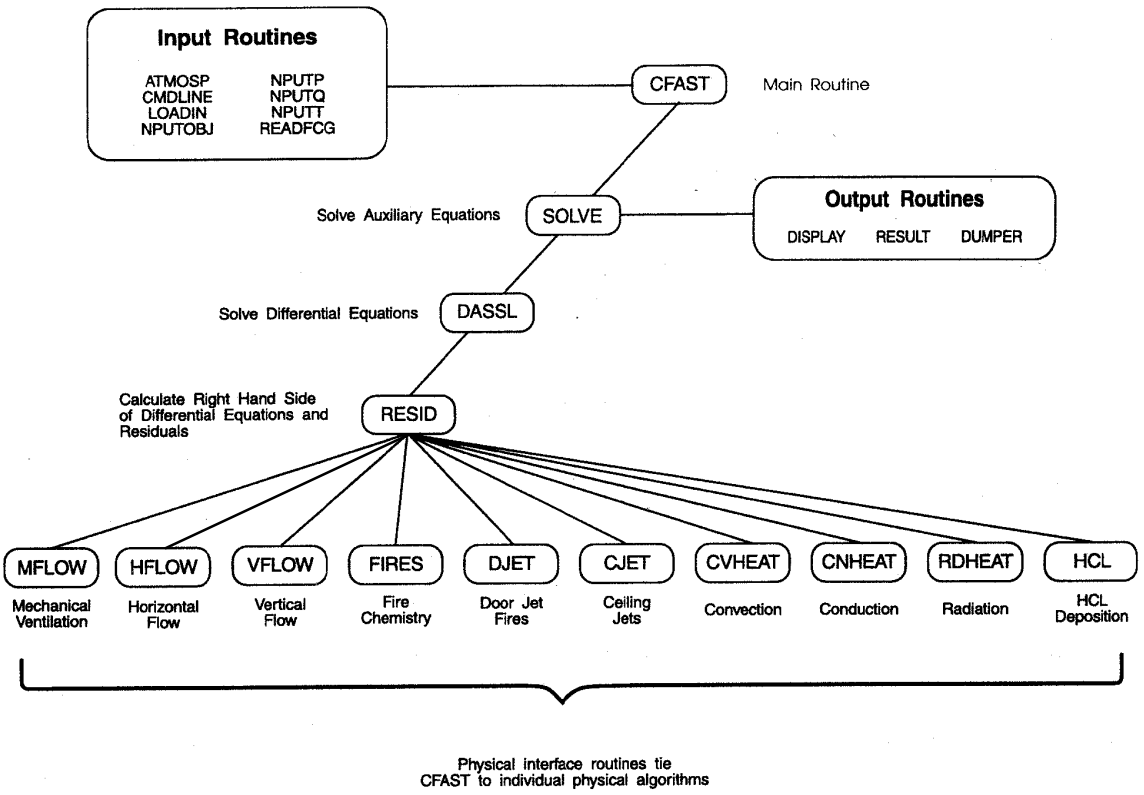

Figure 4-1 – Subroutine structure for CFAST[27]

The first classification is the "main fire." This fire must be completely specified by the user including a heat release rate curve, species production ratios, unconstrained (free-burning) or constrained (oxygen-limited) combustion, and other geometric and combustion properties. Only one main fire may be specified for each simulation, and the main fire starts burning at the very beginning of each simulation. Typical uses for the main fire would be to simulate a burning piece of furniture, stack of wooden pallets, or an ignition burner. For this work, the main fire will be used to simulate the ignition burner in the compartment corner.

The second fire classification is an "object fire." Multiple object fires can be specified in the same manner as the main fire, however more options are available. The most important are the ability to specify or calculate delayed ignition of an object, and the ability to calculate a subsequent heat release rate from the burning object. Once ignition of the object has occurred, the additional changes to the compartment environment are tracked using separate properties for both the main fire, and any object fires. In particular, the different heat release rates and species production rates are permissible for the "main fire" and "object fires." Examples of objects might be a piece of furniture or a slab of wall lining material. Before implementation of the flame-spread algorithm was complete, several types of objects were available in CFAST [26,27] as indicated in Table 4-1.

Table 4-1 – CFAST[26,27] object types

Object Type	*Ignition Criteria*†	*Description*
1	1,2,3	Unconstrained object (free-burning)
2	1,2,3	Constrained object (oxygen limited)
3	2,3	Flame spread object based on Quintiere's algorithm [31]
4	(not implemented)	Pool fire (not implemented)

†Criteria: 1-specified simulation time reached, 2-specified object surface temperature is reached, 3-specified object surface incident flux is reached

Since the goal of this project was to simulate ignition and subsequent fire-spread on wall/ceiling lining materials in the compartment corner scenario, a logical choice for implementation was to create a new object type for the flame spread algorithm. The next section describes how the new flame-spread algorithm fits into the CFAST structure as an object.

4.2 New Flame Spread Algorithm Structure within CFAST

The new flame-spread algorithm was implemented into CFAST[26,27] as a new object type, designated as object type five. Most of the changes to the source code of CFAST were made to the subroutines used within the subroutine *FIRES* (Figure 4-1) However, some changes were necessary in other locations in the source code of CFAST to allow a type five object. These details will not be presented here, but are available in Appendix B.

The structure of the subroutines under *FIRES* is shown in Figure 4-2. This discussion will concentrate on the subroutines contained in the first level below *FIRES*, and the indicated flame spread algorithm subroutines. The remaining subroutines perform other normal functions of CFAST[26,27] simulations and are described in [27]. The three subroutines of interest under *FIRES* are *PYROLS*, *DOFIRE*, and *OBJINT*. *PYROLS* interpolates the time dependent fire data (mass loss rate, heat release rate, species production, etc.) for the main fire, and *OBJINT* is the analogous subroutine for object fires. *DOFIRE* then calculates the heat release rate, species production, plume entrainment rate, etc. for the main fire and all object fires. This information is assembled by *FIRES*, and ultimately used in other subroutines as necessary to converge to a solution at each time-step.

As shown in Figure 4-2, all of the subroutines associated with the new flame spread algorithm are contained within the *OBJINT* subroutine. The approach used is to *calculate* the object fire properties using the flame spread algorithm, instead of just interpolating values from a table (heat release rate vs. time, for example). Table 4-2 gives a brief description of the main flame spread algorithm routines from Figure 4-2.

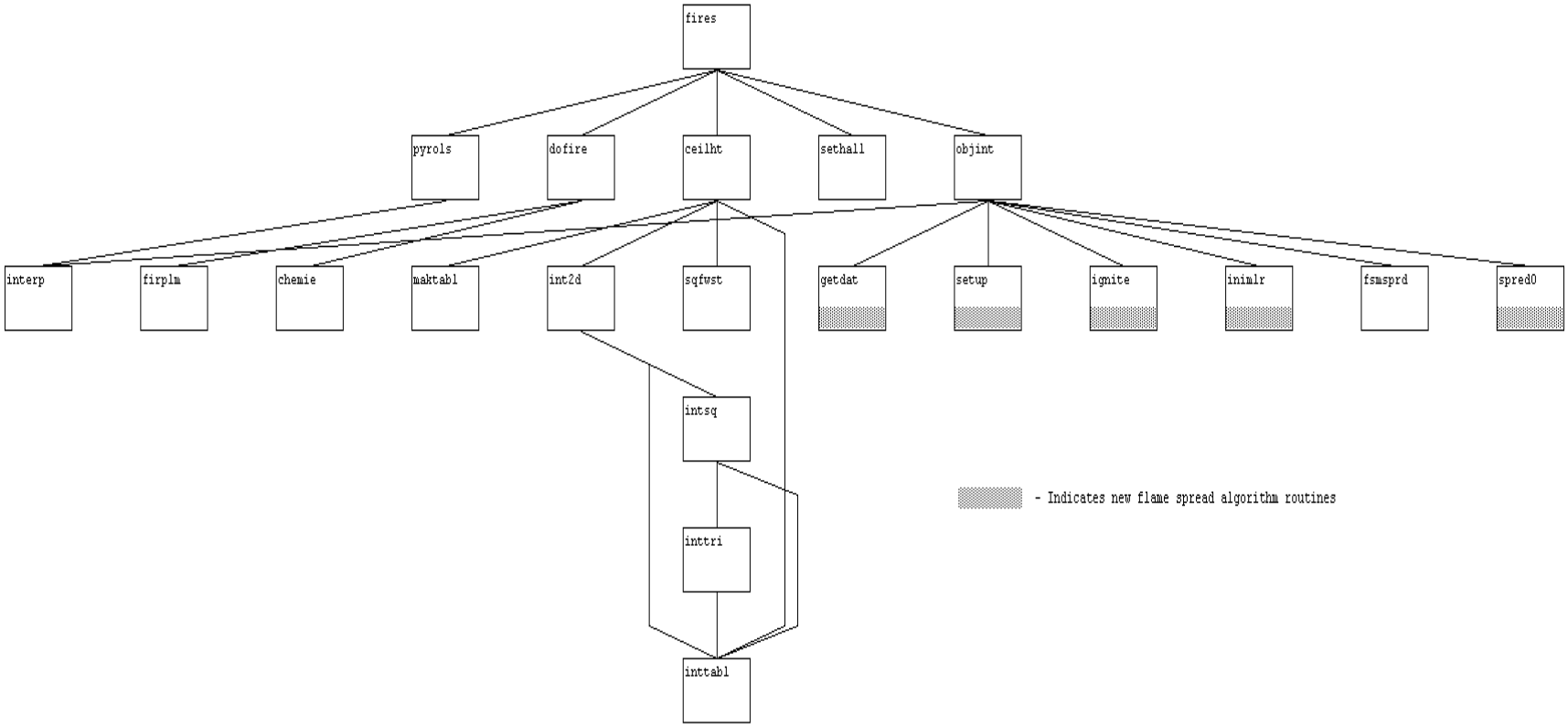

Figure 4-2 – Structure of Subroutines below FIRES

Table 4-2 – Description of main flame spread algorithm routines

Subroutine	*Description*
GETDAT	Gets all flame spread algorithm input data from user or setup files Imports necessary variables from CFAST[26,27]
SETUP	Initializes all flame spread algorithm variables
IGNITE	Checks for ignition, updates local wall temperatures and fluxes
INIMLR	Initializes mass loss rate, once ignition occurs
SPRED0	Calculates flame spread after ignition. Main outputs are heat release rate, mass loss rate, and area of pyrolysis.

The procedure used for using the new flame spread algorithm is as follows:

1) Add type five flame spread object to CFAST[26,27] object database (see Appendix C),
2) add any associated material data (if needed) to CFAST thermophysical database (see Appendix C),
3) specify the type five object in the main CFAST input datafile (see Appendix C),
4) run CFAST with the new input datafile created in step 3,
5) CFAST initializes itself,
6) CFAST increments to the next time-step (first step will be time = 0),
7) CFAST executes subroutine *OBJINT* because an object is in use,
8) *GETDAT* and *SETUP* are executed if this is the first time *OBJINT* has been entered,
9) if ignition has not occurred, *IGNITE* will be executed. It calculates wall fluxes and temperatures, and check for ignition,
10) if ignition has just occurred, *INIMLR* will be executed. For no ignition, the program jumps to step 13,
11) if ignition has occurred, *SPRED0* is executed,
12) values for object mass loss rate, heat release rate, and pyrolysis area calculated and passed back to *OBJINT*,
13) The standard CFAST routines are executed.
14) If flashover conditions or the simulation time have been reached, the simulation ends. Otherwise, the program goes back to step 6

A better representation of the previous procedure is shown in Figure 4-3. For additional reference, Figure 4-4 has been included to show detail on the input procedure used for the flame spread algorithm.

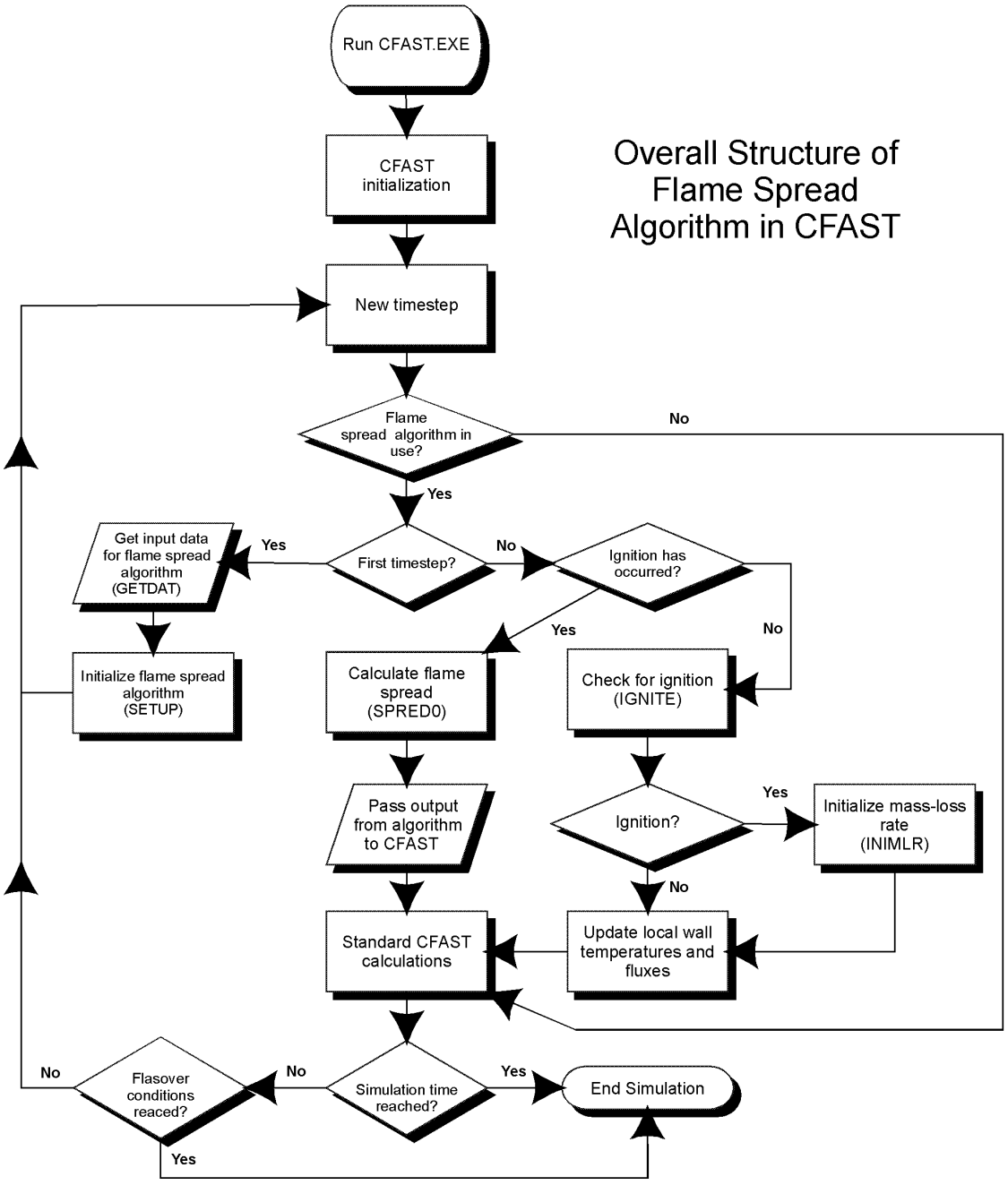

Figure 4-3 – Flow chart of flame spread algorithm when implemented in CFAST

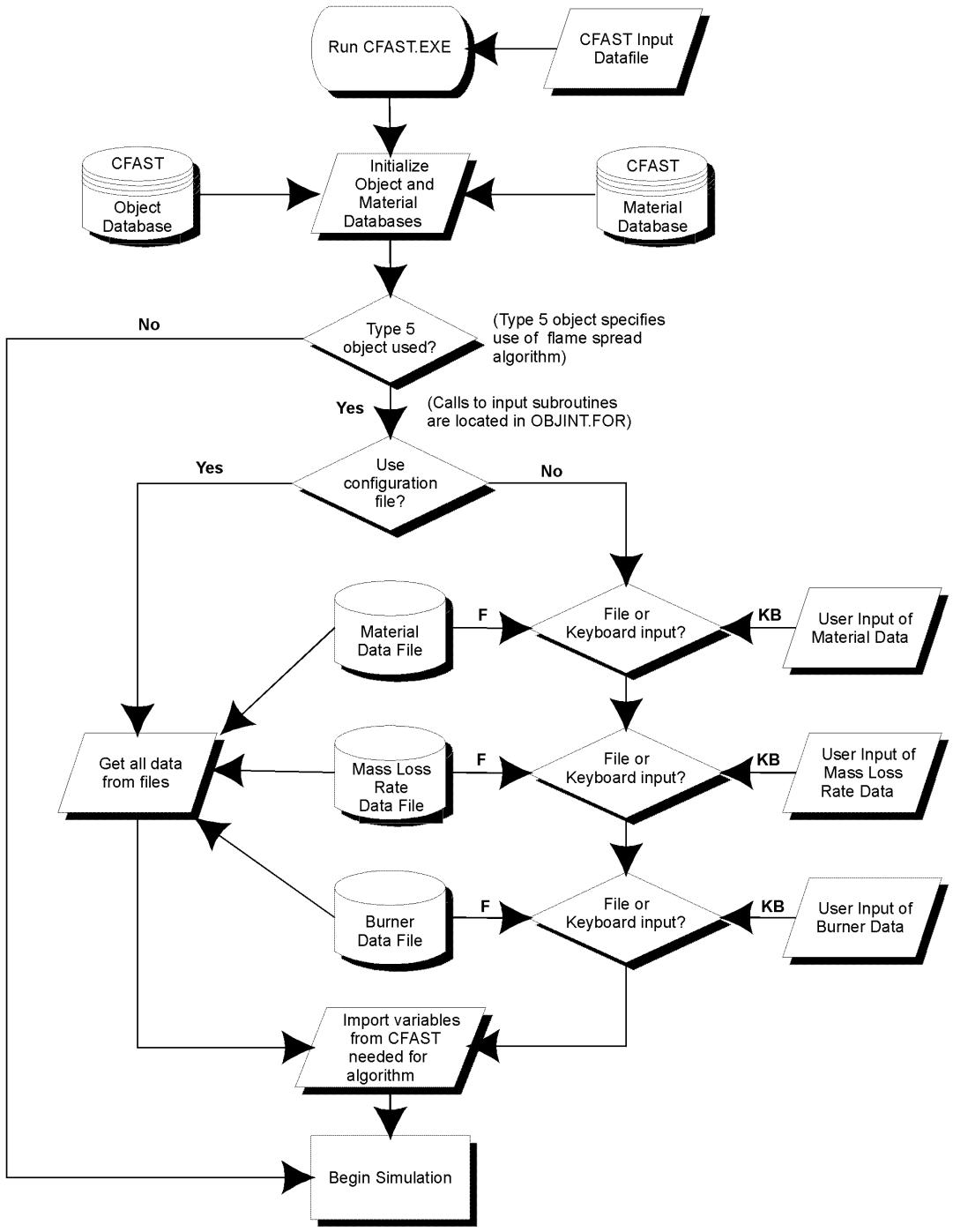

Figure 4-4 – Flow chart showing input data for the flame spread algorithm

Two other general notes must be made about the implementation of the flame spread algorithm into CFAST[26,27]. First, the object ignition handling setup resident in CFAST is bypassed by this algorithm. This is done simply because the algorithm has its own ignition routine and does not need to use the one provided by CFAST. More specifically the algorithm controls the logical array OBJON, used to specify whether or not an object is burning. This variable is set to "FALSE" each time *OBJINT* is executed, until the flame spread ignition algorithm (*IGNITE*) reaches ignition conditions in the simulation. At this point, OBJON is set to "TRUE" to inform CFAST the object has ignited.

The second issue revolves around the simulation time-step. The flame-spread algorithm is not necessarily executed each time the *OBJINT* is executed. This is because CFAST[26,27] can use very small time-steps on the order of 0.0001 seconds, and running the flame spread algorithm at this resolution would be very slow indeed! Instead, the user specifies the minimum amount of simulation time that must pass before the flame spread algorithm is executed again. A value of 0.5 seconds has been shown to provide good results and stability. It is recommended that the maximum CFAST time-step be set to this same value, using the SOLVER.INI file.

The next chapter will provide some detail on the changes to Mitler's original algorithm that were necessary when making the additions outlined in Chapter 3.

5.0 Conversion of Mitler's Original Algorithm

The original flame spread algorithm developed by Mitler[23,24] simulated flame spread on the center of a compartment wall and ceiling. In order to simulate a room corner fire on the walls/ceiling using the zone model CFAST[26,27], the changes described in Chapter 3 needed to be implemented along with some structural changes. These changes were added as an option that can be turned on or off using the input data. By making the changes in this way the original sidewall algorithm is preserved, and may still be used in its original form. The next two sections describe the changes made to the original source code for implementing the specified changes, and structural changes necessary to convert the stand-alone program into a set of subroutines used by CFAST.

5.1 Changes to Mitler's Source Code

Changes in many subroutines of Mitler's original program[23,24] were necessary for simulating the corner configuration. When the corner configuration is used, the logical variable CRNR is set to "TRUE" by either subroutine *FIDAT* (reads material input data from a file) or *KBDAT* (manual input of material data). This logical variable is used throughout the algorithm to determine whether or not to use the changes related to simulating the room corner configuration.

The first change was made to the geometry of flame spread on the ceiling. Other than developing the radiation network with the quarter-circular geometry, only two changes were required to specifically deal with the geometry of the quarter circle. The first was a change in *LATSPR* (lateral flame spread calculations) to the calculation of the average width of the pyrolysis zone. In the original algorithm, the average width was based on the width of the pyrolyzing elements on the upper and lower walls. In the new algorithm, once the pyrolysis zone begins to move across the ceiling in a circular pattern, the calculation of average width accounts for the quarter circular geometry of the elements. The contribution of the quarter circular elements to the average width was made using the arc-length of each burning ceiling element.

The second change was to *MLRATE* (mass loss rate calculations). In this subroutine, the mass loss rate for each element is scaled using the width of that particular element versus the average pyrolysis width. As with the change in *LATSPR*, the circular geometry of the ceiling element is taken into consideration (using an arc-length as before). In retrospect, the continued use of the average width calculation may not have been a good choice. Simulation results (Chapter 6) showed that the calculated mass-loss rate over ceiling elements from this method was probably too large in most cases.

The next change was the altering of the flame height calculations for the corner configuration. The expressions from Section 3.2 were simply inserted into the subroutine *FLAME* (primary flame height calculation routine). There were a few other instances of flame height calculation in subroutines *MLRATE*, *FLXTMP* (calculates post-ignition fluxes and wall temperatures, and *CVCCOM* (calculates convective portion of flux). The calculations were updated in these subroutines as well.

The third change was to add the new radiation network to the algorithm. The logical variable RADCALC (set in *FIDAT* or *KBDAT*) controls use of the radiation

network subroutines. The main controlling subroutine for the radiation network is *RADXFER*. *RADXFER* is called from subroutines *COMBND* (calculates post ignition total flux), *INFLXF* (calculates pre-ignition total flux), and *NBFLUX* (calculates flux at any time when no flame is present) as shown in Figure 5-1. Using inputs from these routines, *RADXFER* calculates the radiative flux. The radiative flux is then added to the convective flux, resulting in the total flux used in the remainder of the algorithm.

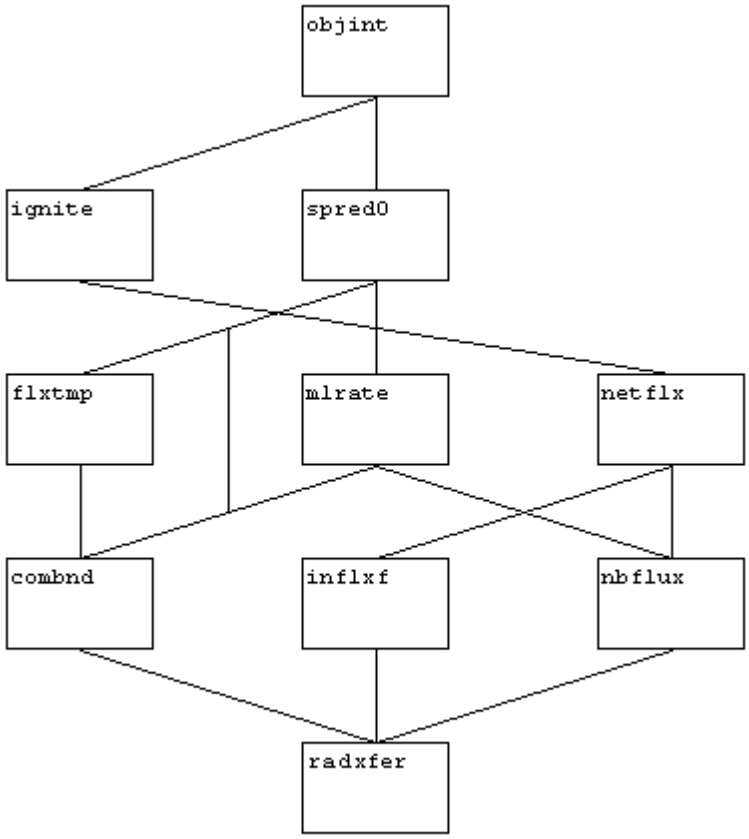

Figure 5-1 – Subroutine structure above RADXFER

The next change was the addition of the heat flux maps from Dillon's work[7]. The logical variable FLUXMAP in subroutines *FIBRN* (reads burner input data from a file) or *KBBRN* (manual input of burner data) controls the use of the heat flux map. At this time, the user cannot change the heat flux map values. The values for both the 100kW and 300kW burner flux distribution are set in the subroutine *SETUP* (initializes flame spread algorithm variables). The routines *IGNITE* and *SPRED0* then pass the values to the appropriate flux calculation routines: *INFLXF*, *COMBND*, and *RADCOM* (calculates post ignition radiative flux). The heat flux values from the heat flux map replace the values calculated for the radiative flux from the burner. Because the heat flux maps simulate a *total* flux (i.e. radiation *and* convection), concessions have been made so that the convection is not added twice to the total heat flux.

The last change was to allow multiple pyrolysis zones. The logical variable MULTIPYR in subroutine *FIDAT* or *KBDAT* controls this option. A separate condition was written into subroutine *BRNOUT* (checks for burnout at each node) to handle the option of calculating multiple pyrolysis zones.

A description of each specific subroutine and the structure of the subroutines are available in Appendices H and G, respectively. A detailed list of specific changes to each subroutine from the original algorithm is also available in Appendix F.

5.2 Structure Changes for CFAST Implementation

Two basic changes to the original program structure were made in order to implement the flame spread algorithm into CFAST[26,27]. The first change was to remove the controlling subroutines used for the original algorithm. As CFAST now controls the flame-spread algorithm, these routines are not necessary. The second change was to store the main variables from the flame-spread algorithm in FORTRAN common blocks to allow easy exchange between the main subroutines and CFAST. The common blocks are included using the include file "MITLER.INC."

6.0 Results

This chapter describes the evaluation process and output of the new flame spread algorithm. A set of experimental data[18] was obtained for several marine composite materials describing test results from the Cone Calorimeter[15], LIFT apparatus[3], and ISO 9705[16] room corner configuration. Data sets from four of these materials were used for algorithm testing because they represented a varied range of experimental behavior (particularly in the ISO9705 tests) and had the most complete material property data. Input files for CFAST and the flame-spread algorithm were developed to model these four cases, based on the material property data from these materials. Next, a sensitivity analysis was developed in order to study the effects of changing key input variables. Finally, simulations were conducted and the results examined. The first part of the chapter gives a description of the input data, followed by an explanation of the setup of the sensitivity study, and finally a discussion of the results of the simulations.

6.1 Description of the Input Data

The data used to test the new algorithm was provided by Southwest Research Institute (San Antonio, TX). The data was accompanied by a report[18] describing the testing of numerous materials, including seven fire retarded (FR) woven glass composite materials, a textile wall covering material, and a standard marine grade woven polyester material. Each material was tested in several ways, including the Cone Calorimeter, LIFT apparatus, and full-scale room corner. The materials were tested in the Cone Calorimeter according to ISO 5660[15], a standard for testing building materials using the Cone Calorimeter. Generally, each material was tested twice at three different irradiance levels. Next, two separate test procedures were used for experiments conducted in the LIFT apparatus. Materials were tested according to IMO Resolution A.653[13] and ASTM E 1321-97-a[3], yielding two sets of lateral flame spread properties for the materials. Finally, each material was tested in a full-scale room according to provisions outlined in ISO 9705[16]. The material ignition and lateral flame spread properties were derived using the procedures of ASTM E 1321.
The following is a list of material data provided from the bench-scale tests:

- density (ρ)
- thickness (δ)
- thermal inertia ($k\rho c_p$)
- ignition temperature (T_{ig})
- effective heat of combustion (ΔH_{eff})
- lateral flame spread parameter (Φ)
- minimum surface temperature for lateral flame spread ($T_{s,min}$)
- heat release rate curve from the Cone Calorimeter at different irradiance levels

The full-scale tests provided total heat release rate and a selection of points describing the upper layer temperature in the room.

Out of the nine materials tested, four produced complete sets of material data. These materials were fire-retarded (FR) polyester (designated material number 3), FR

vinylester (material number 4), standard marine polyester (material number 8), and FR acrylic (material number 9). Since these materials represented a varied range of behavior in the ISO 9705 test (earliest flashover @ 1.8min to latest flashover @ 11.1min) along with the complete material property data sets, they were selected to evaluate the new algorithm.

All of the data listed above are necessary as input to the new algorithm. Figure 6-1 shows an example set of input data needed for the algorithm. The shaded parameters in the figure require additional explanation, however other parameters, such as material density or burner height, are fairly straightforward and will not be discussed further here. Note that one of the inputs shown in Figure 6-1 is for the average heat flux from the ceiling. This value is only used in the *sidewall* version of the flame-spread algorithm, but must always be specified so that the input routines work correctly. Sections 6.1.1 to 6.1.7 explain the shaded parameters of Figure 6-1.

6.1.1 Specific Heat and Thermal Conductivity

The experimental data provides a value for thermal inertia ($k\rho c_p$), however the flame-spread algorithm requires each of these values to be specified separately. The report[18] *does* provide a value for material density, but not for thermal conductivity or specific heat. A study by Grenier[10] on similar composite marine materials was consulted to obtain individual values for k and c_p. The composite materials in this study had a specific heat of 1000 J/kg-K. Since the composite materials in Grenier's study are similar to the composite materials used in the experiments conducted by Southwest Research Institute[18], the value of c_p provided by Grenier was used for all materials in this evaluation. The value for thermal conductivity was then calculated using the values for $k\rho c_p$, ρ, and c_p as follows:

$$k = \frac{\left(k\rho c_p\right)}{\rho c_p} \tag{6-1}$$

6.1.2 Net Heat of Complete Combustion and Combustion Efficiency

Heat of combustion is used to convert between mass loss rate and heat release rate in the flame-spread algorithm. The algorithm is set up to use an effective heat of combustion by multiplying a net heat of complete combustion with combustion efficiency as follows:

$$\Delta H_{eff} = \left(\chi_A\right)\left(\Delta H_{net,c}\right) \tag{6-2}$$

The effective heat of combustion is the value derived from Cone Calorimeter tests, however the inputs to the algorithm are χ_A and $\Delta H_{net,c}$. The composition of the composite material is used to determine the appropriate input values. The primary material that is consumed during combustion of composite materials is the resin that binds the glass together (e.g. polyester, vinylester, acrylic, etc.). Thus, it is desirable to use the net heat of complete combustion for this resin material, and apply a combustion efficiency to arrive at the effective heat of combustion derived from the Cone Calorimeter tests. An argument could be made that some error is introduced by using this

method, however the only heat of combustion used in the algorithm is the effective heat of combustion. Thus, the only uncertainty from this method comes from the Cone Calorimeter data itself. The net heats of complete combustion for these materials were taken from Tewarson[34]. If no data could be found on a particular material (vinylester for example), a combustion efficiency of 0.5 was assumed, and an appropriate net heat of complete combustion used in the input data.

PROP_3?.DAT

MATERIAL PROPERTIES / INPUT PARAMETERS	
Height of bottom of slab above floor	0 m
Material density (ρ)	1650 kg/m^3
Material thickness (δ)	0.0252 m
Material specific heat (c_p)	1000 J/kg·K
Material thermal conductivity (k)	0.782 W/m·K
Material ignition Temperature (T_{ig})	671 K
Material initial uniform temperature	293.15 K
Timestep	0.5 sec
Output interval	1 sec
Simulation length	1200 sec
Specific heat of product gases	1340 J/kg·K
Net heat of complete combustion	3.25E+07 J/kg
Efficiency of combustion (χ_A)	0.347
Radiative fraction (χ_{rad})	0.476
Material emissivity (ε)	0.9
Flame transmissivity (τ_{flame})	0.5
Lateral flame spread parameter (Φ)	12.13 kW^2/m^3
Min. surface temp. for lateral spread ($T_{s,min}$)	639 K
Width of slab (2 x width of shorter wall)	4.8 m
Ceiling present?	1 (yes)
Allow multiple pyrolysis zones?	1 (yes)
Average heat flux from the ceiling	2000 kW/m^2
Paramater p for ceiling/wall arm extensions	1 m^{-1}
Combustible ceiling lining present?	1 (yes)
Corner configuration present?	1 (yes)
Use Complex radiation?	1 (yes)
Use gaslayer calcs. In radiation calcs.?	1 (yes)
Use accurate beam length calculation in radiation calculations?	0 (no)

3_50.MLR

CONE CURVE		
Point #	Time sec	HRR kW/m^2
1	0	0.0
2	30	114.9
3	160	81.1
4	260	73.5
5	375	60.4
6	490	48.1
7	735	43.8
8		
9		
10		
11		
12		
13		
14		
15		
16		
17		
18		
19		
20		
21		
22		
23		
24		
25		
Irrad:	50 kW/m^2	

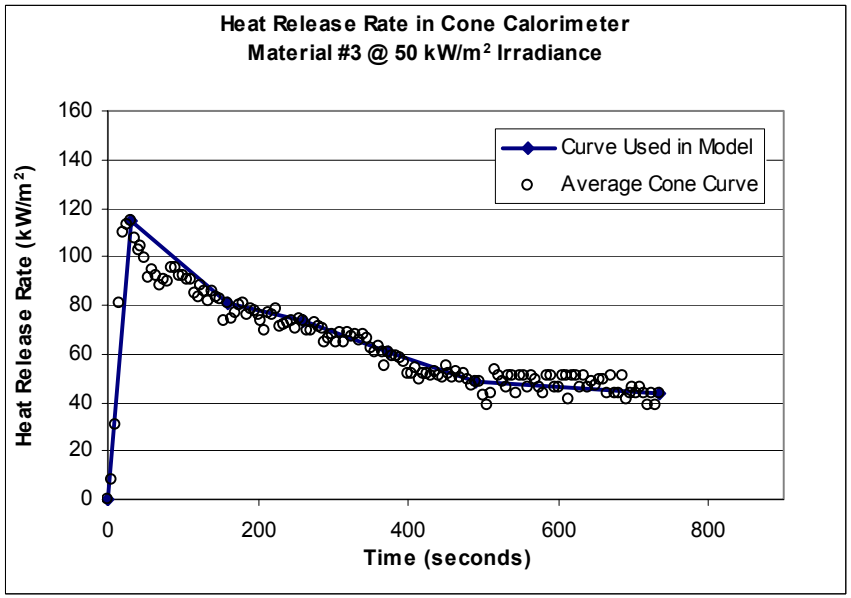

USCG.BRN

BURNER INPUTS	
Burner height above floor	0.152 m
Width of burner side	0.170 m
Use heat flux map?	1 (yes)

Figure 6-1 – Sample of input data for the new flame spread algorithm

6.1.3 Radiative Fraction of Heat Release Rate

The radiative fraction of heat release rate (χ_R) was derived in a similar manner as the combustion efficiency, using an effective heat of combustion and radiative heat of combustion:

$$\chi_R = \frac{\Delta H_{rad}}{\Delta H_{eff}} \tag{6-3}$$

In this case, the effective heat of combustion is for the resin material *alone*, not the value provided from the composite material tests provided by Southwest Research Insitute [18]. As with the net heat of complete combustion, values for ΔH_{rad} and ΔH_{eff} were taken from Tewarson[34]. If these values could not be found, a radiative fraction of 0.3 was assumed to be a representative value[8].

6.1.4 Emissivity

The emissivity of these materials was not determined during testing. Based on the similar composite materials from Grenier's study[10], an emissivity of 0.9 was assumed to be reasonable for these simulations.

6.1.5 Flame Transmissivity

A value for flame transmissivity was also not determined during testing of the composite materials and little guidance on this value could be found in the literature. The only basis found was from Karlsson [19], where he assumed a flame emissivity of 0.5. If the assumption is made that $\varepsilon_{flame} = \alpha_{flame}$, and $\alpha_{flame} = (1 - \tau_{flame})$, then τ_{flame} is 0.5. This is the value currently used for these materials.

6.1.6 Lateral Flame Spread Properties

The lateral flame spread properties required by the algorithm are the minimum temperature for lateral flame spread ($T_{s,min}$) and the lateral flame spread parameter (Φ). Since two values for each lateral flame spread property were available from the provided material property data, the average value was used in the simulations.

6.1.7 Cone Calorimeter Curve

Southwest Research Institute performed several Cone Calorimeter tests on each material. Generally, two tests were completed at each of three irradiance levels for any given material. An average heat release rate curve for each material at each irradiance level was created using the available data, where the average was started from the ignition time of the sample in the experiment. A simple curve fit to the developed average cone curve was used for the actual model input data. An example is shown in Figure 6-2.

In some cases, the duration of one of the experimental tests was longer than the other. This situation appears in Figure 6-2, as experimental curve #2 ends at ~725 seconds, while experimental curve #1 ends at ~850 seconds. The procedure used in this case was to continue the average curve beyond where the shorter experimental curve

ended, using the curvature of the longer test. By examining the average curve after ~725 seconds in Figure 6-2, it can be seen that its curvature matches that of experimental curve #1 beyond this time. Additionally, a five-point moving average was used to help fit the developed average cone curve when it exhibited a large amount of scatter.

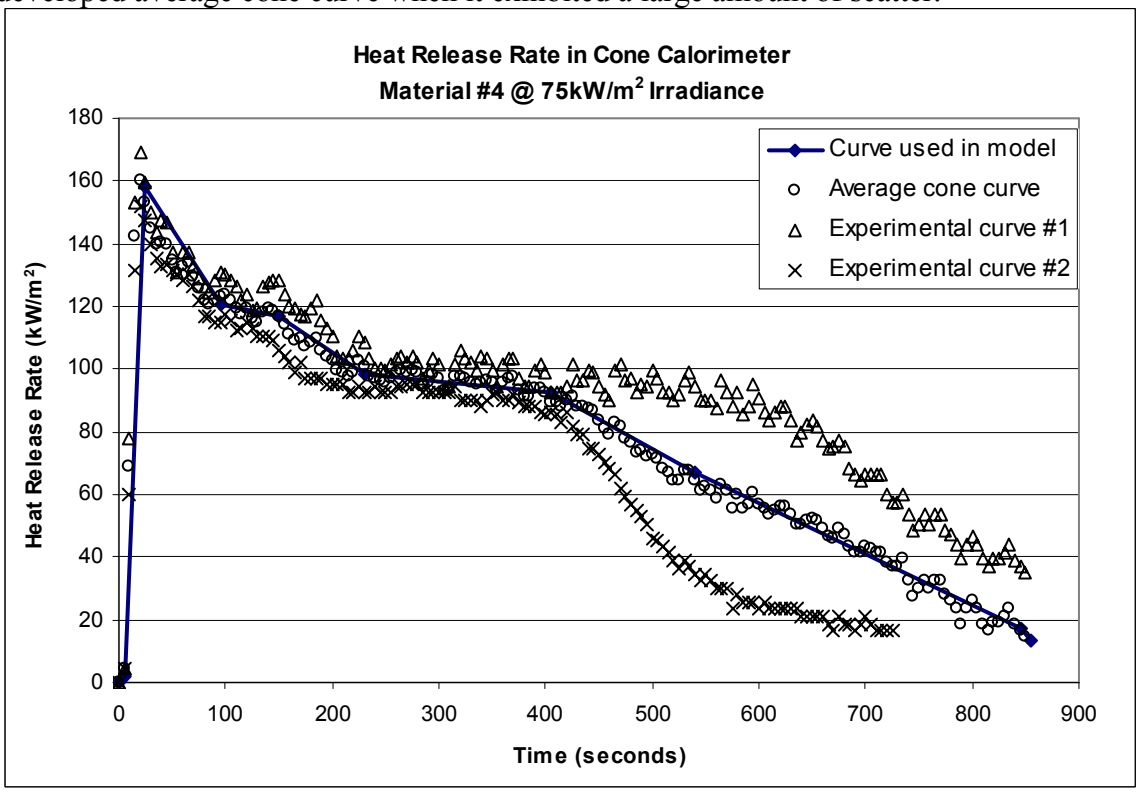

Figure 6-2 – Example Cone Calorimeter data

6.2 Sensitivity Study

A study of the effect of changing key input variables was developed in order to test the new algorithm. The first step was to assemble a baseline set of input data for each material, followed by a matrix of changing variable values.

The baseline input values were intended to be a self-consistent set of data that would be representative of typical input to the algorithm. The values were obtained using the methods outlined in the previous section. A summary of major input values for the baseline simulations of the materials is given in Table 6-1.

Table 6-1 – Summary of baseline simulation inputs

Baseline - Major Input Variables								
Material	Name	T_{ig} K	$T_{s,min}$ K	Φ kW^2/m^3	ε (ND)*	τ_{flame} (ND)*	k W/m·K	ρ kg/m^3
3	FR polyester	671	639	12.13	0.9	0.5	0.782000	1650
4	FR vinylester	671	639	12.32	0.9	0.5	1.221000	1630
8	Polyester	662	479	19.02	0.9	0.5	0.597000	1390
9	FR acrylic	681	569	23.22	0.9	0.5	1.511000	1880

Material	Name	c_p J/kg-K	$k\rho c_p$ $(kW^2 \cdot s/m^4K^2)$	ΔH_{eff}** J/kg	$\Delta H_{net,c}$ J/kg	χ_A (ND)*	χ_R (ND)*
3	FR polyester	1000	1.29	11.28	32.5	0.347	0.476
4	FR vinylester	1000	1.99	13.43	22.7	0.5	0.3
8	Polyester	1000	0.83	21.60	32.5	0.665	0.476
9	FR acrylic	1000	2.84	12.28	25.2	0.489	0.314
				($\times 10^6$)	($\times 10^6$)		

Notes: * Dimensionless variable

** Value from U.S. Coast Guard Report [18]

The Cone Calorimeter curves used for the baseline simulations were from the data provided at an irradiance of $50 kW/m^2$. The complete set of input data for each material's baseline simulation is in Appendix J.

The next step was to develop a matrix of important input variables to vary, in order to determine their effect on the algorithm. The parameters selected for variation were considered to have the largest potential impact on the simulation. The first variable that was examined is the thermal inertia ($k\rho c_p$). This value will affect the conduction of heat through the wall, thus affecting the surface temperature, time to ignition and subsequent fire growth rate. However, each of the parameters in $k\rho c_p$ is specified separately in the input routines to the new algorithm. Variation of thermal conductivity (k) was selected because a value for material density (ρ) was available, and the value for specific heat (c_p) was set to a constant for all materials as indicated previously. A factor of two was selected as the variation level because work completed by Jacoby[17] on similar composite materials showed that the level of uncertainty in calculation of ignition parameters was roughly within a factor of two.

The second input variable modified was the Cone Calorimeter heat release rate curve. Since the mass loss rate is calculated directly from the specified Cone Calorimeter curve, variation of this variable is obviously important. Additionally, the initial mass of material available for pyrolysis at each element is based on the area under the Cone Calorimeter curve. Average Cone Calorimeter curves from irradiance levels of 25 and 75 kW/m^2 were used for this study. These Cone Calorimeter curves may be found in Appendix K.

The material emissivity (ε) and the flame transmissivity (τ_{flame}) were selected for variation because they are used in radiation calculations. In particular, these variables are applied in the developed corner radiation network. Variation of these parameters allows the functioning of the radiation network to be tested.

Next, ignition temperature (T_{ig}) was adjusted. The variation of ignition temperature has a twofold effect. First, the time to ignition will be affected. Secondly, the maximum temperature of the walls (the ignition temperature) will affect the level of radiation exchange. The change was set at ±25% to represent a maximum potential variation due to experimental error or uncertainties in the reduction of data from the Cone Calorimeter or LIFT apparatus. Note that the value of minimum temperature at which lateral flame spread occurs ($T_{s,min}$) is changed proportionally with ignition temperature. This was done because the lowered ignition temperature would generally be less than the value for $T_{s,min}$, which would be unphysical.

Finally, the variables affecting lateral flame spread were altered to determine the importance of lateral flame spread in the simulation. These variables were the minimum temperature at which lateral flame spread occurs ($T_{s,min}$) and the lateral flame spread parameter (Φ). As with the ignition temperature, these parameters were varied by ±25% to represent a maximum range of error or uncertainty. The value for $T_{s,min}$ not increased because its value would often exceed the ignition temperature, resulting in an unphysical condition. The resulting sensitivity matrix is shown in Table 6-2.

Table 6-2 – Input variable sensitivity matrix

Note: The letters are used to conveniently identify simulations. For example, "4f" would be used to denote the simulation where the material emissivity was changed to 0.75 for material #4.

		MATERIAL			
VARIATION		#3 - FR Polyester	#4 - FR Vinylester	#8 - Polyester	#9 - FR Acrylic
k * 0.5 (W/m-K)	a	0.391	0.6105	0.2985	0.7555
k * 2 (W/m-K)	b	1.564	2.442	1.194	3.022
Cone Curve @ Lowest Irradiance (kW/m^2)	c	25	25	25	25
Cone Curve @ Highest Irradiance (kW/m^2)	e	75	75	75	75
$\varepsilon = 0.75$	f	0.75	0.75	0.75	0.75
$\varepsilon = 0.95$	g	0.95	0.95	0.95	0.95
$\tau_{flam} = 0.75$	h	0.75	0.75	0.75	0.75
$\tau_{flam} = 0.25$	i	0.25	0.25	0.25	0.25
T_{ig} + 25% {$T_{s,min}$ + 25%} (K)	j	839 {799}	839 {799}	828 {599}	851 {711}
T_{ig} - 25% {$T_{s,min}$ - 25%} (K)	k	503 {479}	503 {479}	497 {359}	511 {427}
$T_{s,min}$ - 25% (K)	m	479	479	359	427
Φ + 25% ($kW2/m^3$)	n	15.16	15.39	23.78	29.03
Φ - 25% ($kW2/m^3$)	o	9.1	9.24	14.27	17.42

6.3 Discussion of the Simulation Results

The baseline simulations, plus the sensitivity matrix simulations give a total of 64 individual simulations. The key results of these simulations will be presented in this section. Some general observations about the behavior of the materials will be discussed, followed by a review of the sensitivity parameters, and finally presentation of some additional results. The full set of results may be found in Appendix L and on the included CD-ROM (Appendix M). Some of the discussion in this section refers to pyrolysis/burnout front graphs. Because the interpretation of these graphs is not

necessarily intuitive, explanation of a typical pyrolysis/burnout front graph may be found in Appendix I.

6.3.1 – General Observations

The results of the simulations can be broken down into two distinct groups. The simulated behavior of the non-fire-retarded material (polyester) constitutes one group, and the fire retarded (FR) materials fit into another group.

The simulated behavior of the marine grade polyester composite (material #8) follows the experimental curve quite well, as shown by the baseline curve in Figure 6-3 (20-30% error). The fire growth on this material is quite rapid, as the heat release rate reaches 1MW roughly 30-40 seconds after ignition, which is faster than the typical description of an ultra-fast fire growth rate (75 seconds). Note that the entire wall is burning and the ceiling ignites about 15 seconds after ignition. The rapid growth beyond this time is a function of the burning elements reaching the peak burning rate from the Cone Calorimeter curve, and the rapid growth across the ceiling elements. Unlike the wall elements, the ceiling elements increase in area the further they are from the corner. This characteristic of the algorithm is important to remember when examining spread

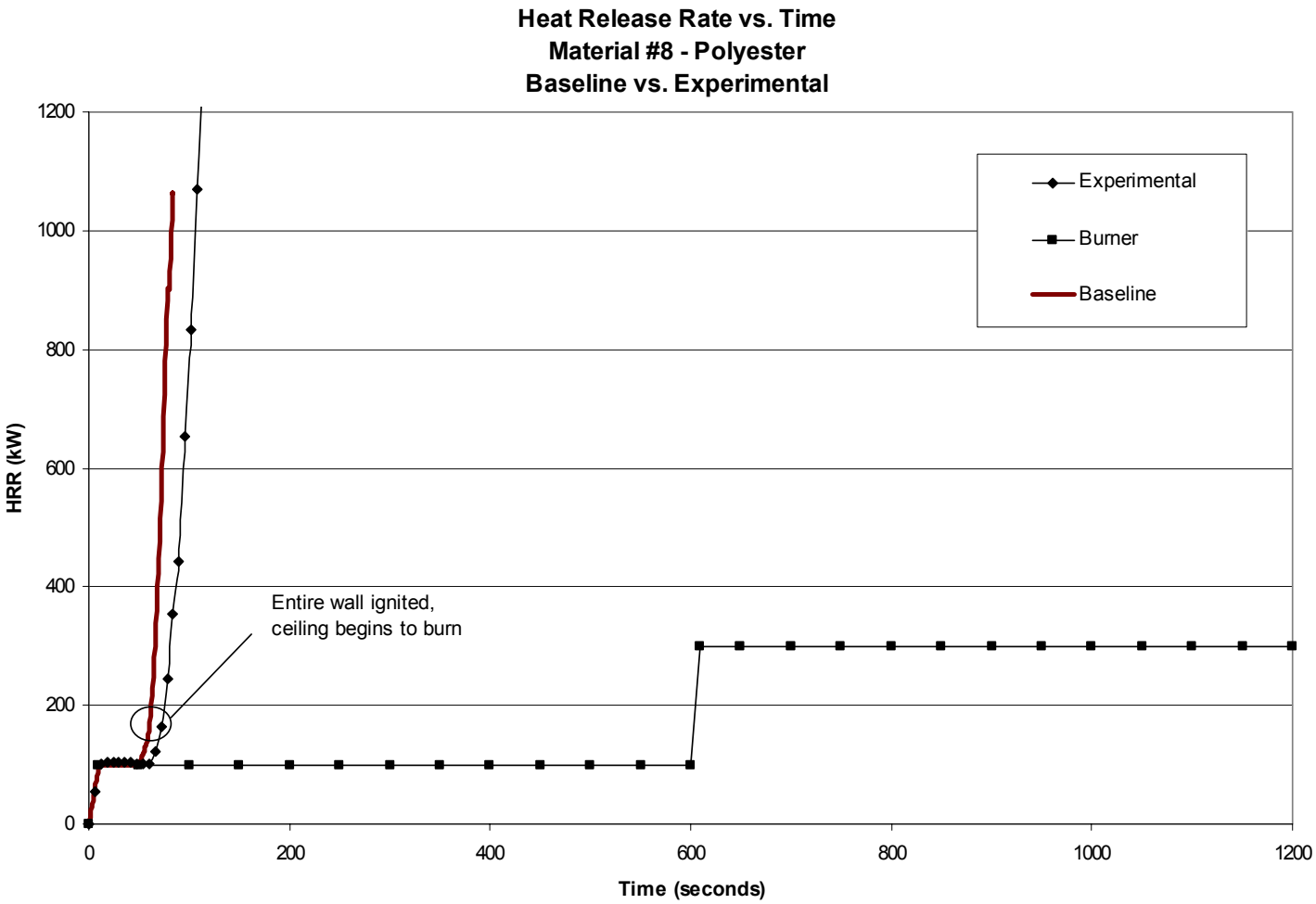

Figure 6-3 – Baseline simulation for material #8 (polyester) versus the experimental data

across the ceiling and the resulting rate of heat release because the larger elements will produce a greater amount of heat release. The peak heat release rate from the Cone Calorimeter is quite high for this material (~350kW/m^2), and is probably the most dominant factor in its rapid fire growth. Some slight variations occur when varying the parameters in the sensitivity matrix, however the general curvature of the simulation remains similar to the baseline in Figure 6-3 through all of the simulations for this material.

The simulated behavior of the fire-retarded (FR) composite materials (material #3, #4, and #9) is quite different from the marine grade polyester composite. Figure 6-4 shows the baselines versus the experimental heat release rate curves for the FR materials. The figure shows that material #3 and #4 do not match the experimental curves except near ignition, and material #9 matches the experimental curve only marginally well. All of these materials exhibit the same general behavior, with some variations caused by the changes outlined in the sensitivity matrix. The baseline simulation in Figure 6-5 may be used to explain this behavior. After ignition, a period of sustained growth occurs as flame spreads over the area of high heat flux on the wall, followed shortly by the spread of flame over the area of constant heat flux specified by the heat flux map (115 seconds to 180 seconds). Figure 6-6 shows the flux distribution at various times. The location of high flux is followed by a location of constant flux that ends at a height of about 2.6m (radius of 0.35m on the ceiling). Figure 6-7 shows the pyrolysis and burnout front locations versus time. The initial rapid growth occurs from 115 seconds to 180 seconds, ending at approximately 2.6m. Because the high/constant flux and initial rapid growth end at approximately the same location on the ceiling, the initial growth is a direct result of the initial flux distribution.

The next part of the curve (180 to 600 seconds in Figure 6-5) is representative of slow flame spread across the ceiling coupled with nodes beginning to burn based on the decay portion of the Cone Calorimeter curve (see Figure 6-2).

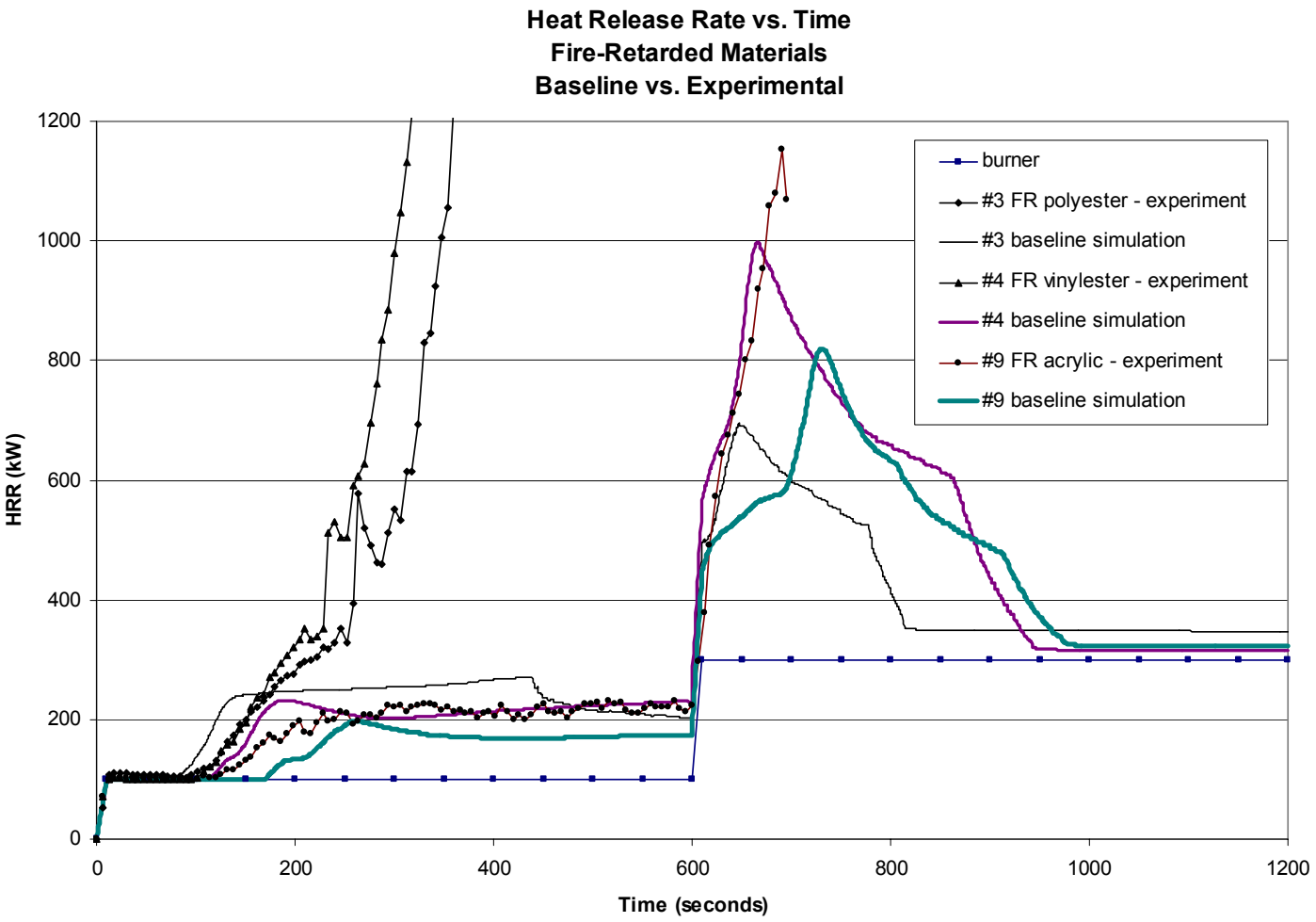

Figure 6-4 – Baseline simulations for the fire-retarded materials versus the experimental data

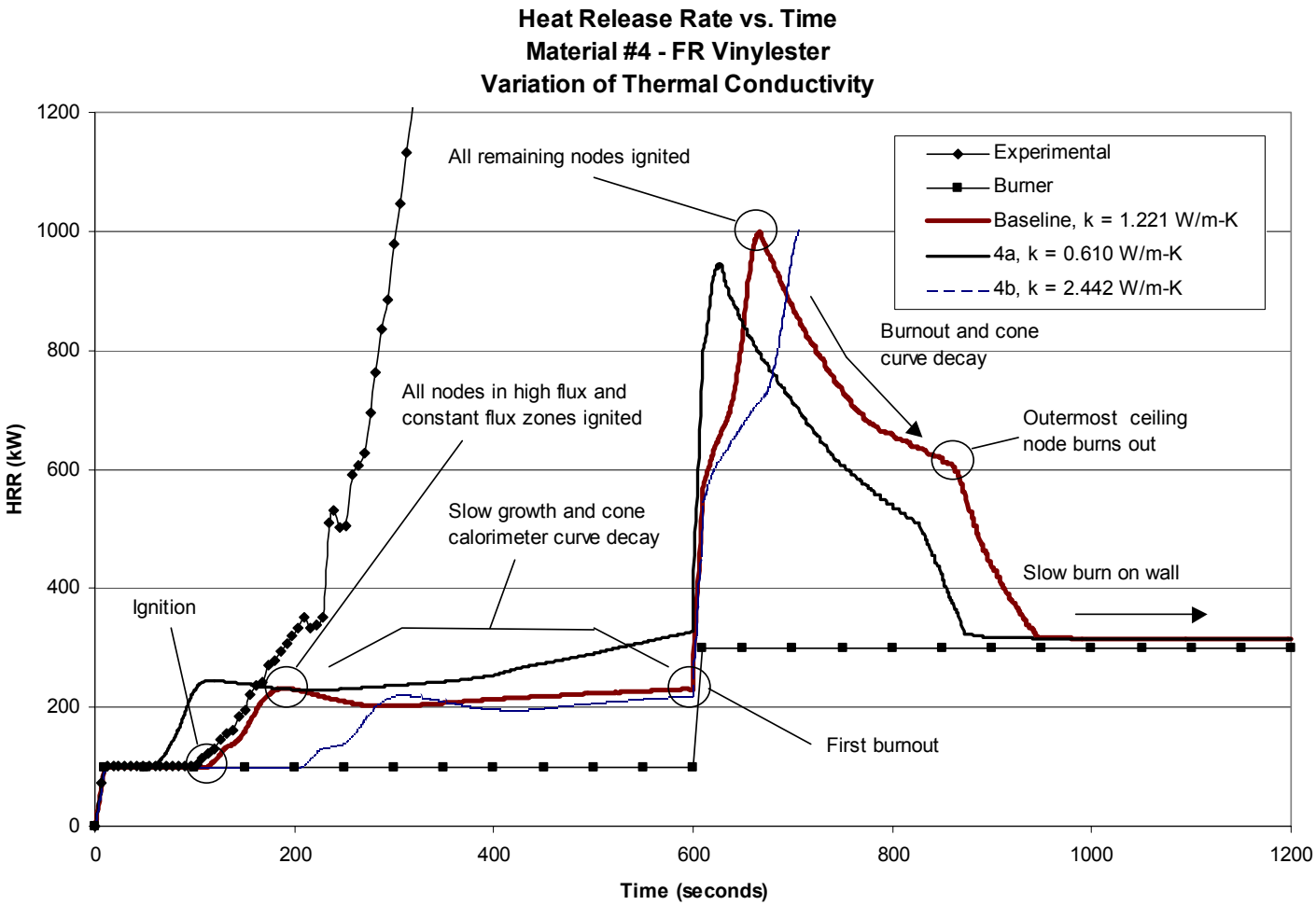

Figure 6-5 – Description of general behavior of simulated fire-retarded materials

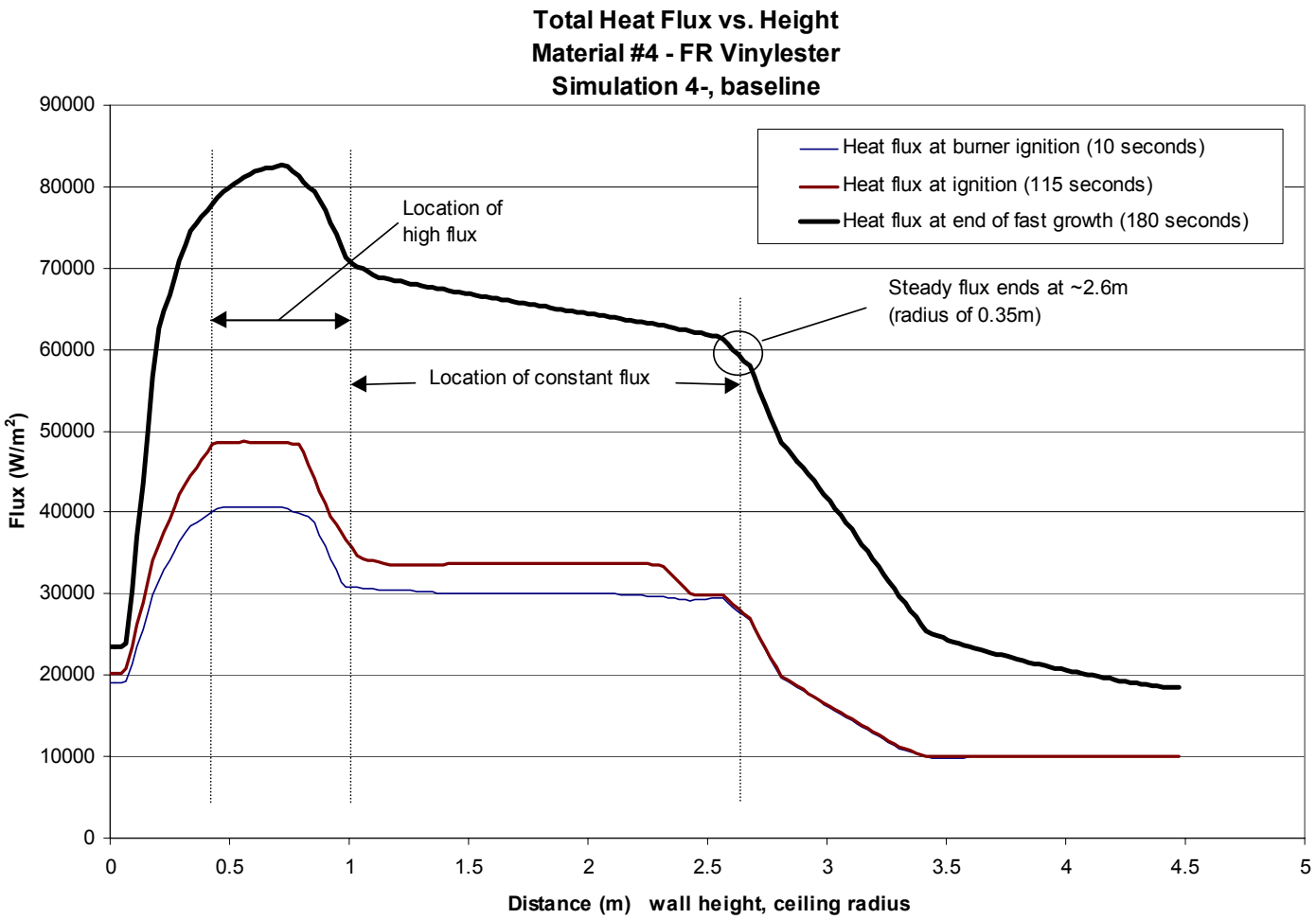

Figure 6-6 – Total flux versus height for material #4 (FR vinylester)

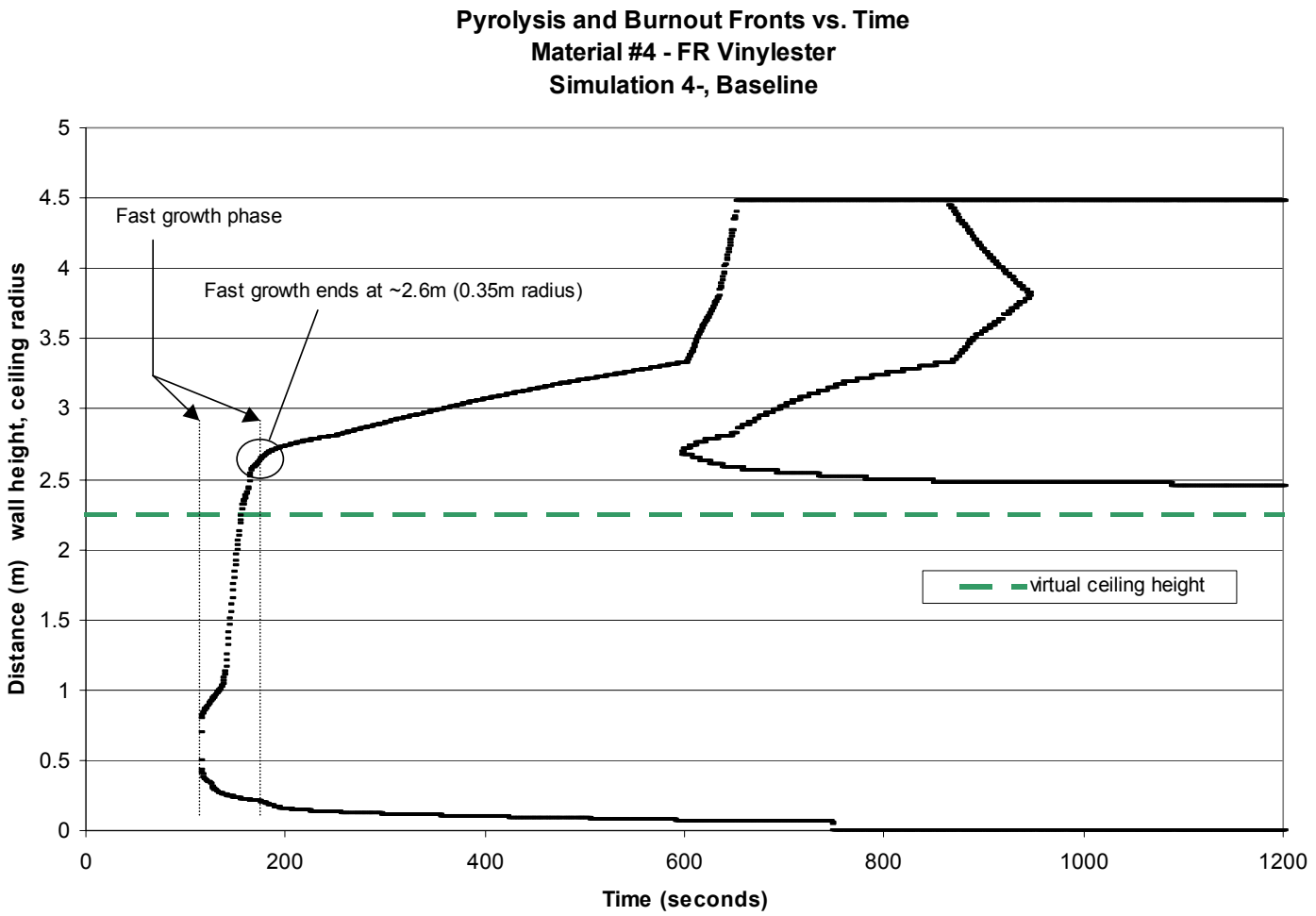

Figure 6-7 – Pyrolysis and burnout fronts for material #4 (FR vinylester)

The result was generally a slower rate of heat release rate growth, or a slight decay in some cases. Additionally, the first occurrence of burnout was frequently simulated during this time period, typically after 400 seconds. The burnout simulated by the algorithm also tends to occur more rapidly on the ceiling as opposed to the wall as illustrated in Figure 6-7 (i.e. the ceiling releases a greater amount of energy in a shorter period of time).

The third part of the baseline heat release rate curve in Figure 6-5 captures the behavior of the material when the ignition burner is increased from an output of 100kW to 300kW. In a typically short span of time (600 to 675 seconds in the example figure), the remaining non-burning nodes ignite. If burnout did not happen before 600 seconds, it generally occurs during this segment of the curve. Note that the slope of heat release rate growth in this segment is also quite steep. This is similar to the slope shown for material #8 in Figure 6-3 after the entire wall is burning. In the baseline case of Figure 6-5, the rapid growth after the burner heat release rate increase is a direct result of the ignition of all remaining nodes and the increasing size of the elements across the ceiling as described previously.

The last segment of the baseline curve in Figure 6-5 (675 to 1200 seconds) characterizes additional burnout and continued burning of nodes based on the decay portion of the Cone Calorimeter curve.

The following sections describe the individual effects of the parameters varied in the sensitivity matrix.

6.3.2 – Thermal Conductivity

The main effect of changing thermal conductivity for all materials was a delay or advance in the ignition time, indicated by Figure 6-8. As shown in the figure, a decrease in thermal conductivity causes ignition to occur at an earlier time. This is because the diffusion of heat through the wall is inhibited, leading to a more rapid surface temperature increase, and hence earlier rise to the ignition temperature. The diffusion of heat though the wall is sufficiently small enough in the example case (3a) that all nodes ignite before the time of increased burner heat release rate. In case 3a, it is interesting to note that although the ceiling nodes ignite quickly in this case, rapid growth does not result as for material #8 in Figure 6-3. This is a result of the Cone Calorimeter curve because the peak heat release rate is lower in magnitude and occurs for only a short period of time (see Figure 6-1).

An increase in thermal conductivity has the opposite effect, as heat readily diffuses through the wall (Case 3b in Figure 6-8). The surface temperature rises more slowly, leading to delayed ignition and fire growth.

A secondary effect of changing the thermal conductivity also exists. When ignition is delayed, a greater amount of unburned material remains at the time when the ignition burner is increased to 300kW. This promotes a longer burning time of the material after the heat release rate increase to the burner. This effect was found only for materials #3, #4, and #9.

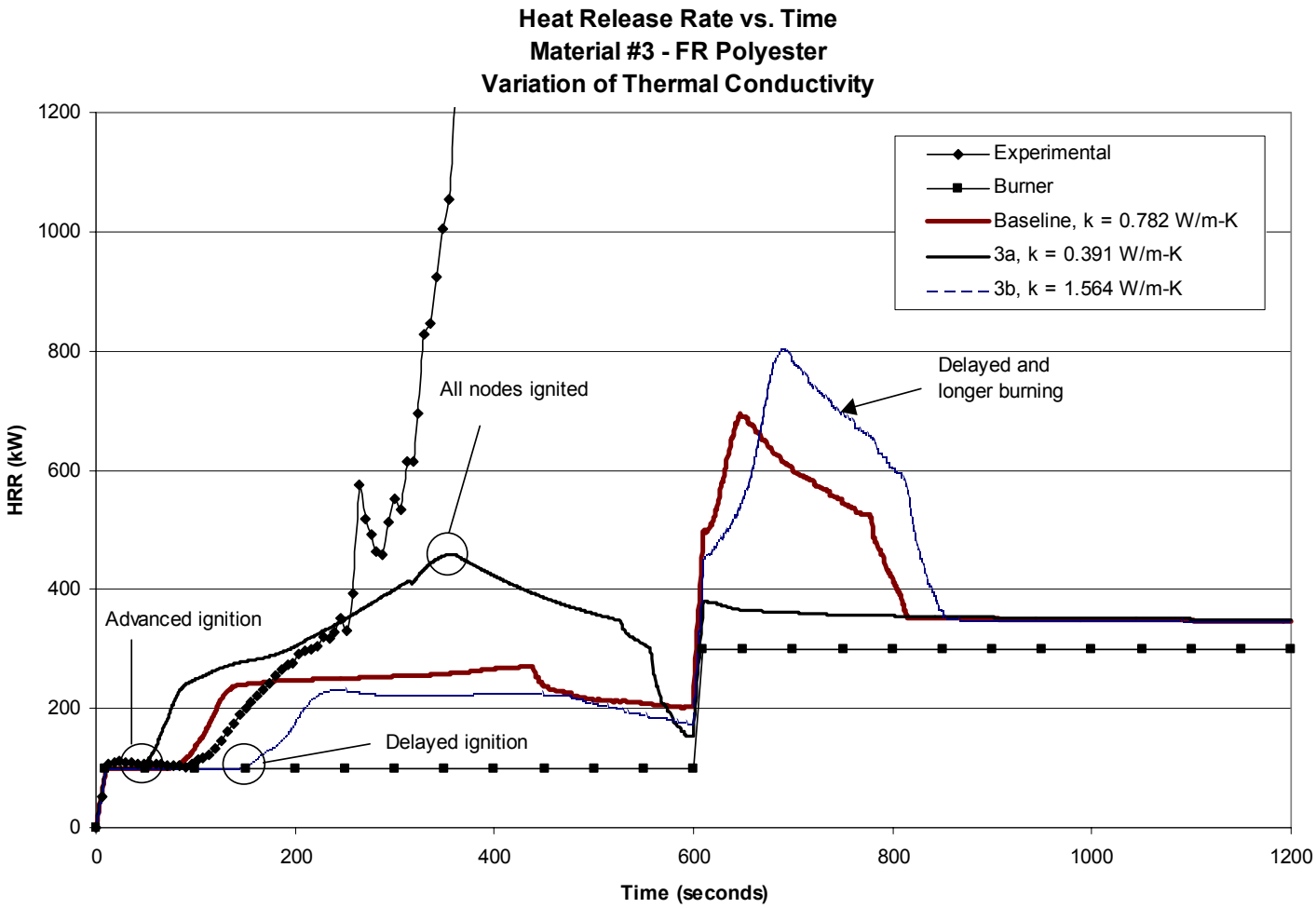

Figure 6-8 – Variation of thermal conductivity for material #3 (FR polyester)

6.3.3 – Cone Calorimeter Curve

The variation of the Cone Calorimeter curve is clearly important, as shown by case 4c in Figure 6-9. Except for the non-FR polyester based material (#8), all of the low-irradiance Cone Calorimeter curves produced significant effects, similar to the one shown in Figure 6-9. Evidently, rapid burnout occurs in these cases. Figure 6-10 confirms this observation by showing the pyrolysis fronts are indeed followed shortly by a burnout front. This rapid burnout is a direct result of the Cone Calorimeter curve for material #4 at 25kW/m^2 shown in Figure 6-11. Note that very little area exists under this curve, leading to a small initial mass at each node and thus rapid burnout. Also important in this simulation is the relative burn time of the wall in comparison with the ceiling. The material on the ceiling is consumed extremely rapidly (some nodes burn for less than 1 minute), indicating that the method of calculation of mass loss on the ceiling may be flawed. As described in Chapter 5, the mass loss rate for each pyrolyzing element is scaled based on its width versus an average width of all the pyrolyzing elements. As an increasing number of larger ceiling elements begin to burn, their width (arc-length) becomes increasingly larger than the average width. Thus, the scaling factor for these elements becomes larger and the elements are likely to being losing mass at an unrealistic rate.

Similar results are found for material #3 and #9, although the effect is less prevalent for material #9. Material #8 did not show significant variation between the different Cone Calorimeter curves.

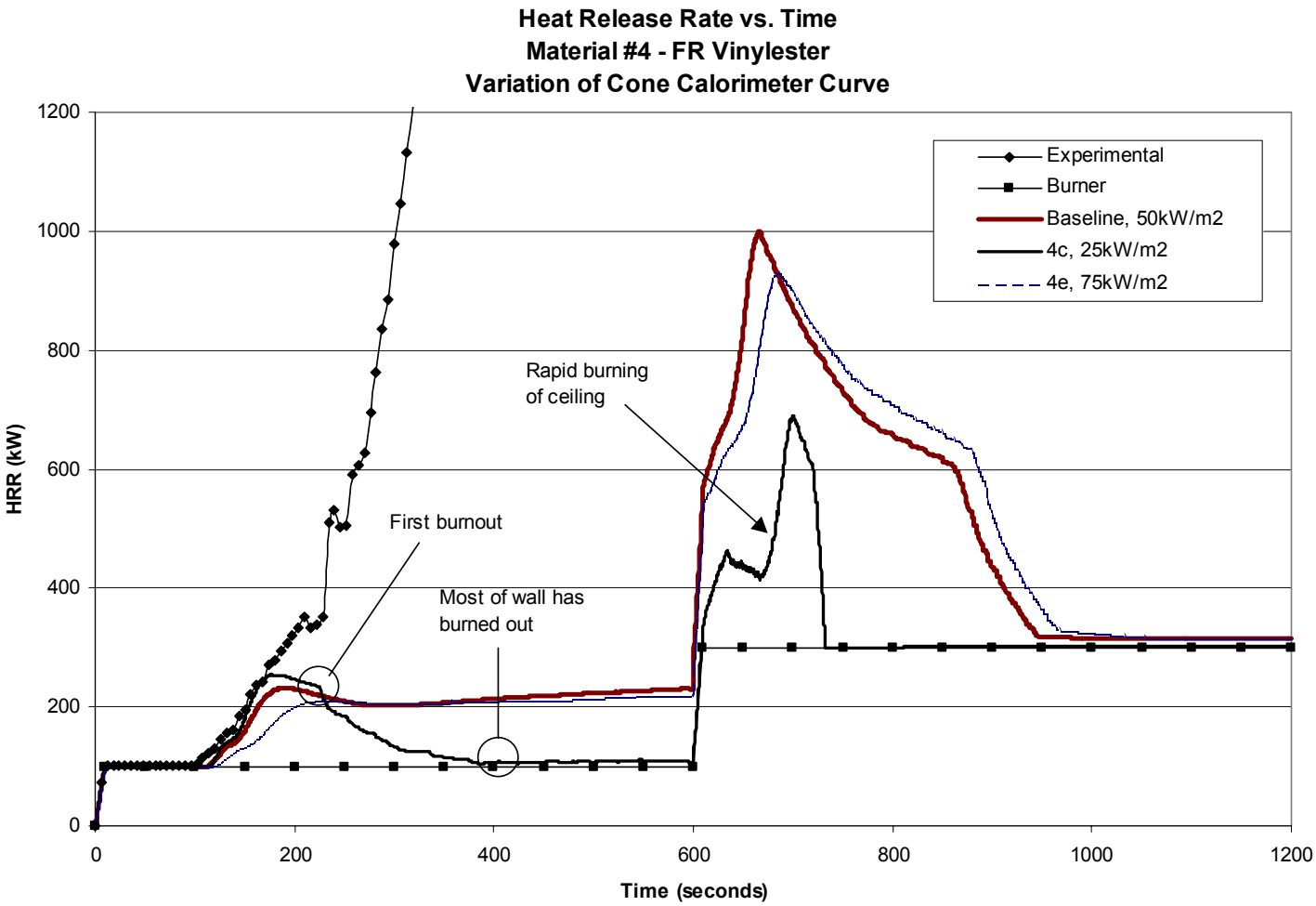

Figure 6-9 – Variation of Cone Calorimeter curves for material #4 (FR vinylester)

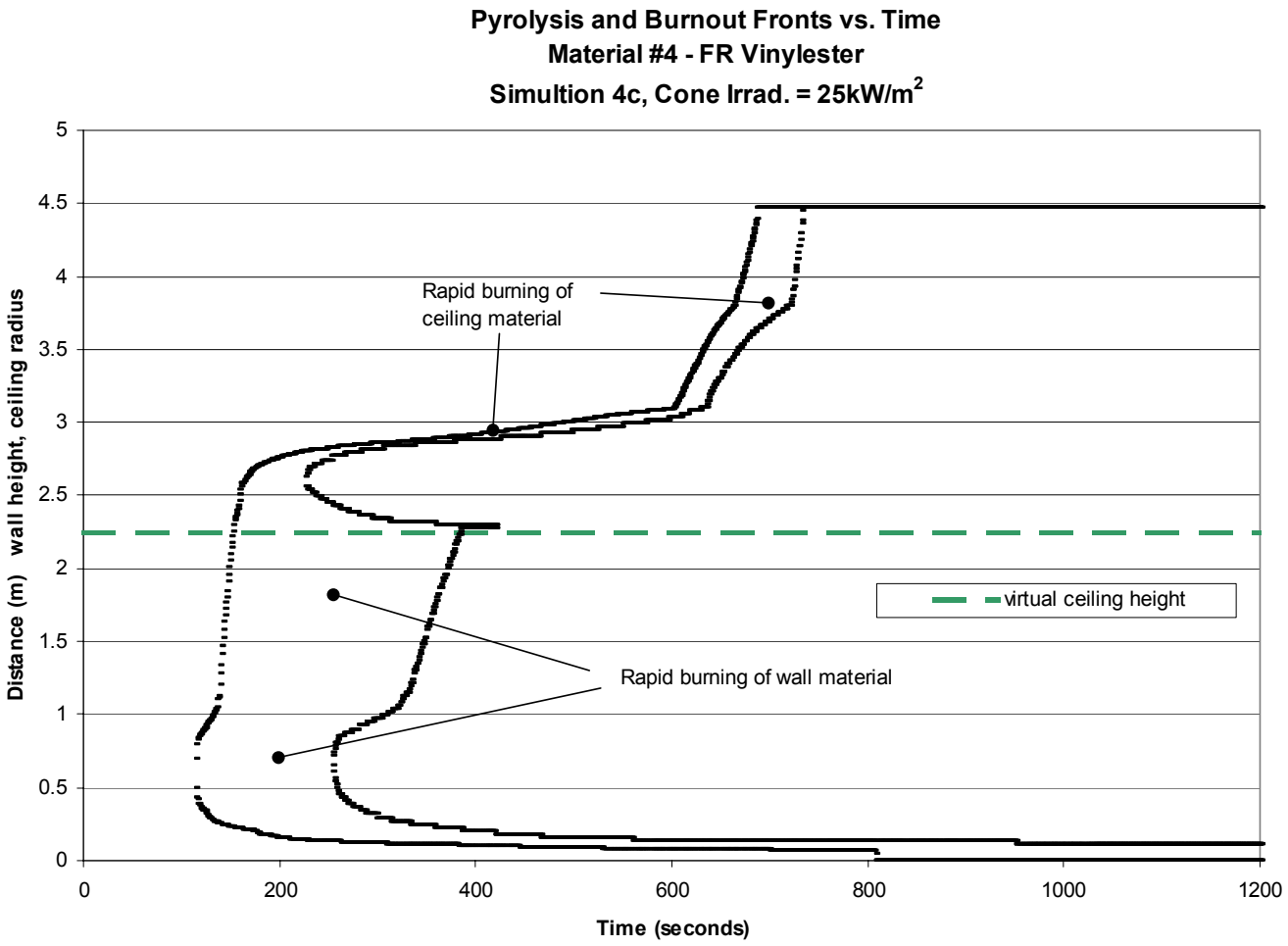

Figure 6-10 – Pyrolysis and burnout fronts for material #4 using 25kW/m^2 irradiance in the Cone Calorimeter data

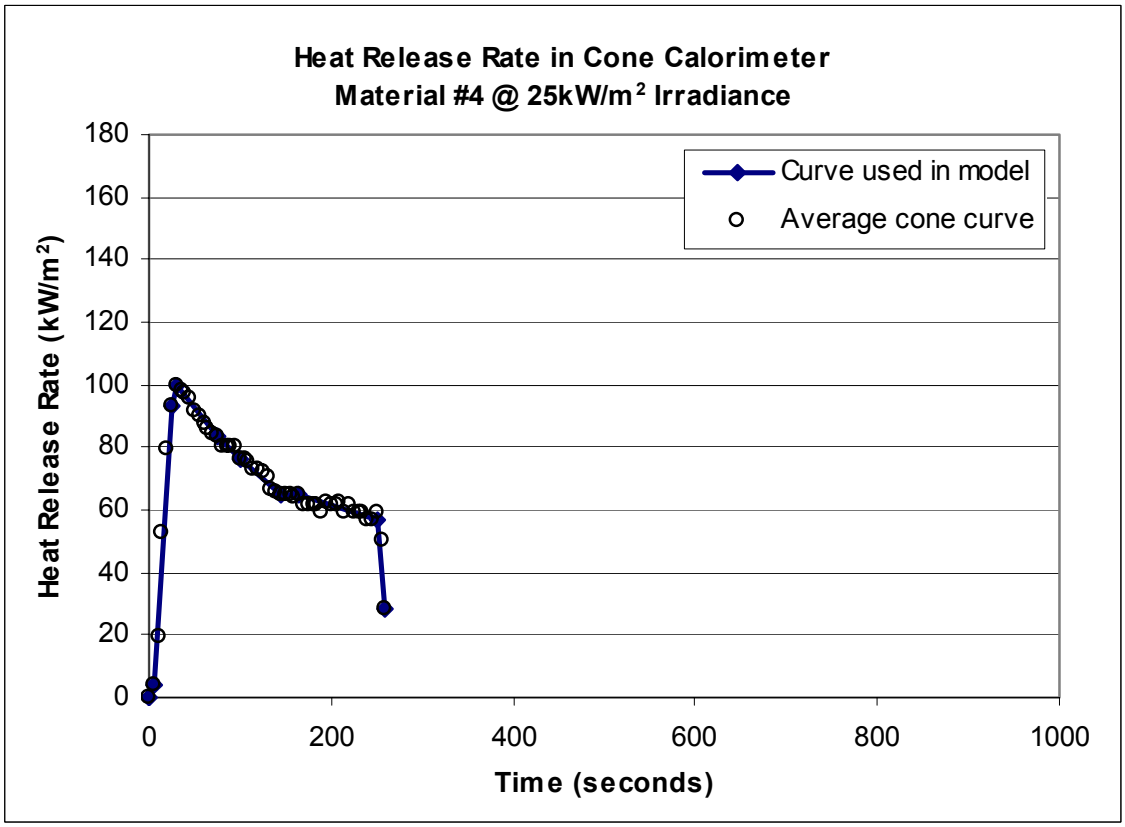

Figure 6-11 – Cone Calorimeter curve for material #4 at 25kW/m^2

6.3.4 – Emissivity and Flame Transmissivity

Variation of material emissivity and flame transmissivity did not produce a significant effect. Figures 6-12 and 6-13 show the variation of these parameters for material #9, where the alteration of these variables clearly had little impact. The other materials reacted in a similar fashion to these changes.

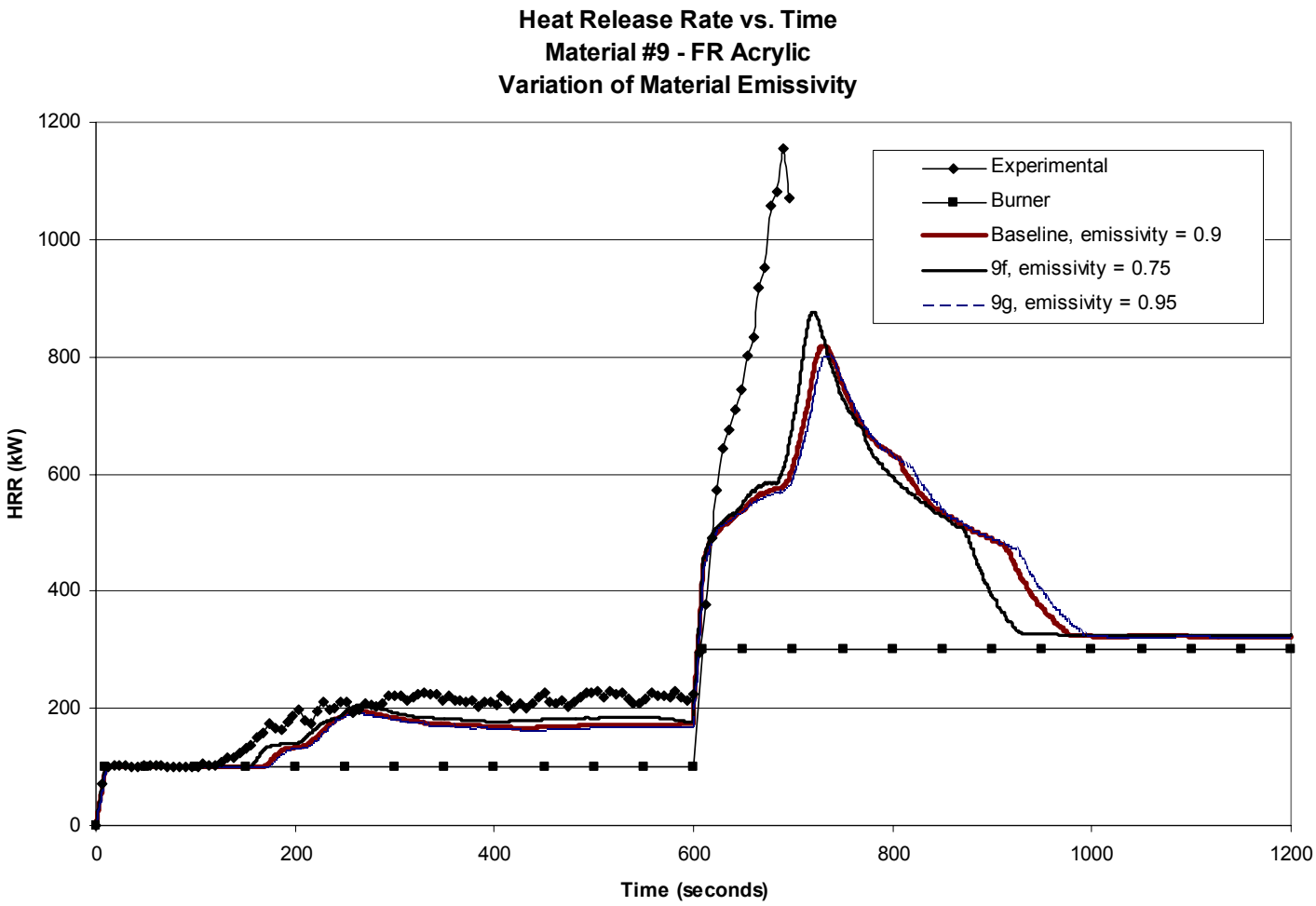

Figure 6-12 – Variation of material emissivity for material #9 (FR acrylic)

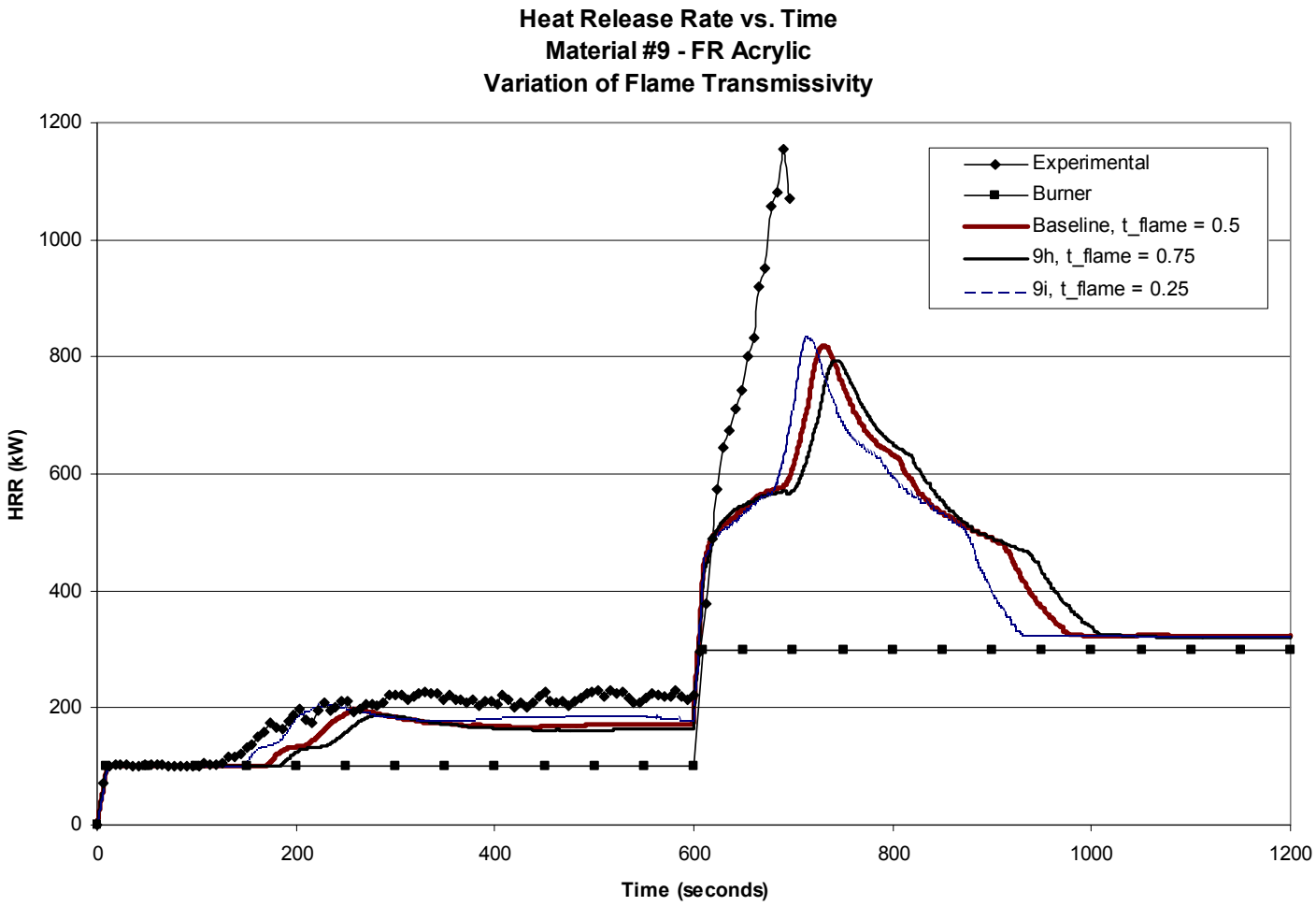

Figure 6-13 – Variation of flame transmissivity for material #9 (FR acrylic)

6.3.5 – Ignition Temperature

Variation of the ignition temperature produced very similar effects as the variation of thermal conductivity. A lower ignition temperature produced faster ignition, subsequent fire growth, and burnout, while a higher ignition temperature produced delayed ignition and more sustained burning. This is shown in Figure 6-14.

6.3.6 – Lateral Flame Spread Parameters

Variation of the minimum temperature for lateral flame spread and the flame spread parameter showed no effects in the conducted simulations. The results presented in Figures 6-15 and 6-16 are typical for all the materials simulated.

6.3.7 – Additional Results

In addition to the sensitivity study, the algorithm was tested for numerical stability. This was accomplished by varying the time-step used for the simulation. The baseline simulation for material #8 (polyester) was tested at numerous time-steps, ranging from 0.05 seconds to 2.0 seconds. The results are presented in Figure 6-17. Note that the time-scale has been reduced to 600 seconds in this case to reveal the effects more clearly. As shown in the figure, variation of the time-step had very little impact except when the time-step became large (2.0 seconds). The consistency of results at small time-steps indicates that the program is numerically stable.

The overall prediction of the behavior of the fire-retarded materials was not accurate, particularly for material #3 and #4. One reason for this could be that the results of the small-scale experiments and the resulting derived material properties do not capture the full-scale behavior of the fire-retardants present in these materials.

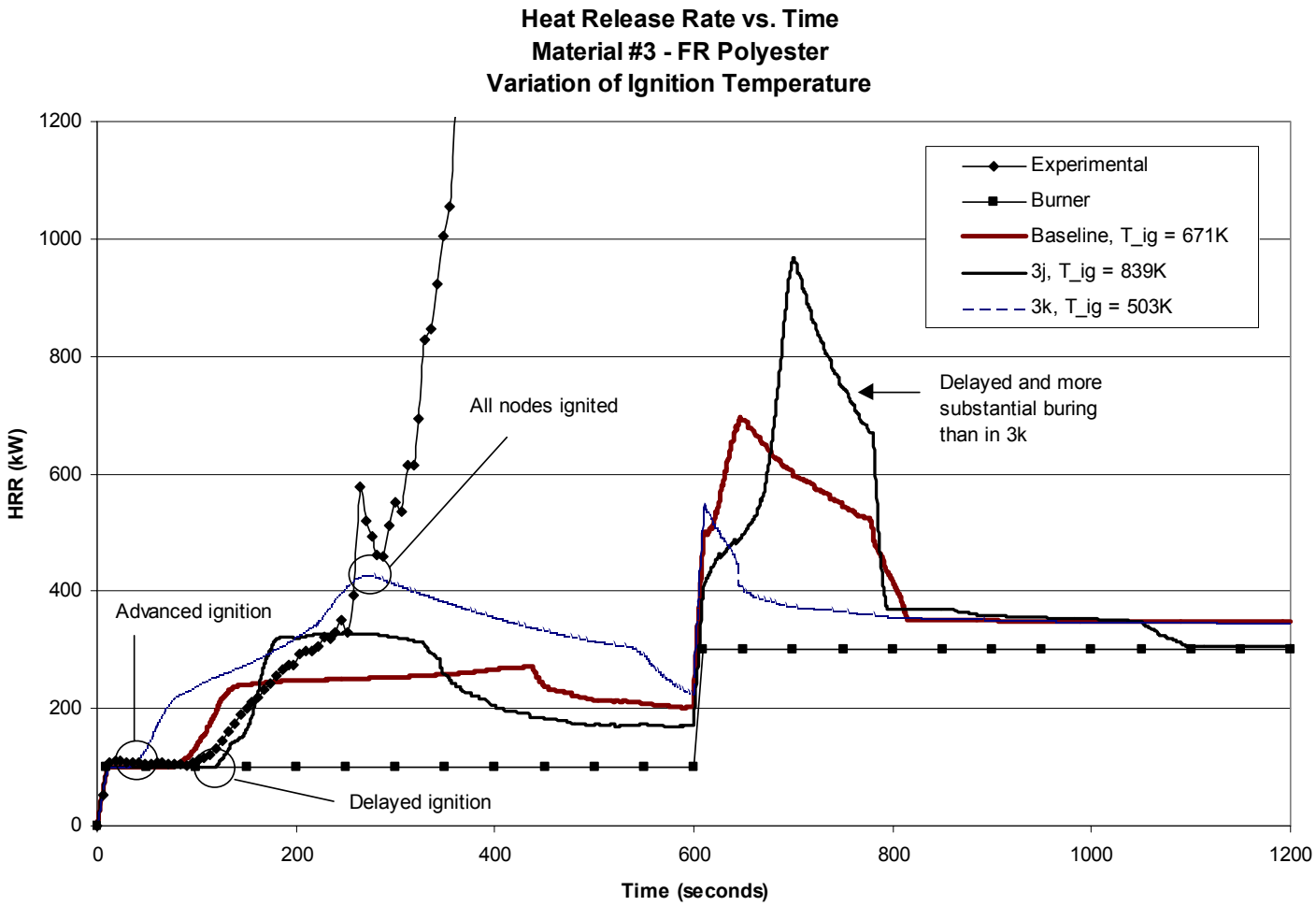

Figure 6-14 – Variation of ignition temperature for material #3 (FR polyester)

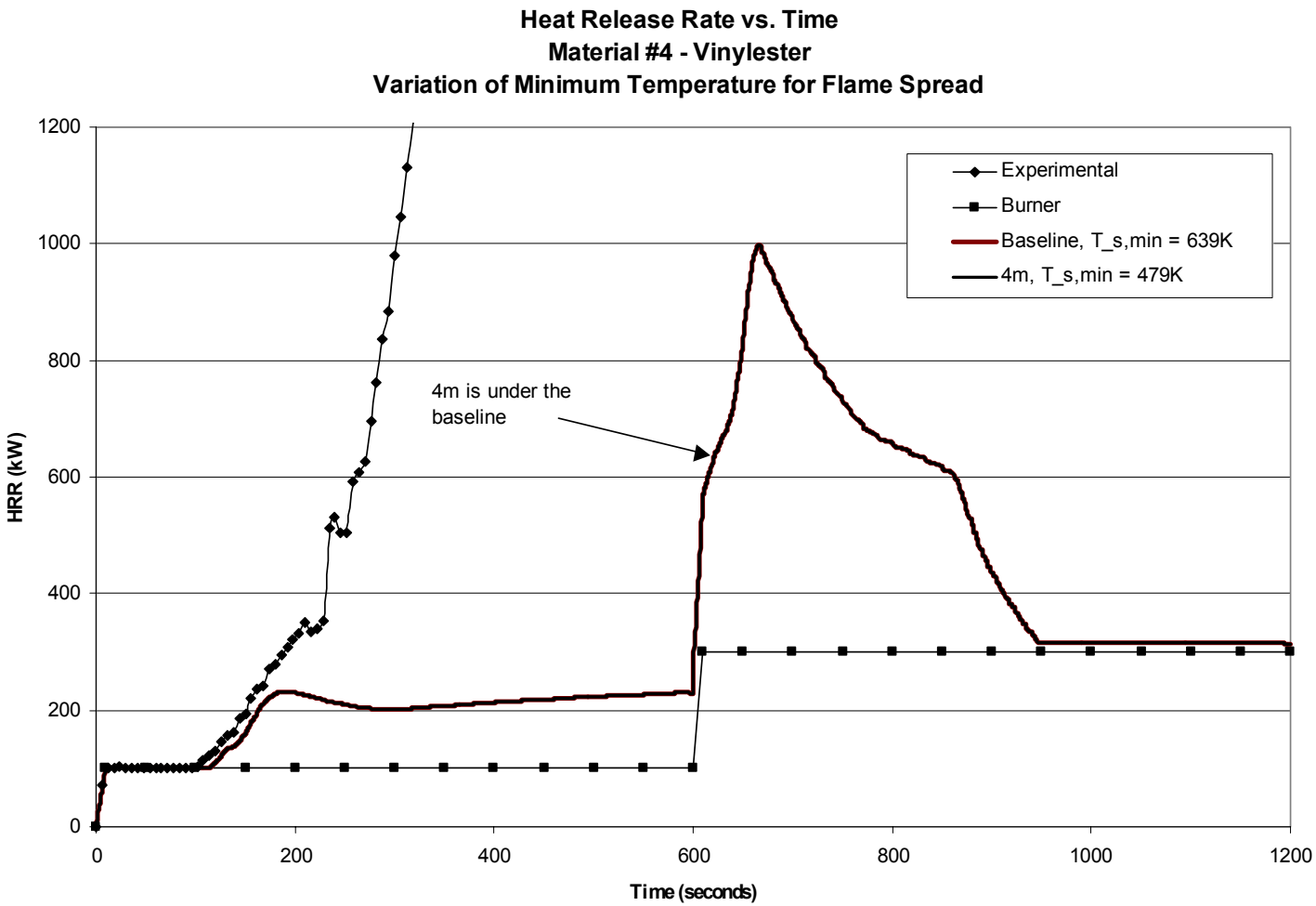

Figure 6-15 – Variation of minimum temperature for lateral flame spread for material #4 (FR vinylester)

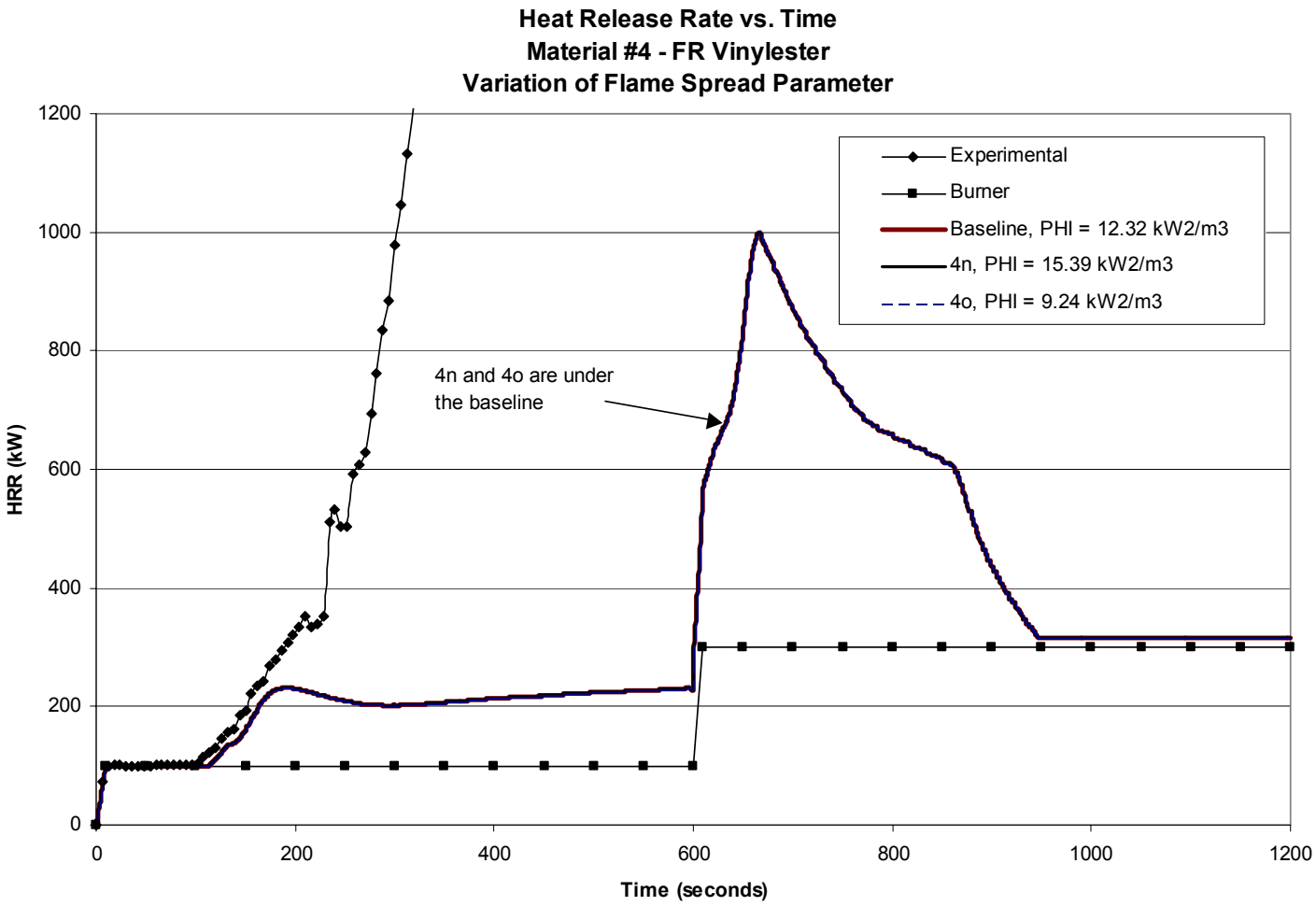

Figure 6-16 – Variation of the flame spread parameter (Φ) for material #4 (FR vinylester)

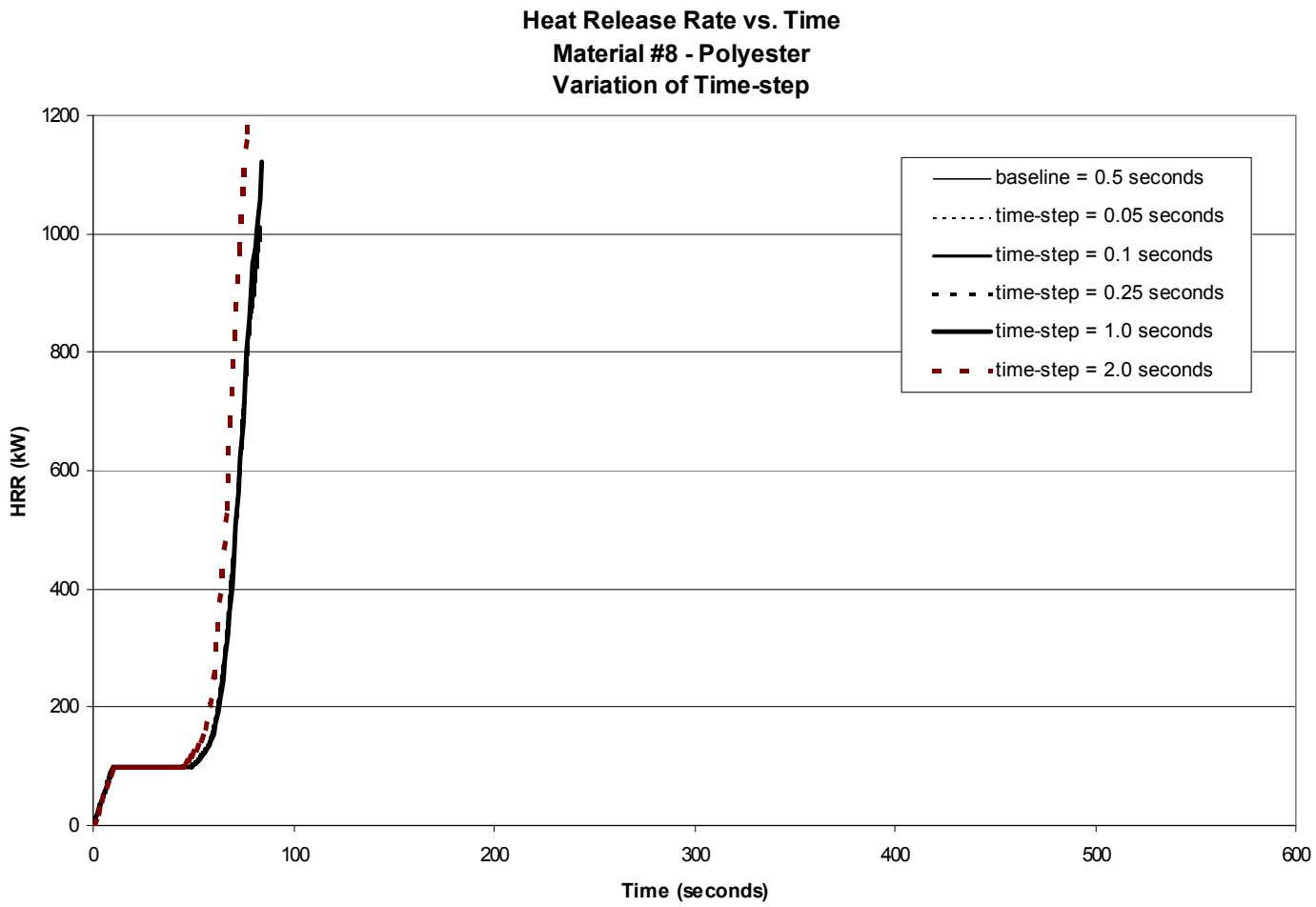

Figure 6-17 – Variation of time-step to demonstrate numerical stability using material #8 (polyester)

Figure 6-18 shows the experimental results from material #3 and #4, indicating potential times where the fire-retardants may be active. Note that there is overlap in the suggested times, as there is a fair degree of uncertainty in the behavior of the fire-retardants. Material #9 is not shown because the fire-retardants appear to have a more constant effect until the time when the heat release rate of the burner is increased and are quickly overcome after this time (see Figure 6-13). In order to test the hypothesis of fire-retardant effects, two additional simulations were conducted. A Cone Calorimeter curve from an equivalent non-fire retarded material was substituted for the fire-retarded Cone Calorimeter curves of materials #3 and #4, to determine if the effects of the retardants could be "removed" from the simulation. The Cone Calorimeter curve for material #8 was substituted for the original material #3 curve, since material #8 is a non-fire retarded, polyester based composite. The substitute for the material #4 Cone Calorimeter curve was taken from a composite material in Jacoby's[17] work that was a non-fire retarded, vinylester based composite material (8mm thick, with a ceramic fiberboard backing). The remaining material properties were unchanged. The new Cone Calorimeter curves used for material #3 and #4 are shown in Figures 6-19 and 6-20. The resulting simulations for material #3 and #4 are presented in Figures 6-21 and 6-22, respectively.

The results from the change in cone curve for material #3 do not offer much support for the hypothesis. Using the cone curve from material #8 causes material #3 to be simulated in a manner very similar to the original baseline for material #8. In this case the Cone Calorimeter curve clearly dominates the simulation because the peak heat release rate is of greater magnitude and has a longer duration. Thus it is difficult to determine the effect of the fire retardant for this material.

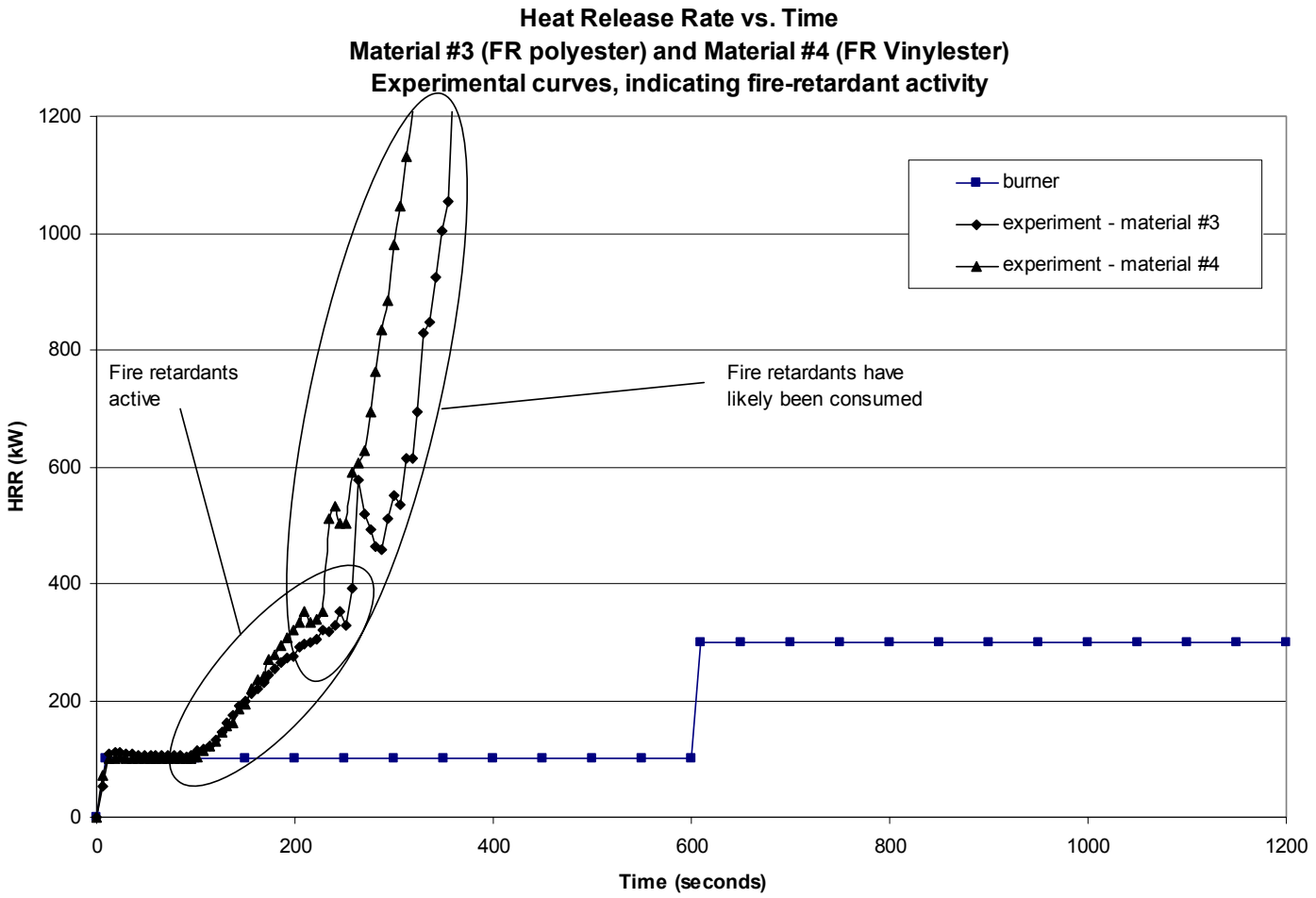

Figure 6-18 – Indication of possible fire-retardant activity for material #3 and #4

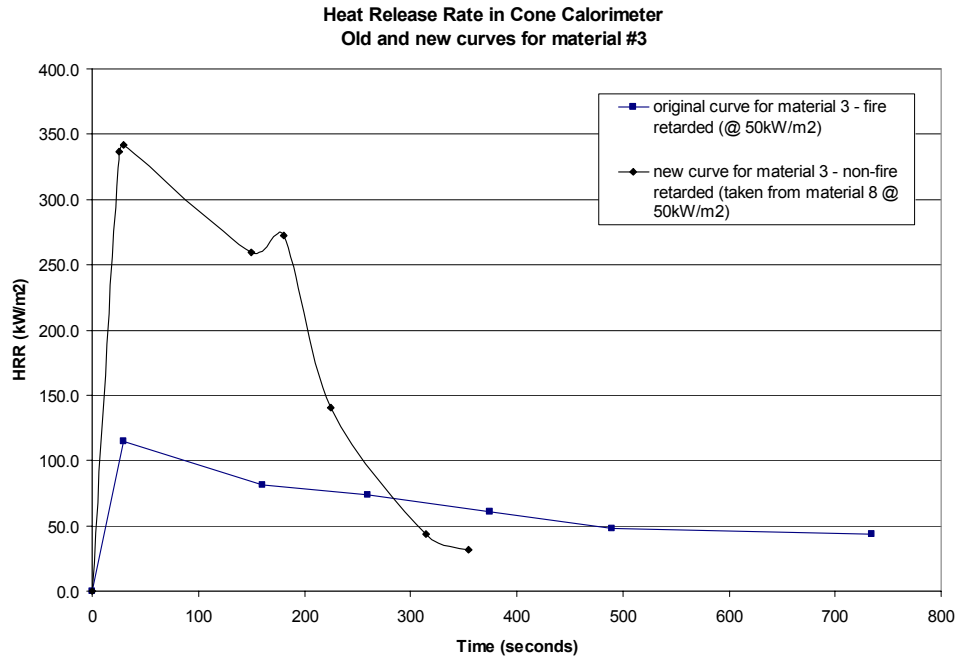

Figure 6-19 – Change of Cone Calorimeter curve for material #3

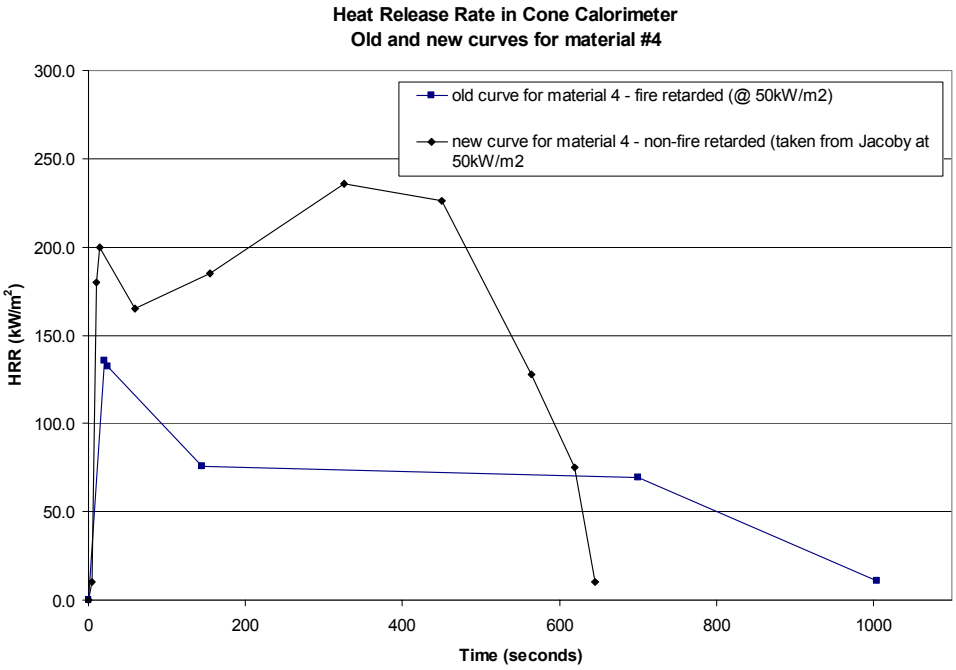

Figure 6-20 – Change in Cone Calorimeter curve for material #4

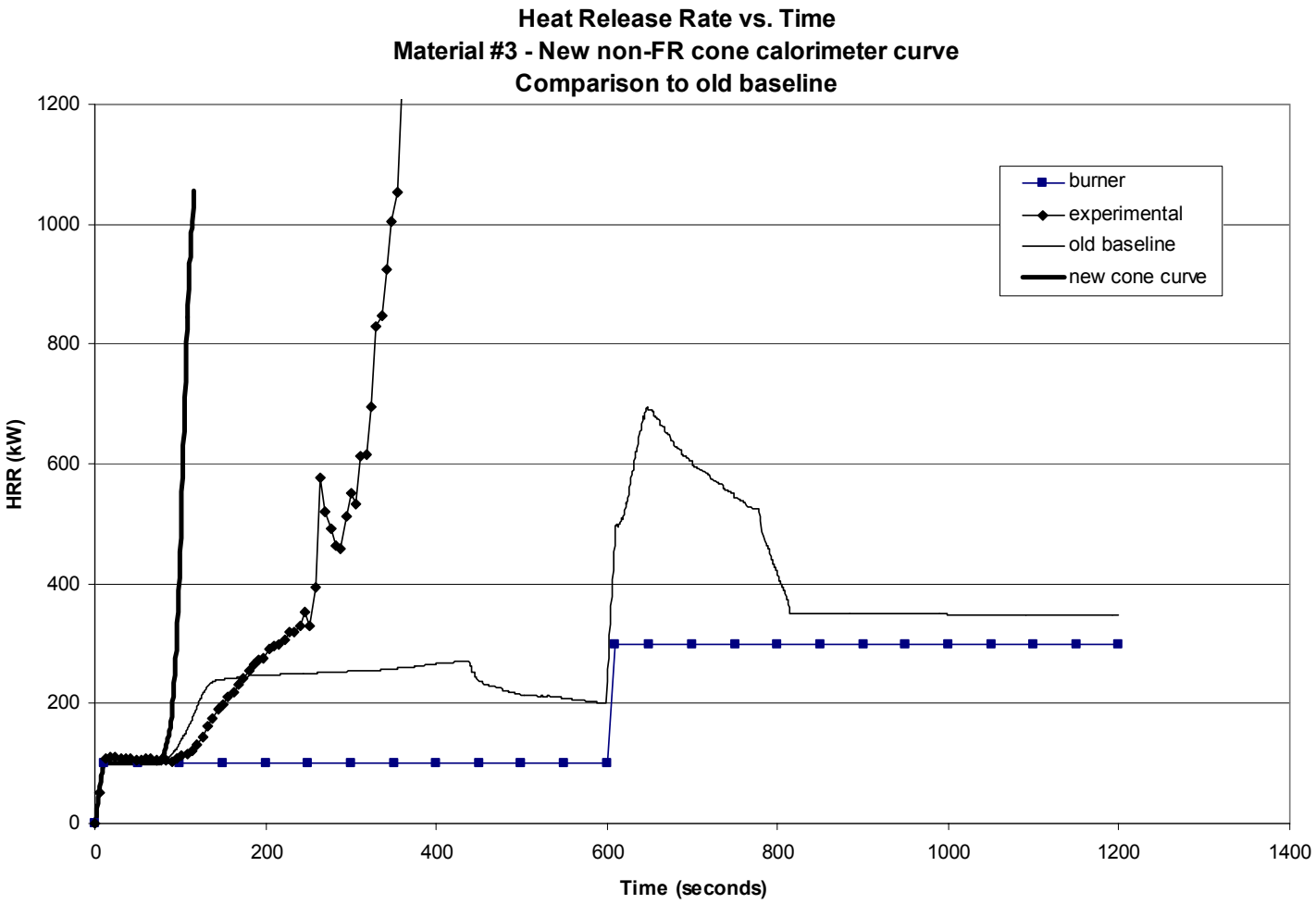

Figure 6-21 – Results from non-fire retarded Cone Calorimeter curve for material #3

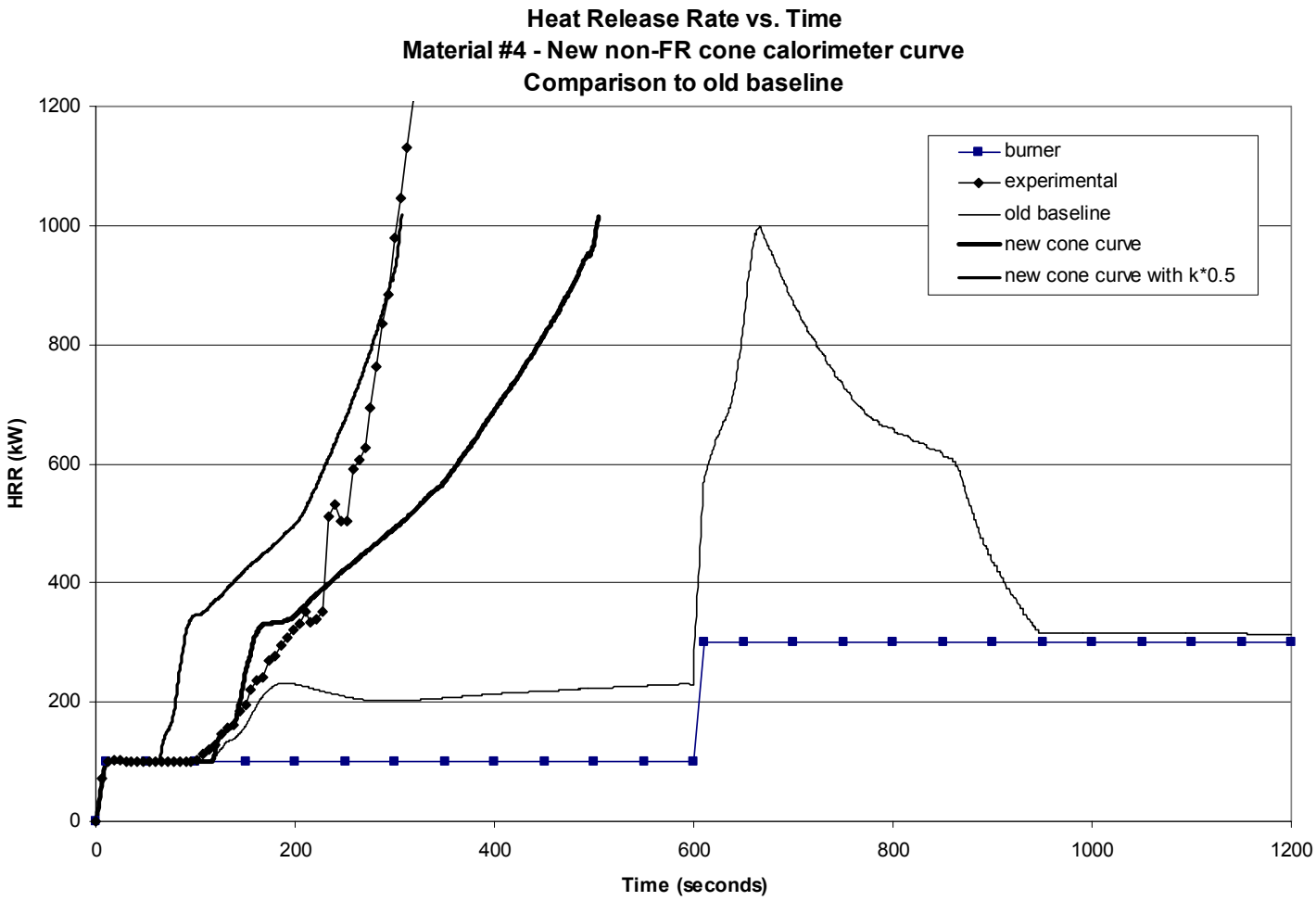

Figure 6-22 - Results from non-fire retarded Cone Calorimeter curve for material #4

The new heat release rate result for material #4 shows more interesting results. The heat release rate continues to grow after the ignition of the high/constant flux zone, instead of leveling off or decaying slightly as in previous simulations. This observation indicates that the simulated effect of the fire-retardant may have been removed, but the slope of the continued growth is still too shallow in comparison with the experimental curve. The possibility exists that one of the material parameters could still be incorrect, so the thermal conductivity was decreased by a factor of two. This change was made to determine if the slope of the continued growth could be corrected. The result is shown in Figure 6-22. The ignition time is advanced as expected, and the slope of this new curve near flashover matches the experimental curve more closely (flashover is also nicely predicted in this simulation). However these results are considered general in scope, as the complex behavior of the fire retardant is probably based on a combination of the factors presented. More research on the effects and modeling of fire retardants is clearly necessary in order to draw any firm conclusions.

7.0 Conclusions and Recommendations

This paper has described the selection, development, and testing of a corner flame spread algorithm embedded within a zone model, used to simulate the behavior of marine composite materials in an ISO 9705[16] room corner configuration. This section presents conclusions of the research and recommendations for future work.

7.1 Conclusions

A flame spread algorithm developed by Mitler[23,24] was selected out of a group of many algorithms to model the spread of flame over wall/ceiling linings in a room corner configuration. The selection was made primarily because this algorithm simulates compartment fire conditions and includes the most detailed representation of upward flame spread, pyrolysis, and distribution of heat flux from burner and wall flames to the wall/ceiling surfaces. The original algorithm was developed to simulate the spread of fire on a compartment wall away from a corner, so several modifications were necessary to correctly simulate the corner configuration. These changes included ceiling flame spread geometry (quarter-circular), flame height, enhanced radiation exchange, heat flux maps, and multiple pyrolysis zones. Once the algorithm was developed, it was implemented into the zone model CFAST.

Experimental data from several marine composite materials was obtained in order to evaluate the new algorithm. The four materials selected for this task had complete material property data sets and represented a variety of full-scale experimental results. These materials were based on polyester, fire-retarded (FR) polyester, FR vinylester, and FR acrylic composites. After developing a basic strategy for obtaining self-consistent input data for these materials, a sensitivity matrix of for changing important input parameters was created. Numerous simulations were conducted based on the sensitivity matrix to evaluate the new flame spread algorithm.

Out of the four materials simulated, only the non-fire retarded material matched the experimental curve to any degree of accuracy. All of the fire retarded materials showed varying degrees of deviation from the experimental curves. The FR polyester and FR vinylester demonstrated the greatest amount of deviation, while FR acrylic showed only modest deviation. These deviations were likely caused by the inability of the small-scale tests (with their derived parameters) to effectively capture the large-scale effects of the fire-retardants. The simulations conducted showed that the algorithm was most sensitive to the Cone Calorimeter curve, thermal inertia, and the ignition temperature. Additionally, the simulations revealed a potential problem with the algorithm's calculation of mass loss rate on the ceiling, as burnout occurred too quickly in some cases.

7.2 Recommendations for Future Work

Several tasks were identified that would be beneficial as follow-up work to this project. These are listed in descending order of importance as follows:

(1) The calculation of the mass loss rate on the ceiling must be examined. Currently, a weighting scheme (carried over from the original algorithm) is used in the

mass loss rate calculations. This scheme may be incorrect because of the circular geometry of the ceiling elements.

(2) The calculations for multiple pyrolysis fronts must also be checked. The algorithm currently calculates several parameters based on the height of a *single* pyrolysis zone. The validity of calculations (particularly flame height and heat flux) must be examined once multiple pyrolysis zones occur.

(3) There is an important need to study the role of fire retardants to determine a more effective way of modeling the complex behavior of these types of materials. One possible improvement might be a time-dependent combustion efficiency to describe the changing state of material combustion from the fire retardant.

(4) Additional "simple" materials should be modeled using the new flame spread algorithm. This would be helpful in verifying the capabilities of the algorithm. In this project only one such material was simulated, leaving the possibility that other issues concerning "simple" materials may still exist.

Note that although this algorithm was developed for the purpose of simulating the burning behavior of marine composites, it is certainly not limited to these materials. Simulation of particleboard, wood paneling, and similar materials could easily conducted using available small-scale data from the literature or experiments

(5) The assumptions made in the use of the heat flux map must be reviewed. The area of high flux near the ceiling was removed because the algorithm simulated ignition near the ceiling, while experimental observation showed ignition occurred further down on the wall. Experiments designed to determine why sustained ignition does not occur at the area of highest flux would be a good first step in attempting to implement the "real" heat flux map into the algorithm.

(6) Finally, there should be a check on the use of the flame transmissivity in the radiation network. This parameter was used as an approximation for calculating the attenuation of radiation as it passes through a flame. The possibility exists that the use of this factor does not conserve energy within the radiation network. If energy is not being conserved, the effects of this parameter may be removed by simply setting the value of this parameter to one.

References

[1] Ahmed, Gamal N., Mark A. Dietenberger, and Walter W. Jones. Calculating flame spread on horizontal and vertical surfaces. U.S. Dept. of Commerce. National Institute of Standards and Technology: Gaithersburg, MD. 1994.

[2] Alston, J., S. Ayers, T. Fay, C. Lautenberger, C. Prueher, and J. Watson. Flame Spread Modeling and Full-Scale Calibration. Worcester Polytechnic Institute: Worcester, MA. 1999.

[3] ASTM. Standard Test Method for Determining Material Ignition and Flame Spread Properties. ASTM E-1321-97a. American Society for Testing and Materials: West Conshohocken, PA. 1997.

[4] Bailey, J., G. Forney, W. Jones, and P. Tatem. Proceedings of the Fire Safety Conference on Performance Based Concepts. "Comparison of CFAST Predictions to Real Scale Fire Tests." Paper 25; Institut de Securite: Zurich, Switzerland. 1996. Pp 1-14.

[5] Baroudi, D., M. Kokkala, and W. Parker. Fire Safety Science – Proceedings of the Fifth International Symposium. "Upward Flame Spread on Wooden Surface Products: Experiments and Numerical Modeling." International Association for Fire Safety Science: 1997.

[6] Beyler, Craig L., Sean P. Hunt, Naeem Iqbal, and Frederick W. Williams. Fire Safety Science – Proceedings of the Fifth International Symposium. "A Computer Model of Upward Flame Spread on Vertical Surfaces." International Association for Fire Safety Science: 1997.

[7] Dillon, S. E. Analysis of the ISO 9705 Room/Corner Test: Simulations, Correlations, and Heat Flux Measurements. U.S. Dept. of Commerce. National Institute of Standards and Technology: Gaithersburg, MD. 1998.

[8] Drysdale, Dougal. An Introduction to Fire Dynamics. 2nd ed. John Wiley and Sons: Chichester, England. 1999.

[9] Grenier, A. T., Fire Characteristics of Cored Composite Materials for Marine Use. Worcester Polytechnic Institute: Worcester, MA. 1996.

[10] Grenier, A.T., N. A. Dembsey, and J. R. Barnett. "Fire Characteristics of Cored Composite Materials for Marine Use." *Fire Safety Journal*. V.30. 1998. Pp. 137-159.

[11] Hasemi, Y. and T. Tokunaga. "Some Experimental Aspects of Turbulent Diffusion Flames and Buoyant Plumes from Fire Sources Against a Wall and in a Corner of Walls." *Combustion Science and Technology*. V.40. 1984. Pp 1-17.

[12] International Maritime Organization. FTP Code: International Code for Application of Fire Test Procedures (Resolution MSC.61(67)). "Resolution MSC.40(64) – Standards for Qualifying Marine Materials for High-Speed Craft as Fire Restricing Materials (1994)." International Maritime Organization: London. 1998.

[13] International Maritime Organization. FTP Code: International Code for Application of Fire Test Procedures (Resolution MSC.61(67)). "Resolution A.653(16) – Recommendation on Improved Fire Test Procedures for Surface Flammability fo Bulkhead, Ceiling and Surface Finish Materials (1989)." International Maritime Organization: London. 1998.

[14] International Maritime Organization. International Code of Safety for High-Speed Craft. International Maritime Organization: London. 1995.

[15] International Organization for Standardization. International Standard ISO 5660: Fire Tests – Reaction to Fire – Part 1: Rate of Heat Release from Building Products (Cone Calorimeter Method). Reference number ISO 5660-1:1993. International Organization for Standardization: Geneva, Switzerland. 1993.

[16] International Organization for Standardization. International Standard ISO 9705: Fire Tests – Full-scale room test for surface products. Reference number ISO 9705:1993(E). International Organization for Standardization: Geneva, Switzerland. 1993.

[17] Jacoby, D. Ignition Characteristics of Marine Cored Composites: Effect of Skin Thickness and Core Composition. Worcester Polytechnic Institute: Worcester, MA. 1998.

[18] Janssens, M.L., A.Garabedian, and W. Gray. Establishment of international Standards Organization (ISO) 5660 Acceptance Criteria for Fire Restricting Materials Used on High Speed Craft. U.S. Dept. of Transportation. U.S. Coast Guard. Marine Safety and Environmental Protection (G-M): Washington, DC. 1998.

[19] Karlsson, Björn. Modeling Fire Growth on Combustible Lining Material in Enclosures. Lund University: Sweden, 1992.

[20] Kulkarni, A. K., E. Brehob, S. Manohar, and R. Nair. Turbulent Upward Flame

Spread on a Vertical Wall Under External Radiation. U.S. Department of Commerce. National Institute of Standards and Technology: Gaithersburg, MD. 1994.

[21] McCaffrey, Bernard. SFPE Handbook of Fire Protection Engineering. 2nd ed. "Flame Height." National Fire Protection Association: Quincy, MA. 1995.

[22] Mills, A. F. Heat Transfer. Irwin, Inc.: Boston,MA. 1992.

[23] Mitler, Henri E. and Kenneth D. Steckler. SPREAD – a Model fo Flame Spread on Vertical Surfaces. U.S. Dept. of Commerce. National Institute of Standards and Technology: Gaithersburg, MD. Written 1993, Issued 1995.

[24] Mitler, Henri E. An Algorithm to Describe the Spread of a Wall Fire Under a Ceiling. U.S. Dept. of Commerce. National Institute of Standards and Technology: Gaithersburg, MD. 1994.

[25] Ohlemiller T., S. Dolan. Ignition and lateral flame spread characteristics of certain composite materials. U.S. Dept. of Commerce. National Institute of Standards and Technology: Gaithersburg, MD: Center for Fire Research, 1989.

[26] Peacock, R. D., P. A. Reneke, W. W. Jones, and R. W. Bukowski. A User's Guide for FAST 3.0: Engineering Tools for Estimating Fire Growth and Smoke Transport. U.S. Department of Commerce, National Institute of Standards and Technology: Gaithersburg, MD. 1997.

[27] Peacock, R. D., G. P. Forney, P. Reneke, R. Portier, and W. W. Jones. CFAST, the Consolidated Model of Fire Growth and Smoke Transport. U.S. Department of Commerce, National Institute of Standards and Technology: Gaithersburg, MD. 1993.

[28] Saito, K., J. G. Quintiere, F. A. Williams. Upward Turbulent Flame Spread. Fire Safety Science, Proceedings of the First International Symposium. Washington D. C.: Hemisphere Publishing Corp. 1986.

[29] Siegel, R., and J. Howell. Thermal Radiation Heat Transfer. 3rd ed. Taylor and Francis: Washington D.C., 1992.

[30] Qian, Cheng, and Saito. Fire Safety Science – Proceedings of the Fifth International Symposium. "An Empirical Model for Upward Flame Spread Over Vertical Flat and Corner Walls." International Association for Fire Safety Science: 1997.

[31] Quintiere, James, G. "A Simulation Model for Fire Growth on Materials Subject to a Room-Corner Test." *Fire Safety Journal.* V.20. 1993. Pp.313-339.

[32] Quintiere, James, G. "Growth of Fire in Building Compartments." *Fire Standards and Safety Journal, ASTM STP 614*. A. F. Robertson, Ed. American Society for Testing and Materials. 1977. Pp. 131-167.

[33] Satterfield, D.B., and J.R. Barnett. User's Guide for WPI/Fire Version 2: Compartment Fire Model. Worcester Polytechnic Institute: Worcester, MA. 1990.

[34] Tewarson, A. SFPE Handbook of Fire Protection Engineering. 2nd ed. "Generation of Heat and Chemical Compounds in Fires." National Fire Protection Association: Quincy, MA. 1995.

[35] Tien, C.L., K.Y. Lee, and A.J. Stretton. SFPE Handbook of Fire Protection Engineering. 2nd ed. "Radiation Heat Transfer." National Fire Protection Association: Quincy, MA. 1995.

Appendices

Appendix A – Differential Element to Finite Quarter Circle Configuration Factor

This appendix describes the derivation of a configuration factor for a differential element to a finite quarter-circular area within a plane perpendicular to the plane of the quarter circle, and contiguous with one of it's edges. This is more evident from Figure A-1**.** The development of this configuration factor proceeded in a manner similar to the one outlined in Chapter 6-3.2 of Siegel and Howell[29] (example 6.4 in particular) The notation of Figure A-1 is used in the following derivation:

1) Find equivalent values for $\cos\theta_1$, $\cos\theta_2$, and S in the following equation:

$$F_{d1-2} = \int_{A_2} \frac{\cos\theta_1 \cos\theta_2}{\pi S^2} dA_2 \tag{A.1}$$

$$\cos\varphi = \frac{a}{\rho} \qquad a = \rho\cos\varphi$$

$$\cos\theta_1 = \frac{a}{S} = \frac{\rho\cos\varphi}{S} \tag{A.2}$$

$$\cos\theta_2 = \frac{H}{S} \tag{A.3}$$

$$S^2 = B^2 + H^2$$

$$B^2 = a^2 + (L-b)^2 \qquad b = \rho\sin\varphi$$

$$B^2 = (\rho\cos\varphi)^2 + (L-\rho\sin\varphi)^2$$

$$S^2 = (\rho\cos\varphi)^2 + (L-\rho\sin\varphi)^2 + H^2 \tag{A.4}$$

2) Substitute equations A.2, A.3, and A.4 into equation A.1.

$$F_{d1-2} = \int_{A_2} \frac{H\rho\cos\varphi}{\pi S^4} \rho d\rho d\varphi$$

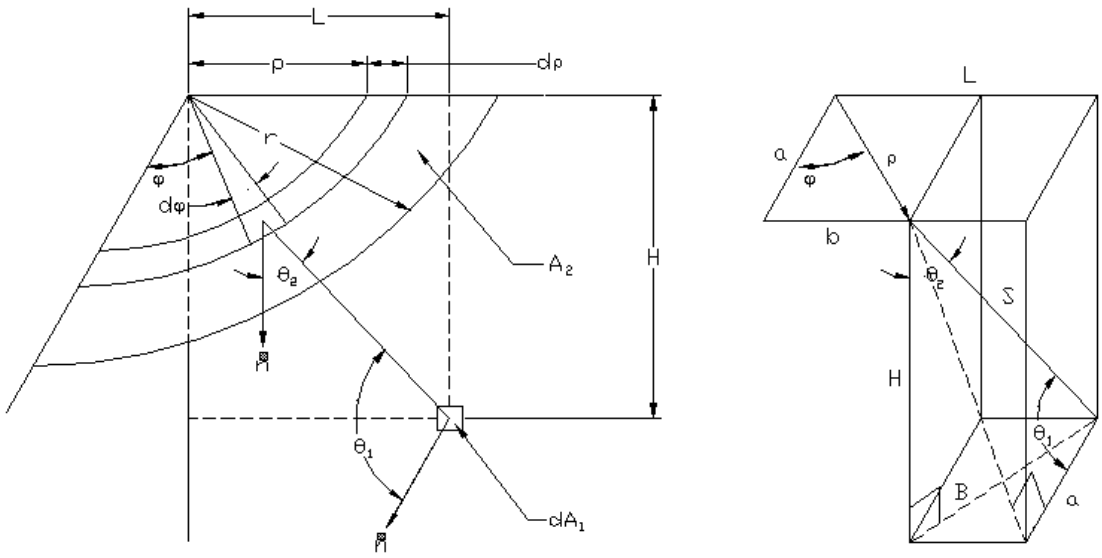

Figure A-1 – Setup for configuration factor between differential element and quarter circle

$$F_{d1-2} = \frac{H}{\pi} \int_{\rho=0}^{r} \int_{\varphi=0}^{\frac{\pi}{2}} \frac{\rho^2 \cos\varphi}{\left[(\rho\cos\varphi)^2 + (L-\rho\sin\varphi)^2 + H^2\right]^2} d\rho d\varphi \tag{A.5}$$

3) Itegrating and simplifying equation 5 yields,

$$F_{d1-2} = \frac{1}{4\pi L}\left[\begin{array}{l} \ln\left(H^2 + r^2 + L^2 + 2rL\right)H - 2\tan^{-1}\left(\frac{-r+L}{H}\right)L \\ \qquad -\ln\left(H^2 + r^2 + L^2\right)H + 2\tan^{-1}\left(\frac{L}{H}\right)L \end{array}\right] \tag{A.6}$$

The next step was to verify this derivation. In order to do this the standard configuration factor shown in Figure A-2a is used to construct an equivalent to the derived configuration factor. This construction is shown in Figure A-2b. Essentially the quarter circle is divided up into many small strips and the configuration factor for each strip is calculated as follows:

If $a_2 \le L$ then,

$$CF_{strip} = (CF_1 - CF_2) + (CF_3 - CF_4) \tag{A.7}$$

otherwise

$$CF_{strip} = (CF_1 - CF_2) - (CF_3 - CF_4) \tag{A.8}$$

The configuration factor for all the strips are then summed to get the equivalent configuration factor for the quarter-circular area to the differential area. The following values were used to check the derivation:

r = 1m
H = 1m
L = 0.5m

# of strips for check method = 1000

Using the check method:

$F_{d1\text{-}2} = 0.05399$

Using the derived method:

$F_{d1\text{-}2} = 0.05403$

This gives an error of 0.075%, thus proving that the new derivation was correct.

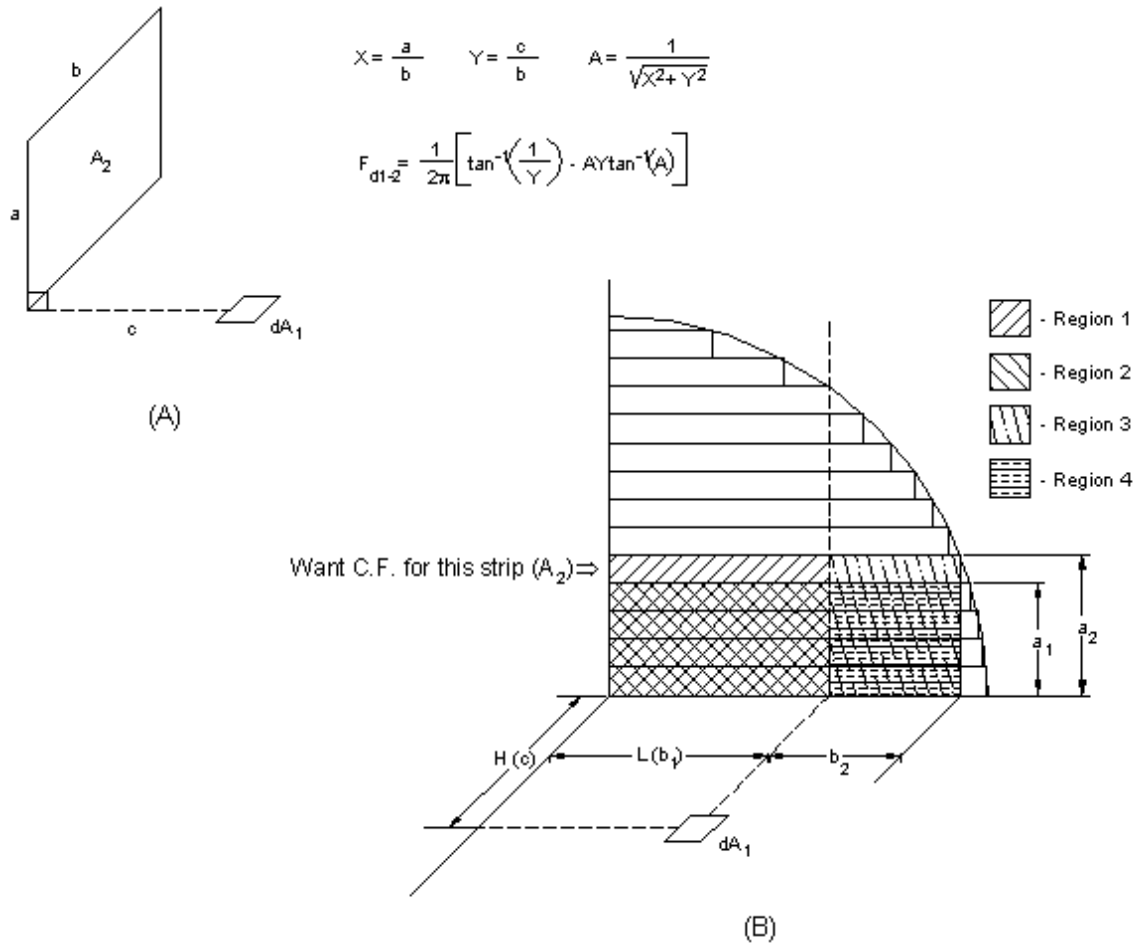

Figure A-2 – Setup for verification of configuration factor

Appendix B – List of Changes Made to the CFAST Source Code

Routine	*Date*	*Change*
CNHEAT	4/9/99	-FLXTOT now defined in CFAST.INC
	6/22/99	-Removed FLXTOT from main arg. list.
FIRES	4/8/99	-Added XFIRE(1,9) and to argument call list for OBJINT
INITSLV	5/6/99	-Opened new debugging file "stpmax.err"

INITSOLN	4/6/99	-Changed if-statement conditional from
		IF (OBJTYP(I).EQ.3) THEN
		to
		IF (OBJTYP(I).EQ.FSM) THEN

NPUTOB	4/6/99	-Changed criteria for unsupported object type error check from FSM to MAXTYP
NPUTQ	4/29/99	-Added write statements to show object parameters.
OBJINT	4/8/99	-Added BURNER to argument list. (for Mitler FSM) -Added MITLER.INC to include file list
	4/9/99	-Added BURNER and IROOM to argument list in call to IGNITE and SPRED0
	4/12/99	-Changed UPDATE to UPDAT1 to avoid interference with Mitler's spread algorithm (uses a variable "UPDATE")
	4/28/99	-Added conditional so that Mitler's algorithms (ignition and spread) are only accessed when the time has increased a certain increment. DT is calculated for use in these algorithms. It is no longer specified in subroutine GETDAT as before. Variable PREVTIME is used for these purposes.
	4/28/99 – 5/5/99	-Added sections to handle interfacing with new flame spread algorithm developed by Mitler and MTW
RESID	4/8/99	-Moved definition of FLXTOT to common block /MOCO1A/ in CFAST.INS. This is for use in the Mitler flame spread model.
	6/22/99	-Removed FLXTOT from arg. list in call to CNHEAT
UPDOBJ	4/29/99 – 5/4/99	-Changed DT to DTNEW to avoid interference with MITLER's flame spread module. Added "MITLER.INC" to include list.
		-Added sections to deal with a Mitler flame spread type object. Essentially, these lines bypass the calculations normally reserved for CFAST objects, and allows the new algorithm to handle them.

Routine	*Date*	*Change*
UPDOBJ (cont'd)	5/4/99	-Added following variables: MASSMTW - mass loss rate from MTWFSM algorithm QDOTMTW - heat release rate from burning wall AREAMTW - pyrolysis area of burning wall These variables are used to hold the previous values for the variables OMASST,OQDOTT, and OAREAT as the algorithm does not calculate these variables at each iteration.

Appendix C – CFAST Input Datafiles

CFAST Main Input Datafile

```
VERSN    3One Compartment Base Case
TIMES    1200     1     1     1      0
DUMPR cfcgmt3.HI
ADUMP cfcgmt3.CSV NFSW
TAMB  293.150        101300. 0.000000
EAMB  293.150        101300. 0.000000
HI/F  0.000000
WIDTH  3.60000
DEPTH  2.40000
HEIGH  2.40000
CEILI FRPOLYST
WALLS FRPOLYST
FLOOR PLYWOOD
HVENT  1  2  1 0.800000  2.00000 0.000000 0.000000 0.000000 0.000000
CVENT  1  2  1       1.00000       1.00000       1.00000       1.00000
CHEMI  16.0000  50.0000  10.0000 1.95000E+007  293.150  493.150 0.300000
LFBO 1
LFBT 2
CJET ALL
FPOS -1.00000 0.0500000 0.000000
FTIME       10.0000       600.000       610.00
FMASS      0.000000    0.00512820    0.00512820    0.01538462
FQDOT      0.000000        100000.       100000.        300000.
HCR       0.0800000     0.0800000     0.0800000     0.0800000
OD        0.0300000     0.0300000     0.0300000     0.0300000
CO        0.0300000     0.0300000     0.0300000     0.0300000
OBJECT   USCGMAT3 1      450  2  1.20000 0.000000 0.000000 0.000000  1.00000 0.000000
MITCF 1 USCGMT3.CFG USCGMT3.CSV
```

The highlighted portions of the main input file are the most important to for using the new flame spread algorithm, and will be discussed briefly here. A more thorough explanation of the remainder of this file can be found in 26.

ADUMP – This line is used to specify a comma-delimited output file for reading by a spreadsheet.

CEILI and WALLS – The material that lines the walls should be specified here. This will be the same material that is specified in the objects database for the object defined by the OBJECT line.

CHEMI, FTIME, FMASS, FQDOT – These lines specify the main fire. For use of the new flame spread algorithm, the burner should be specified using at least these lines.

OBJECT – This line specifies the object to use in the simulation. The most important variables here are the object name, compartment number, ignition value, and ignition type. These are shown below for clarity:

```
OBJECT   USCGMAT3 1      450  2  1.20000 0.000000 . . .
```

The ignition type (2) in this case is for temperature, and the ignition value is set to 450 K. These numbers are not used by the flame spread algorithm, but a value must be specified to avoid initialization errors from CFAST.

MITCF – This line is a new line interpreted by CFAST. This sets up automatic use of the new flame spread algorithm. The values specify whether or not to use this feature (1=yes, 0=no), the name of the configuration file to use for the new algorithm, and the name of the output file from the algorithm.

CFAST Object Database Entry Example

The object database for flame-spread objects that use the new flame spread algorithm follow the standard CFAST object database format. The highlighted parameters can be altered as necessary for the material, and parameters that are crossed out must be given the value shown in the second example #2. This format can be added to the end of the object database file *OBJECTS.DF*. Note that the heat of combustion shown in the database below is the *effective* value, not a heat of *complete* combustion.

A plus in the leftmost column indicates a continuation of the previous line. Great care should be taken when altering this database, as CFAST is very precise in interpreting entries to this database. It is suggested that a text only editor be used when editing this database.

```
 #  Example #1
 #  Description of the object can go anywhere in this header
 #
 #
 #
 OBJECT NAME
 Type Ignition_flux Ignition_temp Total_mass Gram_molecular_wt
+ Volatilization_temp Heat_of_combustion Thermophysical_material
 Panel_length Panel_height_or_width Panel_thickness X_normal_component
+ Y_normal_component Z_normal_component
 {blank—this is required!}
 Object_time_history
 Pyrolysis_rate_time_history
 Rate_of_heat_release_time_history
 Area_of_fire_time_history
 Height_of_flame_time_history
 CO/CO2_time_history
 OD_or_soot_time_history
 H/C_time_history
 O/C_time_history
 CT_time_history
 HCN_time_history
 HCl_time_history
```

```
#  Example #2
#
#  Mitler flame spread object
#
#
OBJECT USCGMT3
5 0 450 500 16 450 1.13E+007 FRPOLYST
2.4 3.6 2.4 0 0 0

1000 2000 3000
0 0 0 0
0 0 0 0
0 0 0 0
0 0 0 0
0 0 0.0172 0.0176
0 0.012 0.014 0.023
0.16 0.16 0.16 0.16
0 0 0 0
1 1 1 1
0 0 0 0
0 0 0 0
```

CFAST Thermal Database Entry Example

Materials that can be used in the new flame spread algorithm must be placed in the CFAST thermophysical database. All of these fields are up to the user. No special changes need to be made in order to use any of these materials in Mitler's algorithm. The next line describes each entry for a material in the database, followed by a few examples. All of these entries should be a single line. Highlighted parameters are the most important. The plus in the left column indicates that the line is continued from the previous line.

```
 Name  Thermal_conductivity Specific_heat Density Thickness Emissivity
+ HCl_coefficients(7)  Description
```

A few examples are:

```
COMBRICK  0.72 835 1920 0.076 0.9 0 0 0 0 0 0 0  Common brick (3")
CONCRETE  1.75 1000 2200 0.15 0.94 0 0 0 0 0 0 0  Concrete, Normal
     Weight (6")
GLASS     1.4 750 2500 0.006 0.1 0 0 0 0 0 0 0  Plate Glass (1/4")
```

Note that the name has a maximum of eight characters, and if it is less that that, blank spaces fill the remainder. Also note that there are two spaces after the name and two spaces before the description. These spaces are important for CFAST to be able to interpret the database correctly.

Appendix D – Structure of the Radiation Network Routine: RADXFER

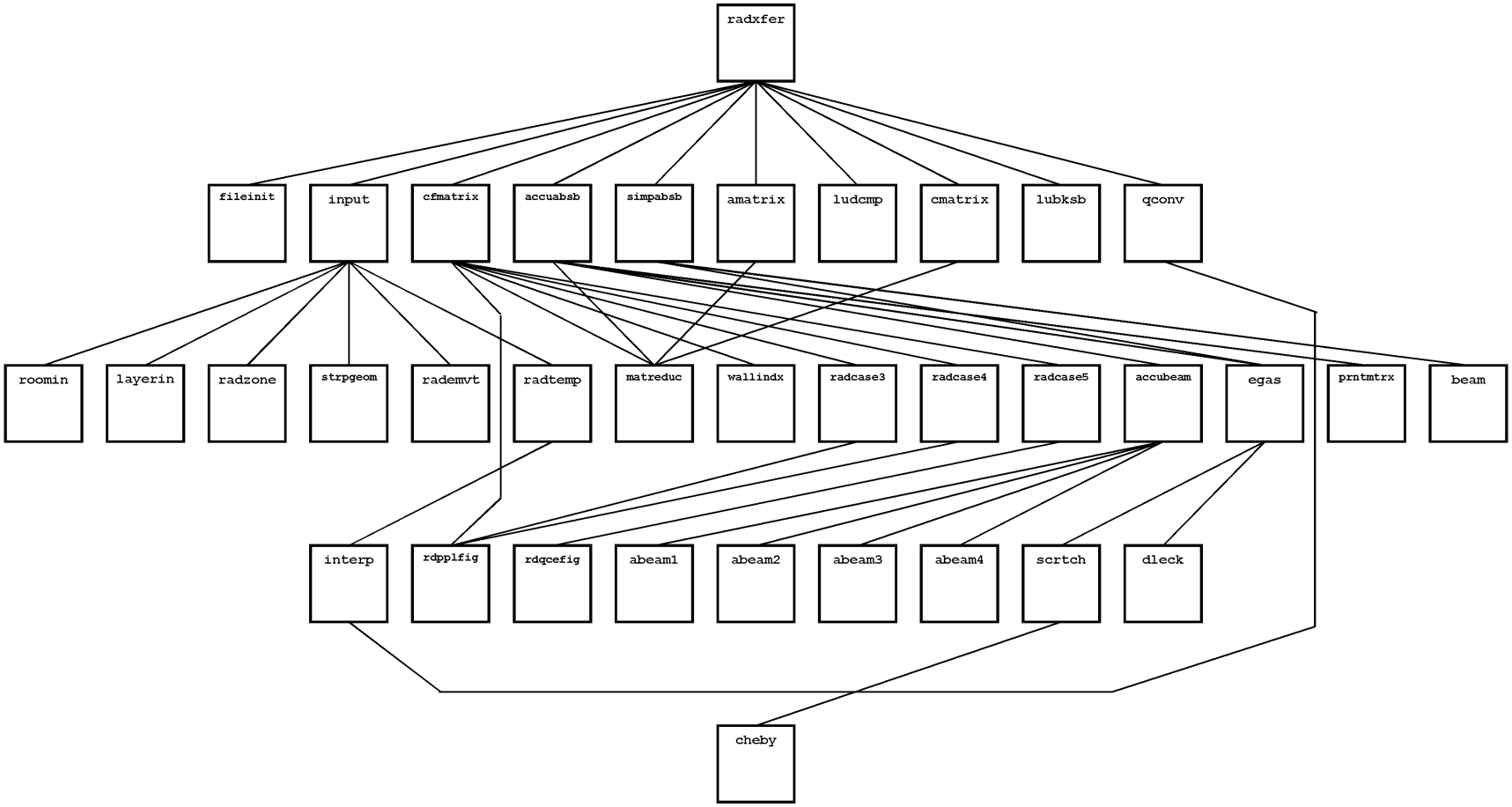

Appendix E – Description of Subroutines for RADXFER

ABEAM1	:	Calculates the geometric beam length through the hot gas layer from an upper layer element to a ceiling element.
ABEAM2	:	Calculates the geometric beam length through the hot gas layer from a lower layer element to a ceiling element.
ABEAM3	:	Calculates the geometric beam length through the hot gas layer from an upper layer element to a lower layer element.
ABEAM4	:	Calculates the geometric beam length through the hot gas layer from an upper layer element to an upper layer element.
ACCUABSB	:	Calculates absorptivity of the upper gas layer using precise beam lengths between individual elements (validity not verified)
ACCUBEAM	:	Calculates the geometric beam length through the hot gas layer between individual elements.
AMATRIX	:	Builds the [a] matrix for the radiation network calculations
BEAM	:	Calculates the mean beam length of the upper gas layer
CFMATRIX	:	Calculates a matrix of configuration factors between all elements
CHEBY	:	Calculate Chebyshev polynomial. Used for SCRTCH.
CMATRIX	:	Builds the [c] matrix for the radiation network calculations
DLECK	:	Calculates overlap correction for gas mixtures of CO_2 and H_2O. Used for routine EGAS
EGAS	:	Routine borrowed from WPI/Fire to calculate the emissivity of a gas layer.
FILEINIT	:	Writes program header to screen and/or output file
INPUT	:	Control subroutine for input subroutines
INTERP	:	Generic CFAST routine for interpolation
LAYERIN	:	Gets in input data for the upper gas layer from CFAST
LUBKSB	:	Generic LU back-substitution routine for matrix inversion
LUDCMP	:	Generic LU decomposition routine for matrix inversion
MATREDUC	:	Converts a two dimensional matrix to a one dimensional matrix [for example, a(#,#) is represented by a(1,1) = 1, a(1,2) = 5, a(2,1) = 10, a(2,2) = 20, then the new matrix a(#) would be a(1) = 1, a(2) = 5, a(3) = 10, a(4) = 20]
QCONV	:	Converts the incident flux output data to the scale used in the flame spread algorithm (the element width is typically not the same in both programs)

RADCASE3	:	Calculates the view factor for wall elements that are on perpendicular planes, and they are contiguous only on one corner.
RADCASE4	:	Calculates the view factor for a wall elements that are on perpendicular planes, and they separated (i.e. the elements do not touch anywhere)
RADCASE5	:	Calculates the view factor for a quarter-circular element from a strip element located in a plane that is contiguous and perpendicular to an edge of the quarter circle. A selection of points over the area of the strip is used to get an average value using the base differential view factor calculation.
RADEMVT	:	Sets the emissivity of each element to the value used in the flame spread algorithm
RADTEMP	:	Sets the surface temperature of each element using the distribution provided by the flame spread algorithm.
RADXFER	:	Main control subroutine for the radiation network subprogram
RADZONE	:	Calculates the number of elements for each zone based on current simulation conditions
RDPPLFIG	:	Basic configuration factor calculation for two perpendicular areas contiguous along one edge
RDQCEFIG	:	Basic configuration factor calculation to a quarter-circular area from a differential element located in a plane that is contiguous and perpendicular to an edge of the quarter circle
ROOMIN	:	Gets the input data for room geometry, location of the layer interface, width of the upper and lower pyrolysis zones, and extent of ceiling pyrolysis zone from the flame spread algorithm and CFAST.
SCRTCH	:	Interpolates values from the Hottel charts for CO_2 and H_2O. Used for routine EGAS
SIMPABSB	:	Calculates absorptivity of the upper gas layer using the mean beam length approximation
STRPGEOM	:	Calculates the geometric dimensions of each element
WALLINDX	:	Sets a zone index for each element

Appendix F – List of Changes Made to Mitler's Original Algorithm

Routine	*Date*	*Change*
BRNFLX	4/8/99	-Changed variable FLUX to FLUXAR for CFAST compatibility
	4/12/99	-Added "PRECIS.INC" to include file list
	5/6/99	-Added conditional so that layer temperatures are used in the re-radiation loss, instead of the general ambient temperature. -Added "MITLER.INC","CENVIRO.INC", and "CPARAMS.INC" to include file list
	5/10/99	-Removed prior conditional - unsure if working. Can be used for tweaking later.
	5/19/99	-Changed range in do loop from NTOP to NCEIL. Added in enhanced corner radiation call (RADXFER).
	5/23/99	-Added variable BFCASE to main arg. list This variable denotes which subroutine called BRNFLX: BFCASE=1 -- called by either MLRATE or SPRED0 BFCASE=2 -- called by FLXTMP BFCASE=3 -- called by NETFLX Different combinations of temperature and flux are used by these subroutines, as illustrated in the code below.
	6/20/99	-Removed call to RADXFER.FOR (now in COMBND.FOR and INFLXF.FOR) -Added conditional to simply copy the flux array in the corner case from PHIIN(I) or UFLUX(I) to FLUXAR(I) in the pre-ignition and post-ignition cases, respectively.
	7/27/99	-Removed BFCASE from this routine, no longer used.
BRNOUT	4/12/99	-Added "PRECIS.INC" to include file list
	7/29/99	-Added routine to deal with multiple pyrolysis zones if they are in use. -XP1, TIME, and MULTIPYR added to main arg. list.
COMBND	4/12/99	-Added "PRECIS.INC" to include file list
	5/27/99	-Added IROOM and CRNR to main arg. list. -Added conditionals to deal with the corner configuration and enhanced corner radiation routine handling (RADXFER).

Routine	*Date*	*Change*
COMBND (cont'd)	6/30/99	-Added conditional for inclusion of complex radiation calculations. This is represented by logical variable RADCALC. -Added RADCALC to main arg. list. -Added TFLM to main arg list and arg list for RADXFER. -Added XF to arg list for RADXFER.
	7/21/99	-Added XPB1, FLUXVAL, and FLUXMAP to main arg. list. -Added routines to handle the use of heat flux maps,if selected.
COMBST	4/12/99	-Added "PRECIS.INC" to include file list
CVCCOM	4/12/99	-Added "PRECIS.INC" to include file list.
	5/23/99	-Added CRNR to main arg. list. -Added conditional for corner flame height.
	6/2/99	-Added WIDTH to main arg. list.
	7/19/99	-Added CLINING to main arg. list and added conditional so that PHCXFP is always calculated when CLINING is true.
CVFLX	4/12/99	-Added "PRECIS.INC" to include file list
DLTCLC	4/12/99	-Added "PRECIS.INC" to include file list
FIBRN	4/12/99	-Removed the burner power input part of this routine. -The burner HRR will be taken from the main CFAST fire, which should be specified as the HRR of the burner. -The radiant fraction of the HRR from the burner will also be taken from CFAST. -Added "CFAST.INC" and "PRECIS.INC" to include file list
	7/21/99	-Added logical variable FLUXMAP to control whether a heat flux map from the burner in the ISO9705 configuration is to be used in the algorithm.
FIDAT	4/8/99	-Multiple additions made to allow use of CFAST variables as inputs (see comments in code for specifics) -Added "CFAST.INC" and "CENVIRO.INC" to include file list -Changed variable P to P5 for CFAST compatibility
	4/12/99	-Added "PRECIS.INC" to include file list
	5/3/99	-Re-instated user input of DT.
	5/11/99	-Added CRNR, GASLAYER, and ACCUGAS to list of input variables for the subroutine RADXFER and main arg. list.
	6/2/99	-Added variable CLINING to deal with the no-ceiling lining case. This variable was added to the main arg. list.

Routine	*Date*	*Change*
FIDAT (cont'd)	6/30/99	-AMPP0 is now calculated instead of input by the user. -Added RADCALC variable to input list. This is a logical variable that controls whether complex radiation calculations will be used in the corner configuration. -RADCALC added to main arg. list. -Added variable TFLM (transmissivity of flame) to inputs and main arg list.
	7/15/99	-AMPP0 is now an input variable again.
	7/26/99	-Changed AMPP0 yet again! This will be calculated based on the Cone Calorimeter data in routine SETUP. The user will not be able screw it up this way :)
	7/27/99	-Added error handling for variables P5,EW,TFLM, and TCRIT.
	7/29/99	-Added variable MULTIPYR to input routines and main arg. list.
FIMLR	4/12/99	Added "PRECIS.INC" to include file list
	7/26/99	Moved routine to convert cone curve data from kW/m2 to g/m2 to routine SETUP
FLAME	4/12/99	-Added "PRECIS.INC" to include file list
	4/27/99	-Changed "WRITE(11..." statements to "WRITE(51..." to avoid a unit file conflict error with CFAST
	5/9/99	-Added "MITLER.INC" to include file list. -Removed XP1 and XPB1 from main arg. list as they are in the include file. -Added conditional for corner flame spread flame height calculation.
	5/26/99	-Changed main arg. list to reflect inclusion of "MITLER.INC" (removed XP1, and XPB1)
	6/19/99	-Changed flame height calculations so that all uses of AWIDTH become AWIDTH/2. This is because in SETUP.FOR when the corner is used, AWIDTH is multiplied by 2 to get the correct pyrolysis width from the dimension of the burner. We need to reduce this value again so that it makes sense when calculating the flame height.
	6/25/99	-Removed "MITLER.INC" and reinstated arg. list variables
FLLTMP	4/8/99	-Changed variable FLUX to FLUXAR for CFAST compatibility
	4/12/99	-Added "PRECIS.INC" to include file list
FLXTMP	4/1/99	-Moved calculation of XFB to correct location

Routine	*Date*	*Change*
FLXTMP (cont'd)	4/8/99	-Changed variable BW to BW1 for CFAST compatibility -Changed variable ETA to ETA1 for CFAST compatibility -Changed variable FLUX to FLUXAR for CFAST compatibility
	4/12/99	-Added "PRECIS.INC" to include file list
	5/6/99	-Changed argument list for BRNFLX to (IROOM). -Added IROOM to main argument list.
	5/23/99	-Added integer variable BFCASE, because there are three types of calls to subroutine BRNFLX. BFCASE=2 describes a call from this subroutine. Added this variable to the arg. list for BRNFLX.
	5/30/99	-Added IROOM and CRNR to arg. list for COMBND. -Added CRNR to main arg. list
	5/31/99	-Removed call to BRNFLX for the corner case.
	6/2/99	-Added WIDTH to arg. list for CVCCOM.
	6/3/99	-Added conditional for corner flame height.
	6/6/99	-Added convergence criteria routine for surface temperature, in the same manner that was used in IGNITE.FOR -Added NUNOUT to main arg. list.
	6/7/99	-Added CRNR to arg. list for RADCOM.
	6/17/99	-Added call to wall temperature routines after convergence loop so that the fluxes will be updated as before
	6/19/99	-Changed loop (using statement label 20) condition from NTOP to NCEIL -Changed loop (using statement label 90) condition from MXNODS to NCEIL
	6/20/99	-Reinstated call to BRNFLX in the corner case. Copying of the flux array from UFLUX to FLUXAR was necessary. -Moved call to RADCOM into convergence loop.
	6/22/99	-Changed FLOAT(NCEIL) to DBLE(NCEIL).
	6/23/99	-Added conditional for the corner configuration where WIDTH is changed to WIDTH*2.0 in calculation of THETA
	6/30/99	-Added RADCALC to main arg list and arg list for COMBND. -Added TFLM to main arg list and arg list for COMBND.
	7/19/99	-Added CLINING to main arg. list and added conditional so that PHRXFP is always calculated when CLINING is true.
	7/21/99	-Added FLUXVAL and FLUXMAP to main arg. list and to arg. lists for RADCOM and COMBND. -Added XPB1 to arg. list for COMBND.
	7/23/99	-Added AWIDTH to arg. list for RADCOM.
Routine	*Date*	*Change*

FLXTMP (cont'd)	7/27/99	-Removed variable BFCASE, no longer used.
GETDAT	4/12/99	-Added IROOM to subroutine argument list and also to arg. lists for calls to SETDAT, FIDAT, and KBDAT. Last input section removed, as these values will be taken from CFAST.
	4/8/99	-Changed variable P to P5 for CFAST compatibility
	4/10/99	-Added "MITLER.INC" and "PRECIS.INC" to include list.
	5/11/99	-Added CRNR, GASLAYER, and ACCUGAS to FIDAT arg. list.
	5/20/99	-Removed use of setup file. -Added CRNR, GASLAYER, and ACCUGAS to KBDAT arg. list.
	6/1/99	-Added CLINING to arg. lists for KBDAT and FIDAT.
	6/30/99	-Added RADCALC to arg. lists for KBDAT, FIDAT, and SETDAT. -Added TFLM (flame transmissivity) and RADCALC to arg lists for KBDAT, FIDAT, and SETDAT. -Reinstated use of setup file.
	7/15/99	-Added provisions for auto-start using file information found in the CFAST data file.
	7/21/99	-Added FLUXMAP to arg. list for SETDAT, KBBRN, and FIBRN.
	7/29/99	-Added MULTIPYR to arg. list for SETDAT, KBBRN, and FIBRN.
IGNCHK	4/8/99	-Changed variable BW to BW1 for CFAST compatibility -Changed variable FLUX to FLUXAR for CFAST compatibility
	4/12/99	-Added "PRECIS.INC" to include file list
	6/1/99	-Added HW and CLINING to main arg. list -Added conditionals for no ceiling lining case.
IGNITE	4/9/99	-Changed BW to BW1 for CFAST compatibility -Changed FLUX to FLUXAR for CFAST compatibility -Added "CFAST.INC" and "MITLER.INC" to include file list. -Added BURNER and IROOM to main argument list. -Changed calculation of QDOTB, EXFLXU, and EXFLXL to be handled by CFAST. -Changed structure so program control is returned to CFAST after each time-step/iteration.

Routine	*Date*	*Change*
IGNITE (cont'd)	4/12/99	-Added "PRECIS.INC" to include file list
	5/1/99 - 5/3/99	-Added DT calculation. Added calculation for TEMP since DT can now change. TEMP was originally set in subroutine SETUP. Added conditional to set fluxes to zero in initial time-step if fluxes are less than zero.
	5/6/99	-Added IROOM to argument list in calls to NETFLX
	5/20/99	-Added conditional for setting of EXFLXU and EXFLXL so that when the corner configuration is present, these values are set to zero, and the external radiation exchange is handled by the subroutine RADXFER.
	5/24/99	-Changed setting of M, so that it can extend to NCEIL instead of only NTOP.
	5/26/99	-Changed FLAME arg. list to reflect inclusion of "MITLER.INC" (removed XP1, and XPB1)
	5/27/99	-Added CRNR to arg. list for NETFLX.
	6/1/99	-Added HW and CLINING to arg. list for IGNCHK. -Added conditional to set UPEND to true for the no ceiling lining case where the pyrolysis front has reached the ceiling.
	6/2/99	-Added conditional to stop program if RULNEN is reached.
	6/6/99	-Added new sections to do dynamic iteration/convergence for the surface temperature routine. The convergence criteria will be 0.25 degrees K.
	6/19/99	-Removed opening of file PROFILE.DAT and write statement to this file. -Changed loop (using statement label 90) condition from MXNODS to NCEIL
	6/25/99	-Reverted to old arg. list for FLAME
	6/30/99	-Added RADCALC AND TFLM to arg. list for NETFLX.
	7/21/99	-Added FLUXVAL, and FLUXMAP to arg. lists for NETFLUX. -Added interpolation routine for heat flux map values during times when burner is ramping up to steady state values.
INFLX	4/12/99	-Added "PRECIS.INC" to include file list
	5/27/99	-Added IROOM and CRNR to main arg. list.
	5/31/99	-Added CONVEC to main arg. list. This variable holds the convective flux in an array. -Removed IROOM from main arg. list. -Added conditionals to deal with corner configuration

Routine	*Date*	*Change*
INFLXF	4/12/99	-Added "PRECIS.INC" to include file list
	5/31/99	-Added IROOM, CRNR, CONVEC, and PHIFC to main arg. list. -Added conditionals and calculations to deal with the corner configuration.
	6/30/99	-Added conditional for inclusion of complex radiation calculations. -This is represented by logical variable RADCALC. -Added RADCALC to main arg. list. -Added TFLM to main arg. list and XF and TFLM to arg list for RADXFER.
	7/21/99	-Added FLUXVAL and FLUXMAP to main arg. list. -Added routine to use heat flux map, if selected.
INIMLR	4/8/99	-Changed variable FLUX to FLUXAR for CFAST compatibility
	4/11/99	-Added "PRECIS.INC" and "MITLER.INC" to include file list.
KBBRN	4/12/99	-Removed the burner power input part of this routine. The burner HRR will be taken from the main CFAST fire, which should be specified as the HRR of the burner. The radiant fraction of the HRR from the burner will also be taken from CFAST. -Added "PRECIS.INC" and "CFAST.INC" to include file list
	7/21/99	Added logical variable FLUXMAP to control whether a heat flux map from the burner in the ISO9705 configuration is to be used in the algorithm.
KBDAT	4/12/99	-Multiple additions made to allow use of CFAST variables as inputs (see comments in code for specifics)
	4/8/99	-Changed variable P to P5 for CFAST compatibility
	4/12/99	-Added "PRECIS.INC" to include file list
	5/3/99	-Re-instated user input of DT.
	5/11/99	-Added CRNR, GASLAYER, and ACCUGAS to list of input variables for the subroutine RADXFER and main arg. list
	6/2/99	-Added variable CLINING to deal with the no-ceiling lining case. This variable was added to the main arg. list.
	6/5/99	-Changed input routine for variables after WSLAB. Errors seemed to be generated from this part of the routine. -Removed writing variables obtained from CFAST to output file.

Routine	*Date*	*Change*
KBDAT (cont'd)	6/30/99	-AMPP0 is now calculated instead of input by the user. -Added RADCALC variable to input list. This is a logical variable that controls whether complex radiation calculations will be used in the corner configuration. RADCALC added to main arg. list. -Added variable TFLM (transmissivity of flames) to input list and main arg list.
	7/15/99	-AMPP0 is now an input by the user again.
	7/26/99	-Changed AMPP0 yet again! This will be calculated based on the Cone Calorimeter data in routine SETUP. The user will not be able screw it up this way :)
	7/27/99	-Added error handling for variable P5, EW, TFLM, and TCRIT.
	7/29/99	-Added variable MULTIPYR to input routines and main arg. list.
KBMLR	4/12/99	-Added "PRECIS.INC" to include file list
	7/26/99	-Moved routine to convert cone curve data from kW/m2 to g/m2 to routine SETUP.
LATSPR	4/12/99	-Added "PRECIS.INC" to include file list
	5/24/99	-Added HW and CRNR to main arg. list. -Added conditionals to take into account the presence of the corner configuration. This addition relates to the calculation of AWIDTH. Basically, an equivalent rectangular area is calculated from the quarter-circular area. An equivalent width is then found by using the standard pyrolysis length as one side i.e. ZP - HW or ZP - ZPB (if all the pyrolysis is on the ceiling) of this equivalent rectangular area. Using this equivalent width, AWIDTH is calculated in the same way as before.
MLRATE	4/8/99	-Changed variable ETA to ETA1 for CFAST compatibility
	4/8/99	-Changed variable FLUX to FLUXAR for CFAST compatibility
	4/12/99	-Added "PRECIS.INC" to include file list
	5/4/99	-Changed calculation of RMDOT from RMDOT = RMLEN * WIDTH to RMDOT = RMLEN * AWIDTH
	5/6/99	-Added IROOM to main argument list -Changed argument list for BRNFLX to (IROOM).
	5/20/99	Added "MITLER.INC" to include file list. Revised main arg. list as necessary.

Routine	*Date*	*Change*
MLRATE (cont'd)	5/23/99	-Added CRNR to arg. list for RADCOM and CVCCOM. -Added integer variable BFCASE, because there are three types of calls to subroutine BRNFLX. BFCASE=1 describes a call from this subroutine or from subroutine SPRED0. -Added this variable to the arg. list for BRNFLX.
	5/24/99	-Added conditional to calculation of TABMLR so that if the corner configuration is used, the area of the ceiling as a quarter circle is included. Additionally, ceiling lining conditionals were also added.
	5/26/99	-Changed FLAME arg. list to reflect inclusion of "MITLER.INC" (removed XP1, and XPB1)
	5/30/99	-Added IROOM and CRNR to arg. list for COMBND.
	5/31/99	-Removed call to BRNFLX for the corner case.
	6/1/99	-Added CRNR,MXNODS, and IROOM to arg. list for NBFLUX.
	6/2/99	Added WIDTH to arg. list for CVCCOM.
	6/6/99	Added convergence scheme similar to that found in INGITE.FOR and FLXTMP.FOR. The difference is that RMLEN is the variable used for convergence criteria instead of surface temperature. The criteria will be set to 0.01 g/m-sec.
	6/20/99	-Reinstated call to BRNFLX in the corner case. Copying of the flux array from UFLUX to FLUXAR was necessary.
	6/22/99	-Changed all occurrences of FLOAT(NCEIL) to DBLE(NCEIL).
	6/23/99	-Added conditional for the corner configuration where WIDTH is changed to WIDTH*2.0 in calculation of THETA.
	6/25/99	-Reverted to old arg. list for FLAME
	6/30/99	-Added RADCALC to main arg list and arg list for NBFLUX and COMBND. -Added CLINING to main arg list and added conditionals to modify TABMLR(I) depending on CLINING. -Added TFLM to main arg list and to arg list for COMBND. This is for the complex radiation program. For module NBFLUX, the flame height is zero, so the transmissivity is set to one, and the flame height to zero for this routine.
	7/19/99	-Added CLINING to arg. lists for RADCOM and CVCCOM.
	7/21/99	-Added FLUXVAL and FLUXMAP to main arg. list and to arg. lists for RADCOM and COMBND. -Added XPB1 to arg. list for COMBND
	7/23/99	-Added AWIDTH to arg. list for RADCOM.

Routine	*Date*	*Change*
MLRATE (cont'd)	7/27/97	-Removed variable BFCASE, no longer used.
	7/29/99	-Added conditional to deal with multiple pyrolysis zones, if used. -Added MULTIPYR to main arg. list.
NBFLUX	4/12/99	-Added "PRECIS.INC" to include file list
	6/1/99	-Added CRNR, MXNODS, and IROOM to main arg. list.
	6/30/99	-Added conditional for inclusion of complex radiation calculations. This is represented by logical variable RADCALC. -Added RADCALC to main arg. list. -Added TFLM and XF to main arg list and arg list for RADXFER.
NETFLUX	4/8/99	-Changed variable FLUX to FLUXAR for CFAST compatibility
	4/12/99	-Added "PRECIS.INC" to include file list
	5/6/99	-Added IROOM to main argument list. -Changed argument list for BRNFLX to (IROOM).
	5/23/99	-Added integer variable BFCASE, because there are three types of calls to subroutine BRNFLX. BFCASE=3 describes a call from this subroutine. Added this variable to the arg. list for BRNFLX.
	5/27/99	-Added CRNR to main arg. list. -Added IROOM and CRNR to arg. list for INFLX, INFLXf, and NBFLUX.
	5/31/99	-Added CONVEC to arg. list for INFLX. -Added calculation of PHIFC (convective flux at XF) -Added IROOM, CRNR, CONVEC, and PHIFC to arg. list for INFLXF. -Removed IROOM from arg. list for INFLX. -Added conditional so that call to BRNFLX occurs only in a non-corner case.
	6/1/99	-Added CRNR, MXNODS, and IROOM to arg. list for NBFLUX.
	6/20/99	-Reinstated call to BRNFLX. Flux array copying is now handled by that routine for the corner case.

Routine	*Date*	*Change*
NETFLUX (cont'd)	6/30/99	-Added RADCALC to main arg. list, and arg. lists for NBFLUX and INFLXF. -Added TFLM to main arg list and arg list for INFLXF. -Added 1.0 and 0.0 to arg list for NBFLUX to set transmissivity and flame height for the complex radiation routine.
	7/21/99	-Added FLUXVAL and FLUXMAP to main arg. list and arg list for INFLXF.
	7/26/99	-Removed variable BFCASE. No longer used.
OUTFILE	7/27/99	-Created.
RADCOM	4/8/99	-Changed variable ETA to ETA1 for CFAST compatibility
	4/12/99	-Added "PRECIS.INC" to include file list
	5/23/99	-Added CRNR to main arg. list and call to CEILRAD.
	6/23/99	-Added conditional for corner configuration calculation of XU1. -Changed WIDTH to WIDTH*2.0 for this purpose.
	7/19/99	-Added CLINING to main arg. list and added conditional so that PHRXFP is always calculated when CLINING is true.
	7/21/99	-Added FLUXVAL and FLUXMAP to main arg. list. -Added routines to allow the use of the burner heat flux map.
	7/23/99	-Added AWIDTH to main arg. list. -Changed calculation of XU1 to use AWIDTH. The previous use of WIDTH caused large values of PHIP to be calculated, resulting in erroneously high radiative flux, especially in the corner configuration when the pyrolysis zone started to spread across the ceiling.
RADIAT	4/12/99	-Added "PRECIS.INC" to include file list
RDFLX	4/12/99	-Added "PRECIS.INC" to include file list
	6/25/99	-Removed redundant if statement.
SETDAT	4/8/99	-Changed variable P to P5 for CFAST compatibility
	4/11/99	-Added IROOM to argument list and argument call list to FIDAT
	4/12/99	-Added "PRECIS.INC" to include file list
	6/30/99	-Updated main argument list to work with GETDAT. -Modified to allow the setup procedure to take place using data in the CFAST .DAT input file. -Added TFLM and RADCALC to main arg. list and arg. list for FIDAT.
	7/15/99	-Added provisions for autostart using file information found in the CFAST data file.
	7/21/99	-Added FLUXMAP to main arg. list and arg. list for FIBRN.
	7/29/99	-Added MULTIPYR to main arg. list and arg. list for FIDAT.

Routine	*Date*	*Change*
SETUP	4/8/99	-Changed variable BW to BW1 for CFAST compatibility changed variable ETA to ETA1 for CFAST compatibility -Changed variable FLUX to FLUXAR for CFAST compatibility -Removed variable TIME from setup procedure as it will be handled by CFAST. Added output file open section.
	4/11/99	-Added PRECIS.INC and MITLER.INC to include file list
	4/27/99	-Changed unit number of "flame.dat" from 11 to 51
	6/15/99	-For the corner configuration: Added conditional that sets WUI,WLI,and AWIDTH to 2*WIDTH, because the burner is touching on 2 sides.
	6/22/99	-Changed all references of function FLOAT(int) to DBLE(int) -Changed from 32 nodes/meter to 50 nodes/meter.
	7/26/99	-Added routine to calculate AMPP0 from the cone curve data. -Moved routine to convert cone curve data from kW/m2 to g/m2 from KBMLR and FIMLR to this routine.
SORT	4/12/99	-Added "PRECIS.INC" to include file list
SPRED0	4/8/99	-Changed variable BW to BW1 for CFAST compatibility changed variable ETA to ETA1 for CFAST compatibility -Changed variable FLUX to FLUXAR for CFAST compatibility -Changed variable P to P5 for CFAST compatibility
	4/11/99	-Added "PRECIS.INC","MITLER.INC" and "CFAST.INC". -Changed calculation of QDOTB, EXFLXU, EXFLXL, TWUP, and TWDN so that the values are pulled from CFAST. -Added OMASST, OQDOTT, and OAREAT to output list for CFAST object calculations (species, etc.) -Added calculation procedures for OMASST, OQDOTT, and OAREAT, OMASST – total mass loss rate of the burning wall material (kg/s) OQDOTT - total HRR of the burning wall material (W) OAREAT - total burning area on the wall (m2) -Removed TIME calculation (assigned by CFAST)

Routine	*Date*	*Change*
SPRED0 (cont'd)	4/27/99	-Added CENVIRO.INC to include list
	5/4/99	-Changed calculation of OMASST from OMASST = RMDOT to OMASST = RMDOT*0.001d0*CHIA
	5/6/99	-Changed argument list for BRNFLX to (IROOM). Subroutine BRNFLX now uses MITLER.INC for main variables. -Added IROOM to argument list for FLXTMP and MLRATE
	5/9/99	-Added calculation of TEMP to this subroutine for correct wall temperature calculations.
	5/23/99	-Added integer variable BFCASE, because there are three types of calls to subroutine BRNFLX. BFCASE=1 describes a call from this subroutine or from subroutine MLRATE. -Added this variable to the arg. list for BRNFLX.
	5/24/99	-Added HW and CRNR to arg. list for call to LATSPR
	5/26/99	-Changed FLAME arg. list to reflect inclusion of "MITLER.INC" (removed XP1, and XPB1)
	5/30/99	-Added IROOM and CRNR to arg. list for COMBND. -Added CRNR to arg. list for FLXTMP.
	5/31/99	-Removed call to BRNFLX for the corner case.
	6/2/99	-Added CLINING to arg. list for UPNDWN.
	6/2/99	-Added WIDTH to arg. list for CVCCOM. -Added conditional to stop program if RULNEN is reached.
	6/6/99	-Added NUNOUT to arg. list for FLXTMP.
	6/15/99	-Added CRNR and WUI to the arg. list for UPNDWN.
	6/20/99	-Reinstated call to BRNFLX in the corner case. Copying of the flux array from UFLUX to FLUXAR was necessary.
	6/23/99	-Added CRNR to arg. list for function DELTA. -Added conditional to function DELTA for the corner configuration where the occurrence of WIDTH is replaced by WIDTH*2.0.
	6/25/99	-Reinstated previous arg. list for FLAME
	6/30/99	-Added RADCALC to arg list for COMBND, MLRATE, and FLXTMP. -Added calls to COMBST and FLAME at the beginning, so that DELTAW can be calculated if necessary. -Flashover condition check added. -Added TFLM to arg list for MLRATE, FLXTMP, and COMBND.
	7/18/99	-Additions from 6/23/99 were wrong! Removed them.

Routine	*Date*	*Change*
SPRED0 (cont'd)	7/19/99	-Added CLINING to arg. list for FLXTMP and CVCCOM.
	7/21/99	-Added FLUXVAL, and FLUXMAP to arg. lists for MLRATE, FLXTMP, and COMBND -Added XPB1 to arg. list for COMBND. -Added interpolation routine for heat flux map values during times when burner is ramping up to steady state values.
	7/27/99	-Removed variable BFCASE, no longer used. -Added call to subroutine OUTFILE to open and initialize the standard set of output files.
	7/29/99	-Added MULTIPRY to arg. lists for BRNOUT and MLRATE. Added XP1 and TIME to arg. list for BRNOUT.
SPRED2	4/12/99	-Added "PRECIS.INC" to include file list
	6/20/99	-Added ICODE to arg list of function call to XTWRD2 and XTWRML -Removed minus sign from DELTAZ in call to XTWRD2 for downward spread.
	7/22/99	-Changed error in calculation of XP2B2 for upward spread, in the case where the top of the slab is reached. This was changed from XP2B2 = HW + ZB to XP2B2 = NFINAL * DELTAZ
TMLRP	4/12/99	-Added "PRECIS.INC" to include file list
TMPW04	4/8/99	-Changed variable BW to BW1 for CFAST compatibility
	4/12/99	-Added "PRECIS.INC" to include file list
TRNSFR	4/12/99	-Added "PRECIS.INC" to include file list
UPNDWN	4/12/99	-Added "PRECIS.INC" to include file list
	6/2/99	-Added CLINING to main arg. list. -Added conditionals to set UPEND to true if the no-ceiling lining case is present, and the pyrolysis front has reached the ceiling.
	6/15/99	-Added conditionals to set the initial area of pyrolysis on the ceiling when the corner configuration is present. -Added CRNR and WUI to the main arg. list for this purpose.
	6/21/99	-Changed calculation of L2. Was previously incorrect, as L2 was calculated to be too large by 1, thus the "1 +" was removed. Added error check for L2. In some instances, it is still calculated to be to low by 1. If L2 is found to be wrong, correct it.

Routine	*Date*	*Change*
UPNDWN (cont'd)	6/30/99	-Removed changed made on 6/15/99 (except arg list additions) and 6/21/99. -Removed no ceiling lining conditionals. This will be dealt with in MLRATE.
WALTMP	4/8/99	-Changed variable BW to BW1 for CFAST compatibility -Changed variable FLUX to FLUXAR for CFAST compatibility
	4/12/99	-Added "PRECIS.INC" to include file list
XTWRD2	4/12/99	-Added "PRECIS.INC" to include file list
	6/20/99	-Added ICODE to main arg list. -Added conditional for calling routine to differentiate between upward and downward spread. -Added changed calculations to deal with both conditions correctly.
XTWRML	4/12/99	-Added "PRECIS.INC" to include file list
	6/20/99	-Added ICODE to main arg list. -Added conditional for calling routine to differentiate between upward and downward spread. -Added changed calculations to deal with both conditions -correctly.
	6/24/99	-Conditionals added on 6/20 were wrong! Removed them.

Appendix G – Structure of the Flame Spread Algorithm

Primary Routine Structure

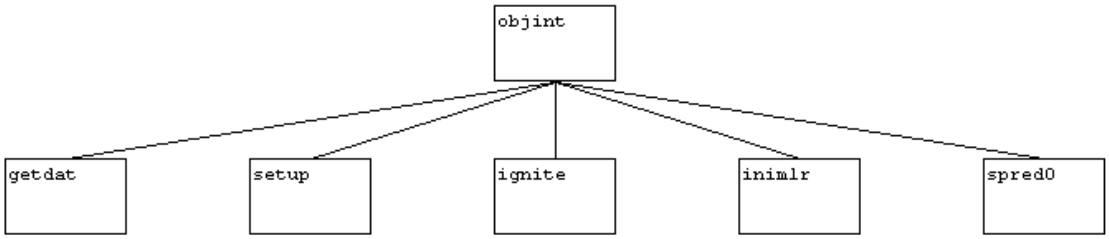

Input Routine Structure

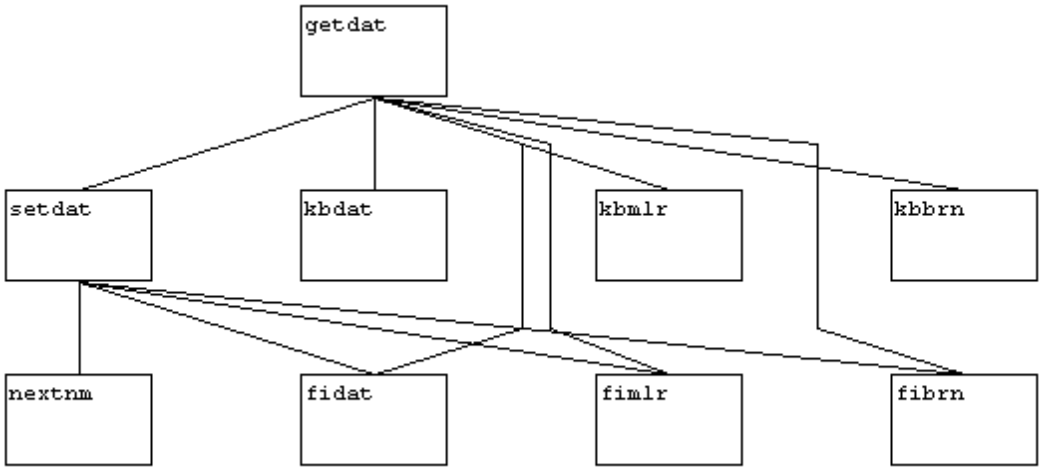

Setup Routine Structure

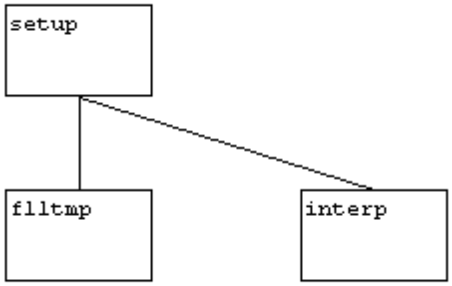

Mass Loss Initialization Routine Structure

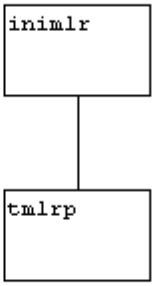

Ignition Routine Structure

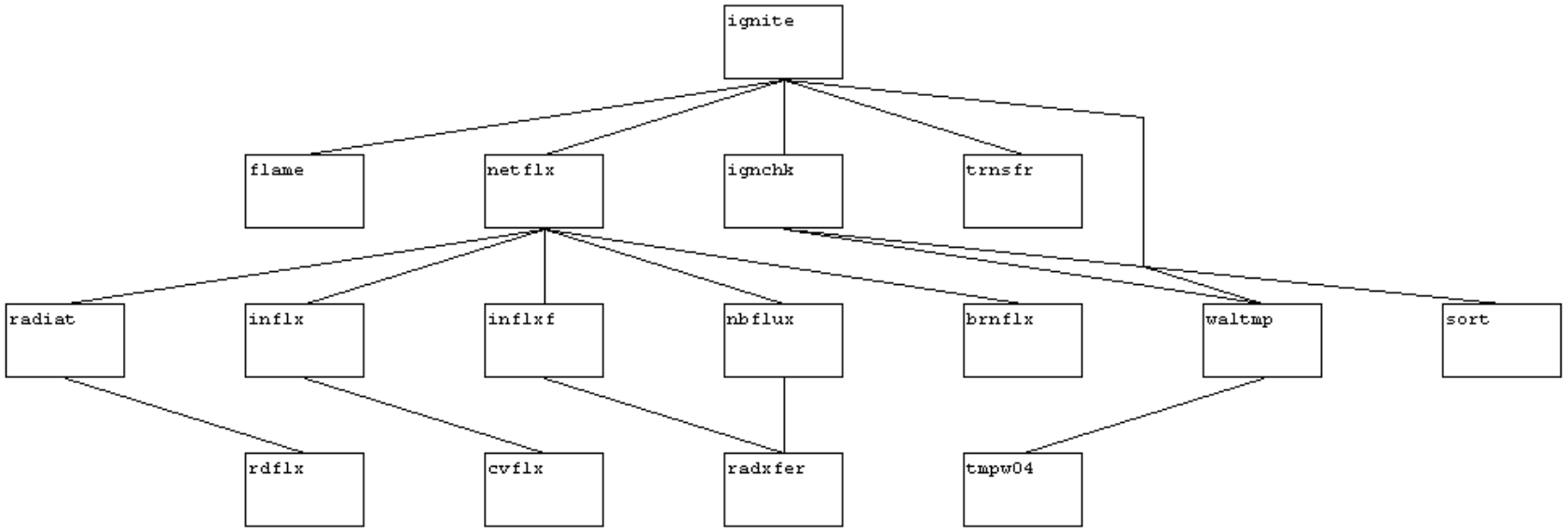

Flame Spread Routine Structure

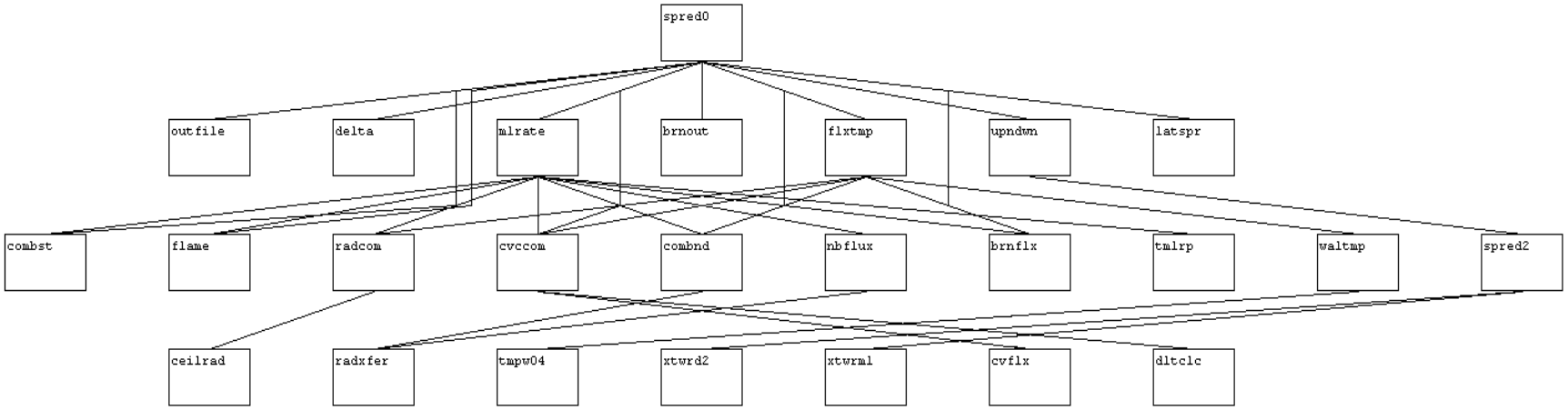

Appendix H – Description of Subroutines for the Flame Spread Algorithm

The following list is adapted from Appendix B in [23].

BRNFLX : Calculates the net wall flux for all the nodes at and above the burner top: takes the incoming flux and subtracts reradiation flux from it. For the corner configuration, the flux is simply transferred to the working array.

BRNOUT : Determines if burnout has occurred at a node. Multiple pyrolysis zones are also calculated is this option is selected.

COMBND : Calculates the combined flux to the wall. Used for post-ignition calculations.

COMBST : Calculates heat release rate from the wall, given the mass-loss rate.

CVCCOM : Calculates the convective flux to the wall.

CVFLX : Function that calculates the convective flux at a given height.

DLTCLC : Calculates delta phi sub c ($\Delta\phi_c$), the jump in convective heat transfer flux (mostly) below the pyrolysis front.

FIBRN : Reads the burner data from a file.

FIDAT : Reads material data and program options from a file.

FIMLR : Reads heat release rate data from a file. The data is from the material's Cone Calorimeter data.

FLAME : Calculates flame height.

FLLTMP : Initializes the arrays used in the program.

FLXTMP : Calculates the total heat flux and temperature distributions over all nodes after ignition.

GETDAT : Main subroutine that drives the input subroutines

IGNCHK : Obtains temperatures at all nodes, checks each for ignition

IGNITE : Main subroutine for driving ignition routines.

INFLX : Calculates incoming flux at and above the burner, and below the flame height. Used during pre-ignition.

INFLXF : Calculates incoming flux above the flame height. For the corner configuration, the total flux is also calculated in this routine. Used during pre-ignition.

INIMLR : Initializes the mass loss rate, upon ignition.

KBBRN : Prompts the user to enter the burner data from the keyboard. The data are then saved in a file.

KBDAT	:	Prompts the user to enter the material data and program options from the keyboard. The data are then saved in a file.
KBMLR	:	Prompts the user to enter heat release rate data from the keyboard. The data is from the material's Cone Calorimeter data. The data are then saved in a file.
LATSPR	:	Calculates the lateral spread and the average width of the pyrolysis zone.
MLRATE	:	Main routine for calculating the mass loss rate.
NBFLUX	:	Calculates the incident flux when there is no burner (i.e. from room feedback effects)
NETFLX	:	Main routine to calculate incident flux, pre-ignition.
OUTFILE	:	Opens standard output files.
RADCOM	:	Calculates the combined radiative flux (burner + wall), post-ignition.
RADXFER	:	Radiation network main subroutine for calculating room feedback effects.
RADIAT	:	Calculates radiative flux from the burner, pre-ignition.
RDFLX	:	Function to calculate radiative flux from the burner.
SETUP	:	Initializes variables for *IGNITE*, *INIMLR*, and *SPRED0*
SORT	:	Array sorting subroutine.
SPRED0	:	Main routine for driving post-ignition flame spread calculations.
SPRED2	:	Tests for spread above or below the pyrolysis area.
TMLRP	:	Function that calculates the total mass loss rate per unit width.
TMPW04	:	Calculates the temperature within the slab using a discrete grid. The wall is heater or cooled on each side by fluxes and the heat diffuses through it by conduction. The heat diffusion is calculated using an explicit method. One dimensional heat flow is assumed.
TRNSFR	:	Transfers current temperature array to array TEMP1.
UPNDWN	:	Checks for upward and downward spread.
WALTMP	:	Finds the temperature profile at each node. The array TEMP(i,j), where i corresponds to the i^{th} node, and j to the depth y_j, contains all the temperatures; the element TEMP(i,1) is the surface temperature at node i.
XTWRD2	:	Calculates next XP or XPB of the pyrolysis zone if spread occurred when highest or lowest pyrolyzing node is higher than M or lower

when highest or lowest pyrolyzing node is higher than M or lower than L-1.

XTWRML : Calculates next XP or XPB of the pyrolysis zone if spread occurred when highest or lowest pyrolyzing node is M or L-1.

Appendix I – A Brief Explanation of the Pyrolysis/Burnout Front Graph

The pyrolysis/burnout front graphs used in the following discussions are somewhat difficult to understand at first glance, so an example is provided here in Figure I-1 for clarity. The arrows indicate the general direction of the fronts, and the hatched area represents burning. The thick dashed line represents the boundary between the wall and the ceiling, where all points above this line are on the ceiling. The height scale does not change for the ceiling, however the main dimension on the ceiling is for a radius instead of a height. In order to get a radius, the virtual height of the room (actual height minus the height of the burner) is simply subtracted from the value on the graph. As an example, consider the time of 800 seconds shown in Figure I-1. At this time the entire wall is burning as well as the ceiling, except for an area of burnout on the ceiling from a radius of about 0.3m to about 1.25m. Another way of interpreting this graph is to examine one particular height versus time, allowing the burning time of a particular element to be determined. For example, consider the ceiling at a radius of 0.75m (3m in the figure). At this particular radius, burning begins at 350 seconds and burnout occurs at 700 seconds. Determining the burning time of a node can help to show if the algorithm is calculating mass loss in a realistic manner. All of these graphs can be interpreted in a similar fashion.

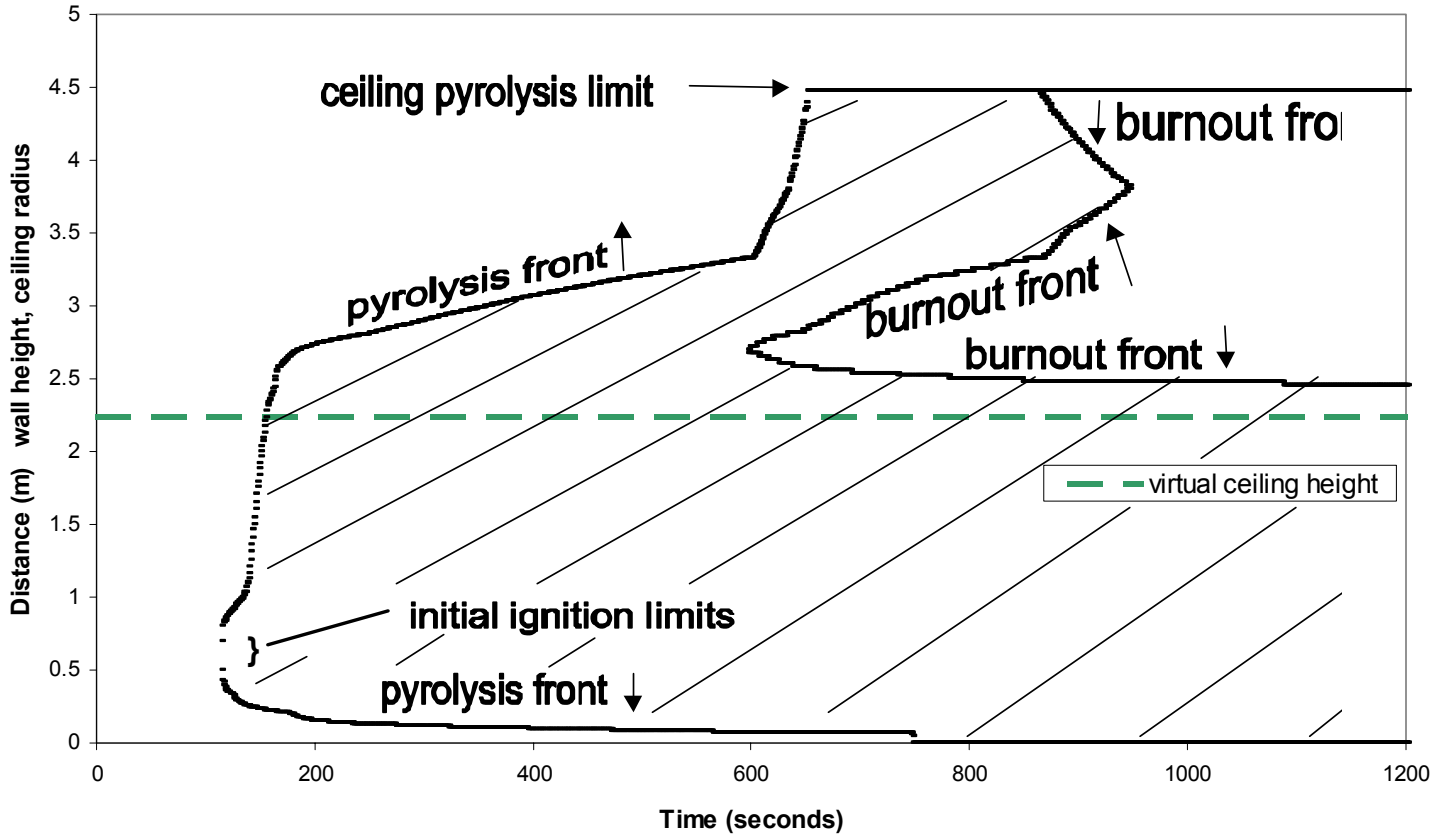

Figure I-1 – Example graph of pyrolysis and burnout fronts

Appendix J – Baseline Inputs to the Algorithm

BASELINE INPUTS FOR MATERIAL #3 - FR POLYESTER

PROP_3?.DAT

MATERIAL PROPERTIES / INPUT PARAMETERS	
Height of bottom of slab above floor	0 m
Material density (ρ)	1650 kg/m^3
Material thickness (δ)	0.0252 m
Material specific heat (c_p)	1000 J/kg·K
Material thermal conductivity (k)	0.782 W/m·K
Material ignition Temperature (T_{ig})	671 K
Material initial uniform temperature	293.15 K
Timestep	0.5 sec
Output interval	1 sec
Simulation length	1200 sec
Specific heat of product gases	1340 J/kg·K
Net heat of complete combustion	3.25E+07 J/kg
Efficiency of combustion (χ_A)	0.347
Radiative fraction (χ_{rad})	0.476
Material emissivity (ε)	0.9
Flame transmissivity (τ_{flame})	0.5
Lateral flame spread parameter (Φ)	12.13 kW^2/m^3
Min. surface temp. for lateral spread ($T_{s,min}$)	639 K
Width of slab (2 x width of shorter wall)	4.8 m
Ceiling present?	1 (yes)
Allow multiple pyrolysis zones?	1 (yes)
Average heat flux from the ceiling	2000 kW/m^2
Paramater p for ceiling/wall arm extensions	1 m^{-1}
Combustible ceiling lining present?	1 (yes)
Corner configuration present?	1 (yes)
Use Complex radiation?	1 (yes)
Use gaslayer calcs. In radiation calcs.?	1 (yes)
Use accurate beam length calculation in radiation calculations?	0 (no)

3_50.MLR

CONE CURVE		
Point #	Time sec	HRR kW/m^2
1	0	0.0
2	30	114.9
3	160	81.1
4	260	73.5
5	375	60.4
6	490	48.1
7	735	43.8
8		
9		
10		
11		
12		
13		
14		
15		
16		
17		
18		
19		
20		
21		
22		
23		
24		
25		
Irrad:	50 kW/m^2	

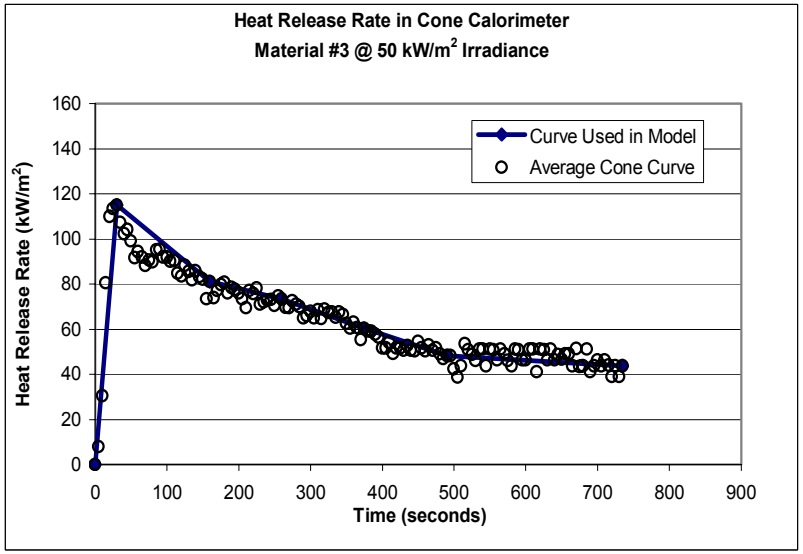

USCG.BRN

BURNER INPUTS	
Burner height above floor	0.152 m
Width of burner side	0.170 m
Use heat flux map?	1 (yes)

BASELINE INPUTS FOR MATERIAL #4 - FR VINYLESTER

PROP_4?.DAT

MATERIAL PROPERTIES / INPUT PARAMETERS	
Height of bottom of slab above floor	0 m
Material density (ρ)	1630 kg/m^3
Material thickness (δ)	0.0248 m
Material specific heat (c_p)	1000 J/kg·K
Material thermal conductivity (k)	1.221 W/m·K
Material ignition Temperature (T_{ig})	671 K
Material initial uniform temperature	293.15 K
Timestep	0.5 sec
Output interval	1 sec
Simulation length	1200 sec
Specific heat of product gases	1340 J/kg·K
Net heat of complete combustion	2.27E+07 J/kg
Efficiency of combustion (χ_A)	0.5
Radiative fraction (χ_{rad})	0.3
Material emissivity (ε)	0.9
Flame transmissivity (τ_{flame})	0.5
Lateral flame spread parameter (Φ)	12.315 kW^2/m^3
Min. surface temp. for lateral spread ($T_{s,min}$)	639 K
Width of slab (2 x width of shorter wall)	4.8 m
Ceiling present?	1 (yes)
Allow multiple pyrolysis zones?	1 (yes)
Average heat flux from the ceiling	2000 kW/m^2
Paramater p for ceiling/wall arm extensions	1 m^{-1}
Combustible ceiling lining present?	1 (yes)
Corner configuration present?	1 (yes)
Use Complex radiation?	1 (yes)
Use gaslayer calcs. In radiation calcs.?	1 (yes)
Use accurate beam length calculation in radiation calculations?	0 (no)

4_50.MLR

CONE CURVE		
Point #	Time	HRR
	sec	kW/m^2
1	0	0.0
2	20	135.3
3	25	132.7
4	145	75.7
5	700	69.3
6	1005	10.8
7		
8		
9		
10		
11		
12		
13		
14		
15		
16		
17		
18		
19		
20		
21		
22		
23		
24		
25		
Irrad:	50	kW/m^2

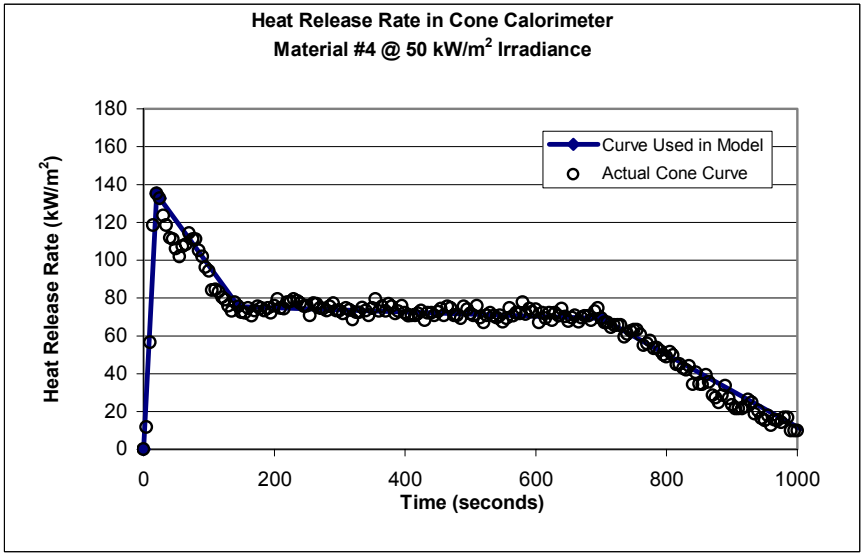

USCG.BRN

BURNER INPUTS	
Burner height above floor	0.152 m
Width of burner side	0.170 m
Use heat flux map?	1 (yes)

BASELINE INPUTS FOR MATERIAL #8 - POLYESTER

PROP_8?.DAT

MATERIAL PROPERTIES / INPUT PARAMETERS	
Height of bottom of slab above floor	0 m
Material density (ρ)	1390 kg/m^3
Material thickness (δ)	0.0241 m
Material specific heat (c_p)	1000 J/kg·K
Material thermal conductivity (k)	0.597 W/m·K
Material ignition Temperature (T_{ig})	662 K
Material initial uniform temperature	293.15 K
Timestep	0.5 sec
Output interval	1 sec
Simulation length	1200 sec
Specific heat of product gases	1340 J/kg·K
Net heat of complete combustion	3.25E+07 J/kg
Efficiency of combustion (χ_A)	0.665
Radiative fraction (χ_{rad})	0.476
Material emissivity (ε)	0.9
Flame transmissivity (τ_{flame})	0.5
Lateral flame spread parameter (Φ)	19.02 kW^2/m^3
Min. surface temp. for lateral spread ($T_{s,min}$)	479 K
Width of slab (2 x width of shorter wall)	4.8 m
Ceiling present?	1 (yes)
Allow multiple pyrolysis zones?	1 (yes)
Average heat flux from the ceiling	2000 kW/m^2
Paramater p for ceiling/wall arm extensions	1 m^{-1}
Combustible ceiling lining present?	1 (yes)
Corner configuration present?	1 (yes)
Use Complex radiation?	1 (yes)
Use gaslayer calcs. In radiation calcs.?	1 (yes)
Use accurate beam length calculation in radiation calculations?	0 (no)

8_50.MLR

CONE CURVE		
Point #	Time sec	HRR kW/m^2
1	0	0
2	25	336.7
3	30	341.8
4	150	259.4
5	180	272.0
6	225	140.7
7	315	43.4
8	355	32.1
9		
10		
11		
12		
13		
14		
15		
16		
17		
18		
19		
20		
21		
22		
23		
24		
25		
Irrad:	50	kW/m^2

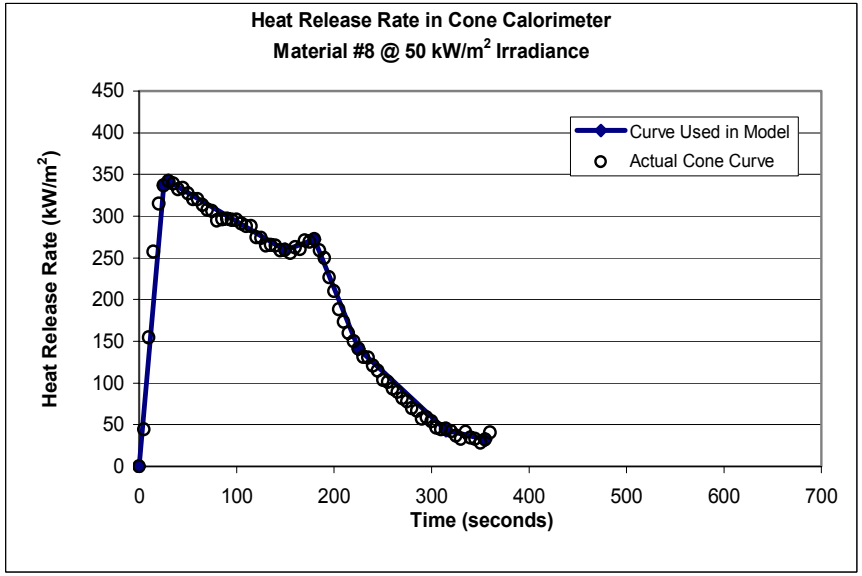

USCG.BRN

BURNER INPUTS	
Burner height above floor	0.152 m
Width of burner side	0.170 m
Use heat flux map?	1 (yes)

BASELINE INPUTS FOR MATERIAL #9 - FR ACRYLIC

PROP_9?.DAT

MATERIAL PROPERTIES / INPUT PARAMETERS	
Height of bottom of slab above floor	0 m
Material density (ρ)	1880 kg/m^3
Material thickness (δ)	0.0252 m
Material specific heat (c_p)	1000 J/kg·K
Material thermal conductivity (k)	1.511 W/m·K
Material ignition Temperature (T_{ig})	681 K
Material initial uniform temperature	293.15 K
Timestep	0.5 sec
Output interval	1 sec
Simulation length	1200 sec
Specific heat of product gases	1340 J/kg·K
Net heat of complete combustion	2.52E+07 J/kg
Efficiency of combustion (χ_A)	0.489
Radiative fraction (χ_{rad})	0.314
Material emissivity (ε)	0.9
Flame transmissivity (τ_{flame})	0.5
Lateral flame spread parameter (Φ)	23.22 kW^2/m^3
Min. surface temp. for lateral spread ($T_{s,min}$)	569 K
Width of slab (2 x width of shorter wall)	4.8 m
Ceiling present?	1 (yes)
Allow multiple pyrolysis zones?	1 (yes)
Average heat flux from the ceiling	2000 kW/m^2
Paramater p for ceiling/wall arm extensions	1 m^{-1}
Combustible ceiling lining present?	1 (yes)
Corner configuration present?	1 (yes)
Use Complex radiation?	1 (yes)
Use gaslayer calcs. In radiation calcs.?	1 (yes)
Use accurate beam length calculation in radiation calculations?	0 (no)

9_50.MLR

CONE CURVE		
Point #	Time sec	HRR kW/m^2
1	0	0
2	5	1.8
3	12	56.0
4	18	98.3
5	28	128.5
6	79	75.6
7	155	59.9
8	550	41.6
9	645	40.3
10	1070	18.0
11		
12		
13		
14		
15		
16		
17		
18		
19		
20		
21		
22		
23		
24		
25		
Irrad:	50	kW/m^2

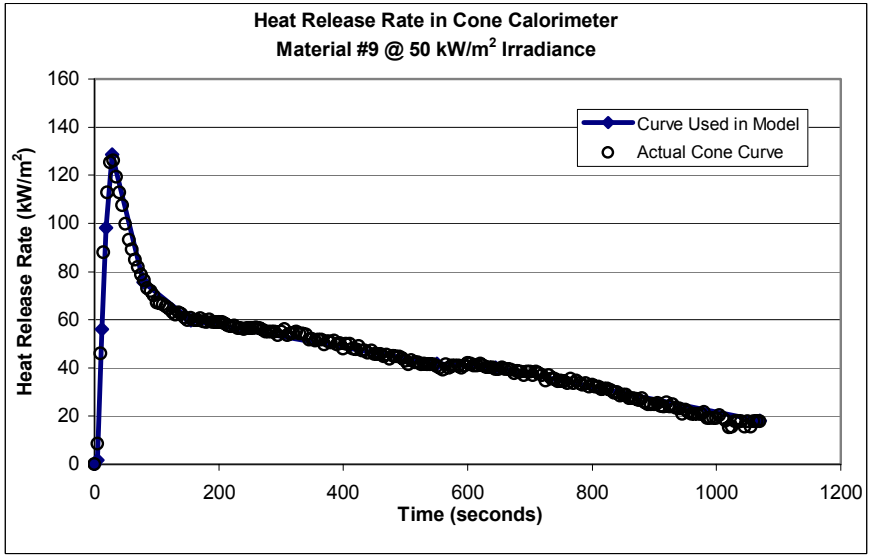

USCG.BRN

BURNER INPUTS	
Burner height above floor	0.152 m
Width of burner side	0.170 m
Use heat flux map?	1 (yes)

Appendix K – Additional Cone Calorimeter Curves

ADDITIONAL CURVES FOR MATERIAL #3 - FR POLYESTER

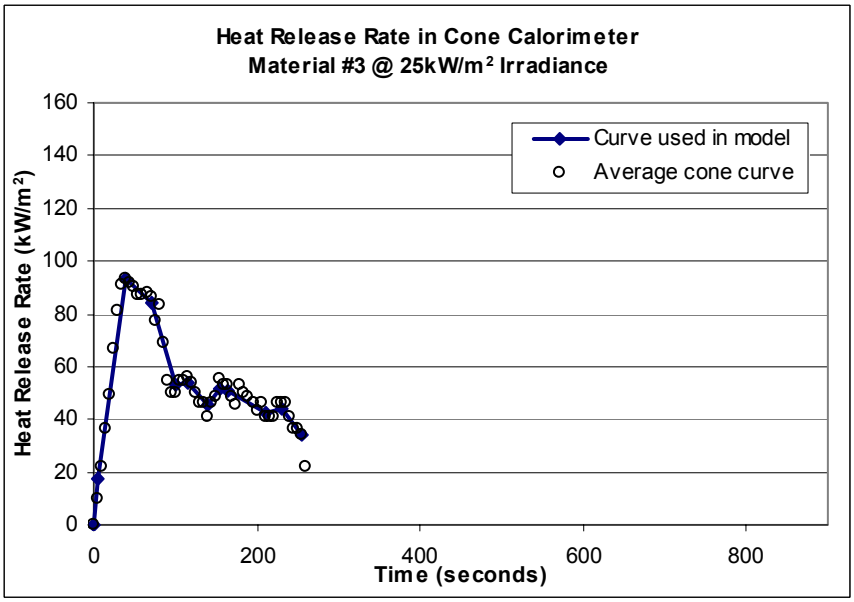

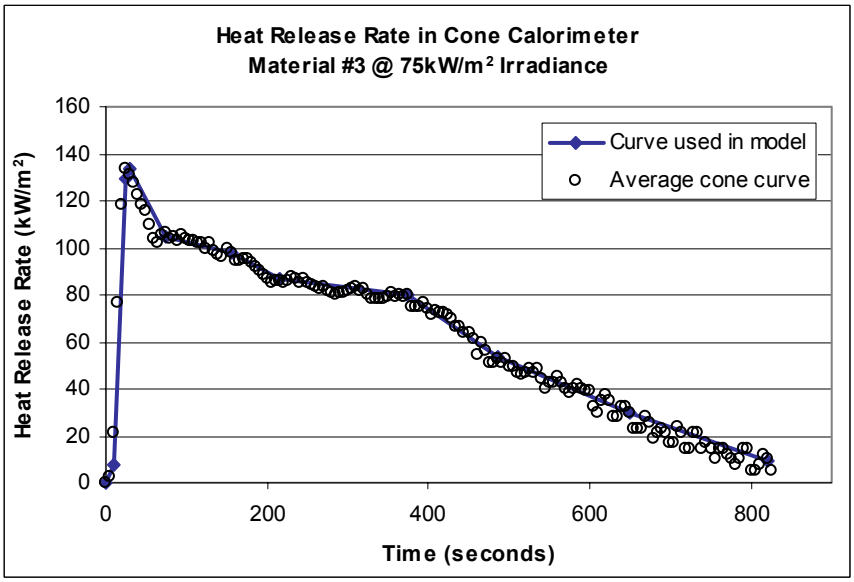

ADDITIONAL CURVES FOR MATERIAL #4 - FR VINYLESTER

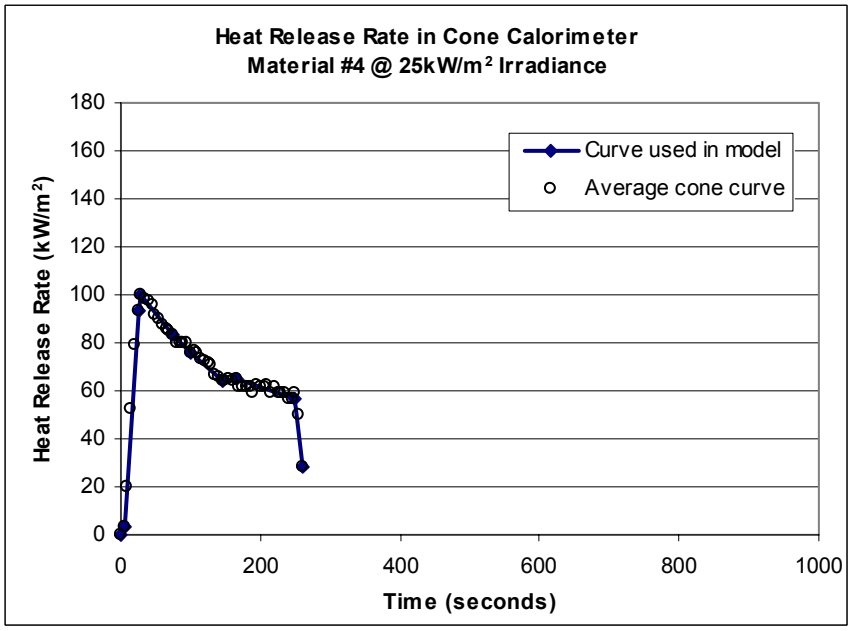

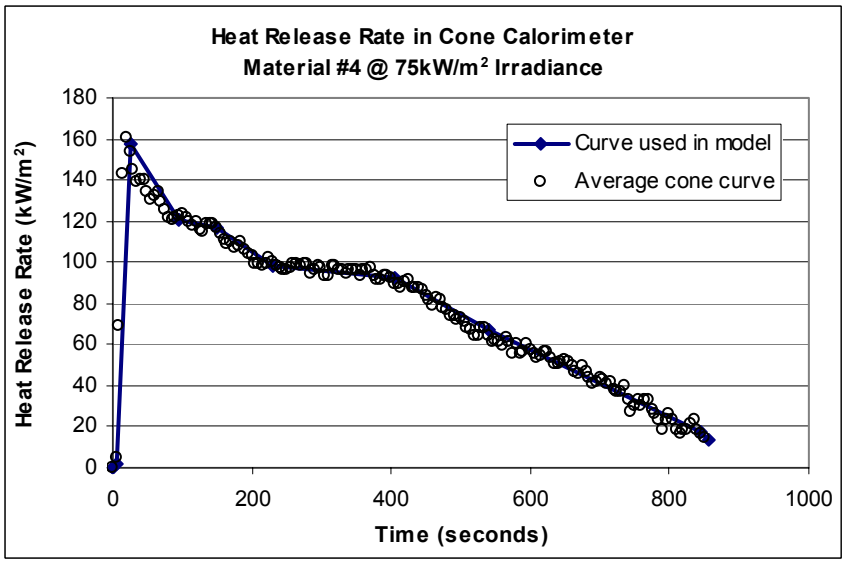

ADDITIONAL CURVES FOR MATERIAL #8 - POLYESTER

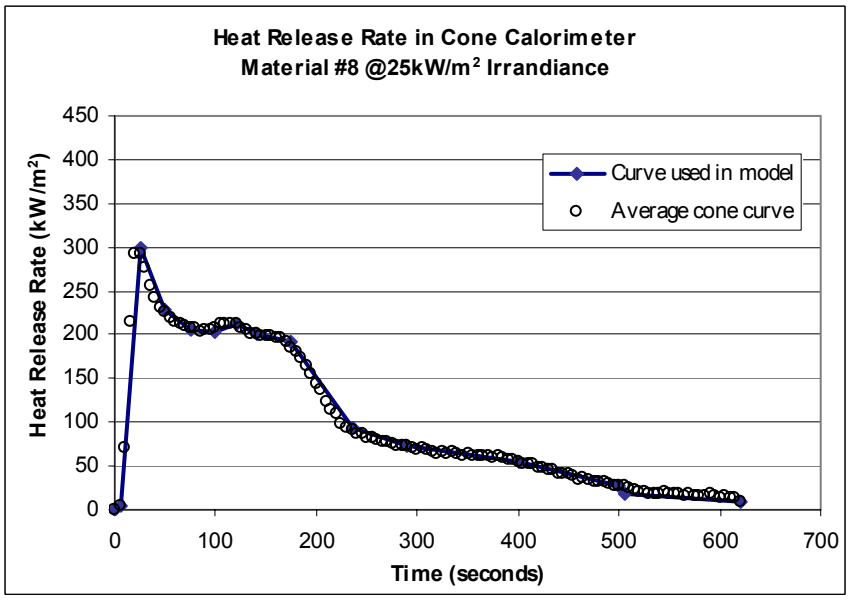

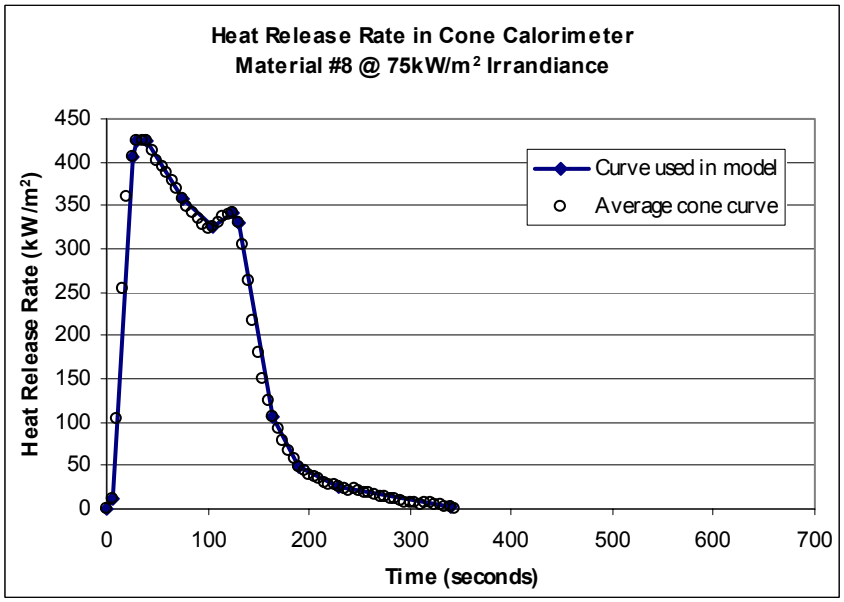

ADDITIONAL CURVES FOR MATERIAL #9 - FR ACRYLIC

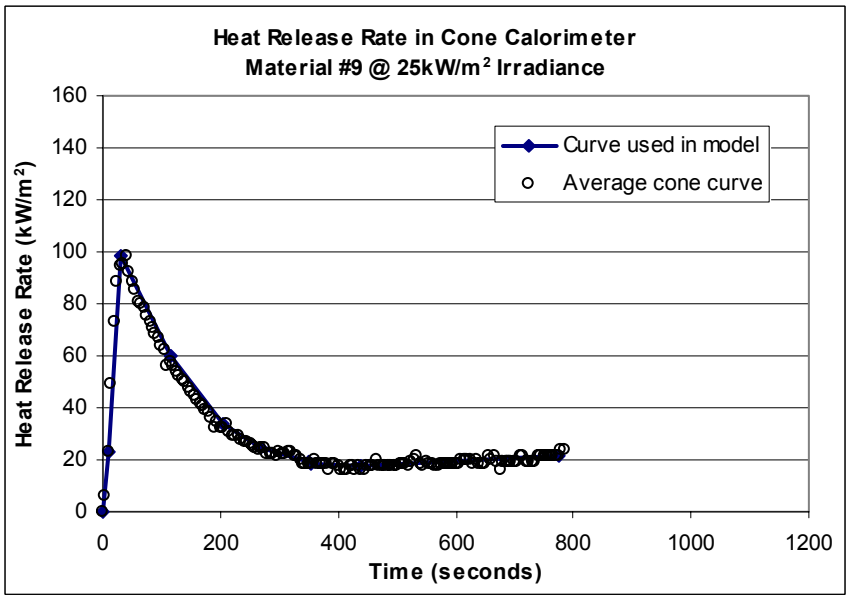

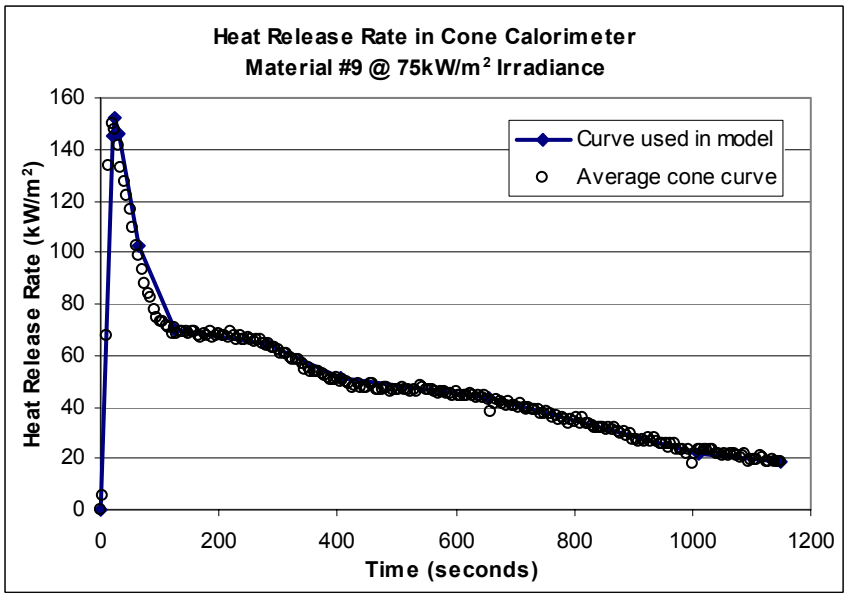

Appendix L – Simulation Results

The results from the simulations are presented in the following order:

1) Material #3 – FR Polyester
- variation of thermal conductivity
- variation of Cone Calorimeter curves
- variation of material emissivity
- variation of flame transmissivity
- variation of ignition temperature
- variation of minimum temperature for lateral flame spread
- variation of flame spread parameter

2) Material #4 – FR Vinylester
- variation of thermal conductivity
- variation of Cone Calorimeter curves
- variation of material emissivity
- variation of flame transmissivity
- variation of ignition temperature
- variation of minimum temperature for lateral flame spread
- variation of flame spread parameter

3) Material #8 – Polyester
- variation of thermal conductivity
- variation of Cone Calorimeter curves
- variation of material emissivity
- variation of flame transmissivity
- variation of ignition temperature
- variation of minimum temperature for lateral flame spread
- variation of flame spread parameter

4) Material #9 – FR Acrylic
- variation of thermal conductivity
- variation of Cone Calorimeter curves
- variation of material emissivity

- variation of flame transmissivity
- variation of ignition temperature
- variation of minimum temperature for lateral flame spread
- variation of flame spread parameter

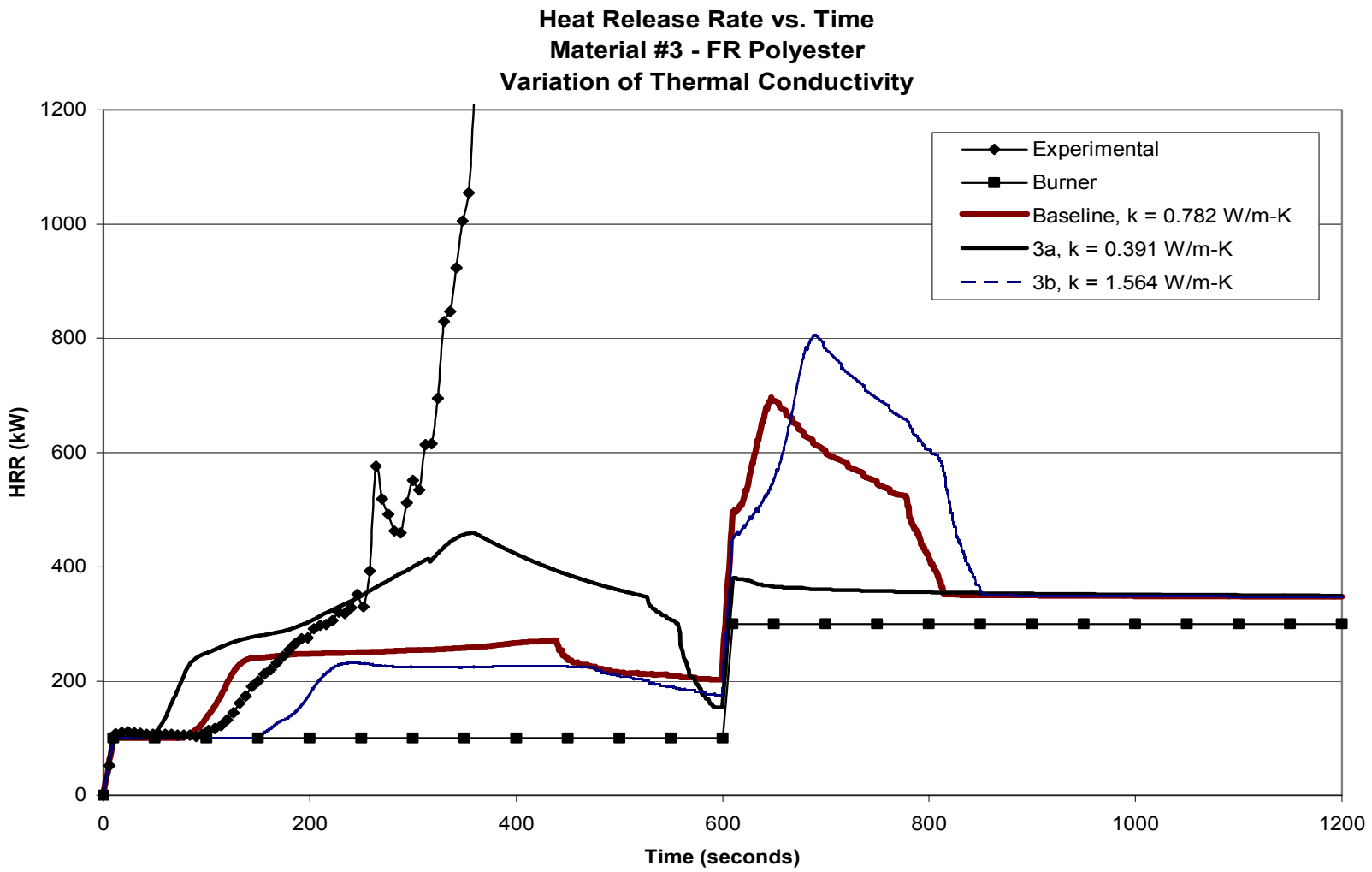
Heat Release Rate vs. Time
Material #3 - FR Polyester
Variation of Thermal Conductivity
HRR (kW)
Time (seconds)
0
200
400
600
800
1000
1200
Experimental
Burner
Baseline, k = 0.782 W/m-K
3a, k = 0.391 W/m-K
3b, k = 1.564 W/m-K

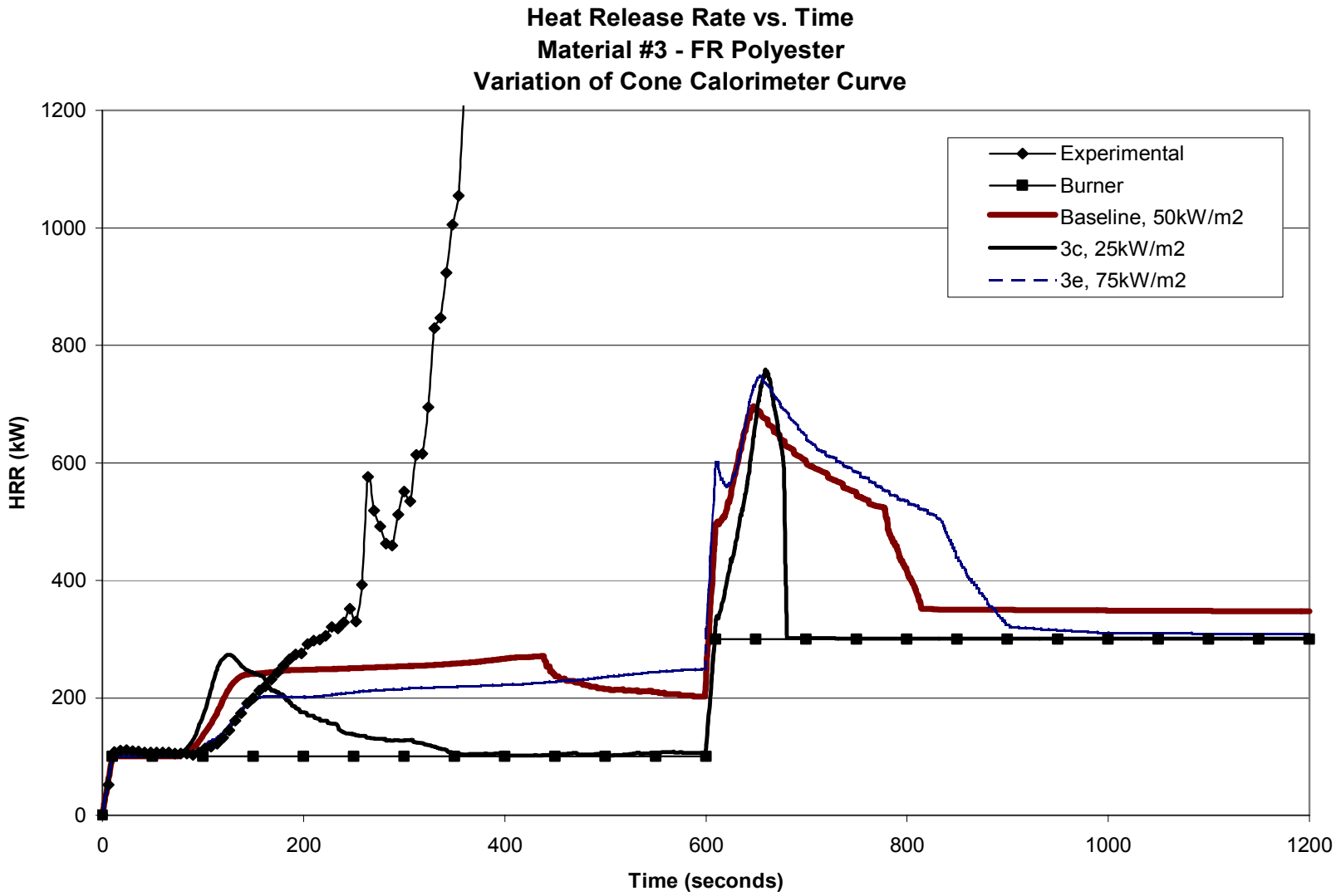
Heat Release Rate vs. Time
Material #3 - FR Polyester
Variation of Cone Calorimeter Curve
HRR (kW)
Time (seconds)
0
200
400
600
800
1000
1200
Experimental
Burner
Baseline, 50kW/m2
3c, 25kW/m2
3e, 75kW/m2

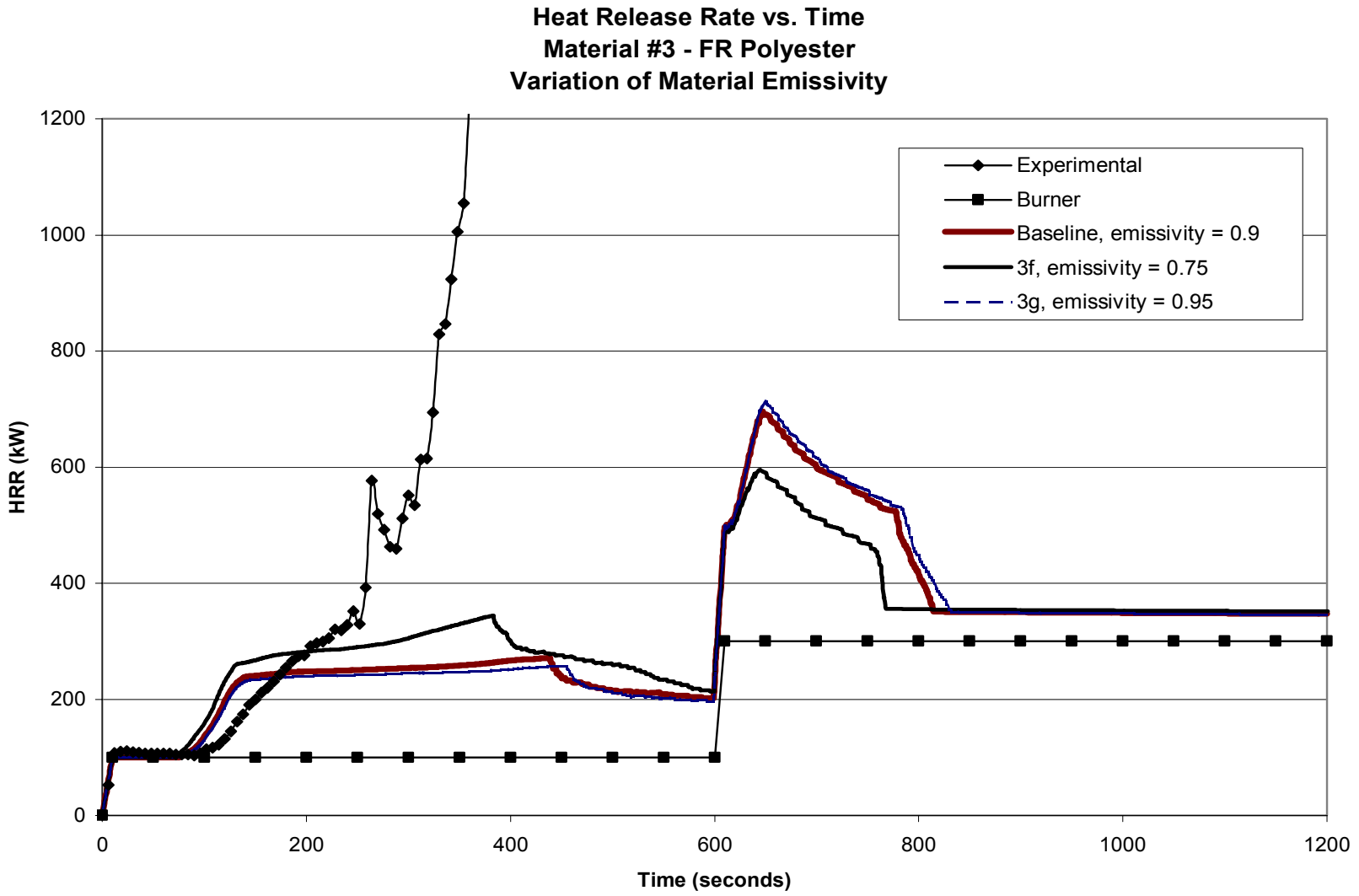
Heat Release Rate vs. Time
Material #3 - FR Polyester
Variation of Material Emissivity
HRR (kW)
Time (seconds)
0
200
400
600
800
1000
1200
Experimental
Burner
Baseline, emissivity = 0.9
3f, emissivity = 0.75
3g, emissivity = 0.95

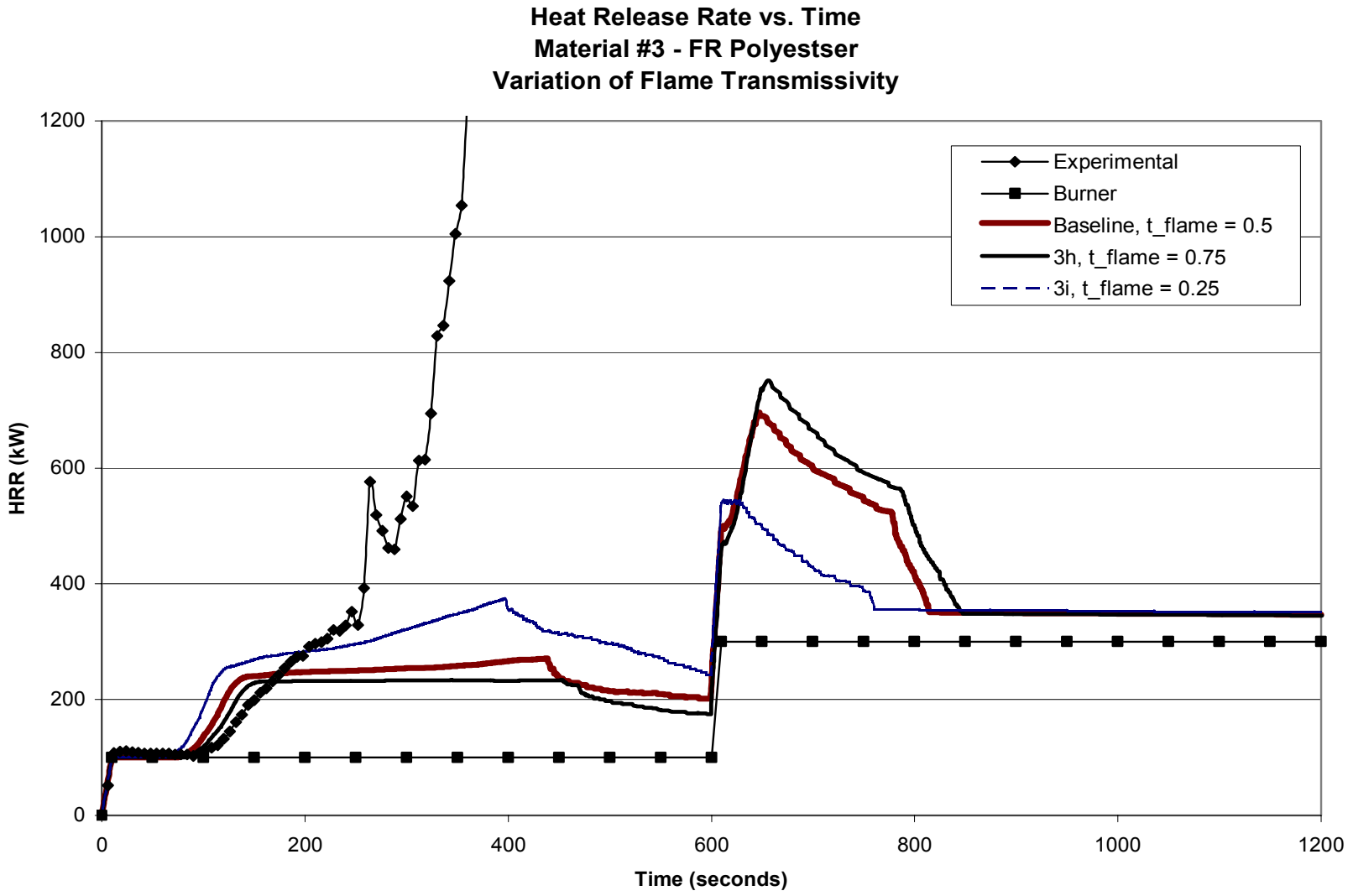
Heat Release Rate vs. Time
Material #3 - FR Polyestser
Variation of Flame Transmissivity
HRR (kW)
Time (seconds)
0
200
400
600
800
1000
1200
Experimental
Burner
Baseline, t_flame = 0.5
3h, t_flame = 0.75
3i, t_flame = 0.25

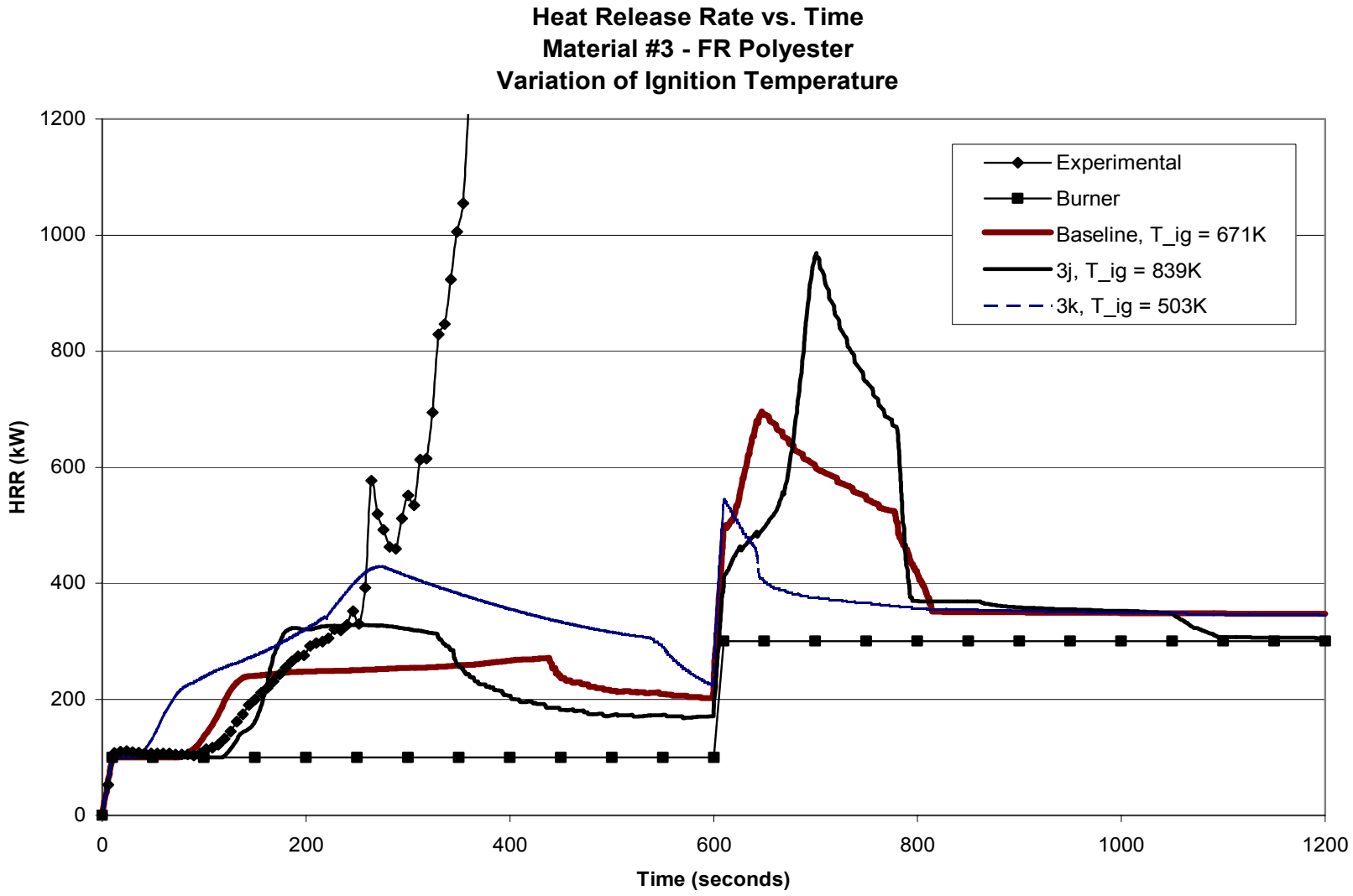
Heat Release Rate vs. Time
Material #3 - FR Polyester
Variation of Ignition Temperature
HRR (kW)
Time (seconds)
0
200
400
600
800
1000
1200
Experimental
Burner
Baseline, T_ig = 671K
3j, T_ig = 839K
3k, T_ig = 503K

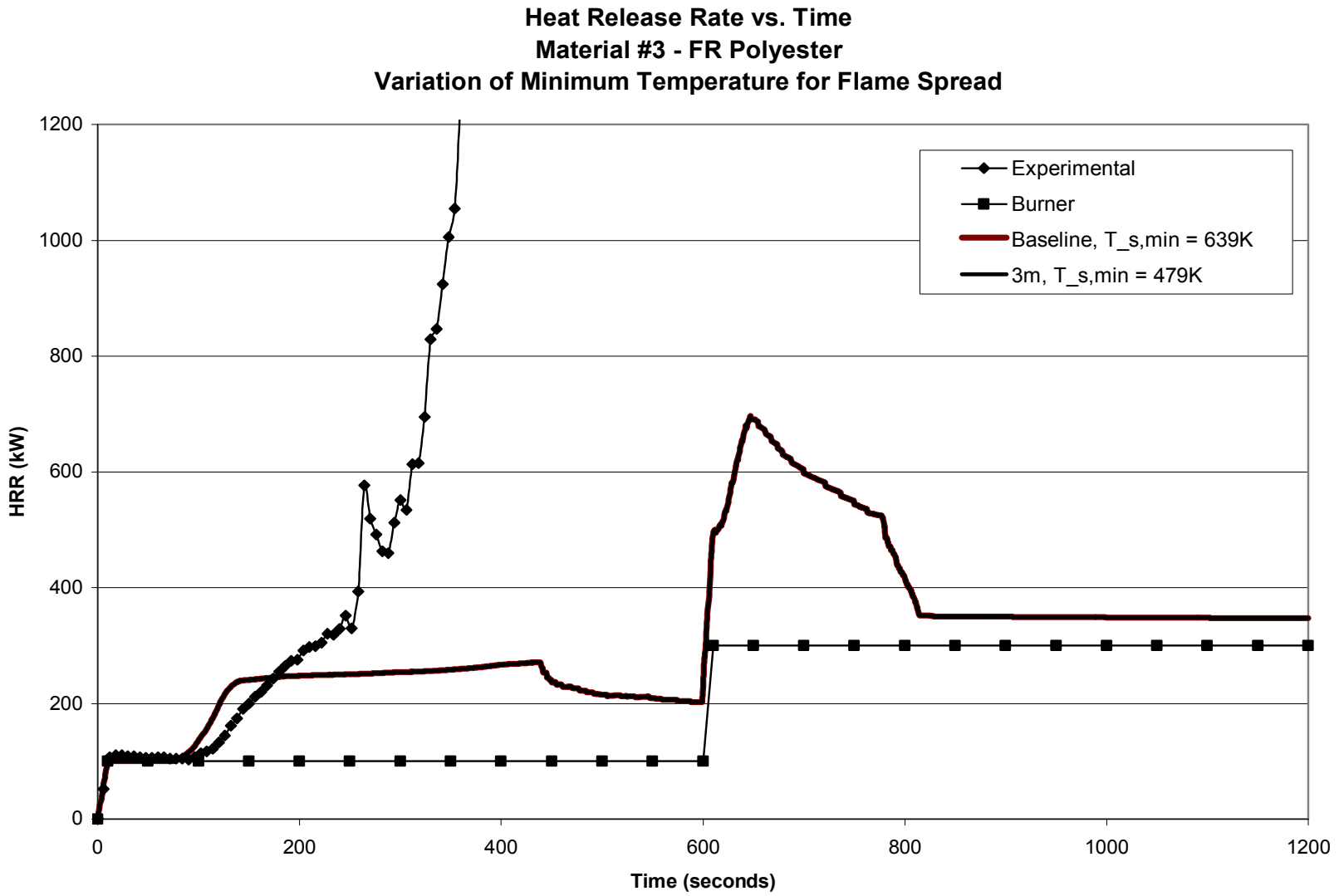
Heat Release Rate vs. Time
Material #3 - FR Polyester
Variation of Minimum Temperature for Flame Spread
HRR (kW)
Time (seconds)
0
200
400
600
800
1000
1200
Experimental
Burner
Baseline, T_s,min = 639K
3m, T_s,min = 479K

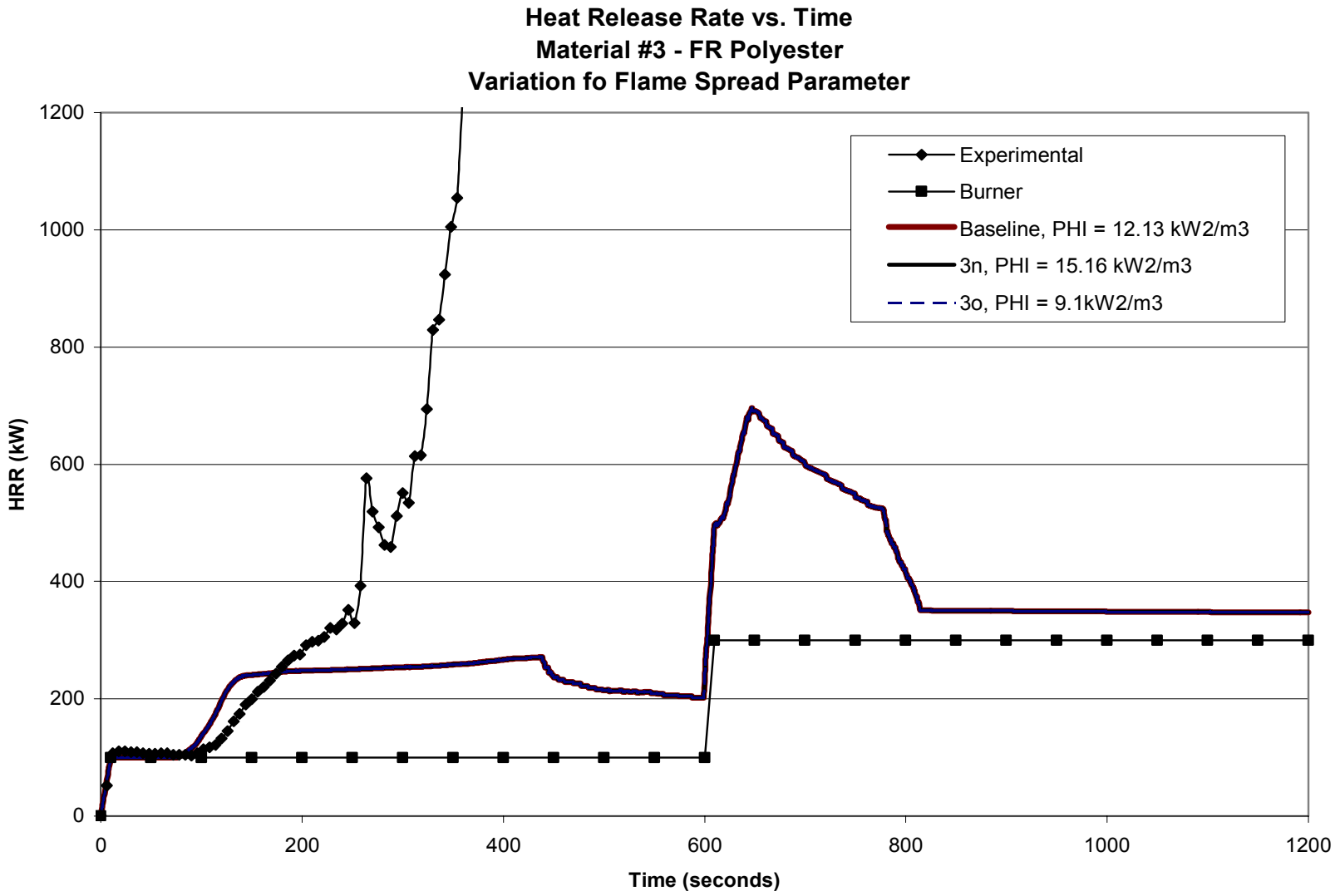
Heat Release Rate vs. Time
Material #3 - FR Polyester
Variation fo Flame Spread Parameter
HRR (kW)
Time (seconds)
0
200
400
600
800
1000
1200
Experimental
Burner
Baseline, PHI = 12.13 kW2/m3
3n, PHI = 15.16 kW2/m3
3o, PHI = 9.1kW2/m3

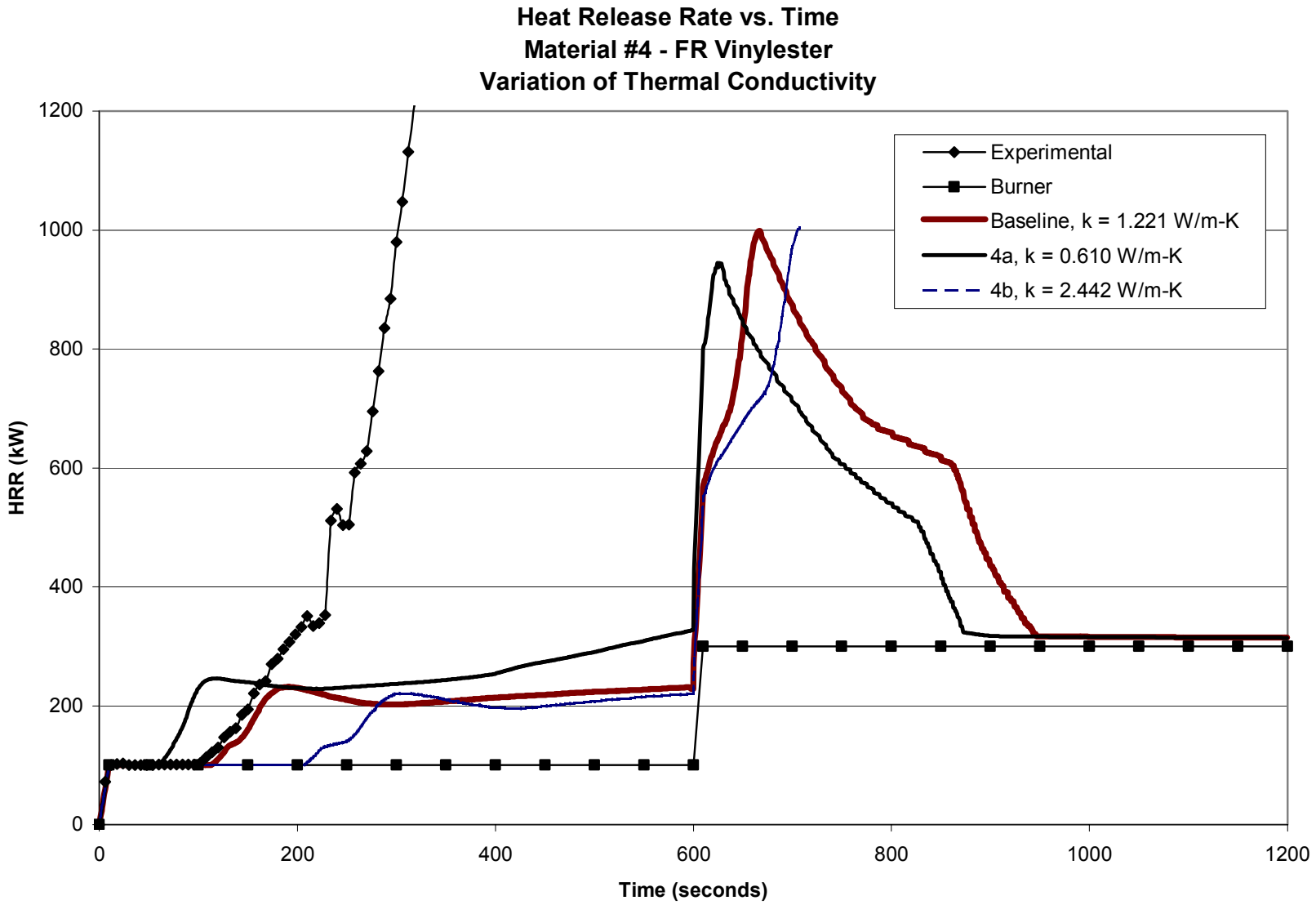
Heat Release Rate vs. Time
Material #4 - FR Vinylester
Variation of Thermal Conductivity
HRR (kW)
Time (seconds)
0
200
400
600
800
1000
1200
Experimental
Burner
Baseline, k = 1.221 W/m-K
4a, k = 0.610 W/m-K
4b, k = 2.442 W/m-K

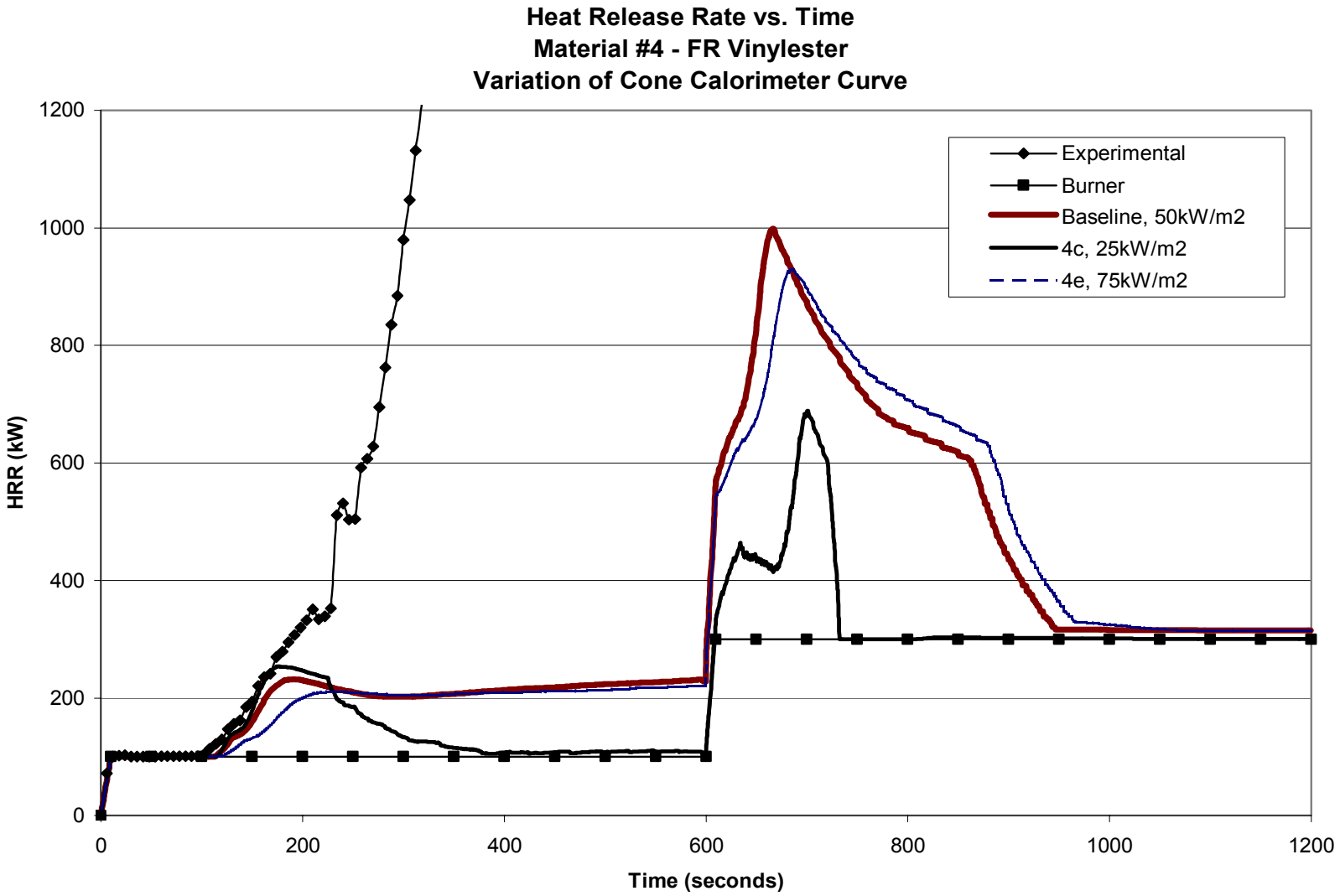
Heat Release Rate vs. Time
Material #4 - FR Vinylester
Variation of Cone Calorimeter Curve
HRR (kW)
Time (seconds)
0
200
400
600
800
1000
1200
Experimental
Burner
Baseline, 50kW/m2
4c, 25kW/m2
4e, 75kW/m2

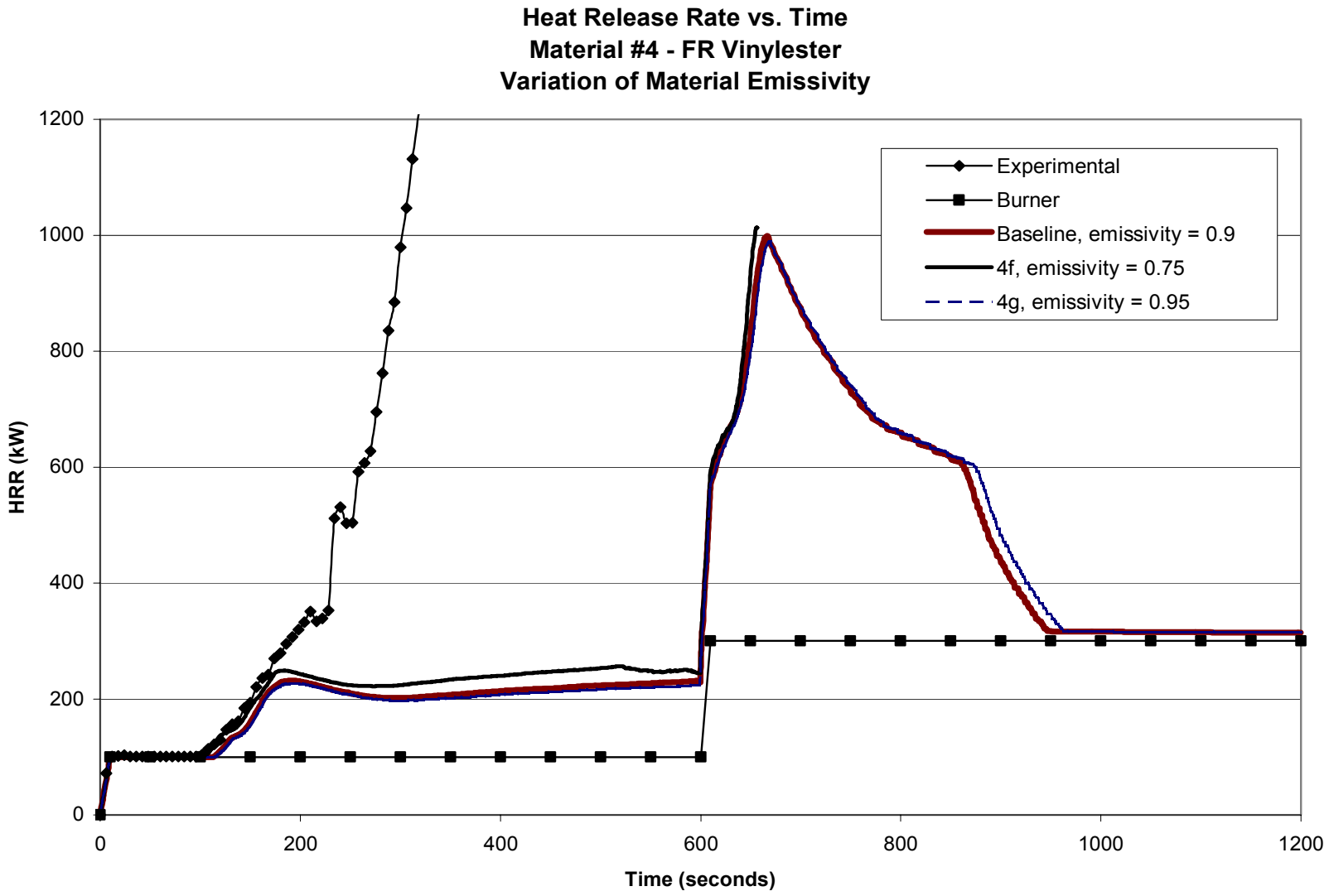
Heat Release Rate vs. Time
Material #4 - FR Vinylester
Variation of Material Emissivity
HRR (kW)
Time (seconds)
0
200
400
600
800
1000
1200
Experimental
Burner
Baseline, emissivity = 0.9
4f, emissivity = 0.75
4g, emissivity = 0.95

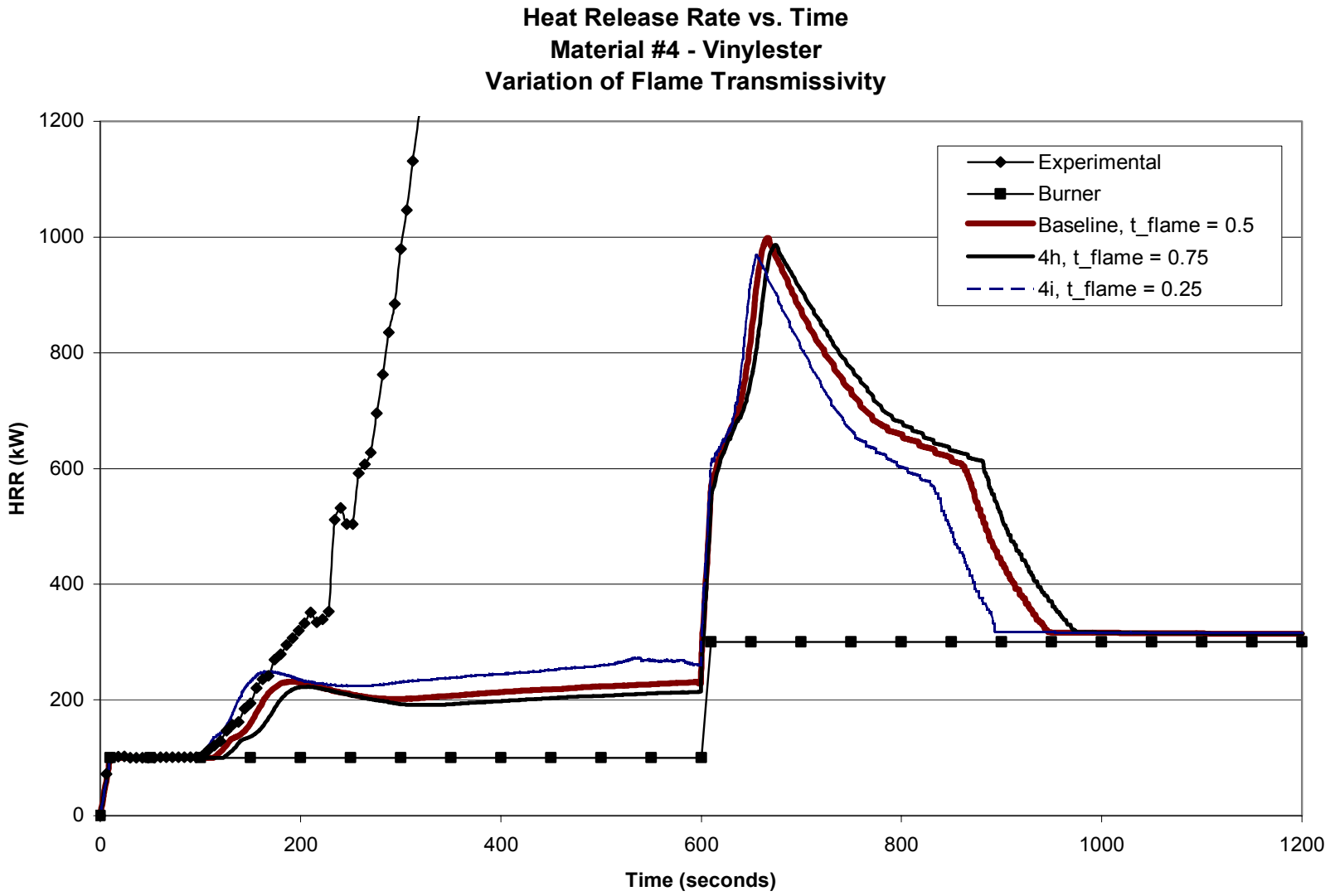
Heat Release Rate vs. Time
Material #4 - Vinylester
Variation of Flame Transmissivity
HRR (kW)
Time (seconds)
0
200
400
600
800
1000
1200
Experimental
Burner
Baseline, t_flame = 0.5
4h, t_flame = 0.75
4i, t_flame = 0.25

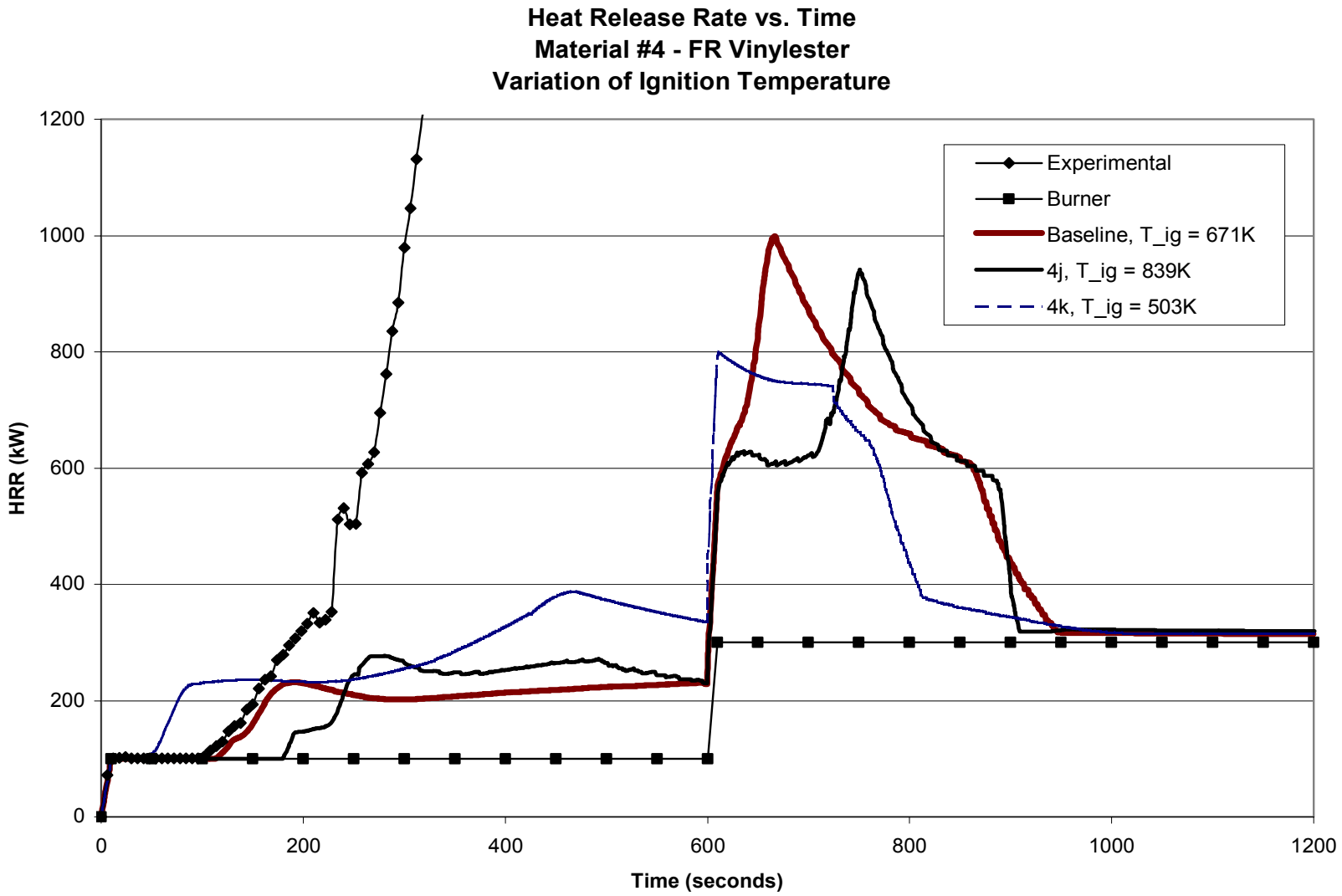
Heat Release Rate vs. Time
Material #4 - FR Vinylester
Variation of Ignition Temperature
HRR (kW)
Time (seconds)
0
200
400
600
800
1000
1200
Experimental
Burner
Baseline, T_ig = 671K
4j, T_ig = 839K
4k, T_ig = 503K

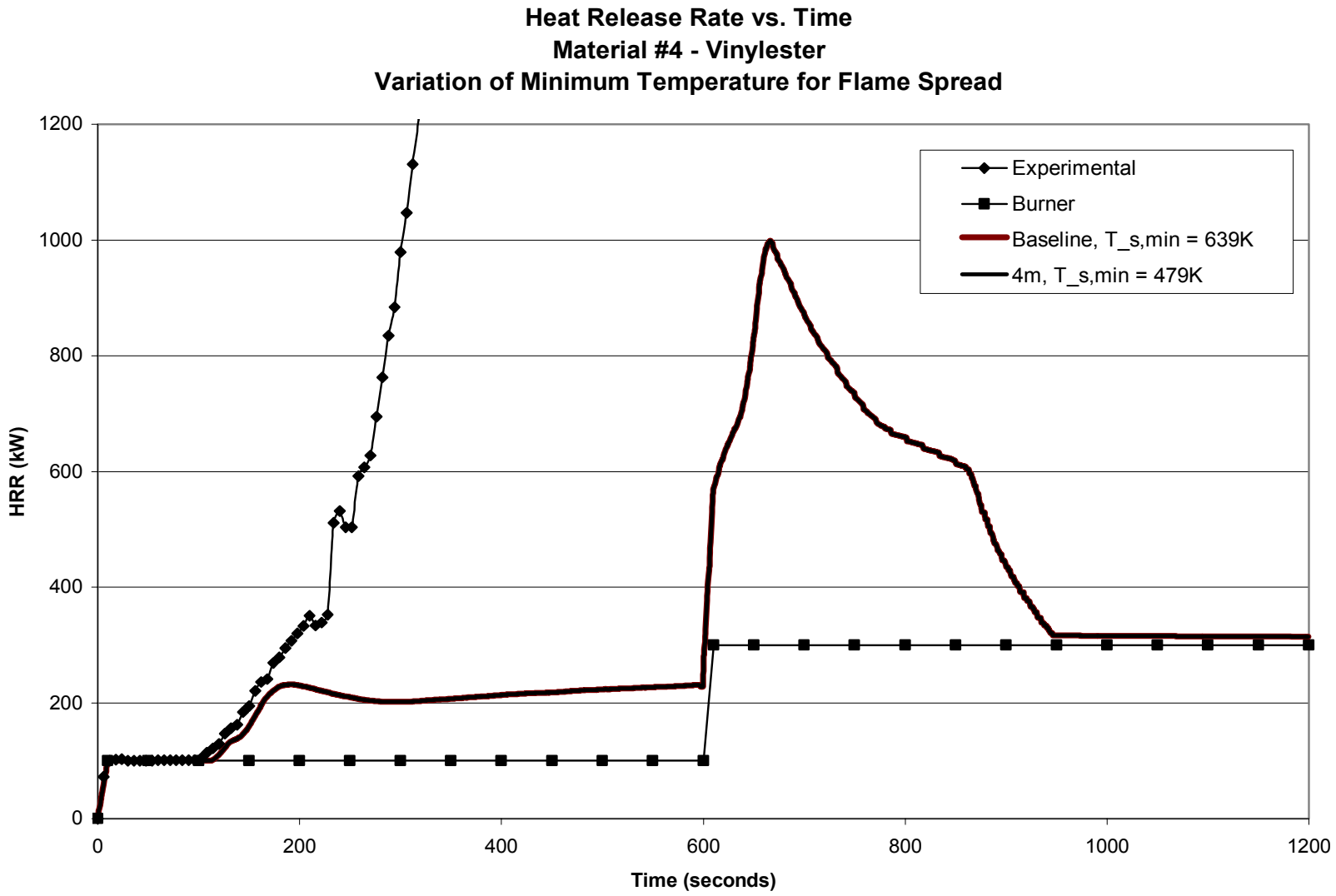
Heat Release Rate vs. Time
Material #4 - Vinylester
Variation of Minimum Temperature for Flame Spread
HRR (kW)
Time (seconds)
0
200
400
600
800
1000
1200
Experimental
Burner
Baseline, T_s,min = 639K
4m, T_s,min = 479K

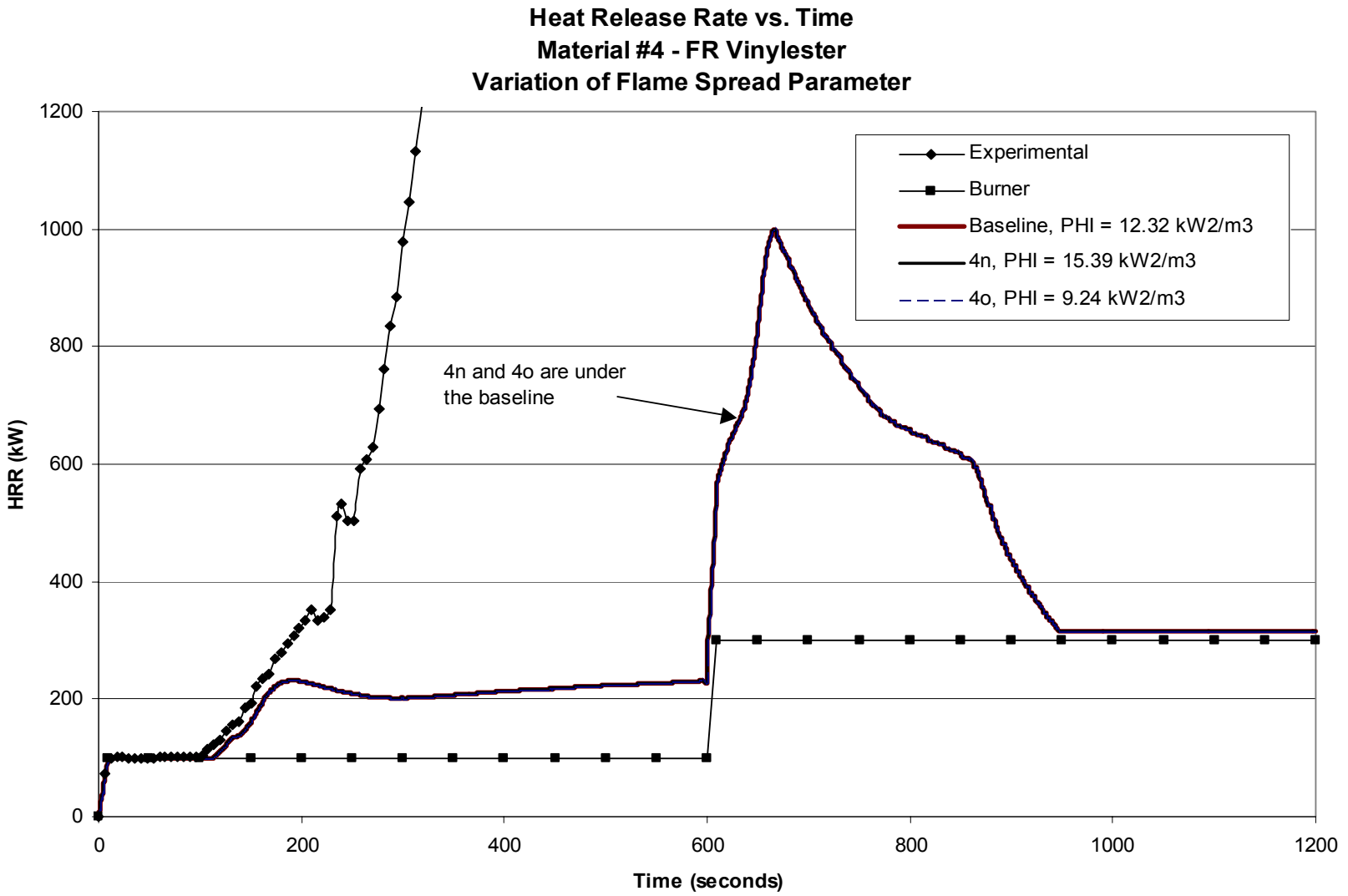
Heat Release Rate vs. Time
Material #4 - FR Vinylester
Variation of Flame Spread Parameter
HRR (kW)
Time (seconds)
0
200
400
600
800
1000
1200
Experimental
Burner
Baseline, PHI = 12.32 kW2/m3
4n, PHI = 15.39 kW2/m3
4o, PHI = 9.24 kW2/m3
4n and 4o are under
the baseline

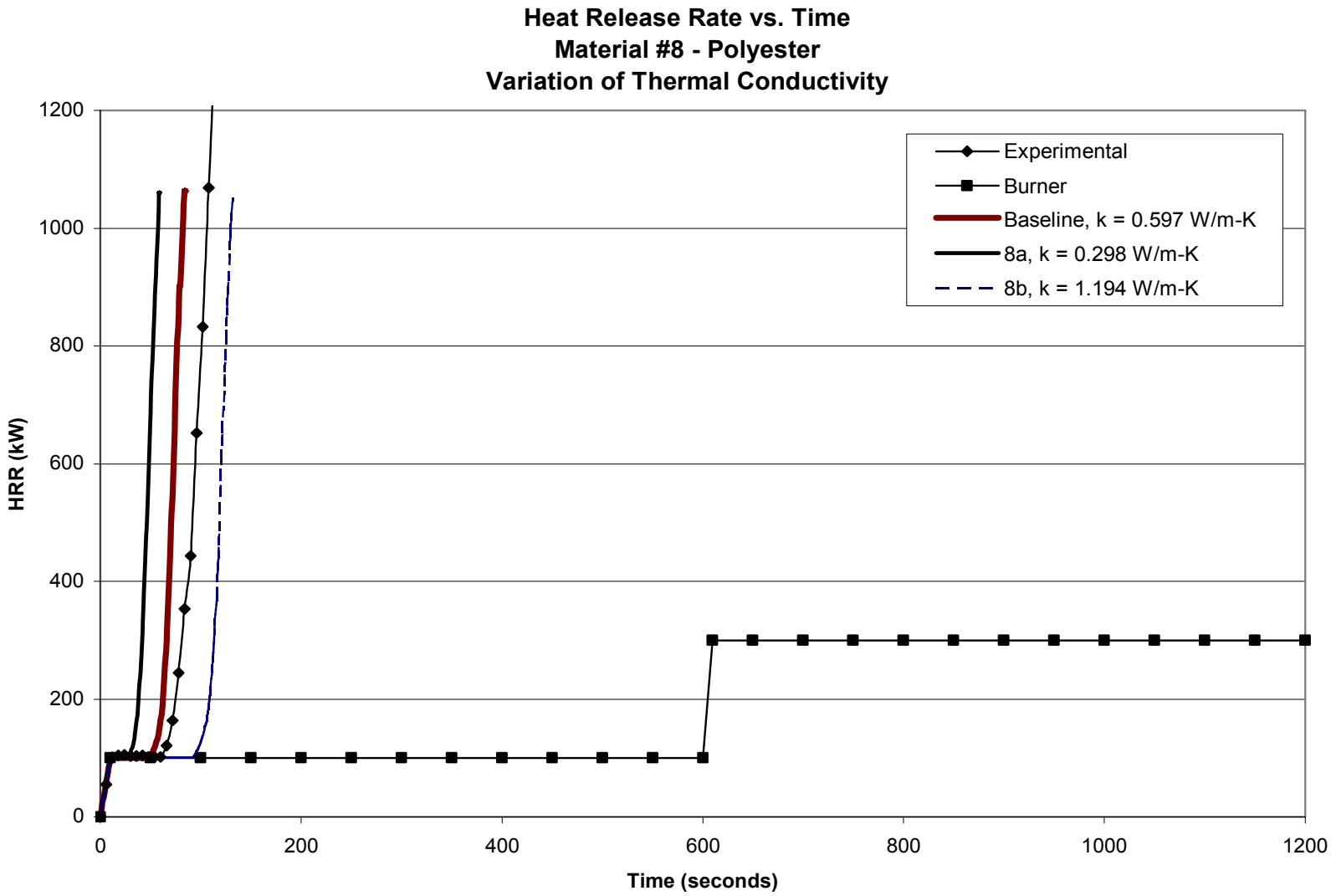
Heat Release Rate vs. Time
Material #8 - Polyester
Variation of Thermal Conductivity
HRR (kW)
Time (seconds)
0
200
400
600
800
1000
1200
Experimental
Burner
Baseline, k = 0.597 W/m-K
8a, k = 0.298 W/m-K
8b, k = 1.194 W/m-K

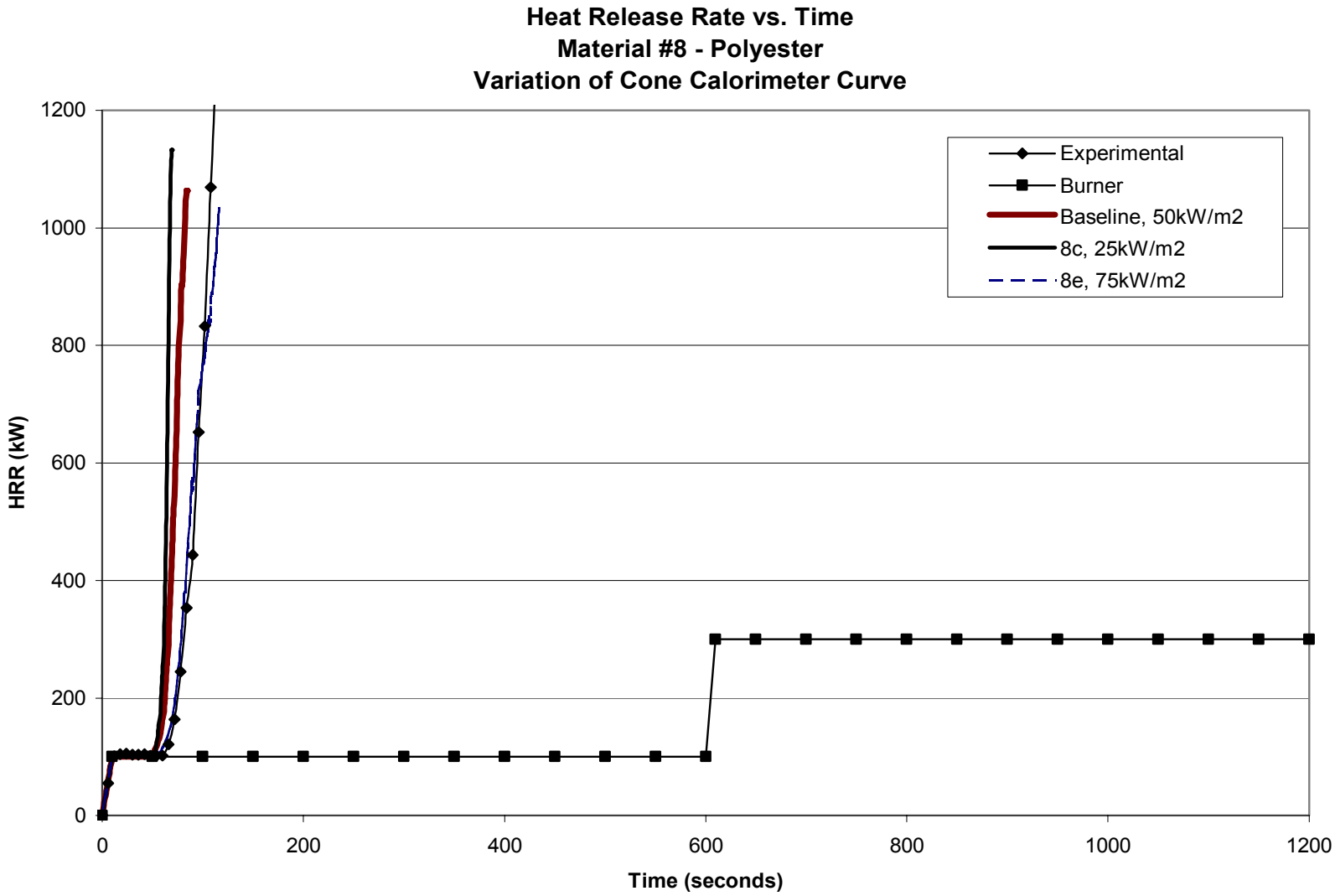
Heat Release Rate vs. Time
Material #8 - Polyester
Variation of Cone Calorimeter Curve
HRR (kW)
Time (seconds)
0
200
400
600
800
1000
1200
Experimental
Burner
Baseline, 50kW/m2
8c, 25kW/m2
8e, 75kW/m2

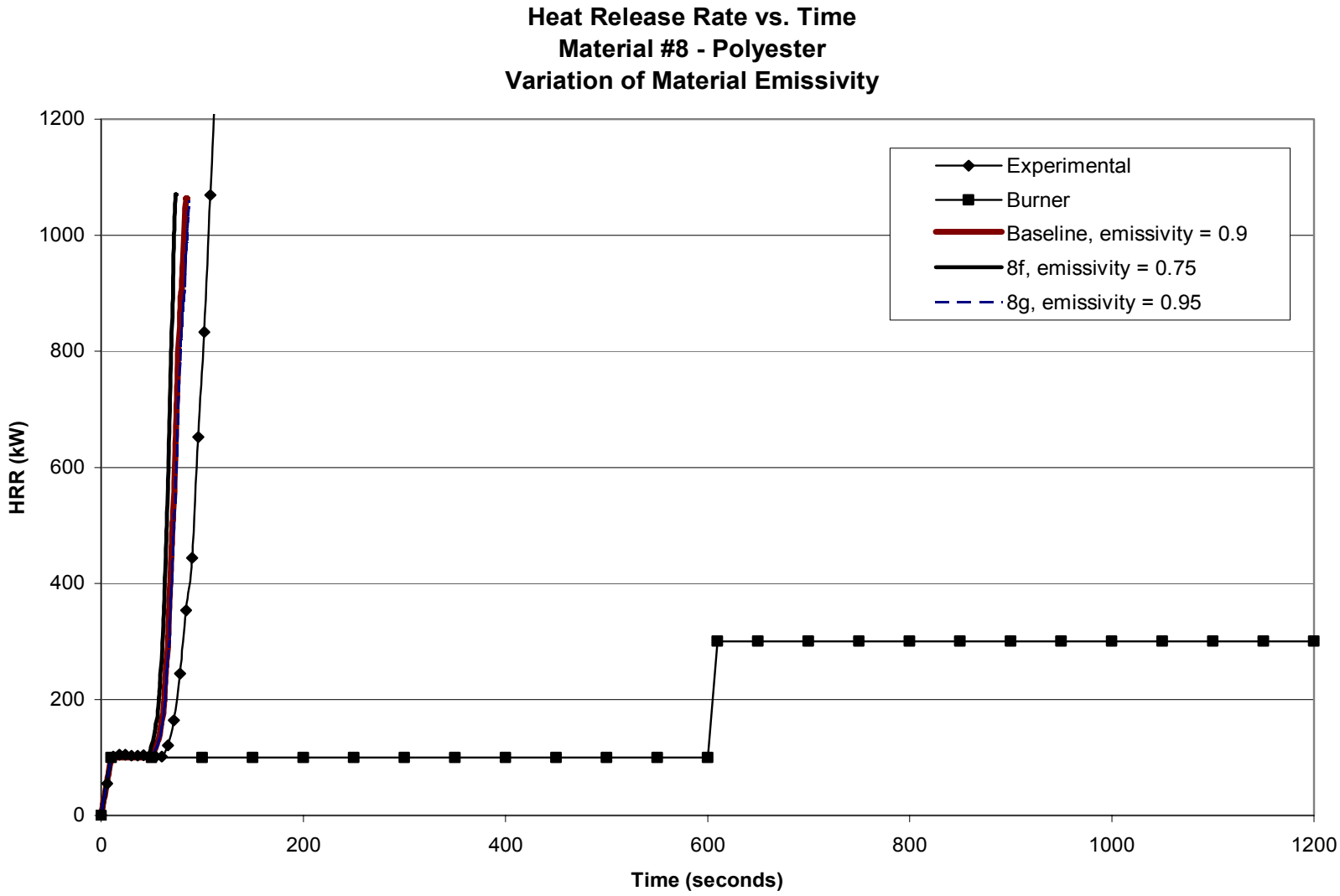
Heat Release Rate vs. Time
Material #8 - Polyester
Variation of Material Emissivity
HRR (kW)
Time (seconds)
0
200
400
600
800
1000
1200
Experimental
Burner
Baseline, emissivity = 0.9
8f, emissivity = 0.75
8g, emissivity = 0.95

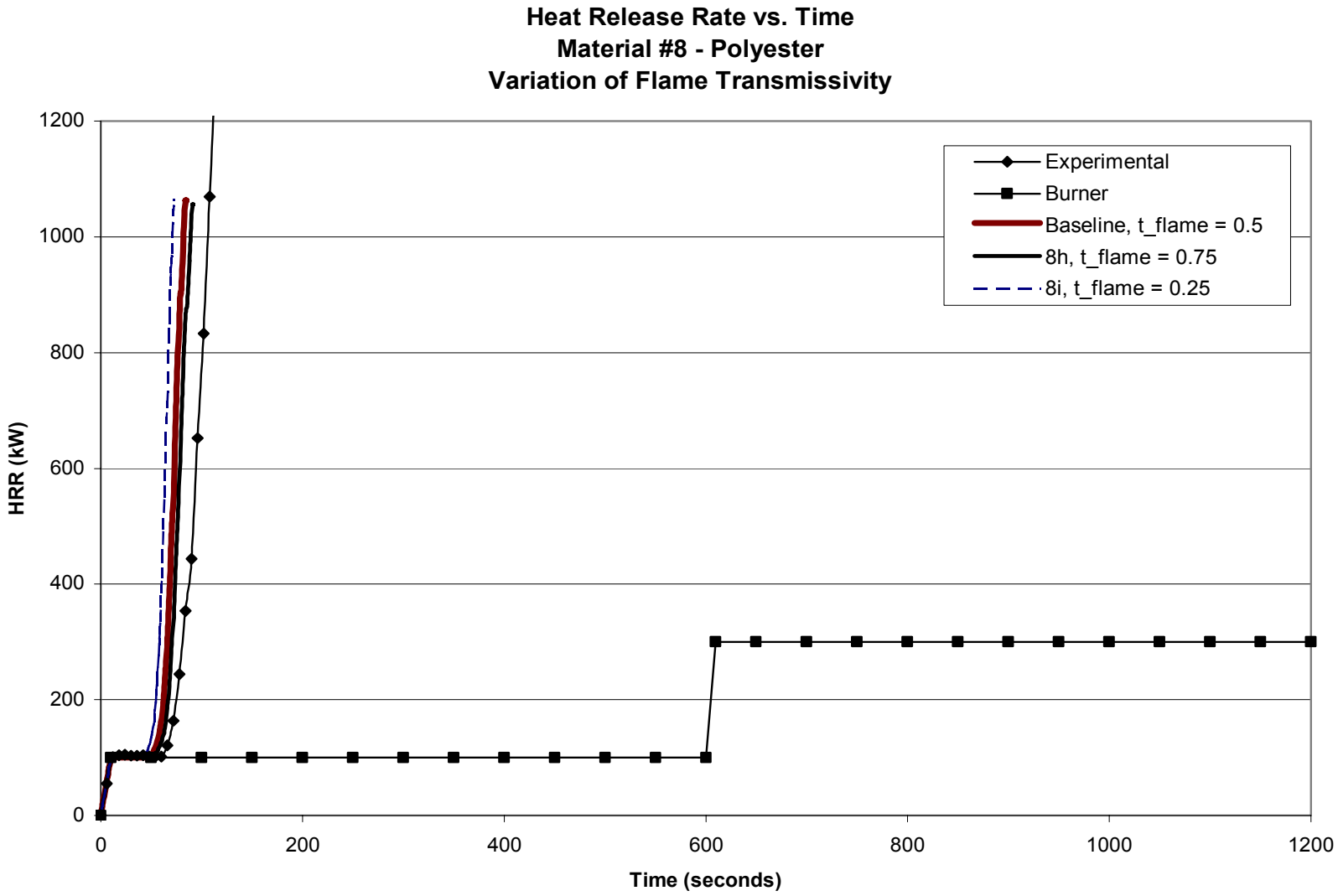
Heat Release Rate vs. Time
Material #8 - Polyester
Variation of Flame Transmissivity
HRR (kW)
Time (seconds)
0
200
400
600
800
1000
1200
Experimental
Burner
Baseline, t_flame = 0.5
8h, t_flame = 0.75
8i, t_flame = 0.25

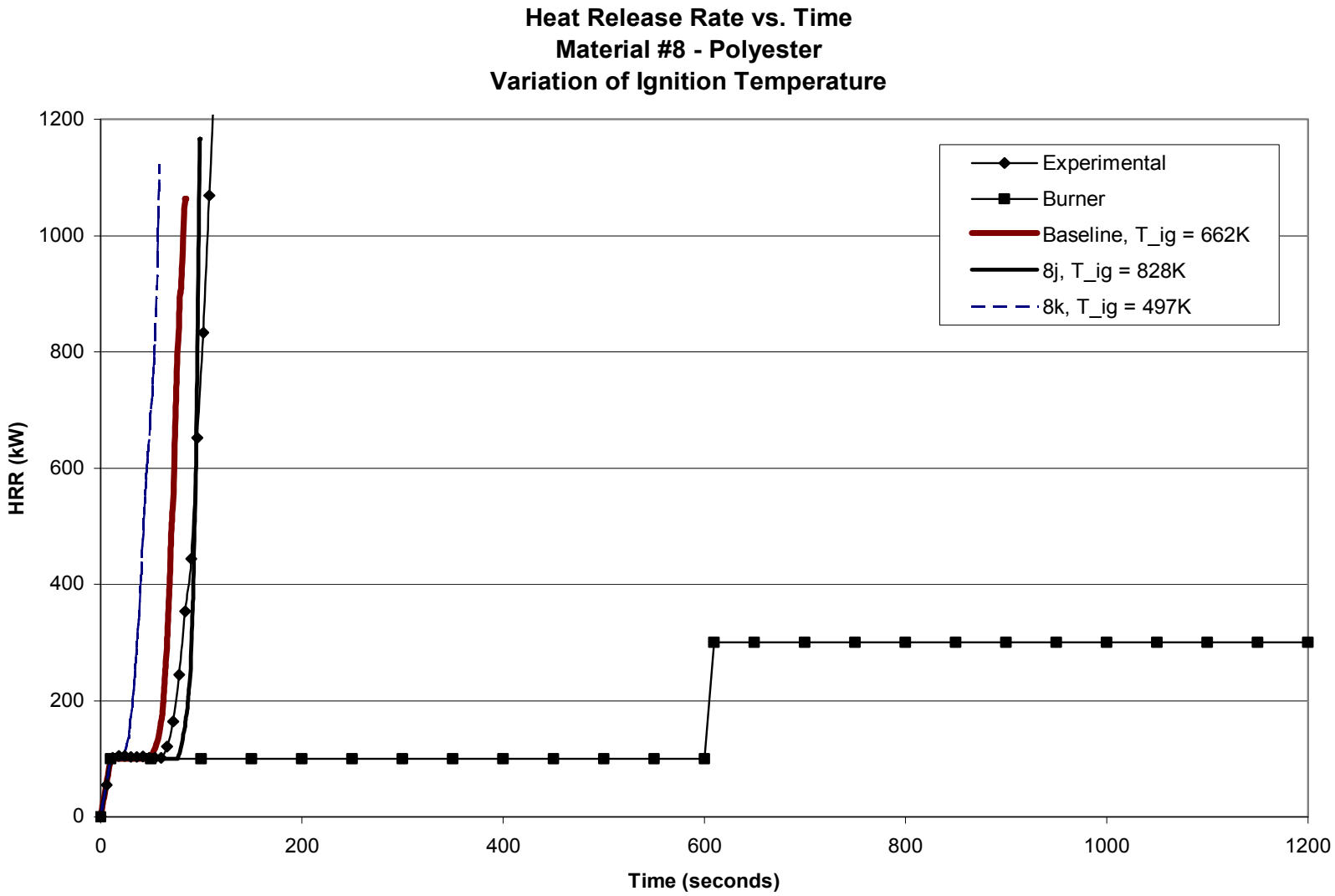
Heat Release Rate vs. Time
Material #8 - Polyester
Variation of Ignition Temperature
HRR (kW)
Time (seconds)
0
200
400
600
800
1000
1200
Experimental
Burner
Baseline, T_ig = 662K
8j, T_ig = 828K
8k, T_ig = 497K

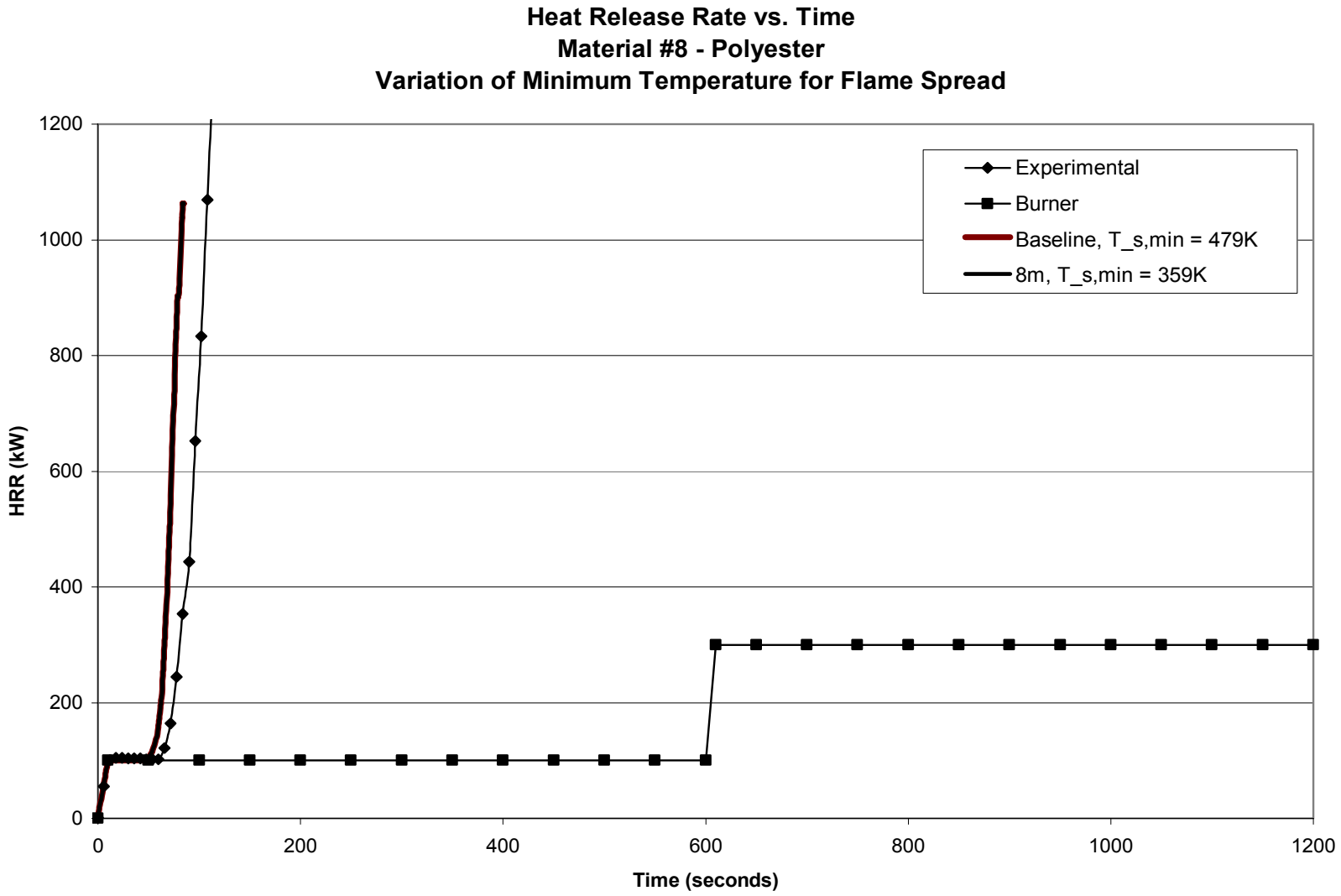
Heat Release Rate vs. Time
Material #8 - Polyester
Variation of Minimum Temperature for Flame Spread
HRR (kW)
Time (seconds)
0
200
400
600
800
1000
1200
Experimental
Burner
Baseline, T_s,min = 479K
8m, T_s,min = 359K

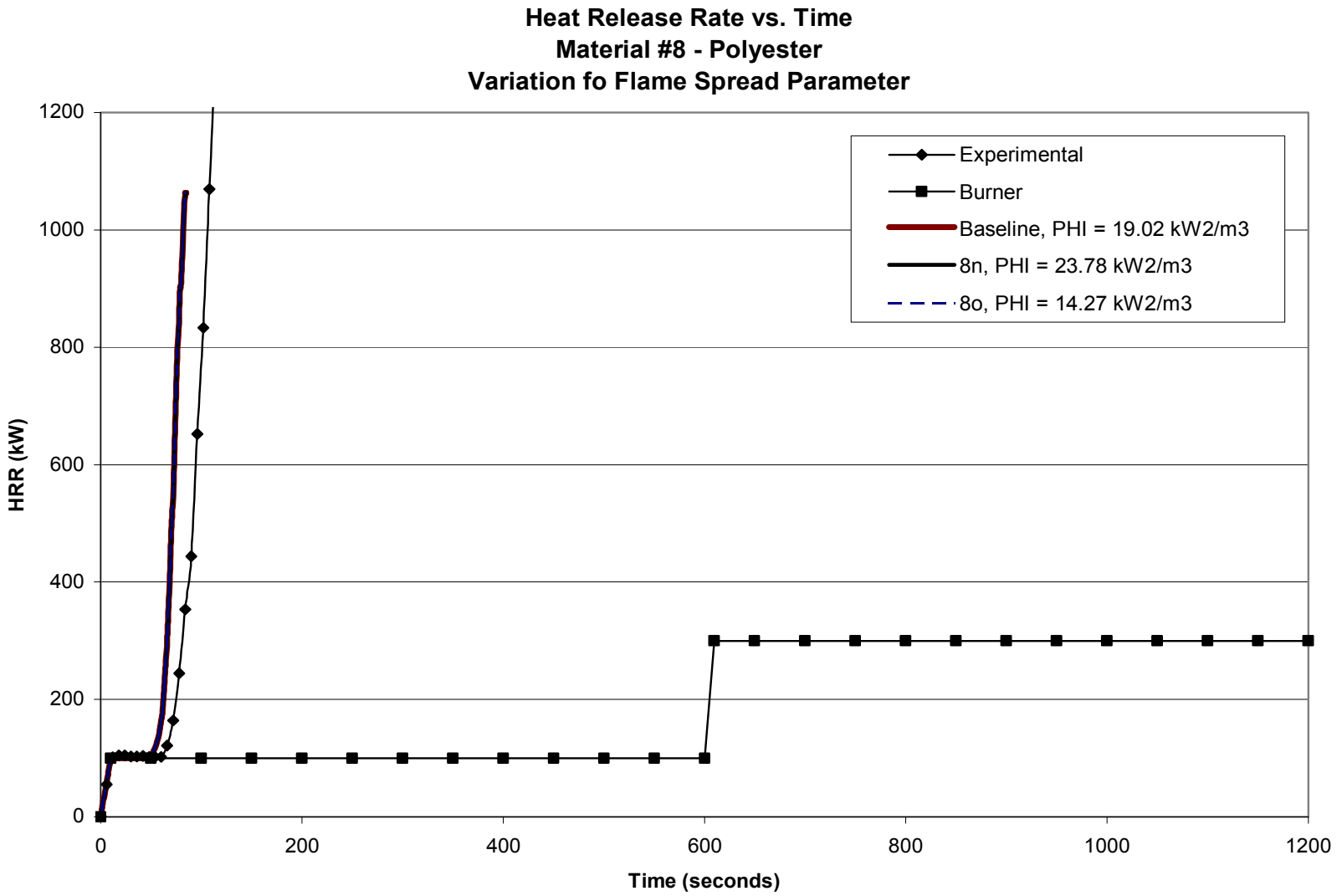
Heat Release Rate vs. Time
Material #8 - Polyester
Variation fo Flame Spread Parameter
HRR (kW)
Time (seconds)
0
200
400
600
800
1000
1200
Experimental
Burner
Baseline, PHI = 19.02 kW2/m3
8n, PHI = 23.78 kW2/m3
8o, PHI = 14.27 kW2/m3

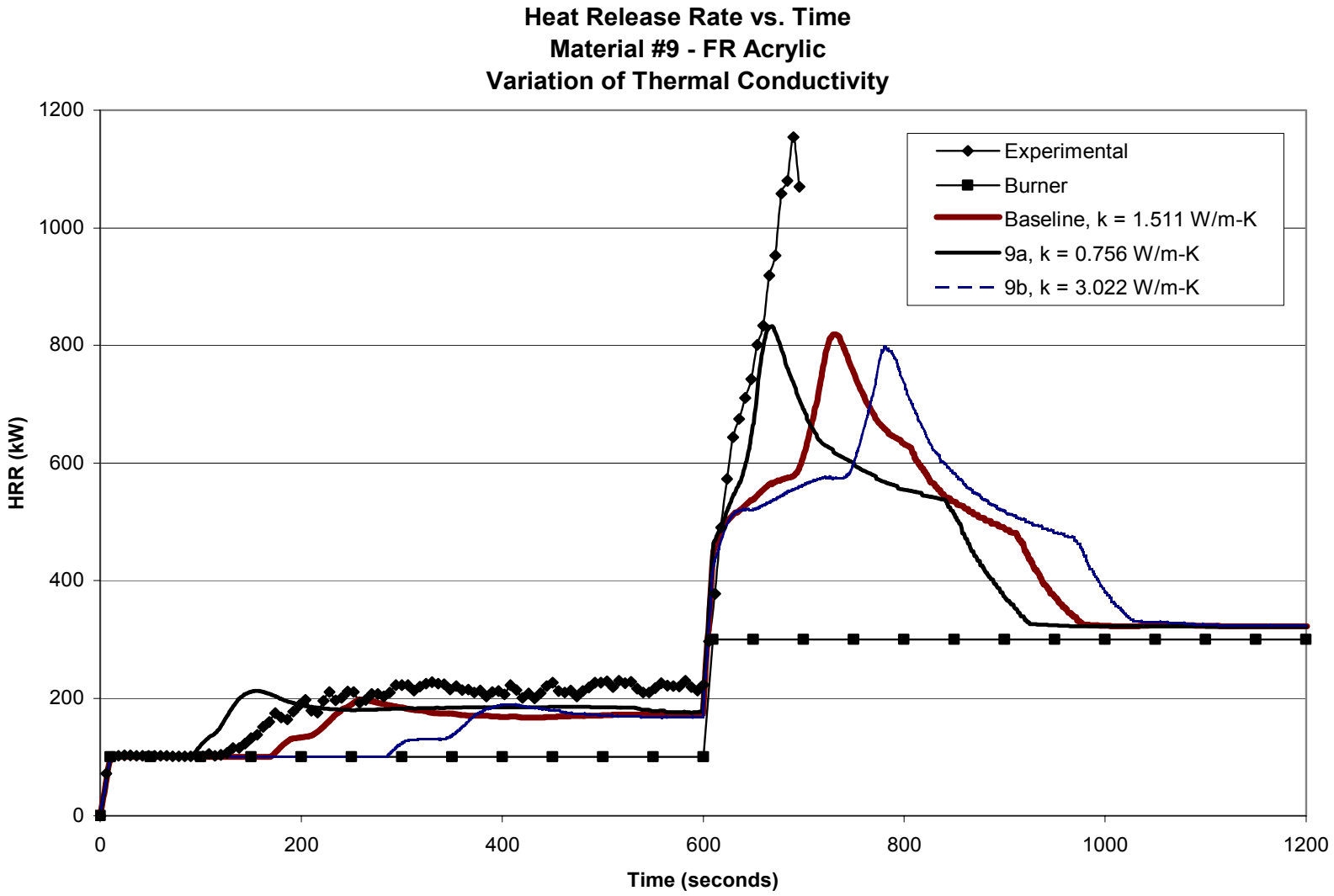
Heat Release Rate vs. Time
Material #9 - FR Acrylic
Variation of Thermal Conductivity
HRR (kW)
Time (seconds)
0
200
400
600
800
1000
1200
Experimental
Burner
Baseline, k = 1.511 W/m-K
9a, k = 0.756 W/m-K
9b, k = 3.022 W/m-K

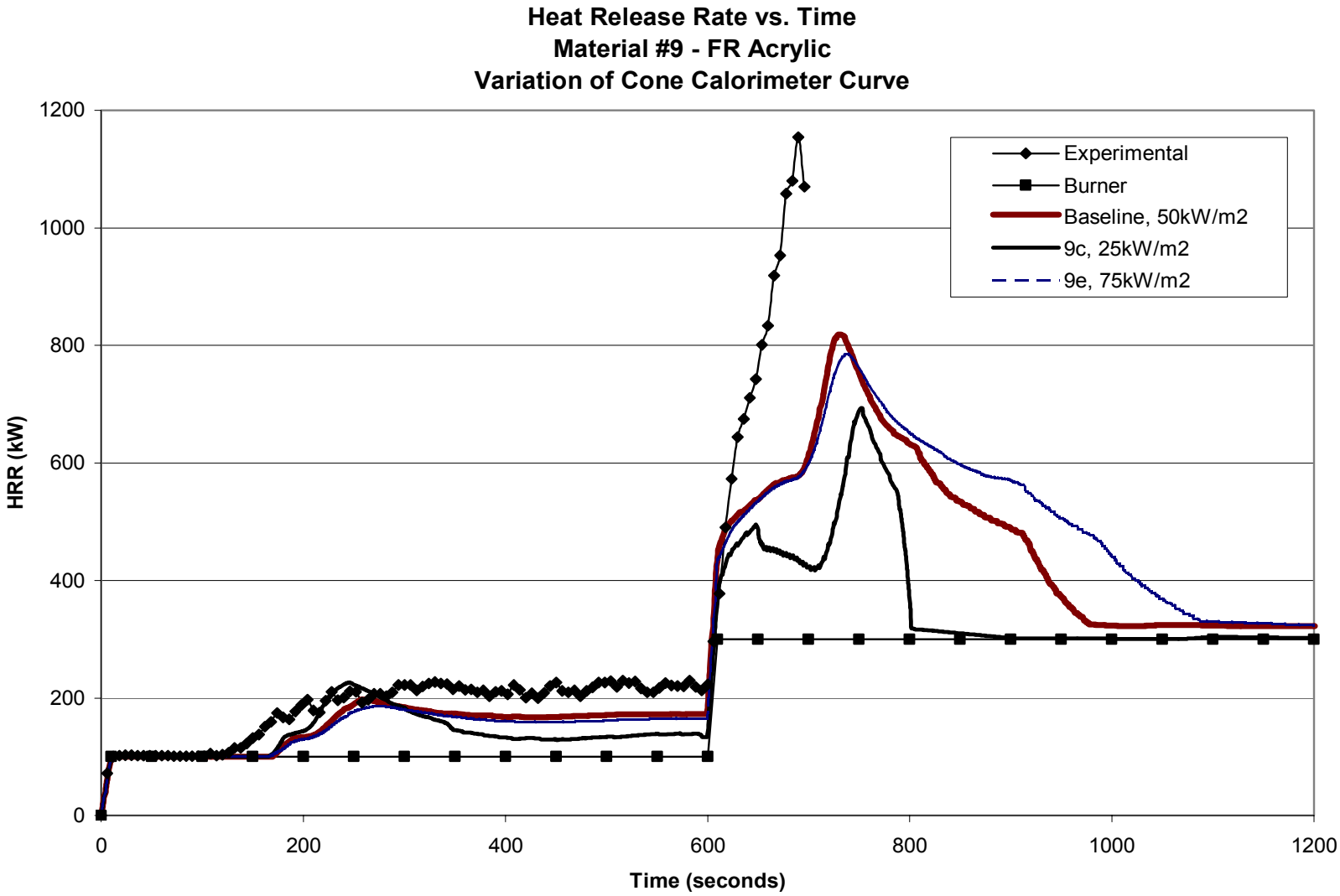
Heat Release Rate vs. Time
Material #9 - FR Acrylic
Variation of Cone Calorimeter Curve
HRR (kW)
Time (seconds)
0
200
400
600
800
1000
1200
Experimental
Burner
Baseline, 50kW/m2
9c, 25kW/m2
9e, 75kW/m2

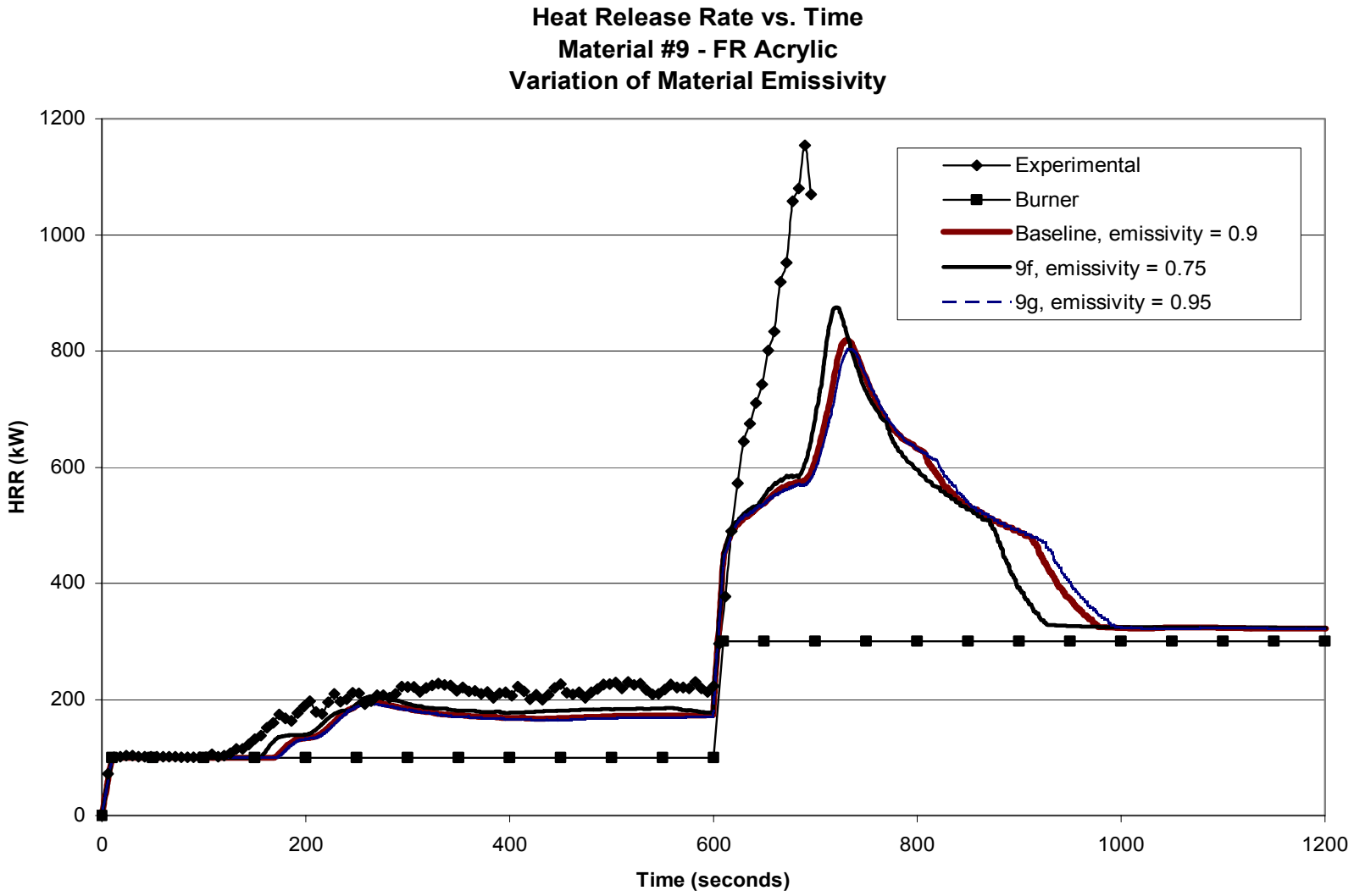
Heat Release Rate vs. Time
Material #9 - FR Acrylic
Variation of Material Emissivity
HRR (kW)
Time (seconds)
0
200
400
600
800
1000
1200
Experimental
Burner
Baseline, emissivity = 0.9
9f, emissivity = 0.75
9g, emissivity = 0.95

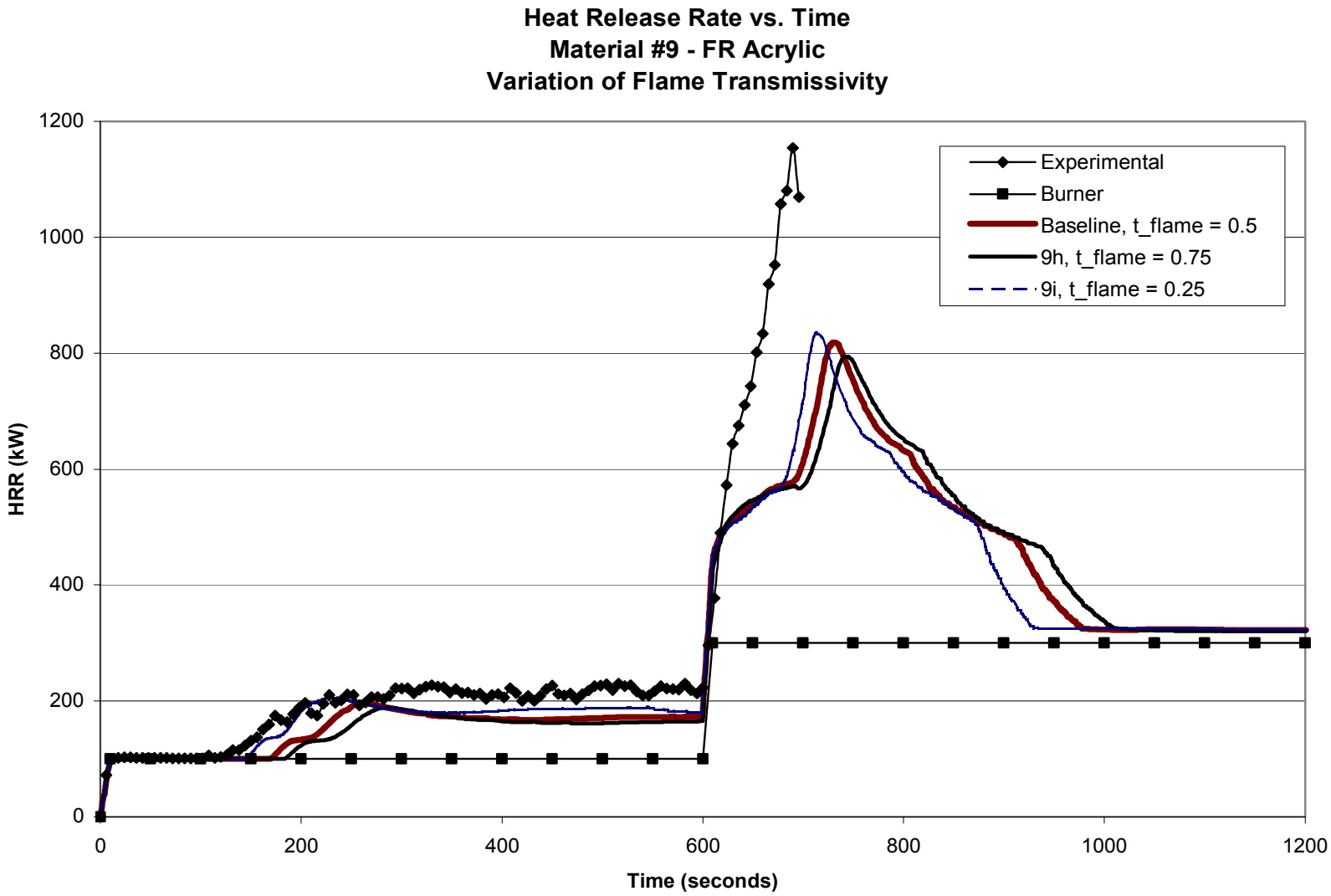
Heat Release Rate vs. Time
Material #9 - FR Acrylic
Variation of Flame Transmissivity
HRR (kW)
Time (seconds)
0
200
400
600
800
1000
1200
Experimental
Burner
Baseline, t_flame = 0.5
9h, t_flame = 0.75
9i, t_flame = 0.25

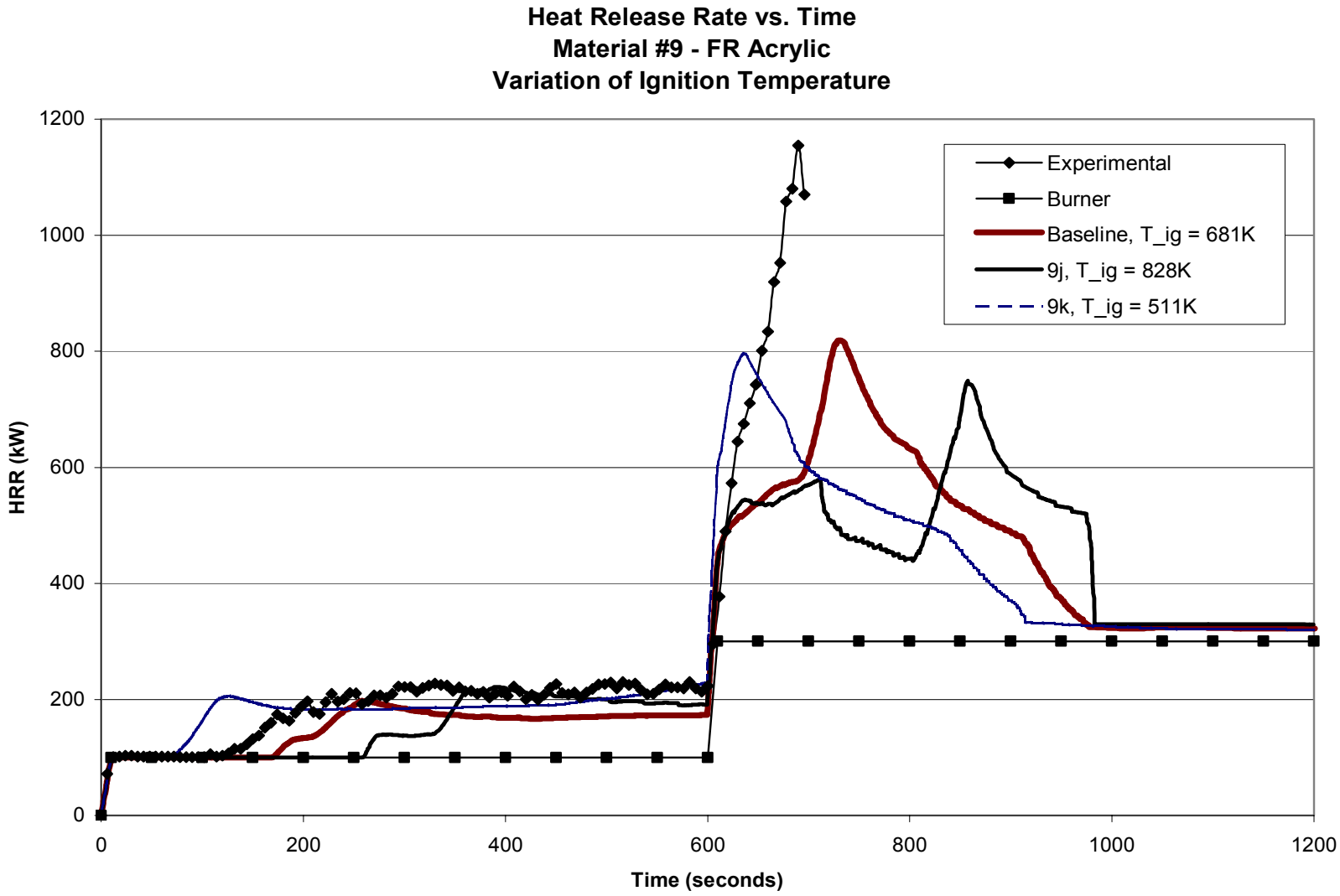
Heat Release Rate vs. Time
Material #9 - FR Acrylic
Variation of Ignition Temperature
HRR (kW)
Time (seconds)
0
200
400
600
800
1000
1200
Experimental
Burner
Baseline, T_ig = 681K
9j, T_ig = 828K
9k, T_ig = 511K

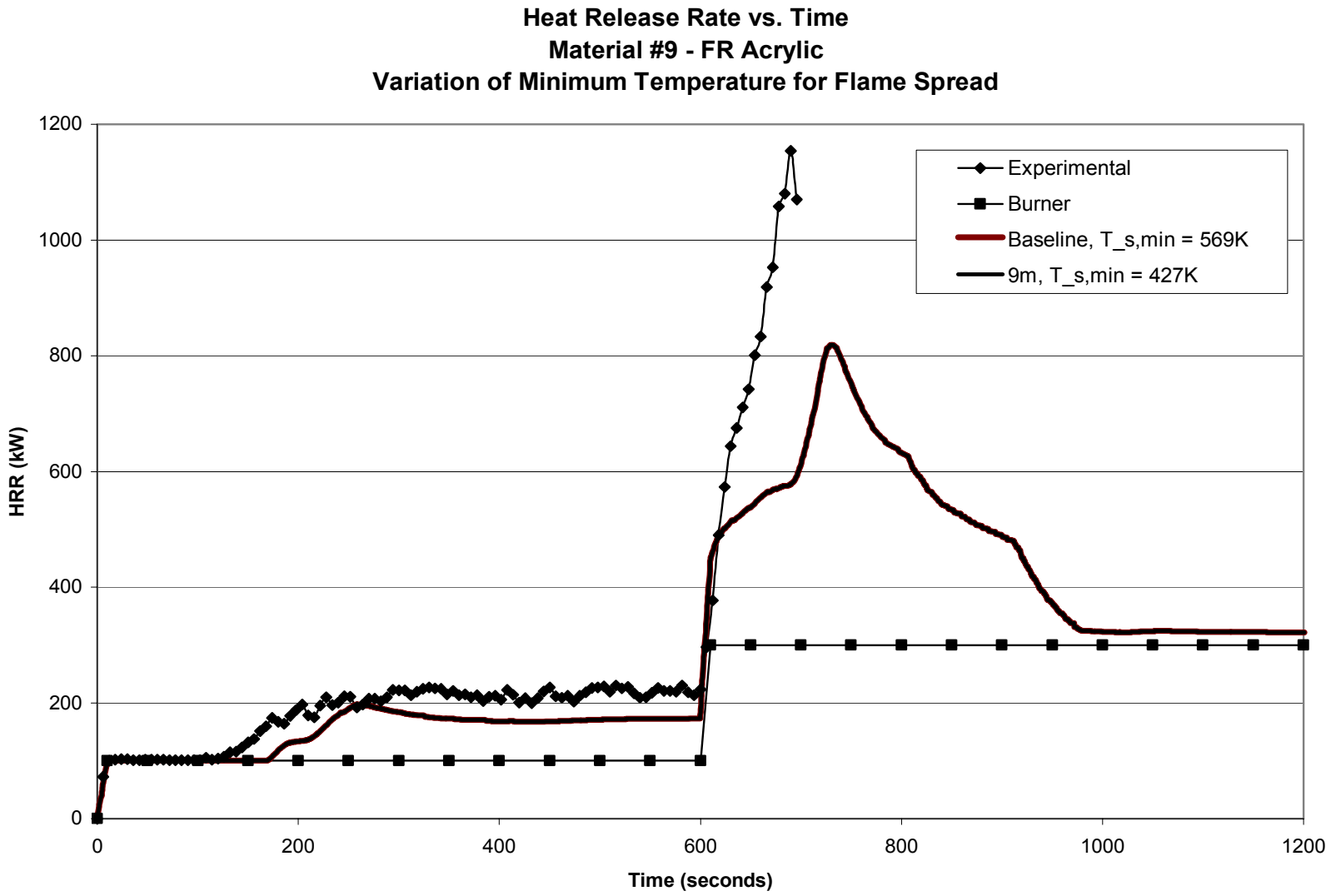
Heat Release Rate vs. Time
Material #9 - FR Acrylic
Variation of Minimum Temperature for Flame Spread
HRR (kW)
Time (seconds)
0
200
400
600
800
1000
1200
Experimental
Burner
Baseline, T_s,min = 569K
9m, T_s,min = 427K

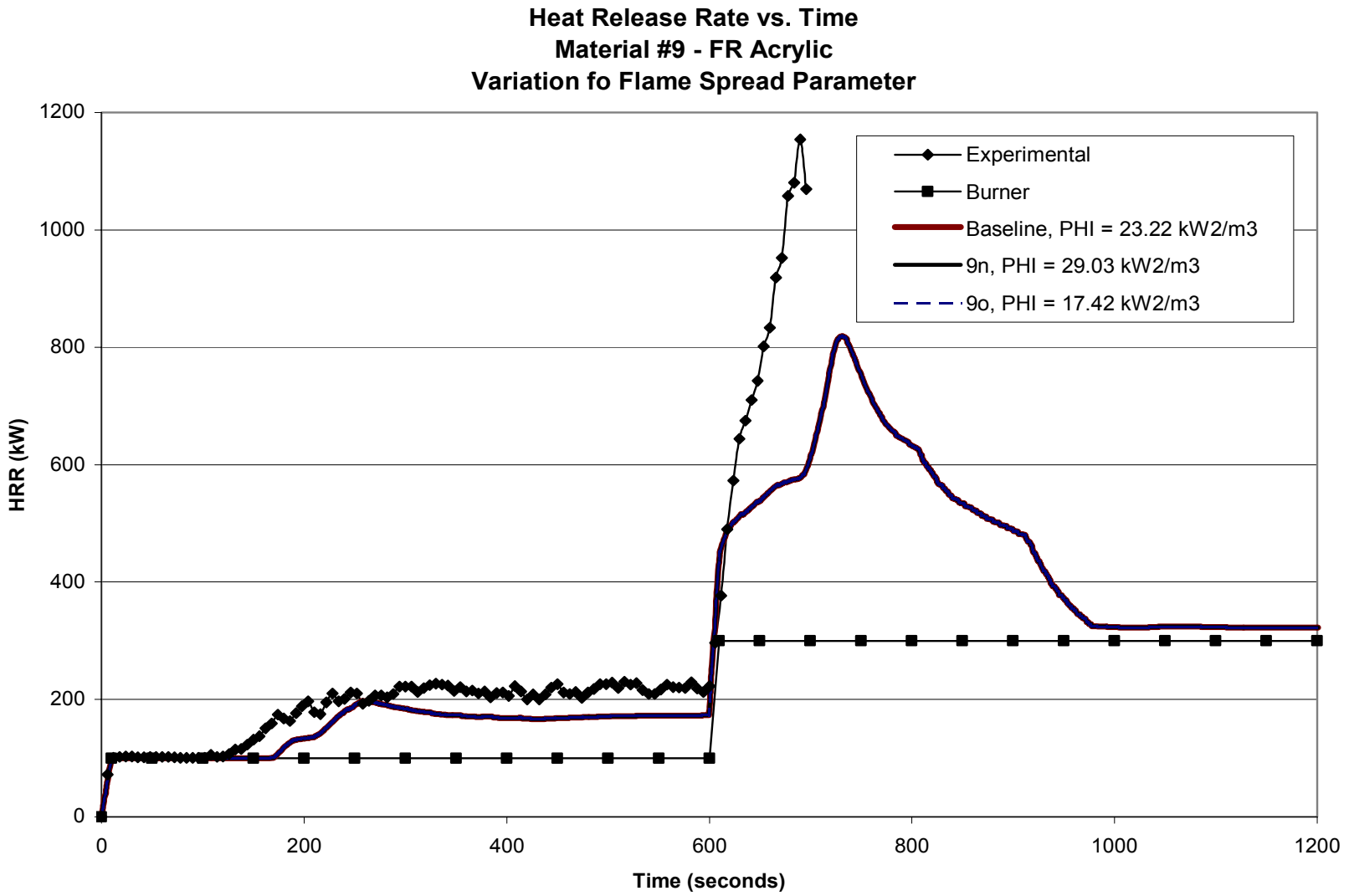
Heat Release Rate vs. Time
Material #9 - FR Acrylic
Variation fo Flame Spread Parameter
HRR (kW)
Time (seconds)
0
200
400
600
800
1000
1200
Experimental
Burner
Baseline, PHI = 23.22 kW2/m3
9n, PHI = 29.03 kW2/m3
9o, PHI = 17.42 kW2/m3

Appendix M – Contents of the Included CD-ROM

This appendix describes the contents of the CD-ROM in the back cover. The main directories are as follows:

src – source code for the model, including compile-time libraries and header files

data – the experimental data used in model verification

inputs – summary of input to the model

docs – electronic version of this document, and associated images

results – results of the simulations

mtech – documents relating to the Maritech (high-speed craft) research project